Accessibility, Reactivity, and Fluoroalkylation Reactions of High-Oxidation-State Organonickel Complexes

by

James R. Bour

A dissertation submitted in partial fulfillment
of the requirements for the degree of
Doctor of Philosophy
(Chemistry)
in the University of Michigan
2018

Doctoral Committee:

Professor Melanie S. Sanford, Chair
Professor Suljo Linic
Professor John Montgomery
Professor Nathaniel Szymczak

James R. Bour

jambour@umich.edu

ORCID iD: 0000-0002-0372-7323

for Cassie, Norma, Jim, Becca, Ryan and Jacob

ACKNOWLEDGEMENTS

I would first like to acknowledge my family both immediate and extended for their seemingly infinite encouragement and support leading to and through graduate school. From the time that I started elementary school to the completion of this degree, my family has always supported me in whatever I endeavored to accomplish. From help with homework to assistance in filing my taxes, every area of my life has been graced with their assistance. I would specifically like to acknowledge my wife and parents. With their help, I had the privilege of focusing on my studies without significant distraction by other areas of my life. I consider myself very lucky to associate with such helpful, intelligent, and understanding people. I hope someday that I can repay all of the time and effort spent helping me with nearly every aspect of my life.

I would next like to acknowledge my advisor, Prof. Melanie Sanford, for her keen scientific insight, leadership, support, and tolerance of me throughout graduate school. I am very fortunate to have been trained by such a talented individual. Her impact on my approach to science cannot be understated. If I have learned even 10% of how Melanie approaches science, I will consider graduate school a success.

I would also like to thank my committee members, Professor Nate Szymczak, John Montgomery and Suljo Linic for their time and intellectual contributions to my research projects. I would specifically like to recognize Prof. Szymczak for his mentorship during my rotation in his lab. During my time in his lab, I learned many skills and perspectives that would prove crucial to the advancements of my research projects in graduate school. I would also like to thank him for his continued interest in me and my research. With so many obligations, it is no small feat to find the time to critically consider aspects of my research.

Since the beginning of my time in the Sanford lab I have been surrounded by brilliant, driven and supportive lab mates. It is safe to say that every single one of my coworkers directly contributed to my projects through daily suggestions and discussions. I would specifically like to thank Courtney, Christo, Doug, Rachel, and Joe for being excellent post-doc role models and taking the time to listen to my ill-conceived ideas and questions. Pablo, Liz, Pronay, Sydonie,

Devin, and Nomaan similarly deserve special recognition for their intellectual contributions to my projects. Though he would never admit it, Nomaan deserves a thanks for calling attention to and challenging my preconceived assumptions about my research. Few were so willing to listen to and correct every nuanced detail of what I had already ruled out of consideration. I would also like to thank Devin and Pronay for their willingness to entertain bad ideas with me. My favorite part of graduate school has been discussions of improbable chemistries with them.

Perhaps the most gratifying part of graduate school has been collaborating with my lab mates on a wide variety of projects. Devin, Eugene, Liz, Nicole, Christian, Ted, Stavros and Ansis have all taught me new perspectives in my approach to science. I am grateful to have worked with them and I am excited to see where our projects will lead.

The department's support staff and management have also been extremely helpful throughout my time at the University of Michigan. I am thankful for all of the help Jeff Kampf, Eugenio Alvarez, Jim Windak, Kate Dyki, Tom Vaid and Andrew Higgs have given me.

Finally, I would like to acknowledge my dear friend Nicole Camasso's contributions to my scientific development through graduate school. Nicole was effectively my graduate student mentor when I first rotated in the Sanford lab. She was the first to welcome me and was always willing to help me with anything at any time throughout my rotation. However, her mentorship did not end after my rotation. Her continued support and advice during the entirety of graduate school was absolutely essential to completion of this degree. I am both proud and grateful to have worked closely with her on numerous projects.

TABLE OF CONTENTS

LIST OF SCHEMES

LIST OF FIGURES

LIST OF TABLES

ABSTRACT

A recent resurgence in nickel catalysis research has demonstrated that nickel-based catalyst systems are promising candidates to solve many outstanding problems in cross-coupling catalysis. Mechanistic studies of these transformations often reveal complicated interconversions of short-lived and consequently poorly characterized organometallic nickel intermediates. This observation is particularly true for highly oxidized nickel centers, which rapidly eliminate C–C and C–X bonds. Thus the rational development of methodologies based on high-valent nickel intermediates remains difficult. This dissertation seeks to address these uncertainties through detailed studies on the accessibility, reactivity and interconversions of model $Ni^{III/IV}$ complexes with a specific focus on fluoroalkylation elimination reactions from $Ni^{III/IV}$ centers

Chapter 2 details the synthesis and $1e^-$ oxidation chemistry of $[Ni^{II}(CF_3)(Ph)]$ complexes bearing diphosphine or tridentate nitrogen donor ligands. Our studies demonstrate that with a judicious choice of ligand, nickel is able to efficiently mediate the formation of $Ar–CF_3$ bonds under oxidatively and thermally mild conditions. Stabilization of the proposed intermediates with a tridentate ligand is found to yield the first example of an isolable diorganonickel(III) complex that undergoes C–C coupling. Detailed mechanistic studies of this transformation rule out the potential intermediacy of Ni^{IV} in this reaction.

Chapter 3 describes the design and reactivity of a model system for a two-part study on elementary organometallic reactions pertinent to $Ni^{II/IV}$ catalysis. Various aryl and alkyl electrophiles are examined for their ability to effect the $2e^-$ oxidation of Ni^{II} to Ni^{IV}. The C–C and

$C(sp^3)$ –X coupling of the reactions of resultant Ni^{IV}(alkyl/aryl) compounds is investigated. Mechanistic studies differentiating $1e^-$ vs $2e^-$ pathways of these transformations are described.

In Chapter 4 the interconversion of organonickel(III/IV) complexes through their reactions with carbon-centered radicals (CCRs) is reported. First we demonstrate that CCRs effect the oxidation of Ni^{III} to Ni^{IV} through inner-sphere radical addition to the nickel centers. Secondly, we show that select Ni^{IV} alkyl complexes are susceptible to homolytic abstraction of a carbon donor ligand by a free carbon-centered radical. This non-traditional C–C coupling pathway opens up previously unprecedented types of reactivity, including mild C–C coupling to form $H_3C–CF_3$.

Chapter 5 describes the synthesis and reactivity the first isolated examples of a copper(I) difluoromethyl complexes. Key to the realization of this strategy was the implementation of a bulky N-heterocyclic carbene ligand to slow bimolecular decomposition. The stoichiometric reactions of these complexes with a variety of organic electrophiles are described culminating with the catalytic difluoromethylation of aryl iodides.

CHAPTER 1

Introduction

1.1. Palladium and Nickel Catalyzed Coupling Reactions

Homogenous transition metal catalysts have transformed approaches to the synthesis of complex organic molecules such as pharmaceuticals and agrochemicals. The overwhelming majority of these transformations are currently performed using palladium-based catalysts, despite the high cost and low earth abundance of palladium. [1,2] Palladium's excellent balance between catalyst activity and stability has made it a practical choice for a wide variety of challenging organic transformations and has thus been adopted as an essential tool in organic synthesis[1,**Error! Bookmark not defined.**]

The broad scope of transformations enabled through palladium catalysis were not initially evident following its initial discovery as a promising catalyst platform. Instead, years of intense organometallic studies generally preceded the practical realization of many of the most difficult transformations (e.g. C–N bond formation).[3] Detailed studies of these transformations revealed that palladium typically cycles between the 0 and +2 oxidation states. However, sporadic proposals suggested that some reactions may be best described through $Pd^{II/IV}$ redox cycling.[4] These proposals were generally dismissed by the community until concrete evidence for the formation and catalytic relevance of Pd^{IV} was achieved through the isolation and reactivity studies of well-defined organometallic Pd^{IV} complexes.[5] These fundamental organometallic studies inspired a paradigm shift in the strategies for catalytic formation of traditionally challenging bonds. The strong driving force for reduction of the Pd^{IV}

center generally accelerates challenging elimination reactions such as C–X and C–CF_3 reductive elimination.[6] While advances in $Pd^{II/IV}$ catalysis have significantly expanded the scope of palladium catalysis, high valent manifolds are not without notable limitation. The $Pd^{II/IV}$ manifold often requires strong oxidants and high catalyst loadings relative to traditional $Pd^{0/II}$ reactions,[7,8] and large scale implementation of this promising catalytic regime is accordingly rare.

Scheme 1.1 Various features of $Pd^{0/II}$ catalysis and $Pd^{II/IV}$ catalysis

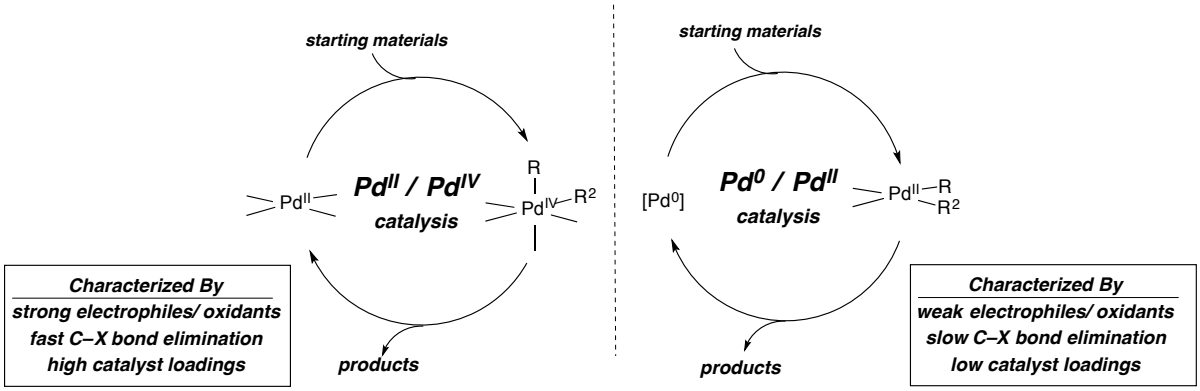

Two strategies have emerged to address the cost and scope limitations. First, detailed studies of catalyst speciation have identified ligands and conditions that can significantly improve catalyst turnover and thus reduce its cost.[9] However, none of these advances have proved general across a broad range of $Pd^{II/IV}$-catalyzed transformations. A second strategy is to replace the palladium catalyst with a less expensive substitute.[10] Palladium's first row group 10 counterpart, nickel, is an obvious choice as an economical and sustainable alternative. Nickel is approximately 2000 less expensive on a cost per mole basis and it is known to catalyze many of the same transformations.[2] However, nickel catalysis has not benefitted from the same depth and breadth of intense organometallic studies as palladium.[11] Specific key aspects of its reactivity, especially in the higher oxidation states, remains largely unknown. Moreover, nickel's propensity to engage organic substrates in both $1e^-$ and $2e^-$ redox events complicates analogies to the more developed areas of palladium catalysis.[2,10] Despite these challenges, a

recent resurgence in nickel catalysis research has identified several areas in which nickel displays significant potential as a practical catalyst for the formation of important bonds.

Though nickel holds promise as an economical and often complementary alternative to high-valent palladium, significant questions remain about the accessibility, reactivity, and interconversions of high-oxidation-state organonickel. And if the history of palladium catalysis serves as an example, answers to this questions will be made on the basis of insights gleaned from detailed mechanistic and organometallic studies. To this end, this thesis describes the synthesis and elementary reactivity of model Ni^{III} and Ni^{IV} complexes with a specific focus on the fluoroalkylation reactions enabled by nickel in these oxidation states.

1.2 High Oxidation State Organometallic Nickel Complexes

Nickel-catalyzed cross-coupling reactions have historically have been historically proposed to occur through one of two pathways.[2,10] The first involves clean $2e^-$ redox cycling between nickel in the 0 and +2 oxidation states. The stability of nickel complexes in these oxidation states has enabled thorough characterization reactivity studies of the key intermediates in these reactions (Scheme 1.2). The other most commonly proposed mechanism is that involving a C–C or C–X elimination from $Ni^{III.}$ Generally known as $Ni^{I/III}$ catalysis, these catalytic manifolds typically involve complicated interconversions between nickel in the 0 to +3 oxidation states. Due to the transient nature of many intermediates in this regime, the key steps of this reaction are typically inferred rather than directly observed (Scheme 1.2).[12] In particular, the remarkable activity of Ni^{III} to C–C and C–X bond-formation has made thorough characterization of these key intermediates difficult. Detailed studies on the generation and bond-forming reactivity are correspondingly limited.

Scheme 1.2. Commonly proposed catalytic manifolds for nickel coupling reactions

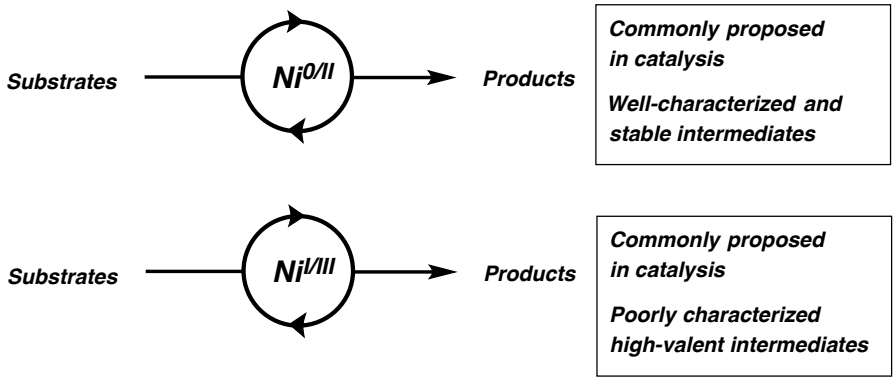

Various strategies have been developed to stabilize and understand the reactivity of organonickel(III) complexes. Though examples are limited, several common features of supporting ligand scaffolds have been reported to stabilize these traditionally reactive complexes.[13] Strongly chelating nitrogen donor ligands are most often employed to enforce saturation of the metal center. A prominent exception is Tilley's 2013 report on a stable but highly unsaturated Ni^{III}–CH_3 complex supported by bulky silylamide ligands. The origin of this molecule's stability is ostensibly a combination between the bulky silylamide ligands and the high barrier to C–N and N–N coupling. Though these complexes represent a significant advance in the stabilization of organonickel(III), none are generally representative of the Ni^{III} intermediates expected in common C–C cross coupling reactions. Chapter 2 of this thesis describes our studies of an isolable non-cyclometallated diorganoNi(III) complex that undergoes high-yielding C–C coupling.

Scheme 1.3. Selected examples of isolated organonickel(III) complexes

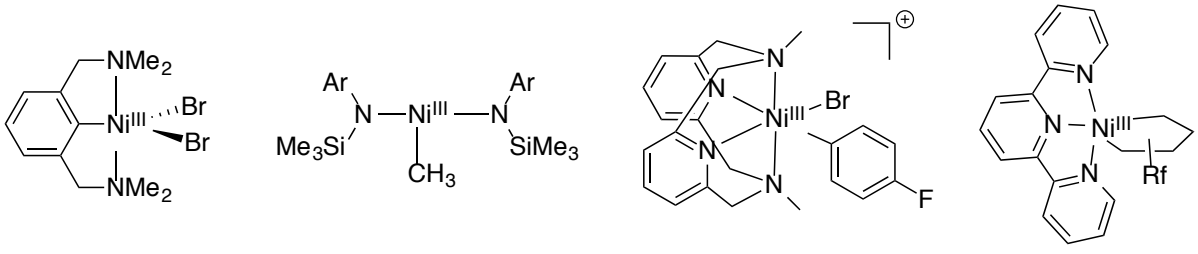

van Koten, **1983** *Tilley*, **2013** *Mirica*, **2014** *Vicic,* **2015**

While the overwhelming majority of nickel-catalyzed coupling reactions are thought to occur through $Ni^{0/II}$ and $Ni^{I/III}$ mechanisms, a growing body of theoretical[14] and experimental[15] evidence supports the feasibility of $Ni^{II/IV}$ catalysis. Similar to the key high-valent intermediates in $Ni^{I/III}$ catalysis, the fast C–C or C-X coupling from Ni^{IV} has prevented the isolation or detection of Ni^{IV} in these reactions. Proposals for these intermediates are generally made when carbon-centered radicals are not detected and the reaction medium is highly oxidizing. Thus there is little experimental support for or against the intermediacy of Ni^{IV} in these transformations outside of recent theoretical studies.

Scheme 1.4. Prominent examples of proposed Ni^{IV} intermediates in (b) nickel-catalyzed directed C–H functionalization reactions and (c) the nickel catalyzed alkylation of benzthiazole derivatives with alkyl iodides

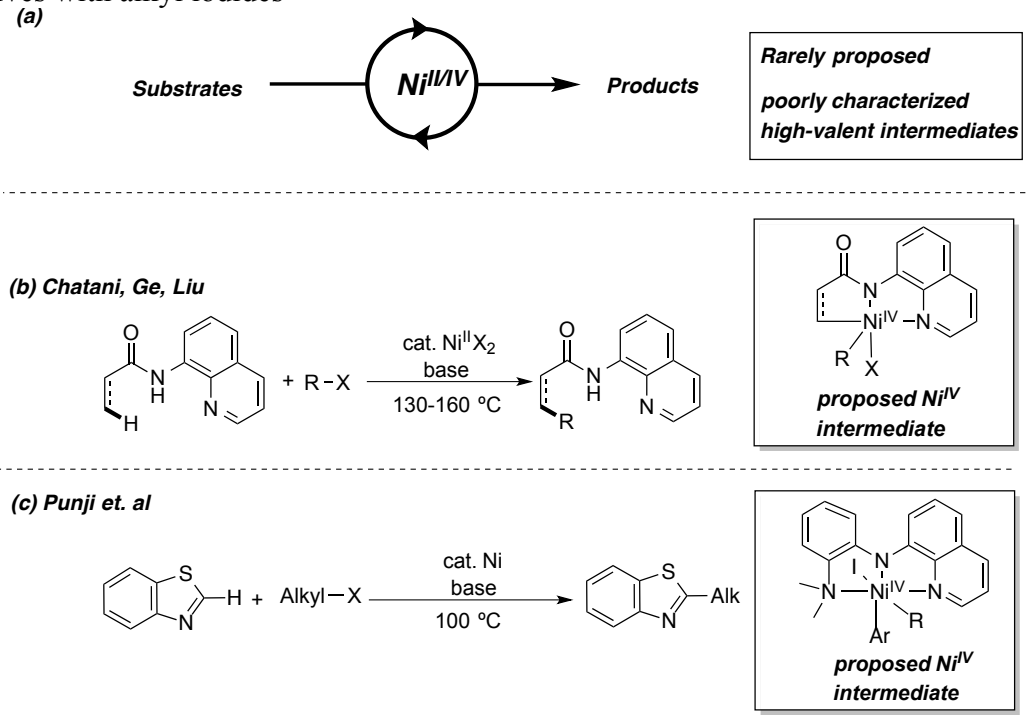

Until recently, Ni^{IV} was not considered a catalytically relevant oxidation state. This is arguably due to the lack of supporting organometallic studies investigating its accessibility and reactivity.[2,10] Until 2015, isolated organonickel(IV) complexes provided little insight into the feasibility of the proposed Ni(IV) intermediates in catalysis (Scheme 1.5).[16] In 2015, Sanford and Camasso published the synthesis and reactivity of a tris-pyrazolylborate-stabilized

cycloneophyl Ni^{IV} that was found to undergo intramolecular C–C coupling and outer sphere C–X coupling (Scheme 1.5).[17] This seminal contribution to the field, was unable to address the broader scope of oxidants leading to the formation of Ni^{IV}– a key component of the overall catalytic relevance of Ni^{IV}. Chapter 3 of this thesis focuses on formation of Ni^{IV} with net $2e^-$ carbon electrophiles as well as the bond-forming eliminations of the product Ni^{IV} compounds. Chapter 4 describes the $1e^-$ interconversions of high-valent nickel complexes mediated by carbon–centered radicals.

Scheme 1.5 Selected examples of isolated organonickel(IV) complexes

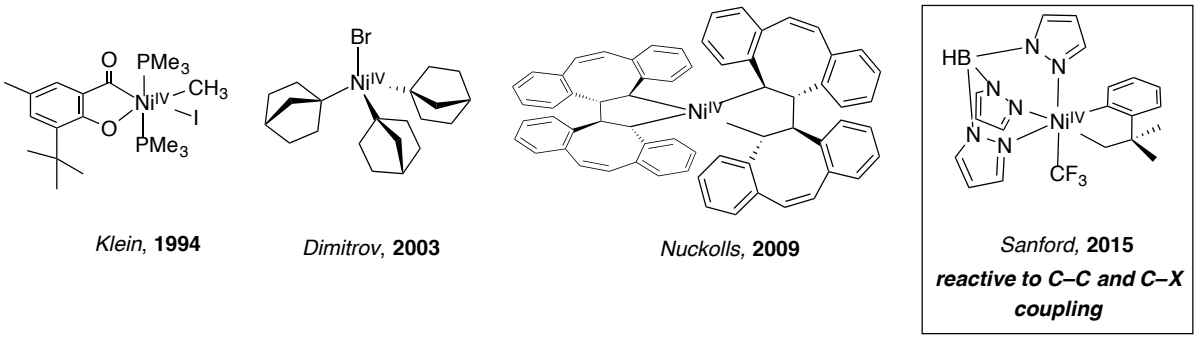

Klein, **1994** *Dimitrov*, **2003** *Nuckolls*, **2009** *Sanford*, **2015**

reactive to C–C and C–X coupling

1.3. Trifluoromethylation Reactions at Oxidized Nickel Centers

One promising application of high-valent nickel catalysis is in the area of trifluoromethylation reactions. Fluoroalkyl groups are important moieties in a variety of pharmaceutical drugs and agrochemicals.[18] However, the incorporation of these famously inert groups to high value fine chemicals is tremendously difficult using traditional organic chemistry. Transition metal mediated/catalyzed strategies have shown promise to enable C–CF_3 bond formation. However, most of these strategies are still generally harsh and/or limited in scope.[19]

Scheme 1.6. Common challenges in C-CF_3 forming reactions from select late transition metals

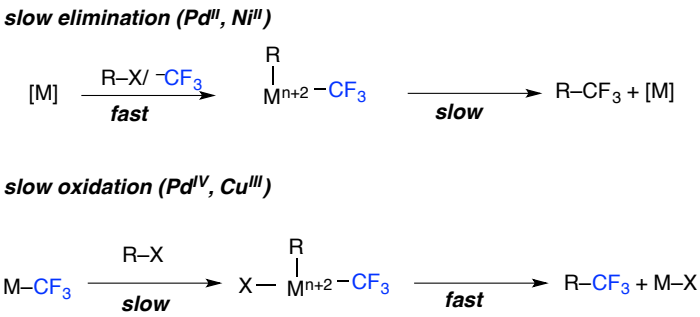

Extensive organometallic studies have identified two common limiting regimes for transition metal trifluoromethylation reactions: slow C–CF_3 elimination from low valent metal centers (i.e Pd^{II}, Ni^{II}) or thermodynamically challenging M-CF_3 oxidation (i.e. to Pd^{IV}, Cu^{III}) (Scheme 1.6).[19,20] In the slow elimination regime, low valent metals (typically Pd) rapidly activate a wide range of electrophiles but subsequent Ar–CF_3 elimination is generally only achieved with specialized ligands and/or high temperatures. In contrast, C–CF_3 elimination from high-oxidation state metals such as Pd^{IV} and Cu^{III} is generally fast, but the generation of these oxidized metal centers is often difficult (Scheme 1.6). Similarly, fast C–CF_3 elimination is also expected to occur from more oxidized nickel species (Ni^{III} and Ni^{IV}). However, at the outset of our studies, the C–CF_3 elimination from Ni^{III} or Ni^{IV} was not known.

The possibility of C–CF_3 bond formation from organonickel(III) is particularly attractive because it may represent an intermediate case between the two limiting regimes shown Scheme 1.7. Carbon-carbon reductive elimination from Ni^{III} is known to be fast *and* Ni^{III} can generally be reached with mild oxidants. Thus a trifluoromethylation methodology constructed around C–CF_3 elimination from Ni^{III} may offer the broad electrophile scope associated with low-valent manifolds and the mild temperatures associated with high-valent regimes. Chapter 2 of this thesis outlines the feasibility and challenges associated with C–CF_3 bond formation from Ni^{III} complexes.

Scheme 1.7 General trends in the generation and C–C coupling of $Ni^{III/IV}$

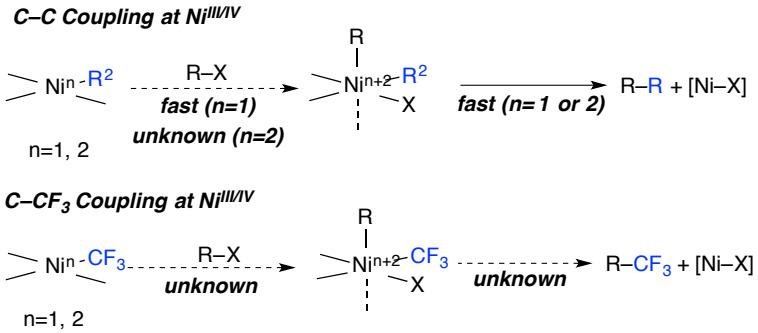

1.4.Copper–Catalyzed Difluoromethylation of Aryl Iodides

Other fluoroalkyl groups have also emerged as attractive targets for incorporation into complex molecules such as pharmaceuticals and agrochemicals.[18,21] In particular, the difluoromethyl group (CHF_2) has garnered significant interest from medicinal chemists as an oxidatively stable bioisostere of the hydroxyl functional group.[22] Given its structural similarity to CF_3 , one might expect similar challenges in the metal-mediated and catalyzed incorporation of this group to organic molecules (i.e. slow C–CHF_2 elimination from low valent metal centers and slow oxidation to high valent M–CHF_2 complexes). However, preliminary organometallic studies suggest that C–CHF_2 elimination can readily occur from low-valent and high-valent metal centers alike.[23] Instead, the limiting challenge in metal-mediated and catalyzed difluoromethylation seems to be efficient transfer of nucleophilic CHF_2 to the metal center.[23a,b] Chapter 5 details the identification of conditions for the transfer of CHF_2 from TMS(CHF_2) to (NHC)CuX complexes and the subsequent application of this organometallic reaction to the catalytic difluoromethylation of aryl iodides.

1.4. References

[1] (a) Magano, J.; Dunetz, J. R. *Chem Rev.* **2011**, *111*, 2177. (b) Corbet, J. P.; Migani, G. *Chem Rev.* **2006**, 106, 2651. (c) Hartwig, J. Organotransition Metal Chemistry: From Bonding to Catalysis. University Science Books: Sausalito, 2010. (d) Torborg, C.; Beller, M. *Adv. Synth. Catal.* **2009**, *351*, 3027.

[2] Tasker, S. Z.; Standley, E. A.; Jamison, J. A. *Nature,* **2014**, *509*, 299.

[3] Hartwig, J. F. *Inorg Chem.* **2007**, *46*,1936

[4] Heck, R. F. *J. Am. Chem. Soc.* **1968**, *90*, 5538. (b) Tremont, S. J; Hu, R. *J. Am. Chem. Soc*. **1984**, *106*, 5759.

[5] Canty, A. J. Dalton Trans. **2009**, *47*, 10409.

[6] Ball, N. D.; Gary, J. B.; Ye, Y.; Sanford M. S. *J. Am. Chem. Soc.* **2011**, *133*, 7577. (b) Ye, Y.; Ball, N. D. Sanford, M. S. *J. Am. Chem. Soc.* **2010**, *132*, 14682. (c) Kalyani, D.; Deprez, N. R.; Desai, L. V.; Sanford, M. S. *J. Am. Chem. Soc.* **2005**, 127, 7330.

[7] (a) Emmert, M. H.; Cook, A. K.; Xie, Y. J.; Sanford, M. S. *Angew Chem Int. Ed.* **2011**, *50*, 9409. (b) D. A. Alonso, C. Najera, I. M. Pastor, M. Yus, *Chem. Eur. J.* 2010, **16**, 5274–5284. (c) T. Jintoku, K. Takai, Y. Fujiwara, Y. Fuchita, K. Hiraki, *Bull. Chem. Soc. Jpn.*1990, **63**, 432. (d) Lyons, T. W.; Sanford, M. S. *Chem. Rev.* **2010**, 110, 1147.

[8] Sehnal, P.; Taylor, J. K.; Fairlamb, J. S. *Chem Rev.* **2010**, 824.

[9] Cook, A. K.; Sanford, M. S. *J. Am. Chem. Soc.* **2015**, *137*, 3109. (b) Engle, K.; Wang, D. H.; Yu, J. Q. *J. Am. Chem. Soc.* **2010**, *132*, 14137.

[10] Aihara, Y.; Chatani, N. *J. Am. Chem. Soc.* **2013**, *136,* 898. (b) Iyanaga, M.; Aihara, Y.; Chatani, N. *J. Org. Chem.* **2014**, *79*, 11933. **(c)** Wu, X.; Zhao, Y.; Ge, H. *J. Am. Chem. Soc*. **2014**, *136*, 1789. (d)

[11] Ananikov, V. V. *ACS Catalysis.* **2015**, *5*, 1964.

[12] Bour, J. R.; Camasso, N. M.; Meucci, E. M.; Kampf, J. W.; Canty, A. J.; Sanford, M. S. *J. Am. Chem. Soc.* **2016,** *138*, 16105.

[13] Grove, D. M.; van Koten, G. D.; Zoet, R.; Murral, N. W.; Welch, A. J. *J. Am. Chem. Soc.* **1983**, *105*, 1379. (b) Yu, S.; Dudkina, Y.; Wang, H.; Kholin, K. V.; Kadirov, M. K.; Budnikova, Y. H.; Vicic, D. A. *Dalton Trans.* **2015** , *44*, 19443 (c) Zheng, B.; Tang, F.; Luo, J.; Schultz, J. W.; Rath, N. P.; Mirica, L. M. *J. Am. Chem. Soc.* **2014**, *136*, 6499.

[14] Omer, H. M.; Liu, P. *J. Am. Chem. Soc.* **2017,** *139*, 9909**.** (b) Singh, S.; K. S.; Sunoj, R.; *J. Org. Chem.* **2017**, *82,* 9619. (c) Li, Y.; Zou, L.; Bai, R.; Lan, Y. *Org. Chem. Front.* **2018** *5*, 615.

[15] Aihara, Y.; Chatani, N. *J. Am. Chem. Soc.* **2013**, *136,* 898. (b) Iyanaga, M.; Aihara, Y.; Chatani, N. *J. Org. Chem.* **2014**, *79*, 11933. **(c)** Wu, X.; Zhao, Y.; Ge, H. *J. Am. Chem. Soc*. **2014**, *136*, 1789. (d) Yan, S.-Y.; Liu, Y.-J.; Liu, B.; Liu, Y.-H.; Zhang, Z.-Z.; Shi, B.-F. *Chem. Commun*. **2015**, *51*, 734. (e). Terao, J.; Kambe, N. *Acc. Chem. Res.* **2008**, *41*, 1545. (f) Soni, V.; Jagtap, R.; Gonnade, *J. Am. Chem. Soc.* **137**, 16064.; Punji, P.; *ACS Catalysis.* **2016**, *6*, 5666. (g) Soni, V.; Khake, S. M.; Punji, B. *ACS Catalysis* **2016,** *6*, 4202**.** (h) Patel, U.; Jain, S.; Pandey, D.; Gonnade, R. G.; Vanka, K.; Punji, B. *Organometallics* **2018**, ASAP DOI: 10.1021/acs.organomet.8b00025

[16] (a) H.-F. Klein, A. Bickelhaupt, T. Jung, G. Cordier *Organometallics* **1994**, *13*, 2557 (b) Carnes, M.; Buccella, D.; Chen, J. Y. C.; Ramirez, A. P.; Turro, N. J.; Nuckolls, C.; Steigerwald, M. *Angew. Chem., Int. Ed.* **2009**, *48*, 290

[17] Camasso, N. M.; Sanford, M. S. *Science* **2015**, *347*, 1218.

[18] Wang, J.; Rosello-Sanchez, M.; Acenal, J. L.; de Pozo, C.; Sorochinsky, A. E.; Fustero, S.; Soloshonok, V. A.; Liu, H. L. *Chem. Rev.* **2014**, *114*, 2432.

[19] Tomashenko, O. A.; Grushin, V. V; *Chem. Rev.* **2011**, 4475.

[20] (a) Grushin, V. V.; Marshall, W. J. *J. Am. Chem. Soc.* **2006**, *128*, 12644. (b) Dubinina, G. G.; Furutachi, K. K.; Vicic, D. A. *J. Am. Chem. Soc.* **2008,** *130,* 8600.
[21] Chen, B.; Vicic, D. A. *Top. Organomet. Chem*. **2014**, *52*, 113.
[22] Sessler, C. D.; Rahm, M.; Becker, S.; Goldberg, J. M.; Wang, F.; Lippard, S. *J. J. Am. Chem. Soc.* **2017,** *139*, 9325.
[23] (a)Gu, Y.; Leng, X.; Shen, Q. *Nature Communications* **2014**, *5*, 5405. (b)Lu, C.; Gu, Y.; Wu, J.; Gu, Y.; Shen, Q. *Chem. Sci.* **2017**, *8***,** 4848. (c) Xu, L.; Vicic, D. A. *J. Am. Chem. Soc.* **2016**, *138*, 2536.

CHAPTER 2

Aryl–CF_3 Coupling from Ni^{III}

2.1 Introduction

Appending trifluoromethyl substituents onto aromatic and heteroaromatic moieties can impart unique properties to organic molecules.[1] As a result, significant recent effort has been focused on the development of mild, selective, and inexpensive methods for the construction of aryl–CF_3 and heteroaryl–CF_3 linkages.[2,3] Group 10 metal-catalyzed cross-coupling reactions between aryl–X and CF_3–Y represent a particularly attractive approach, since analogous transformations have proven exceptionally effective for other C–C bond-forming reactions. However, early efforts to develop such reactions were impeded by the lack of precedent for a key step of the catalytic cycle: Aryl–CF_3 bond-forming reductive elimination from M(aryl)(CF_3) complexes (M = Pd, Ni).[4]

Scheme 2.1. Successful Ar–CF_3 coupling regimes of Pd.[3d, 5]

(***a***) Thermal Coupling Regime from Pd(II)

(***b***) Oxidative Coupling Regime from Pd(IV)

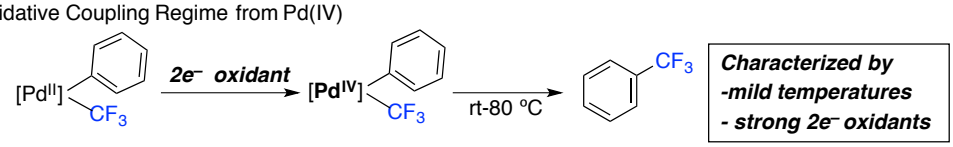

Over the past decade, fundamental organometallic studies of [Pd(aryl)(CF_3)] complexes have identified two successful regimes for high yielding aryl–CF_3 bond-forming reductive elimination from palladium. The first regime, thermally induced elimination, generally requires high temperatures and precise tuning of the electronic/steric properties of the supporting

phosphine ligand (Scheme 2.1a). Only a handful of specialized ligands have been reported to enable this transformation and only one has been successfully translated into catalysis.[4,5] The second regime relies on oxidation of a Pd^{II} center to drive the notoriously challenging coupling reaction (Scheme 2.1b). Though this strategy is thermally mild and effective with a broad range of inexpensive nitrogen donor ligands, it relies on harsh and expensive $2e^-$ oxidants. These fundamental organometallic studies have ultimately enabled the development of several important, albeit harsh, Pd-catalyzed aryl–CF_3 coupling methods. These include the reactions of aryl halides with $TESCF_3$ (Scheme 2.2a)[5] and of aryl–H with CF_3^+ reagents (Scheme 2.2b)[3d].

Scheme 2.2 Examples of Pd-Catalyzed Ar–CF_3 Coupling through (a) a Pd(0/II) manifold and (b) through a Pd(II/IV) manifold

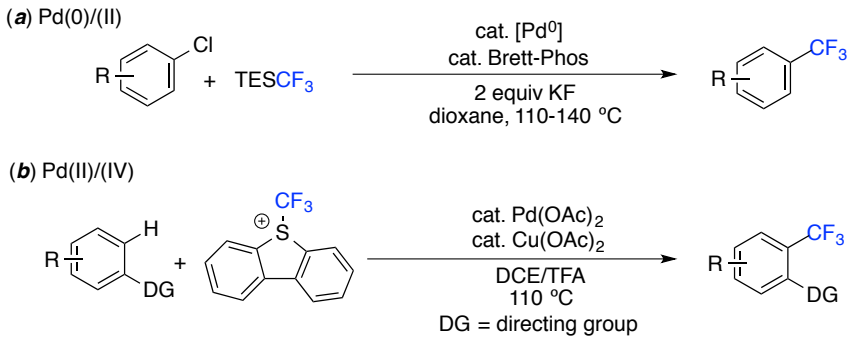

In contrast to the extensive studies of aryl–CF_3 coupling at Pd, there has been very little exploration of analogous reactions at Ni. Promising avenues toward the discovery of nickel-based catalysts for this transformation are accordingly bleak. Moving to Ni would be attractive due to (*i*) its dramatically lower cost versus Pd[6] and (*ii*) the greater diversity of cross-coupling mechanisms and oxidation states at Ni versus Pd (which might potentially enable milder catalytic manifolds that are not viable with Pd-based catalysts).[7,6] Recent reports by Vicic[8] and Grushin[9] have described the synthesis of a limited set of $Ni^{II}(CF_3)(Ar)$ complexes (*e.g.,* **1a** and **1b** in Figure 3.3). However, these complexes were not reported to undergo Ar–CF_3 coupling upon thermolysis and their reactivity to oxidation was not reported in detail. Overall, little is known about the elementary reactivity of (L~L)Ni(CF_3)(Ar) complexes and even less is known about the feasibility of nickel-catalyzed aryl trifluoromethylation reactions.

Scheme 2.3 Previously reported (P~P)Ni(CF_3)(Ar) Complexes[8,9]

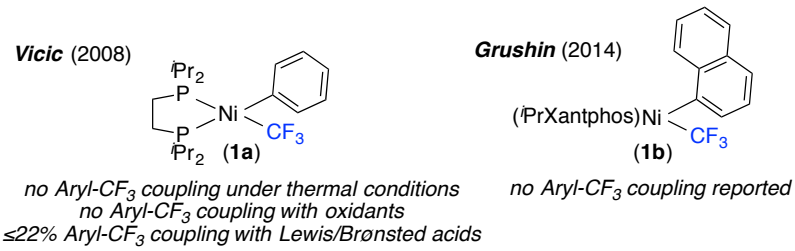

Based on related chemistry at Pd (Scheme 2.1b), we reasoned that Ar–CF_3 coupling at Ni could be enabled through oxidation of the Ni center. In contrast to palladium however, where clean $2e^-$ redox cycling between $Pd^{0/II}$ and $Pd^{II/IV}$ predominates, mononuclear Ni^{III} complexes are thought to be common intermediates in nickel-catalyzed coupling reactions.[10] Moreover, organometallic Ni^{III} complexes are known to readily mediate the formation of challenging C–C and C–X bonds, though the intermediacy of Ni^{III} in these reactions is generally inferred rather than directly observed. Importantly, the $1e^-$ oxidation of organonickel(II) intermediates can often be accomplished with mild oxidants such as O_2 or alkyl halides. Thus Ar–CF_3 reductive elimination from Ni^{III} may offer an intermediate compromise between the two successful Ar–CF_3 coupling regimes demonstrated thus far at Pd (strong $2e^-$ oxidants or high temperatures/specialized ligands).

Scheme 2.4 Strategy for the Development of Ni-catalyzed trifluoromethylation reactions

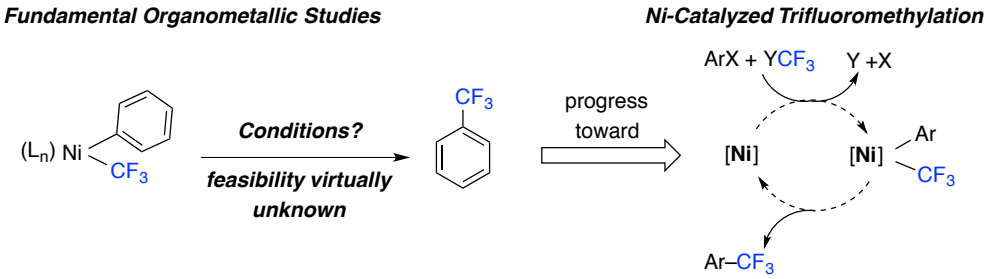

This chapter describes our studies of stoichiometric Ar–CF_3 coupling from nickel centers first through the in-situ generation of $[Ni^{III}(CF_3)(Ph)]^+$ compounds then from an isolated $[Ni^{III}(CF_3)(Ph)]$ compound. The results outlined herein detail insight into this challenging

transformation and provide a stoichiometric basis through which catalytic manifolds could be developed (Scheme 2.4)

2.2. Results and Discussion

2.2.1. Oxidatively Induced Ar–CF_3 Coupling from Diphosphine Nickel Complexes

Synthesis of (L~L) Complexes

A first key challenge was the development of a robust and general synthetic route to (P~P)$Ni^{II}(CF_3)$(Ar) starting materials (1). The previously reported complexes **1a** and **1b** were prepared via the reaction of (P~P)Ni^{II}(aryl)(halide) (2) with $TMSCF_3/F^-$ (Scheme 2.5a). However, transmetalation with $TMSCF_3$ is often accompanied by competing side reactions such as phosphine ligand displacement.[4,8,9] As such, in our hands, many (L~L)Ni(aryl)(CF_3) derivatives could not be accessed using this approach.

Scheme 2.5 (a) Previous strategies for the synthesis of **1**; (b) Our synthetic route to **1**.

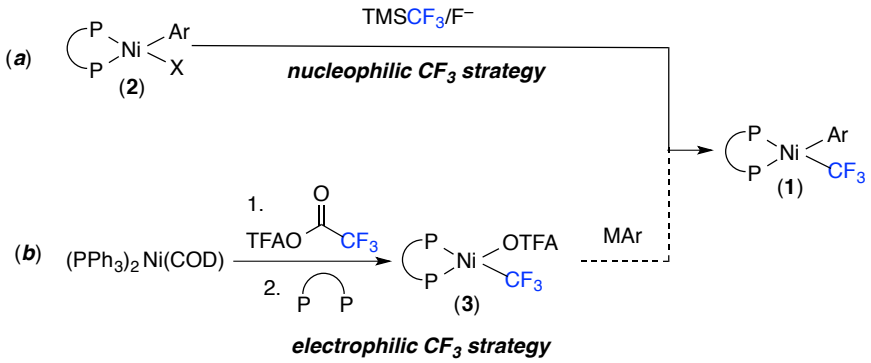

To circumvent these challenges, we designed an alternative synthesis of **1** that avoids the requirement for $TMSCF_3$ (Scheme 2.5b). This process introduces the CF_3 ligand via oxidative addition of trifluoroacetic anhydride at $(PPh_3)_2Ni(COD)$ followed by decarbonylation of the resulting trifluoroacyl intermediate.[11] Ligand exchange with a bidentate phosphine affords (P~P)Ni(OTFA)(CF_3) (**3**). Finally, transmetalation between **3** and an organometallic reagent (MAr) yields the desired product **1**.

Scheme 2.6 Synthesis of complex **1c**

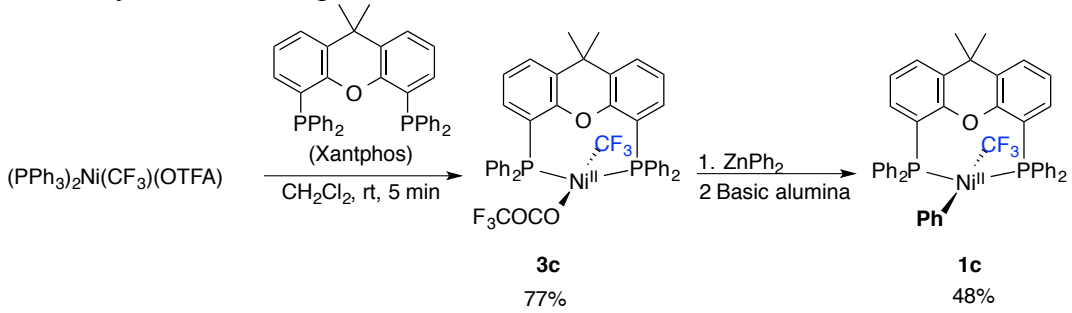

We first targeted (Xantphos)Ni(Ph)(CF_3) (**1c**), since its Pd analogue is known to undergo Ph–CF_3 bond-forming reductive elimination under mild conditions (Scheme 2.1a). The ligand exchange between *trans*-$(PPh_3)_2$Ni(OTFA)(CF_3) and Xantphos afforded **3c** in 77% yield (Scheme 2.6). Subsequent reaction of **1c** with PhMgCl or PhLi yielded a complex mixture of inorganic products. In contrast, the use of $ZnPh_2$ led to relatively clean formation of **1c** as determined by NMR spectroscopic analysis of the crude reaction. However, rapid decomposition of **1c** was observed during work-up.[12]

We hypothesized that the Lewis acidic by-product of this reaction, $Zn(OTFA)_2$, was responsible for this decomposition. Lewis acids are known to react with M–CF_3 complexes to generate unstable difluorocarbenes.[13] Indeed, the removal of $Zn(OTFA)_2$ (via filtration of the crude reaction mixture through basic alumina) afforded a zinc-free solution of **1c** with dramatically enhanced stability. As further confirmation of the proposed Lewis acid sensitivity, isolated **1c** was subjected to of 5 equiv $ZnBr_2$ or LiOTf. Upon addition, the solution immediately changed color and **1c** was completely consumed within 5 minutes as determined by ^{19}F NMR (Scheme 2.7). The instability of **1c** to hard Lewis acids may play a role in the failure of PhMgCl or PhLi to yield **1c** from **3c**.

Scheme 2.7 Reactions of **1c** with selected Lewis acids

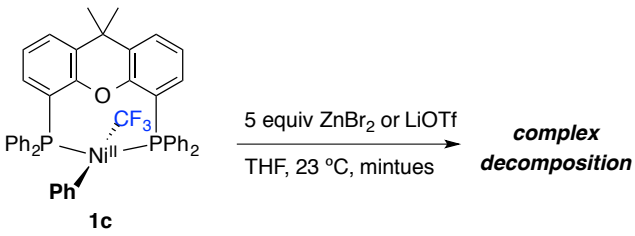

Complex **1c** could be isolated in 48% yield via recrystallization from acetone. ^{1}H, ^{19}F, and ^{31}P NMR spectroscopic characterization shows that the *trans* isomer of **1c** predominates in solution at 25 ºC (>98% *trans*). Notably, the related Ni^{II} $^{i}Pr_2$Xant-Phos complex **1b** is also the *trans* isomer.[9]

Reactivity of (P~P)Ni(CF$_3$)(Ph) Complexes

With **1c** in hand, we next explored the reactivity of this Ni^{II} complex towards aryl–CF_3 coupling. Heating an acetone solution of **1c** at 60 ºC under N_2 for 1 h resulted in complete consumption of the starting material. A mixture of organic products, including benzene and biphenyl, was formed, but no Ph–CF_3 was detected (Scheme 2.8a).[14] Attempts to improve the yield of this reaction through the addition of π-acids or phosphine ligands were unsuccessful. These observations mirror those reported by Grushin for complex **1b**, where complicated decomposition was found to predominate over Ar–CF_3 coupling.

Scheme 2.8 (a) Thermolysis of **1c** in acetone and (b) oxidation of **1c** with Ferrocenium hexafluorophosphate

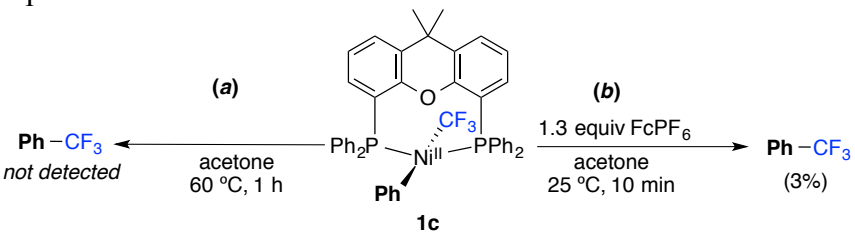

We hypothesized that the oxidation of **1c** might promote the desired Ph–CF_3 coupling reaction. This hypothesis was predicated on our own work studying oxidatively-induced aryl–CF_3 coupling at Pd as well as literature precedent for other oxidatively-induced C–C and C–heteroatom bond-forming reactions at Ni. The treatment of **1c** with 1.3 equiv of ferrocenium hexafluorophosphate ($FcPF_6$; a $1e^-$ oxidant that is commonly used to promote reductive elimination at Ni)[15] resulted in complete consumption of **1c** within 10 min at room temperature and generation of Ph–CF_3 in 3% yield (Scheme 2.8b).

Figure 2.1 (a) X-ray crystal structure of 1d. Thermal ellipsoids drawn at 50% probability and (b) Cyclic voltammogram of complex 1d with 0.1 M NBu4BF4 in MeCN at a scan rate of 50 mV/s.

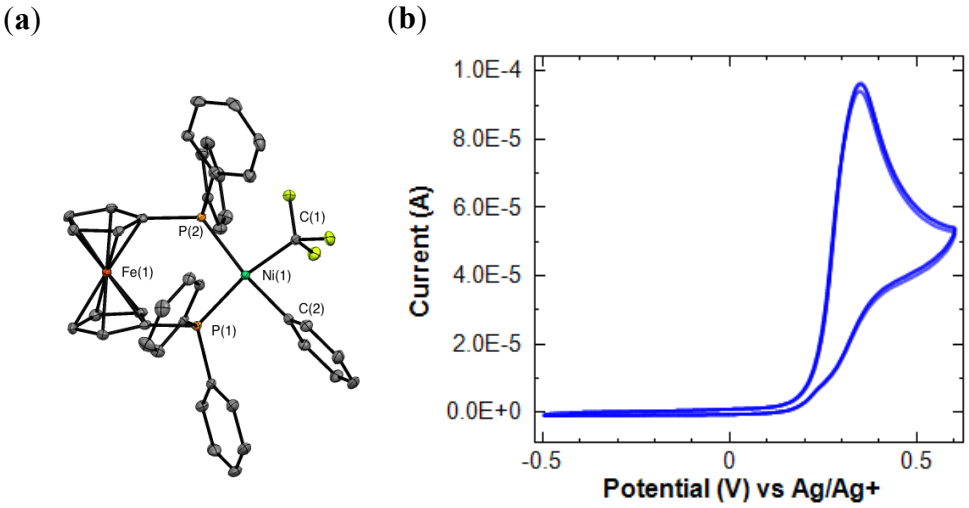

We reasoned that the low yield was likely due to the predominantly *trans* orientation of the Ph and CF_3 ligands in **1c**. Thus, we next targeted $Ni^{II}(Ph)(CF_3)$ complexes bearing dppf, a high bite angle phosphine that is expected to maintain a *cis*-geometry at Ni.[16] The complex (dppf)Ni(Ph)(CF_3) (**1d**) was prepared in 67% yield via the pathway in Scheme 2.5b. Complex **1d** assumes a *cis*-geometry, as determined by NMR spectroscopic analysis[17] as well as X-ray crystallography (Figure 2.1a). The bite angle of dppf in **1d** is 100.2º; as a result, the C_{CF3}(1)-Ni-C_{Ph}(2) angle is relatively acute (83.2º), which is expected to accelerate reductive elimination.

Heating solutions of **1d** at 75 ºC for 12 h under N_2 resulted in complete consumption of the starting material. A mixture of biphenyl, benzoyl fluoride and benzene was formed, but no Ph–CF_3 was detected (Table 2.1, entry 1). In contrast, the treatment of **1d** with 1.3 equiv of $FcPF_6$ in acetone at room temperature under N_2 resulted in rapid consumption of starting material, and formation of Ph–CF_3 in 77% yield (Table 2.1, entry 2). Comparable results were obtained with the stronger oxidant $AcFcBF_4$ (Table 3.1, entry 3), while no reaction was observed with the weaker oxidants Cp_2CoPF_6 (E^0 = –1.33 V vs. Ag/Ag^+) and $Cp^*_2FeBF_4$ (E^0 = –0.59 V vs

Ag/Ag^+) after 1 h at room temperature. These results are consistent with the cyclicvoltammogram of **1d** (Figure 2.1b), which shows an irreversible oxidation wave centered at approximately +0.36 V versus Ag/Ag^+. Notably, exposure of acetone solutions of **1d** to air at room temperature also produced Ph–CF_3, albeit in lower and more variable yield (15%).

Table 2.1 Oxidatively induced Ph-CF_3 coupling from **1d** as a function of oxidant

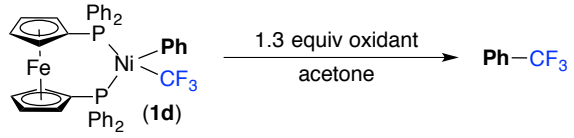

Entry	oxidant	potential vs Ag/Ag^+	yield Ph-CF_3[a]
1	none[b]	n/a	<1%
2	$FcPF_6$[b]	–0.04 V	77%
3	$AcFcBF_4$	0.27 V	71%
4	$Cp^*_2FeBF_4$	–0.59 V	<1%
5	Cp_2CoPF_6[d]	–1.33 V	<1%
6	ambient O_2[b]	n/a	15%

[a]Yields determined by ^{19}F NMR spectroscopy relative to 4,4'-difluorobiphenyl as a standard; [b] 12 h at 75 ºC; [c] 30 min at 25 ºC; [d] 1 h at 25 ºC.

Mechanistic Considerations

There are at least two features of the dppf ligand that could be responsible for the high yielding oxidatively-induced Ph–CF_3 coupling from **1d**: (1) the presence of a redox active ferrocene moiety in the backbone or (2) the high bite angle of the ligand (100.2º). In the former case, oxidation at the Fe (rather than the Ni center) could be responsible for triggering Ph–CF_3 coupling from a nickel center formally in the +2 oxidation state. To test for this possibility, ground state DFT calculations were conducted on $\mathbf{1d}^+$, the cation generated upon oxidizing **1d** by $1e^-$. Complex $\mathbf{1d}^+$ has a square-planar geometry and similar bond-distances and bond angles to **1d**, and DFT shows that the unpaired electron is localized on nickel (Figure 2.2).This

observation suggests that the proximal ferrocene moiety is likely not essential for the desired reactivity.

Figure 2.2 Calculated bond lengths of and spin densities of **1d**$^{+}$. Calculations were performed using the UM06 functional with a SDD basis set on nickel and 6-31G(d) on other atoms.

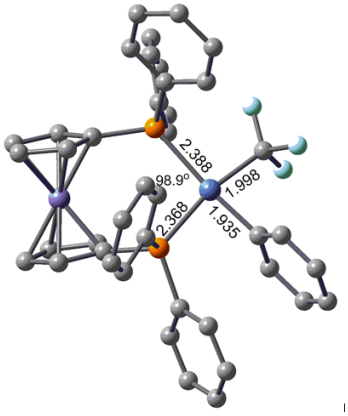

Calculated Spin Density	
Ni =	1.10
C_{ipso}=	-0.05
C_{CF3}=	-0.05

The innocence of the ferrocene backbone raises questions about the origin of the unique reactivity of complex **1b**. Vicic's seminal report on the reactivity of (dippe)Ni(CF_3)(Ar) complexes notes that no Ar-CF_3 coupling is observed in the presence of the related Fe(III) oxidant $Fe^{III}(BiPy)_3$, though no additional conditions were reported. To better understand the origin of this reactivity, we next synthesized a series of (P~P)Ni(Ph)(CF_3) complexes (**1c-f**) bearing electronically similar phosphine ligands with varied bite angles to better understand structure-reactivity relationships. These complexes were treated with 1.3 equiv $FcPF_6$, and in all cases, complete consumption of the Ni^{II} starting material was observed within 30 min at room temperature (Table 2.2). A strong correlation between the bite angle of the phosphine and the yield of Ph–CF_3 was observed, as long as the ligand maintained a primarily cis ground state (Table 2.2). Xantphos-ligated **1c** was not found to afford high yields of coupled product despite its high bite angle, ostensibly due to its *trans* geometry. These results are consistent with phosphine bite angle being an important contributor to the reactivity. Significantly, Ph–CF_3 coupling proceeds rapidly at room temperature in ≥60% yield with several commercially available and relatively inexpensive diphosphines (dppf, diop, and dppb), indicating that these

ligands should be targeted for the development of Ni-catalyzed Ar–CF_3 cross-coupling reactions.

Table 2.2 Oxidatively induced Ph-CF_3 reductive elimination as a function of phosphine ligand

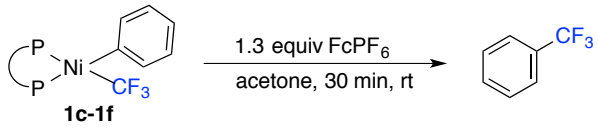

Compound	P~P [a]	E_{pc}	Bite angle	Yield Ph-CF_3 [b,d]
1e	dppbz	0.340	82° [e]	<1 [i] %
1f	dppe	0.333	86.8° [f]	1%
1g	dppp	0.330	87° [e]	2%
1h	dppb	- [j]	98° [e]	70%
1i	diop	0.397	102° [g]	64%
1d	dppf	0.358	100.2° [h]	77%
1c	Xantphos	- [j]	trans	3%

[a]dppbz = 1,2-bis(diphenylphosphino)benzene; dppe = 1,2-bis(diphenylphosphino)ethane; dppp = 1,3-bis(diphenylphosphino)propane; dppb = 1,4-bis(diphenylphosphino)butane; diop = (2,3-*O*-isopropylidene-2,3-dihydroxy-1,4-bis(diphenylphosphino)butane); dppf = 1,1'-bis(diphenylphosphino)ferrocene; xantphos = 4,5-bis(diphenylphosphino)-9,9-dimethylxanthene; [b]Yields determined by ^{19}F NMR spectroscopy relative to 4,4'-difluorobiphenyl as a standard; [c]Bite angle data from reference 18; [d]Bite angle data from the X-ray structure of **1f**; [e]Bite angle data from ref. 19 [f]Bite angle data from the X-ray structure of **1d**; [g]Reaction performed in 2 : 5 benzene : acetone. [j] Compound was not stable under CV conditions.

Though bite angle is well known to play an important role in transition metal mediated C-C coupling reactions, we next sought to investigate the possibility that the observed trend could be better described through bite-angle-dependent effects on the Ni^{II}/Ni^{III} oxidation potential. As seen in table 2.2, compounds **1d-1g** and **1i** exhibit similar electrochemical profiles by CV; a clear relationship between yield and oxidation potentials was not found. Because all

compounds in table 2.2 are fully consumed by Fc+, these results are inconsistent with the observed bite angle trends being mostly dependent on electronic differences between high and low bite angle complexes.

We next directed our attention to better understand the decomposition pathways that outcompete Ar–CF_3 coupling from low bite angle complexes. Analysis of the oxidation products of compounds **1e-g** under standard conditions did not reveal an obvious mode of decomposition. ^{19}F NMR analysis of the reaction mixture indicated that trace quantities of PhCOF are created throughout the course of the reaction (<5%). The formation of benzoyl fluoride implicates the formation of free fluoride ions and trace water in solution. Indeed, fluoride can be observed (^{19}F NMR: bs, -136ppm) when the same reaction is performed in anhydrous DMSO. These observations suggest that fragmentation of the CF_3 ligand outcompetes Ar-CF_3 coupling in low bite angle complexes.

Scheme 2.9 Potential mechanism for the formation PhCOF from **1f**

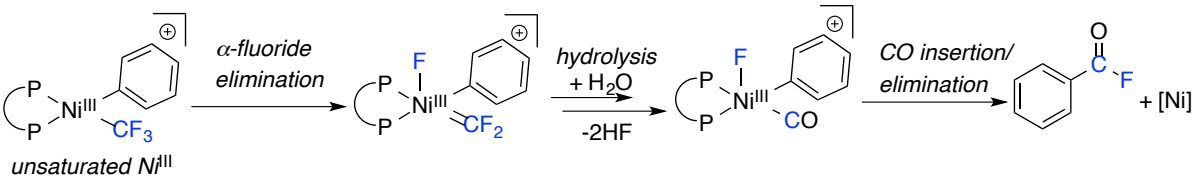

The formation of PhCOF from[$M(CF_3)(Ph)$] complexes in the presence of adventitious water has been previously noted to occur from related palladium complexes.[20] This mode of decomposition is generally proposed to occur through hydrolysis of difluorocarbene formed via α-fluoride elimination. We hypothesized that the observed PhCOF is formed through competitive α-fluoride elimination from the short-lived $[(P\sim P)Ni^{III}(CF_3)(Ph)]^+$ complex immediately following oxidation. Control reactions make carbene formation from Ni^{II} intermediates unlikely as **1d** and **1f** were found to be stable in the presence of water for extended periods. To test for the formation of difluorocarbenes following oxidation, compounds (dppe)Ni(CF_3)(4-F-C_6H_4) (**4d**) and (dppf)Ni(CF_3)(4-F-C_6H_4) (**4f**) were

synthesized so that the fate of aromatic fragments could be conveniently monitored by ^{19}F NMR. Oxidation of **4f** in the presence of 125 equiv of water afforded 4-F-PhCOOH in 68% yield as determined by ^{19}F NMR (Scheme 2.10). Importantly, Ar-CF_3 coupling at the related compound **4d** was nearly unaffected by the addition of water to the reaction. These results imply that the formation of unstable difluorocarbenes directly competes with Ar-CF_3 coupling in the low bite angle complexes.

Scheme 2.10 Effect of added water on the oxidation of **4d** or **4f**

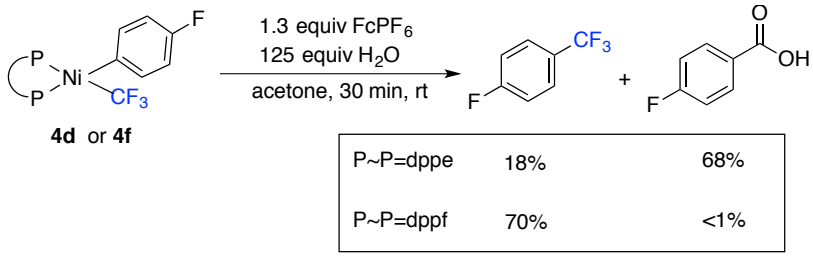

P~P=dppe	18%	68%
P~P=dppf	70%	<1%

Finally, we sought to probe for the intermediacy of free carbon-centered radicals. Vicic and coworkers have demonstrated that Ni^{III} complexes bearing CF_3 ligands can undergo reductive homolysis to generate CF_3 radicals.[21] Though no products associated with reductive homolysis (HCF_3, H–Ar, etc), were noted by ^{19}F NMR, we next probed for the formation of free carbon centered radicals. Under otherwise identical conditions, two equivalents of TEMPO, a common radical trap, were added to the oxidation of **4d**. The anticipated products of intercepted free radicals were not observed (Scheme 2.11). Instead, the coupled product was observed in good, albeit lower yield (55%). We attribute this modestly reduced yield to incomplete conversion of the starting material under these conditions. It is not currently clear why the addition of TEMPO limits full conversion of the nickel complex. Because TEMPO is known to be redox active, it may competitively react with the ferrocenium oxidant. However, the formation of coupled product suggests that this reaction is slower than oxidation of nickel or another active oxidant is also formed in the reaction. As such, we also attempted to trap any

potential radicals using electron rich arenes, which are known to rapidly react with aryl and trifluoromethyl radicals. The addition of 10 equivalents of 1,3,5-trimethoxy benzene was not found to significantly affect the yield (Scheme 2.11). Taken together, these experiments favor a concerted reductive elimination mechanism from transient (P~P)Ni^{III}(CF$_3$)(Ar) complexes.

Scheme 2.11 Attempted interception of carbon-centered radicals in the oxidation of **4d**

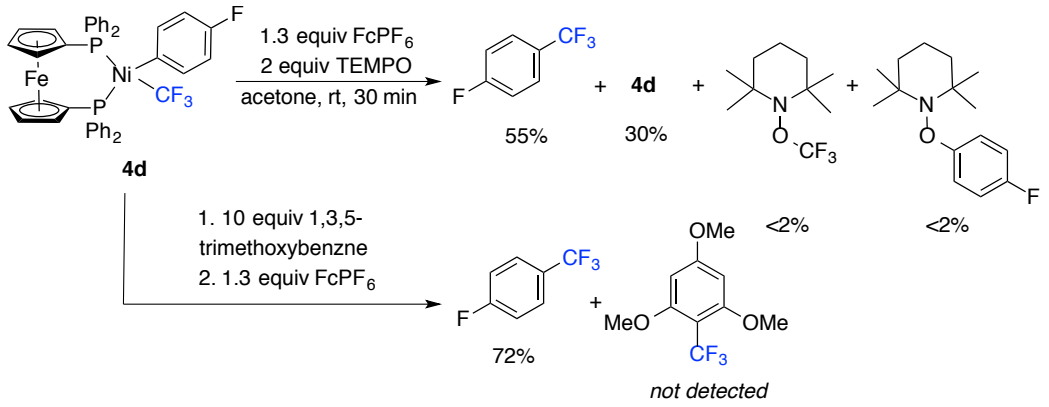

Outlook

The investigations described herein support the feasibility of nickel-catalyzed aryl trifluoromethylation reactions involving C–C coupling at Ni^{III}. The mild nature of the oxidants required in this transformation differentiates this reactivity from related studies of palladium Ar–CF$_3$ coupling, where harsh 2e^- oxidants are needed. In this way, nickel catalyzed aryl trifluoromethylation through a Ni$^{I/III}$ manifold still holds promise as a thermally *and* oxidatively mild method. However, our investigations have also identified unforeseen challenges that will need to be addressed in the development a Ni$^{I/III}$ catalytic cycle. Our synthetic efforts toward the key (P~P)Ni(CF$_3$)(Ar) model complexes demonstrated that these key intermediates exhibit strong sensitivity to Lewis acids. Lewis-acidic ions are commonplace in a variety of nickel-catalyzed cross coupling reactions. Identification of compatible bases (and counterions) or transmetallating agents will likely be necessary in the development of such a method.

2.2.2. Aryl–CF_3 Bond-Forming Reductive Elimination from Isolated Diorganonickel(III): Synthesis, Reactivity, and Mechanism[1,22]

Section 2.2.1 described our studies of oxidatively induced Ar–CF_3 coupling from diphosphine Ni(II) precursors. Though these investigations demonstrated that high-yielding Ar-CF_3 coupling was possible from nickel, the exact nature of the transformation was still unclear. We next sought to stabilize the proposed Ni^{III} intermediate so that we could directly study Ar–CF_3 bond formation, and more generally, features of C–C coupling from diorganonickel(III). Notably, at the outset of these investigations, C–C coupling from an isolated Ni^{III} complex had not been observed. This gap is particularly noteworthy as it has been commonly proposed to be the product-forming step in a variety of nickel-catalyzed cross-coupling mechanisms for over 40 years.

Synthesis of a Stable [$Ni^{III}(CF_3)(Ar)$] complex

Our studies of diphosphine compounds indicate that low temperature isolation of a $[(P\sim P)Ni^{III}(CF_3)Ar)]^+$ would be highly challenging or impossible; reactions using strong oxidants such as $AcFcBF_4$ were complete in less than one minute at room temperature. We instead targeted the synthesis of a $Ni^{II}(CF_3)(Ar)$ complex ligated by trispyrazolylborate (Tp) $[TpNi^{III}(CF_3)(Ph)]^-$ (**5**), which would then be oxidized to the targed Ni^{III} complex ($TpNi^{III}(CF_3)(Ph)$, (**6**) . Our group and others have previously reported that Tp-ligated Pd^{IV} and Ni^{IV} complexes exhibit excellent stability relative to related high oxidation state complexes supported by bidentate or even other tridentate nitrogen donor ligands (Scheme 2.12). Furthermore, the quadrupolar boron atom incorporated within the ligand framework is a convenient paramagnetic NMR handle for monitoring of paramagnetic nickel species.

[1] Work in this section was done in collaboration with Nicole Camasso. She developed the reaction conditions required to exchange the dtbpy ligand with NMe_4Tp. Without this advance, many of the studies in this section would not be possible. I primarily focused on the syntheses of (dtbpy)Ni(CF_3)(Ph) and **6** as well as all of the reactivity studies.

Scheme 2.12 Ligand Effects on the Elimination of 2,2-dimethylbenzocyclobutane from Ni^{IV} Complexes

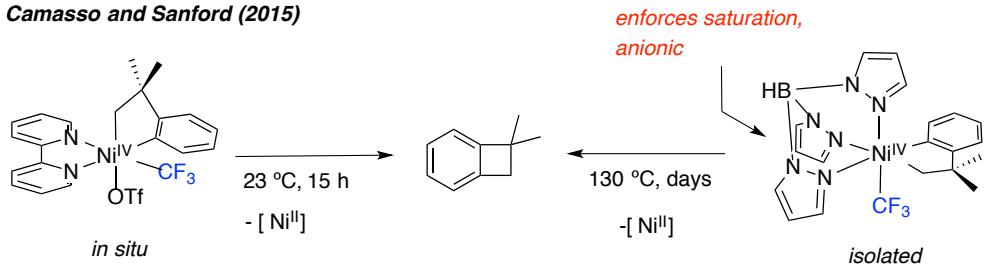

The synthesis of **5** was first attempted through direct analogy to our synthesis of (P~P)Ni(CF_3)(Ph) (**1c-1f**) complexes. Upon mixing (PPh_3)$_2$Ni(CF_3)OTFA with NMe_4TP a light pink powder immediately precipitated (Scheme 2.13). Analysis of the crude reaction mixture by ^{11}B and ^{19}F NMR revealed the formation of NMe_4OTFA, (MeCN)$_2$$Ni^{II}$($CF_3$)$_2$, $Ni^{II}Tp_2$ and free PPh_3. This reaction outcome can be rationalized through sequential Tp/PPh_3 ligand exchange and Tp/CF_3 ligand exchange between nickel centers. The irreversible and unavoidable formation of $Ni^{II}Tp_2$ has been noted during attempted ligation of other Ni^{II} salts.[23] Presumably, the negatively charged Tp ligand labilizes weakly bound X-type ligands such as OTFA or Cl.

Scheme 2.13 Attempted synthesis of NMe_4[TpNi(CF_3)OTFA]

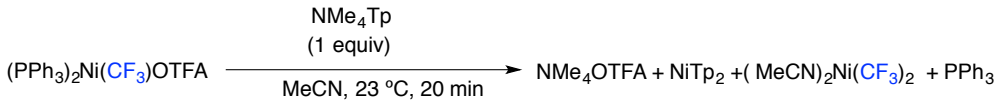

We hypothesized that the unwanted ligand exchanges may be due to the liberation of a coordination site through loss of NMe_4OTFA. To avoid this unwanted side reaction, we next targeted the installation of the phenyl ligand before Tp ligand exchange. Attempts to isolate (PPh_3)$_2$Ni(CF_3)(Ph) through transmetallation with $ZnPh_2$ were unsuccessful (Scheme 2.14a) Filtration through celite and removal of the volatiles only returned PPh_3, potentially suggesting that the lability of PPh_3 was resulting in decomposition of the desired product. On the basis of this observation we pursued an alternate route where the PPh_3 ligands were first exchanged with a more stabilizing ditertbutyl bipyridine (dtbpy) (Scheme 2.14b). Subsequent addition of

diphenyl zinc and filtration through basic alumina yielded (dtbpy)Ni(CF_3)(Ph) in 61% yield. Gratifyingly, the dtbpy proved to be an excellent compromise between stability and lability. This dtbpy complex underwent ligand exchange when treated with 1 equivalent of NMe_4Tp to yield **5** in 76% yield.

Scheme 2.14 Alternate Synthetic Routes to **5**

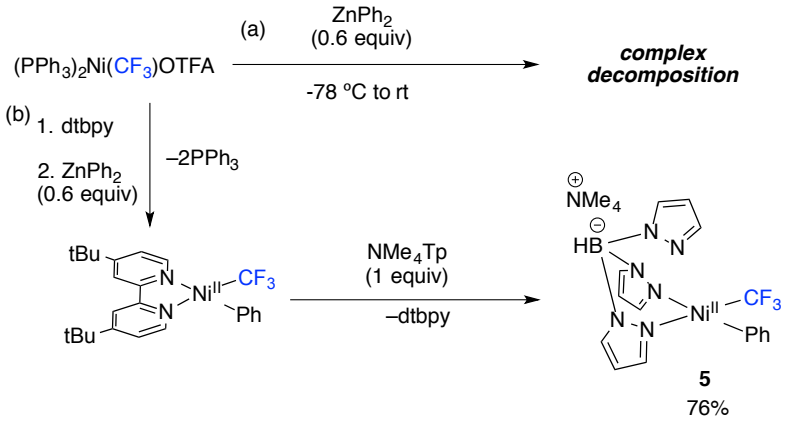

The stability and accessibility of the +3 oxidation state was next evaluated by cyclic voltammetry. In contrast to the diphosphine complexes in section 2.2.1, the CV of **5** exhibits a chemically reversible but widely separated oxidation wave centered at about -700 mV vs Fc/Fc+ (Figure 2.3). Perhaps more importantly, the reversibility of this redox couple was found to be largely invariant with changes in scan rate (25 mv/s to 200 mv/s), suggesting that the +3 oxidation state may indeed be quite stable. We attribute the large peak separation to an EC mechanism wherein oxidation or reduction results in the association or dissociation of a pyrazole.

Figure 2.3 Cyclic Voltammogram of complex **5**. Conditions: [Ni] = 0.01 M in CH_3CN; $[NBu_4BF_4]$ = 0.1 M; Scan Rate = 100 mV/s

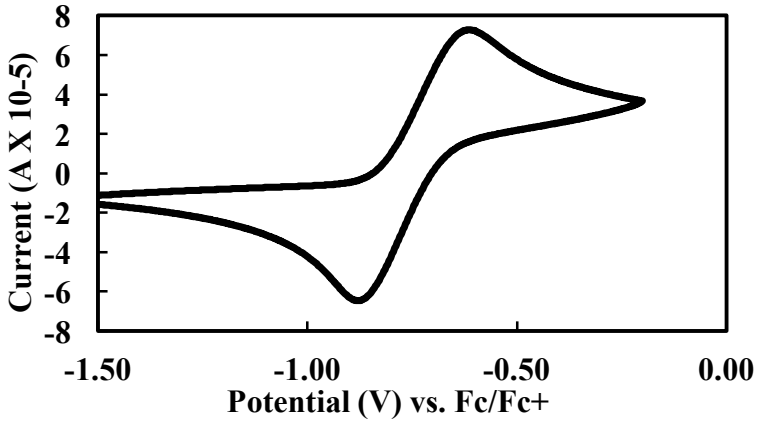

We next examined the chemical oxidation of **5** with $AgBF_4$ to generate the corresponding Ni^{III} product. This oxidant was selected because it is expected to be sufficiently oxidizing (0.04V vs Fc/Fc+) and it generates Ag^0 as an insoluble and thus easily removed by-product. Treatment of **5** with 1.05 equiv $AgBF_4$ at -35ºC resulted in an immediate color change and concomitant precipitation of Ag^0.[20] Analysis of the ^{11}B NMR revealed complete conversion to a new NiTp bound product (Scheme 2.15). Filtration and recrystallization at -35 ºC yielded elementally pure **6** in 87% yield.

Scheme 2.15 Oxidation of **5** with $AgBF_4$ to yield **6**

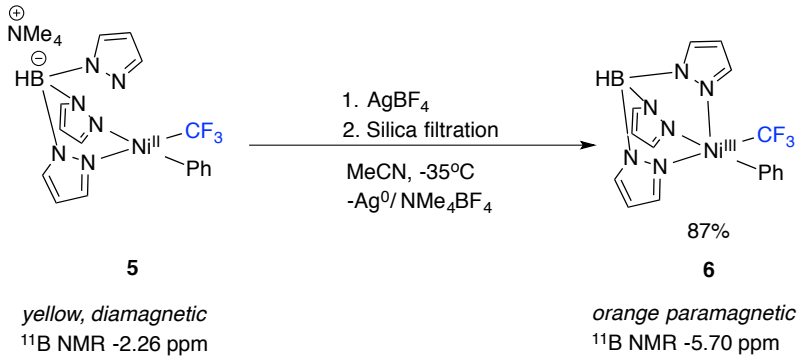

Characterization of $TpNi^{III}(CF_3)(Ph)$

Characterization of **6** by EPR spectroscopy and effective magnetic moment (u_{eff} = 1.81) measurements is consistent with a low spin (S = ½) Ni^{III} electronic structure (Figure 2.4a). As seen in figure 2.4b, single crystal X-ray diffraction reveals that **6** displays a distorted square

base pyramid structure ($\tau \approx 0.15$) in the solid state. Interestingly, the EPR spectrum of **6** in 3:1 PrCN/MeCN glass at 100 K suggests that it adopts an octahedral geometry through coordination of a nitrile ligand to the axial position of the Ni^{III} center. Strong hyperfine coupling to two nitrogen atoms was consistently observed under these conditions. Attempts to obtain an X-ray quality crystal of the MeCN adduct of **2e** were unsuccessful.

Figure 2.4 (a) EPR spectrum of **6** at 100K in 3:1 PrCN:MeCN. Top(Red)=Simulated, Bottom(blue) =Experimental. EPR fit using following parameters g_x= 2.22, g_y= 2.19, g_z= 2.01 A_N(2N)=18G. (b) X-Ray Crystal Structure of **6**. Thermal Ellipsoids drawn at 50% Probability

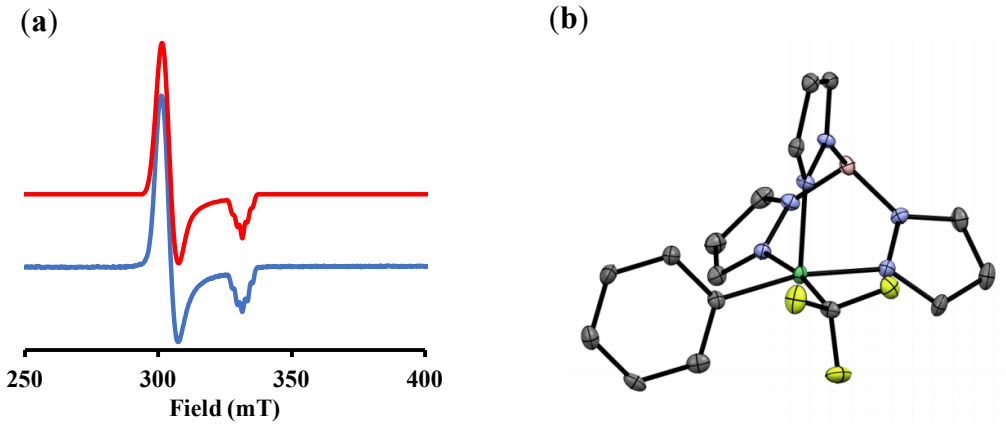

Ar–CF_3 Coupling from 6

With a stable [$Ni^{III}(CF_3)(Ph)$] complex in hand, reactivity of **6** to Ar–CF_3 reductive elimination was studied next. Heating a solution of **6** in MeCN for 3 h at 40 ºC led to complete consumption of starting material and concomitant formation of the C(sp^2)–CF_3 coupling product, Ph–CF_3 in 47% yield (Scheme 2.16). Raising the temperature of the reaction to 80 ºC and lowering the reaction time to 5 min resulted in an increase to 59% yield (Scheme 2.16). This reactivity was found to be unique to the +3 oxidation state; less than 5% of Ph–CF_3 was formed when the Ni^{II} precursor **5** was heated for 12 h at 75 ºC.

Scheme 2.16 Thermolysis of **6** in CH_3CN

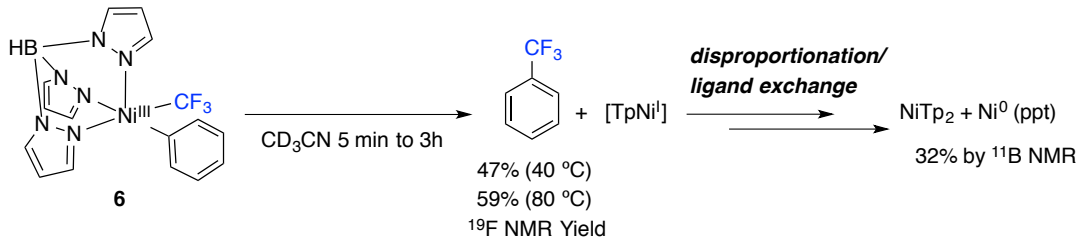

The nickel-containing products of this transformation were also investigated. No Ni^I species were detected by EPR spectroscopy in any of these conditions. Instead, analysis of the crude reaction mixtures by ^1H and ^{11}B NMR spectroscopy revealed the presence of $Ni^{II}Tp_2$ in 32% yield based on nickel (theoretical maximum = 50% yield) (Scheme 2.16). This product is likely formed via disproportionation and ligand exchange between two $TpNi^I$ reductive elimination products to yield Ni^0 and $Ni^{II}Tp_2$. A black precipitate consistent with nickel black was noted in the reaction mixtures. Analogous disproportionation reactions of $[Ni^I]$ species to form 0.5 equiv of $[Ni^{II}]$ and 0.5 equiv of $[Ni^0]$ have been reported under similar conditions.[24] More detailed discussion of the fate of the reduced nickel fragments is provided below.

Mechanistic Details

We next sought to gain insights into the mechanism of Ph-CF_3 coupling from complex **6**. As summarized in Scheme 2.17, there are at least three possible pathways for this transformation. The first (pathway a) involves initial homolysis of the Ni^{III}–CF_3 bond followed by reaction of the resulting F_3C• with a second equivalent of **6** to yield Ni^{IV} complex **7**.[25] Ph–CF_3 reductive elimination from **7** would then release the product. The second (pathway b) involves direct Ph-CF_3 bond formation from the Ni^{III} center. Finally, the third (pathway c) involves the *in situ* formation of a cationic Ni^{IV} intermediate **8** via redox disproportionation between two Ni^{III} centers. Importantly, the maximum possible yield of Ph-CF_3 in pathway b is 100%, while for pathways a and c it is 50%. As such, the observed yield of 59% provides initial

evidence in support of pathway b. Nonetheless, we sought to gain additional data regarding the feasibility of each of the alternate pathways.

Scheme 2.17 Potential Mechanisms for the Formation of Ph–CF_3 from **6**

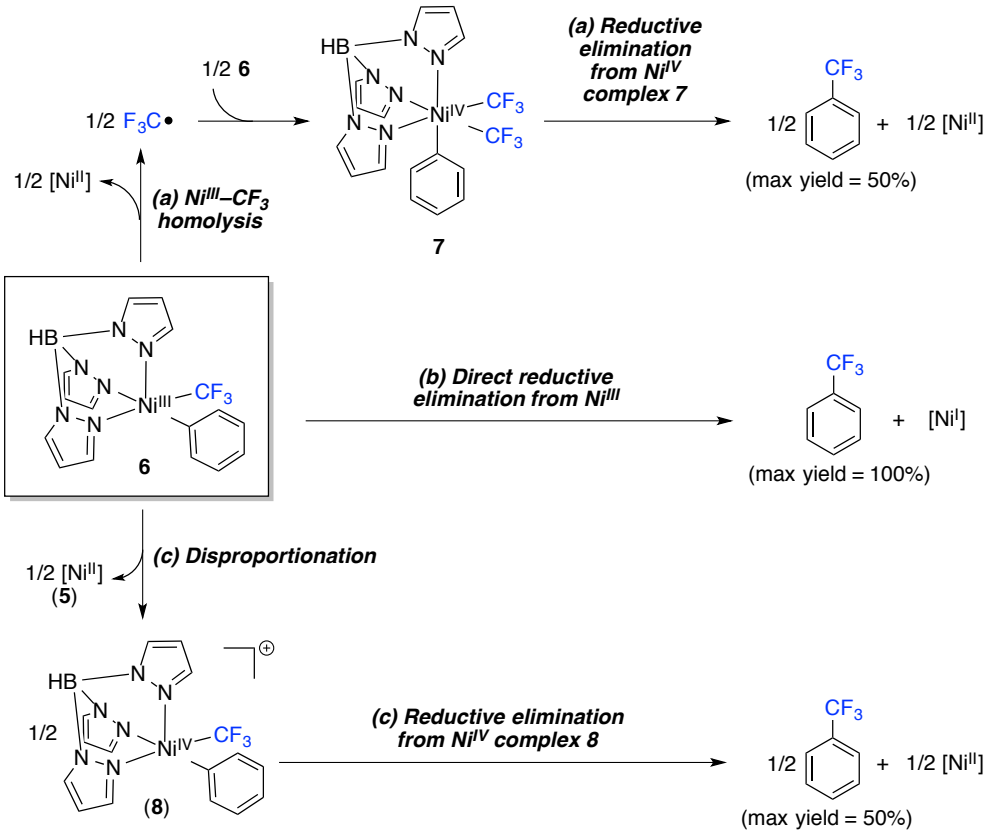

We first interrogated pathway a in more detail. Notably, the key intermediate in this pathway, Ni^{IV} complex **7**, has been fully characterized, and its reactivity is known (Chapter 3). Furthermore, our previous studies showed that Ph–CF_3 bond-forming reductive elimination from **7** requires heating at 55 ºC for 14 h (compared to 40 ºC for 3 h from **6**). Thus, if pathway a were operating, we would expect to observe a build-up of intermediate **7** under the milder reaction conditions. However, **7** was not detected when the thermolysis of **6** by was monitored by ^{19}F NMR spectroscopy, providing further evidence against this pathway.

Two additional experiments were conducted to probe for the intermediacy of F_3C• in this transformation. First, **6** was heated in CD_3CN at 40 ºC for 3 h in the presence of 2 equiv of the organic radical trap TEMPO. As shown in Scheme 2.18a, the presence of TEMPO did

not reduce the yield of Ph-CF_3 under these conditions (47% yield without TEMPO versus 57% yield with TEMPO). Furthermore, neither TEMPO-CF_3 nor H/DCF_3, products expected to form in the presence of free CF_3 radicals, were detected. Second, the thermolysis of **6** was conducted in neat C_6D_6, which is known to react with F_3C• to form $C_6D_5CF_3$.[26] However, the only detectable organic product was $C_6H_5CF_3$ (formed in 54% yield, Scheme 2.18b) This experiment demonstrates that the Ph in the organic product is derived from the ligand rather than the solvent. Collectively, these results are inconsistent with mechanism (a) or any other mechanism involving F_3C• intermediates.

Scheme 2.18 Radical Trapping Experiments in the Thermolysis of **6**

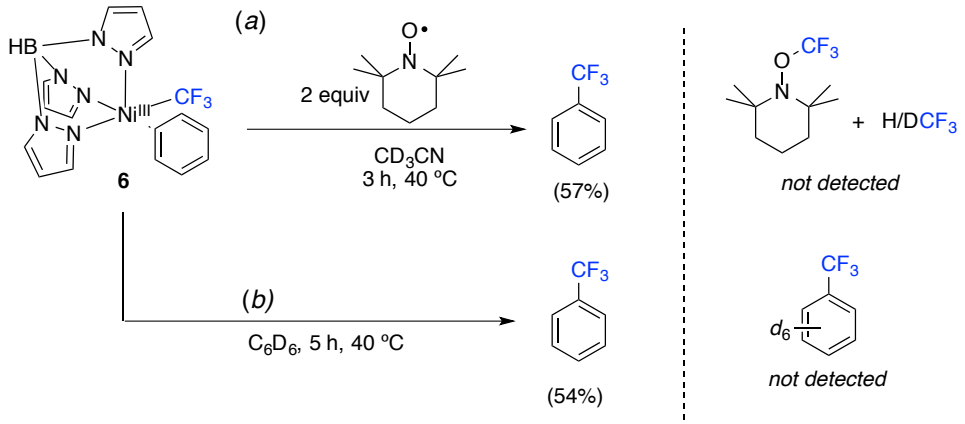

We next investigated the feasibility of Ph-CF_3 coupling via pathway c. A first set of experiments probed the accessibility and reactivity of the cationic Ni^{IV} complex **8**, which would be the key intermediate in this disproportionation mechanism. The CV of **5** at higher potentials reveals a second oxidation with an onset potential of approximately +0.35 V vs Fc/Fc^+ (Figure 2.5). We attribute this to a $Ni^{III/IV}$ couple, which interconverts **6** and proposed cationic Ni^{IV} intermediate **8**.[27] The observed quasi-reversibility of this couple suggests that **8** should be detectable using chemical oxidants with potentials of ≥0.35 V vs. Fc/Fc^+.

Figure 2.5 Cylic Voltammogram of **5**. Conditions: [Ni] = 0.01 M in CH_3CN; [NBu_4BF_4] = 0.1 M; Scan Rate = 100 mV/s

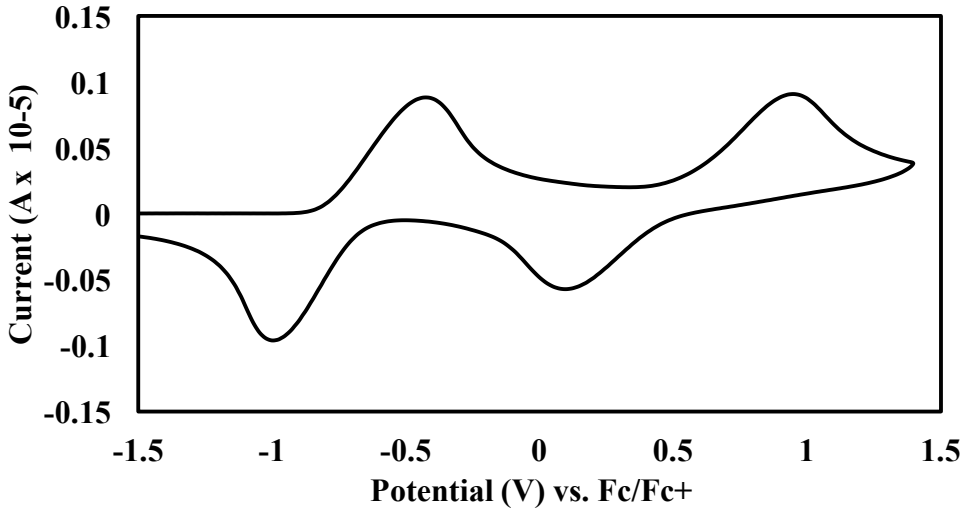

To test this possibility, we treated **6** with 1 equiv. of the 1e^- oxidant $NOBF_4$ (E^o = +0.84 V vs. Fc/Fc^+).[28] ^{19}F NMR spectroscopic analysis of the reaction mixture at –30 ºC showed immediate formation of a new singlet at –31 ppm, consistent with the formation of a diamagnetic Ni^{IV}–CF_3 intermediate (Scheme 2.19). When the temperature was increased to 25 ºC over 3 min, this intermediate decayed with concomitant appearance of Ph-CF_3 (50% yield). While attempts to isolate the unknown compound were unsuccessful, these data are consistent with the formation of Ni^{IV} complex **8**, which undergoes subsequent Ph–CF_3 reductive elimination.

Scheme 2.19 Oxidation and Subsequent Ph–CF_3 Elimination Reaction of **6**

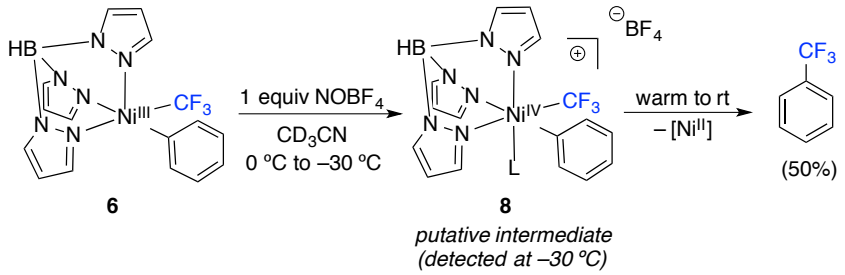

The proposed Ni^{IV} intermediate **8** appears to be accessible from **6** in the presence of a strong oxidant; however, it remains unclear whether **8** is relevant to Ph-CF_3 coupling in the absence of an external oxidant. The only oxidant available during the thermolysis of **6** is a

second equivalent of **6** (Scheme 2.17c); therefore, the maximum yield of Ph-CF_3 via this pathway would be 50%. As noted above, the yield of Ph-CF_3 is >50% (Scheme 2.16), indicating that pathway c could not be the exclusive mechanism operating in this system. In addition, redox disproportionation would involve the formation of 0.5 equiv of the starting Ni^{II} complex **5**, which is expected to be stable and observable by NMR spectroscopy under the reaction conditions. However, **5** was not detected by ^{1}H or ^{19}F NMR spectroscopy during the thermolysis of **6** in CD_3CN at 40 ºC, again providing evidence against pathway c as the primary mechanism.

Finally, pathway c is expected to exhibit a second order dependence on [Ni], while pathways a and b should be first order in [Ni]. The initial rates of Ph-CF_3 coupling from **6** were determined in C_6D_6 by monitoring the formation of Ph–CF_3 via ^{19}F NMR spectroscopy at different concentrations of [Ni].[29] The method of initial rates was then used to determine the order in nickel to be 0.8 (R^2 = 0.994; Figure 2.6). This result provides further evidence against a redox disproportionation mechanism (or any other pathway that is bimolecular in Ni^{III} before the rate determining step).[30] Collectively, the available mechanistic data are inconsistent with pathways a and c and support direct reductive elimination from Ni^{III} complex **6** as the most likely mechanism for Ph–CF_3 coupling.

Figure 2.6 A plot of Initial Rates of Ph–CF_3 Formation versus [Ni] for Ph–CF_3 coupling from **6** at 30 ºC in C_6D_6

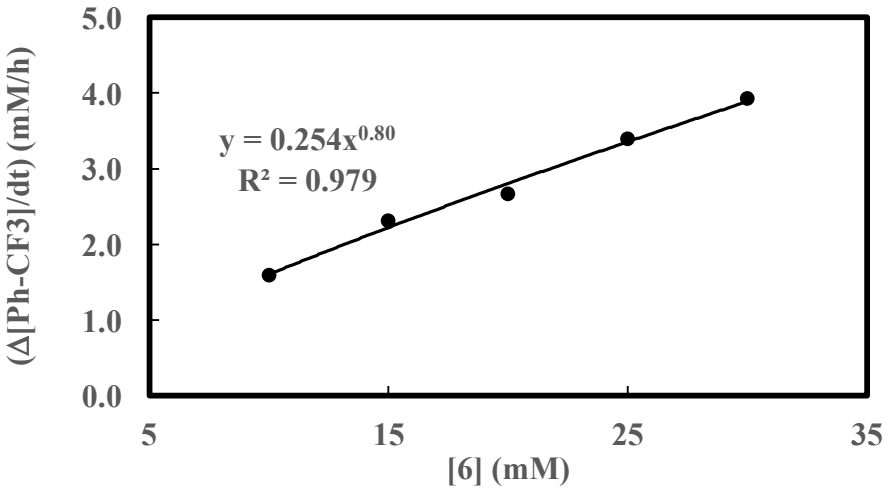

A final important consideration is the moderate yield of Ph-CF_3 and the mass balance in these C–C coupling reactions. Depending on the reaction conditions, the thermolysis of **6** affords Ph-CF_3 in yields ranging from 47-59% along with small quantities of biphenyl (≤4%). Analysis of the crude reaction mixture did not reveal evidence for competitive α-fluoride elimination (likely due to enforced saturation at nickel), as was the case for our diphosphine studies. Instead, we hypothesize that the moderate yields/low mass balance result from side reactions promoted by the coordinatively unsaturated low-valent Ni products formed after reductive elimination. There is ample literature precedent for similar issues in stoichiometric reductive elimination reactions from Ni and Pd centers.[31] These are most commonly resolved by the addition of exogenous ligands, which can quench the reactive low valent metal product(s) by saturating open coordination sites. However, in the current system, the addition of exogenous phosphine or pyridine ligands did not improve the yield or mass balance; in fact, these additives generally resulted in diminished yields of Ph-CF_3 . We attribute this result to the coordination of these ligands to the Ni(III) starting material(Figure 2.7). There is some literature evidence suggesting that octahedral Ni^{III} complexes can have quite different reactivity from their pentacoordinate analogues. In this scenario coordination of added ligand could form an octahedral complex from which non-productive decomposition may occur. Indeed, recrystallization of **6** in the presence of PMe_3 yielded the octahedral PMe_3 adduct of **6** (**6-PMe_3**), which was not found to yield Ph–CF_3 upon thermolysis.

Figure 2.7 (a) Effect of added ligands on the coupling of Ph–CF_3 from **6** and (b) the X-ray crystal structure of **6-PMe$_3$.** Thermal ellipsoids are drawn at 50% probability and hydrogen atoms have been omitted for clarity.

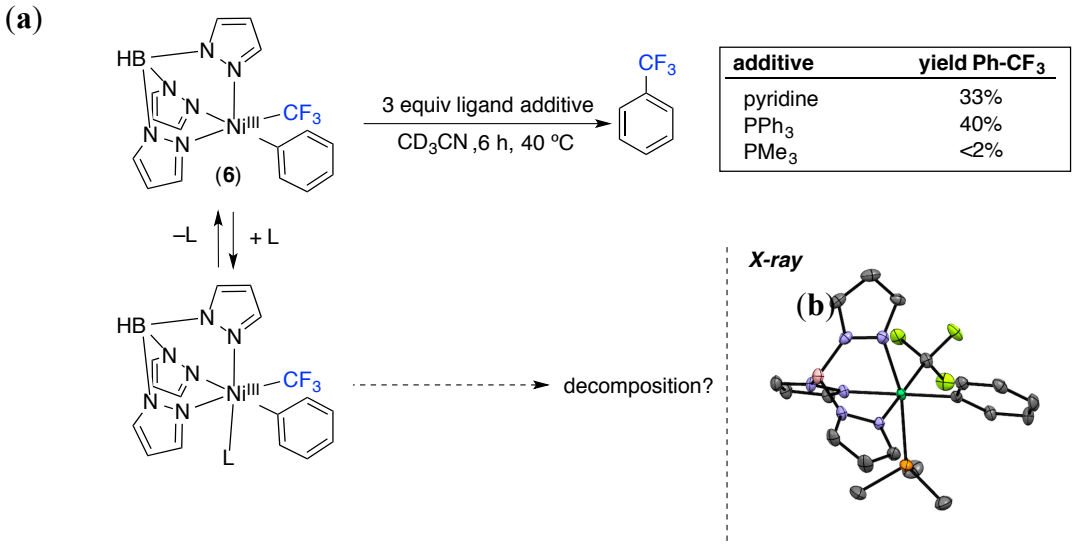

additive	yield Ph-CF_3
pyridine	33%
PPh_3	40%
PMe_3	<2%

An alternative approach to quench reactive Ni^I products would involve the addition of a weak oxidant such as decamethylferrocenium tetrafluoroborate ($Cp^*_2FeBF_4$). The potential of this oxidant (E^o = –0.59 V vs. Fc/Fc^+) is approximately 0.9 V lower than the onset potential for the oxidation of **5** to **6** as determined by CV. However, $Cp^*_2FeBF_4$ is expected to be capable of oxidizing Ni^I by-products to Ni^{II} species, and could thereby decrease undesired side reactions. Indeed, the addition of 1 equiv of $Cp^*_2FeBF_4$ to the thermolysis of **6** in MeCN (3 h at 40 ºC) resulted in an increase from 47% to 68% yield of Ph–CF_3 (Scheme 2.20). The use of 5 equiv of $Cp^*_2FeBF_4$ under otherwise analogous conditions further enhanced the yield of Ph–CF_3 to 82%.

Scheme 2.20 Effect of added $Cp^*_2FeBF_4$ on the Ph–CF_3 coupling yield from **6**

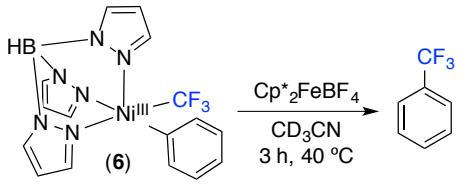

equiv $Cp^*_2FeBF_4$	yield Ph-CF_3
0	47%
1	68%
5	82%

Conclusions

In conclusion, this chapter describes a two-part study on Ar–CF_3 coupling from organonickel(III) compounds. In section 2.2.1 we established for the first time that high-yielding Ar–CF_3 coupling can occur from [Ni(CF_3)(Ph)] complexes. These studies were enabled through a previously unreported strategy for the synthesis of the (P~P)Ni(CF3)(Ph) precursor. In the course of this investigation, heterolytic fragmentation of the CF_3 ligand proved to be problematic before oxidation in the presence of Lewis acids, and after oxidation with low bite angle ligands. This observation represents a previously unrecognized or underappreciated challenge in the discovery of a nickel-catalyzed aryl trifluoromethylation methodology. Previous studies have largely focused on the high kinetic barrier of Ar–CF_3 coupling from Ni(II) as the primary difficulty in such a transformation. While true, our studies suggest that the high coupling barrier is only problematic insofar as apparent and ultimately irreversible -fluoride elimination reactions are facile. Indeed, combined experimental and DFT studies by Grushin predict moderate to low Ar–CF_3 reductive elimination barriers from Ni(II). However, in their report, high-yielding coupling was not observed, instead decomposition of the precursor was found to predominate. Future efforts in this area may need to focus on the mitigation of unproductive decomposition reactions rather than the coupling step itself.

The second part of our studies focused on the isolation of an organonickel(III) complex for detailed studies on Ar–CF_3 coupling from Ni^{III}. This compound was found to undergo Ar–CF_3

coupling under some of the most thermally and oxidatively mild conditions ever reported. The stability of **6** ultimately allowed us to study nuanced aspects of the coupling mechanism that would normally be too fast for thorough characterization. Three different mechanistic pathways were considered for C–C coupling: (a) C–C bond formation via free radical intermediates; (b) direct C–C coupling from Ni^{III}; and (c) redox disproportionation to generate transient Ni^{IV} species and subsequent C–C bond-forming reductive elimination from these intermediates. A series of experiments, including the synthesis/reactivity studies of possible Ni^{IV} intermediates, rate studies, and radical traps were designed to distinguish between these possibilities for the Ph–CF_3 coupling reaction. Collectively, the data suggest that Ph–CF_3 bond-formation occurs via direct C–C coupling from Ni^{III}. Furthermore, these studies show that the yield/mass balance of this reaction can be enhanced through the addition of a weak oxidant, which is believed to quench Ni^{I} by-products and thereby minimize undesired side reactions.

Overall, our combined studies suggest that a nickel-catalyzed aryl trifluoromethylation methodology through a $Ni^{I/III}$ manifold may indeed be feasible. The remarkably mild oxidants and temperatures required to enable this transformation may be an ideal compromise between the oxidative and thermal coupling regimes previously established for Pd. However, our investigations also suggest that careful choice of ligand may be necessary to realize this transformation. Ongoing studies in our lab seek to implement these discoveries into a general and mild nickel-catalyzed trifluoromethylation methodology.

2.3. Experimental Procedures and Characterization of Compounds

2.3.1 General Procedures and Materials and Methods

General Procedures

All manipulations were performed inside an N_2 filled glovebox unless otherwise noted. NMR spectra were obtained on a Varian VNMR 700 (699.76 MHz for ^{1}H; 175.95 MHz for ^{13}C) or a Varian VNMR 500 (500.09 MHz for ^{1}H; 470.56 MHz for ^{19}F; 125.75 MHz for ^{13}C; 225 or 128

MHz for ^{11}B) spectrometer. ^{1}H and ^{13}C NMR chemical shifts are reported in parts per million (ppm) relative to TMS, with the residual solvent peak used as an internal reference. ^{19}F NMR chemical shifts are reported in ppm relative to CCl_3F. ^{11}B NMR spectra are referenced to BF3/Et_2O. Abbreviations used in the NMR data are as follows: s, singlet; d, doublet; t, triplet; q, quartet; m, multiplet; bq, broad quartet; br, broad signal; quint, quintet. Due to significant peak overlap of the diphosphine complexes and extensive ^{13}C-^{31}P and ^{13}C-^{19}F coupling, ^{13}C shifts are not reported as a list. Yields of reactions that generate fluorinated products were determined by ^{19}F NMR analysis using a relaxation delay of 12 s. Quantitative 11B NMR were recorded according to the literature1 at a 90º pulse angle with a 125 s relaxation delay (longest T_1 = 23 s) and a 10 s acquisition period and were checked against a calibration curve. Magnetic susceptibilities were determined by the Evans method in CH_3CN at 23 ºC on a 700 MHz spectrometer.2 Mass spectral data were obtained on a Micromass Magnetic Sector Mass Spectrometer in electrospray ionization mode. Elemental analyses were conducted by Midwest Microlabs. Cyclic voltammetry was performed using a CHI600C potentiostat from CH Instruments. EPR spectra were collected at –176 ºC using a Bruker EMX ESR Spectrometer with a nitrogen-cooled cryostat. X-ray crystallographic data were collected on a Rigaku AFC10K Saturn 944+ CCD-based X-ray diffractometer. Flash chromatography was performed using a Biotage Isolera One system with cartridges containing high performance silica gel.

Materials and Methods

The following compounds were prepared via literature procedures: (PPh_3)2Ni(CF_3)(OTFA), 3 (dtbpy)Ni(CF_3)(Ph), $AcFcBF_4$[32], $Cp^*_2FeBF_4$. Ni(COD)2, biphenylene, $NOBF_4$, $AgBF_4$, and Ph_2Zn were purchased from Strem Chemicals. 4,4'-di-tert-butylbipyridine (dtbpy), Cp_2FePF_6, PPh_3, dppe, dppbz, (–)-diop, and dppp and were purchased from Aldrich. 4,4'-difluorobiphenyl was purchased from Oakwood Chemicals. Xantphos, dppf, and dppb were purchased from ArkPharm. KTp was purchased from Alfa Aesar. Dichloromethane (Fisher), pentane (Fisher), diethyl ether (EMD), toluene (Fisher), and tetrahydrofuran (Fisher) were deaerated via a N2 sparge and were purified by a solvent purification system. Acetonitrile (Acros) and benzonitrile (Acros), diisopropyl ether (Acros) were sparged and used without further purification. CD_2Cl_2, $C6D_6$, CD_3CN, and acetone-d^6 were obtained from Cambridge Isotopes Laboratories and were stored over activated 4 Å molecular sieves (EMD Millipore). Basic alumina (Aldrich) was dried for 48 h under vacuum at 210 °C. Celite was dried for 12 h under vacuum at 100 °C. Unless otherwise noted, all glassware was dried overnight in an oven at 150 °C and cooled under an inert atmosphere before use. All commercial reagents were used without further

purification/drying unless explicitly stated in the experimental section. Unless otherwise noted, all manipulations were performed under an inert atmosphere in a N_2 glovebox.

2.3.2 Synthesis and Characterization of Compounds

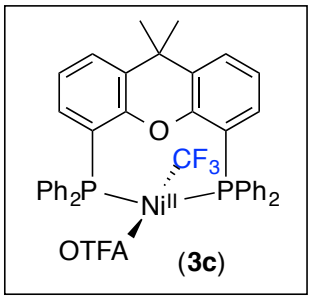

(**3c**)

Synthesis of (Xantphos)Ni(CF_3)(OTFA): Under ambient conditions, a 50 mL round bottom flask was charged with $(PPh_3)_2Ni(CF_3)(OTFA)$ (750 mg, 0.98 mmol, 1.0equiv), Xantphos (581 mg, 1.01 mmol, 1.0 equiv), and dry dichloromethane (35 mL). The resulting dark purple solution was stirred at 25°C for 5 min. The volatiles were removed under reduced pressure, and the residue was dissolved in diethyl ether (10 mL). The product gradually crystallized from solution over 10 min in the form of dark purple crystals. The product was collectedon a fritted filter by vacuum filtration, washed with diethyl ether (3 x 5 mL) and pentane (10 mL), and dried under reduced pressure to afford (Xantphos)Ni(CF_3)(OTFA) (**3c**)as a purple crystalline solid (631 mg, 77% yield). NMR spectra were recorded at –5 °C in order to resolve the fluxional phenyl signals. ^{1}H NMR (700 MHz, CD_2Cl_2at –5 °C): δ 7.82 (d, J_{HH} = 7.4 Hz, 8H), 7.64 (dt, J_{HH} = 7.0, 1.8 Hz, 2H), 7.52 (t, J_{HH} = 7.4 Hz, 4H), 7.43 (t, J_{HH} = 7.6 Hz, 8H), 7.27-7.12 (multiple peaks, 4H), 1.76 (multiple peaks, 6H).^{19}F NMR (471 MHz, CD_2Cl_2 at –5 °C): δ–7.18 (br s, 3F), –75.95 (brs, 3F). ^{31}P NMR (283 MHz, CD_2Cl_2at –5 ºC): δ 10.78(br s).HRMS-electrospray (m/z): $[M – OTFA]^+$calcd for $C_{40}H_{32}OP_2F_3Ni$, 705.1234; found, 705.1216.

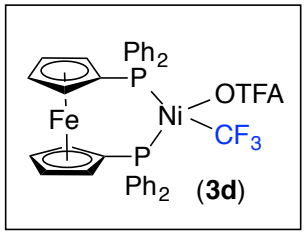

(**3d**)

Synthesis of (dppe)Ni(CF_3)(OTFA) 3d: Under ambient conditions, a 50 mL round bottom flask was charged with $(PPh_3)_2Ni(CF_3)(OTFA)$ (761 mg, 0.99mmol, 1.0equiv), dppf (552 mg, 0.99mmol, 1.0equiv), and dry dichloromethane (35 mL). The resulting solution was stirred at 25°C for 5 min. The volatiles were then removed under reduced pressure, and the residue was dissolved in diethyl ether (10 mL). The product immediately crystallized from solution in the form of a microcrystalline red solid. The product was collected by vacuum filtration, washed with diethyl ether (3 x 5 mL) and pentane(10 mL), and dried under reduced pressure to afford (dppf)Ni(CF_3)(OTFA) (**3d**)as an orange powder (730 mg, 92% yield). The NMR spectra were recorded at –5 °C to resolve the fluxional phenyl resonances.^{1}H NMR (500 MHz, $CDCl_3$at –5 °C): δ 7.92 (brs, 8H), 7.68-6.75

(multiple peaks, 12H), 4.29 (brs, 8H). ^{19}F NMR (471 MHz, $CDCl_3$, –5 ºC): δ –29.87 (s, 3F), –75.38 (s, 3F). ^{31}P NMR (202 MHz, $CDCl_3$, –5 °C):δ28.87 (brs, 1P), 21.32 (brs,1P).HRMS-electrospray (m/z): $[M - OTFA]^+$calcd for $C_{35}H_{28}F_3P_2FeNi$, 681.0321; found, 681.0310.

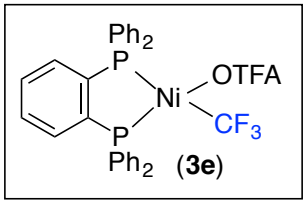

(**3e**)

Synthesis of (dppe)Ni(CF_3)(OTFA) 3e: Synthesis of [(dppbz)Ni(CF_3)(Ph)]: Under ambient conditions, a 50 mL round bottom flask was charged with $(PPh_3)_2Ni(CF_3)(OTFA)$ (765 mg, 1.00mmol, 1.0 equiv), dppbz (448 mg, 1.00mmol, 1.0equiv), and dry dichloromethane (35 mL). The resulting solution was stirred at 25 ºC for 5 min. The volatiles were then removed under reduced pressure, and the residue was dissolved in diethyl ether (10 mL). The product immediately crystallized from solution in the form of a microcrystalline yellow solid. The product was collected by vacuum filtration, washed with diethyl ether (15 mL) and pentane (25 mL), and dried under reduced pressure to afford(dppbz)Ni(CF_3)(OTFA)(**3e**) as a yellow crystalline solid (610 mg, 89% yield). ^{1}H NMR (700 MHz, CD_2Cl_2at 23 °C): δ 7.93-9.79 (multiple peaks, 4H), 7.75-7.14 (multiple peaks, 20H). ^{19}F NMR (471 MHz, CD_2Cl_2 at 23 ºC): δ –28.65 (dd, J_{PF}= 47.1, 9.3 Hz, 3F), –75.22 (s, 3F).^{31}P NMR (283 MHz, CD_2Cl_2at 23 °C): δ 55.0 (d, J_{PP} = 47.1 Hz, 1P), 46.6 (app. quint, J_{PF}= J_{PP} =47.1 Hz, 1P). HRMS-electrospray (m/z): $[M - OTFA]^+$calcd for $C_{31}H_{24}F_3P_2Ni$, 573.0659; found, 573.0650

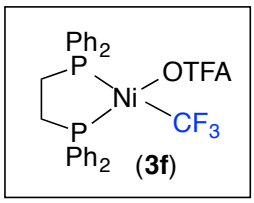

(**3f**)

Synthesis of (dppe)Ni(CF_3)(OTFA) 3f: Under ambient conditions, a 50 mL round bottom flask was charged with $(PPh_3)_2Ni(CF_3)(OTFA)$ (613 mg, 0.80mmol, 1.0equiv), dppp (414 mg, 1.01mmol, 1.25 equiv), and dry dichloromethane (35 mL). The resulting solution was stirred at 25 °C for 10 min. The volatiles were then removed under reduced pressure, and the residue was dissolved in a 1:1 mixture of diethylether anddiisopropyl ether (10 mL). The product slowly precipitated from solution in the form of a yellow powder. The product was collected by vacuum filtration, washed with diethyl ether (3 x 5 mL) and pentane (15 mL), and dried under reduced pressure to afford (dppp)Ni(CF_3)(OTFA) (**3g**)as a yellow solid (386 mg, 73% yield).^{1}H NMR (500 MHz, acetone-$d_6$at 23 °C): δ 8.00 (t, J_{HH} = 9.8 Hz, 4H), 7.86 (t, J_{HH} = 9.1 Hz, 4H), 7.58-7.44(multiple peaks, 12H), 2.63-2.52 (multiple peaks, 4H), 1.88 (m, 2H). ^{19}F NMR (471 MHz, acetone-$d_6$at 23 °C): δ –27.82 (dd, J_{FP}= 43.6, 10.2 Hz, 3F), –73.67 (s, 3F).^{31}P NMR (202 MHz,acetone-$d_6$at 23 °C): δ 19.49 (d, J_{PP} = 82.8 Hz, 1P), –0.56 (dq, J_{PP} = 82.8

Hz;J_{PF}=43.6 Hz, 1P). HRMS-electrospray (m/z): [M – OTFA]$^+$calcdfor $C_{28}H_{26}F_3P_2Ni$, 539.0815; found, 539.0806.

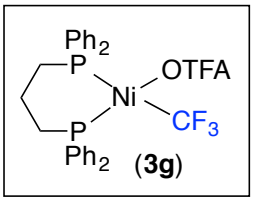

Synthesis of (dppp)Ni(CF_3)(OTFA) 3g Under ambient conditions, a 50 mL round bottom flask was charged with (PPh_3)$_2$Ni(CF_3)(OTFA) (613 mg, 0.80mmol, 1.0equiv), dppp (414 mg, 1.01mmol, 1.25 equiv), and dry dichloromethane (35 mL). The resulting solution was stirred at 25 °C for 10 min. The volatiles were then removed under reduced pressure, and the residue was dissolved in a 1:1 mixture of diethylether anddiisopropyl ether (10 mL). The product slowly precipitated from solution in the form of a yellow powder. The product was collected by vacuum filtration, washed with diethyl ether (3 x 5 mL) and pentane (15 mL), and dried under reduced pressure to afford (dppp)Ni(CF_3)(OTFA) (**3g**)as a yellow solid (386 mg, 73% yield).^{1}H NMR (500 MHz, acetone-$d_6$at 23 °C): δ 8.00 (t, J_{HH} = 9.8 Hz, 4H), 7.86 (t, J_{HH} = 9.1 Hz, 4H), 7.58-7.44(multiple peaks, 12H), 2.63-2.52 (multiple peaks, 4H), 1.88 (m, 2H). ^{19}F NMR (471 MHz, acetone-$d_6$at 23 °C): δ –27.82 (dd, J_{FP}= 43.6, 10.2 Hz, 3F), –73.67 (s, 3F).^{31}P NMR (202 MHz,acetone-$d_6$at 23 °C): δ 19.49 (d, J_{PP} = 82.8 Hz, 1P), –0.56 (dq, J_{PP} = 82.8 Hz;J_{PF}=43.6 Hz, 1P). HRMS-electrospray (m/z): [M – OTFA]$^+$calcdfor $C_{28}H_{26}F_3P_2Ni$, 539.0815; found, 539.0806.

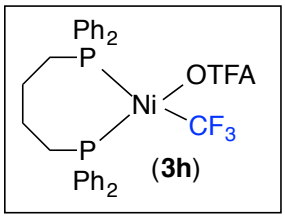

Synthesis of (diop)Ni(CF_3)(OTFA) 3h: Under ambient conditions, a 50 mL round bottom flask was charged with (PPh_3)$_2$Ni(CF_3)(OTFA) (521 mg, 0.68mmol, 1.00equiv),dppb (353 mg, 0.84mmol, 1.2equiv), and dry dichloromethane (25 mL). The resulting solution was stirred at 25°C for 10 min. The volatiles were removed under reduced pressure to give a thick film. Diethyl ether (50 mL)was added,followed by pentane (5 mL). The resulting suspension was then sonicated for 2 min. At this point, the product started to precipitate in the form of an orange powder. Additional pentane (5 mL) was added, and the solution was sonicated for another 2 min. The precipitate was collected by vacuum filtration, washed with pentane (4 x 10 mL), and dried under reduced pressure to afford (dppb)Ni(CF_3)(OTFA)(**3h**) as an orange powder (730 mg, 52% yield). ^{1}H NMR (500 MHz, in C_6D_6at 23 °C): δ 7.76 (brs, 8H), 7.32-6.70 (multiple peaks, 12H), 2.06 (brs, 4H), 1.73 (brs, 4H). ^{19}F NMR (471 MHz,in C_6D_6at 23 °C): δ –9.85 (br s, 3F), –75.45 (brs, 3F). ^{31}P NMR (202 MHz, in C_6D_6at 23 °C): δ 21.20 (brs). HRMS-electrospray (m/z): [M – OTFA]$^+$calcd for $C_{29}H_{26}F_3P_2Ni$, 553.0972; found, 553.0971.

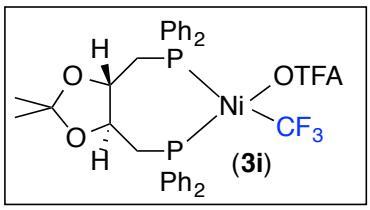

Synthesis of (diop)Ni(CF_3)(OTFA) 3i: Under ambient conditions, a 50 mL round bottom flask was charged with (PPh_3)$_2$Ni(CF_3)(OTFA) (410 mg, 0.53 mmol, 1.0equiv), (+)-diop(470 mg, 0.64 mmol, 1.2equiv), and dry dichloromethane (25 mL). The resulting solution was stirred at 25 ºC for 25 min. The volatiles were removed under reduced pressure until ~5 mL remained. The viscous yellow-orange solution was poured into vigorously stirring pentane (80 mL). The product immediately precipitated from solution in the form of a yellow powder. The product was collected by vacuum filtration, washed with pentane (4 x 5 mL), and dried under reduced pressure to afford (diop)Ni(CF_3)(OTFA) (**3i**)as a yellow-orange powder (238 mg, 61% yield). ^{1}H NMR (700 MHz, in CD_2Cl_2 at 23°C): δ 8.19-7.66 (multiple peaks, 8H), 7.72-7.07 (multiple peaks, 12H), 4.05 (brs, 2H), 2.7-2.2 (multiple peaks, 4H) 1.21 (brs, 6H). ^{31}P NMR (202 MHz, in CD_2Cl_2 at 23 °C):δ 19.79 (br s, 1P), 4.63 (brs, 1P). ^{19}F NMR (471 MHz, CD_2Cl_2) δ –29.63 (t, J_{FP} = 25.0 Hz, 3F), –75.23 (s, 3F). HRMS-electrospray (m/z): [M – OTFA]$^+$calcd for $C_{32}H_{32}O_2F_3P_2Ni$, 625.1183; found, 625.1170.

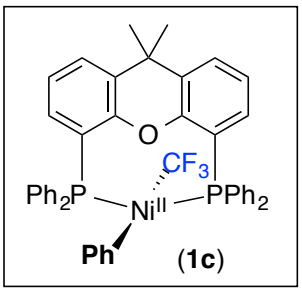

Synthesis of (Xantphos)Ni(CF_3)(Ph) 1c: A Schlenk flask was charged with a stir bar, (Xantphos)Ni(CF_3)(OTFA) (490 mg, 0.59mmol, 1.0equiv), and THF (55 mL). The resulting purple solution was cooled to –35°C. $ZnPh_2$ (77 mg, 0.35mmol, 0.55 equiv) in THF (4 mL) was added. The resulting orange solution was stirred for 15 minand then vacuum filtered through a 3 cm pad of basic alumina. The volatiles were removed under reduced pressure. The resulting orange-yellow powder was collected by vacuum filtration and washed with Et_2O (3 x 1 mL)and then pentane (2 x 1 mL).Complex **1c** was purified further by recrystallization from acetone/pentane, and the crystals were washed with diethyl ether (1 x 2 mL at –35 ºC),and then dried under vacuum to yield **1c** as a yellow-orange powder (227mg, 48% yield). NMR spectra of compound **1c** were recorded at –60 °C because the resonances associated with the phenylgroups were broad at room temperature. Additionally, the compound was not sufficiently stable over the time period needed to collect a ^{13}C NMR spectrum at room temperature. However, at room temperature the ^{19}F and ^{31}P NMR resonances are still consistent with a trans geometry. ^{1}H NMR (500 MHz, in acetone-d_6 at –60 °C): δ 7.92 (brs, 4H), 7.85 (d, J_{HH} = 7.7 Hz, 2H), 7.71-7.36 (multiple peaks, 8H), 7.32 (t, J_{HH} = 7.7 Hz, 2H), 7.26-7.13 (multiple peaks, 4H), 7.08 (t, J_{HH} = 7.7 Hz, 4H), 6.75 (brs, 4H), 6.10 (t, J_{HH} = 7.3 Hz, 1H), 5.94 (brs, 2H), 1.96 (s, 3H), 1.73 (s, 3H). ^{19}F NMR (471 MHz, in acetone-d_6 at –60 °C): δ –11.76 (t, J_{FP} = 17.1 Hz. ^{31}P NMR (202 MHz, in acetone-d_6

at –60 °C): δ 15.78 (q, J_{PF} = 17.1 Hz). HRMS-electrospray (m/z): [M – F]$^+$calcd for $C_{46}H_{37}OF_2P_2Ni$, 739.0723; found, 739.0718. [M – CF_3] calcd for $C_{45}H_{37}OP_2Ni$, 689.0755; found, 689.0740.

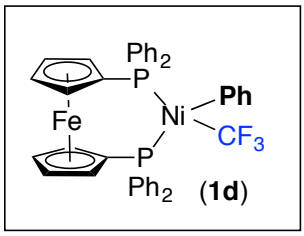

Synthesis of (dppf)Ni(CF_3)(Ph) 1d A 100 mLSchlenk flask was charged with a magnetic stir bar, (dppf)Ni(CF_3)(OTFA) (631 mg, 0.79 mmol, 1.0equiv), and THF (70 mL). The resulting solution was cooled to –78°C in a dry ice/acetone bath. $ZnPh_2$ (96 mg, 0.44 mmol, 0.55 equiv) in THF (4 mL) was added. The solution was stirred at –78 ºC for 30 minand then vacuum filtered through a 3 cm thick pad of basic alumina. The pad was washed with additional THF (10 mL). The volatiles were removed under reduced pressure to afford a red-orange powder. The powder was collected and washed with acetone (3x1 mL at –35 ºC) and then acetonitrile (1 mL) and then diethyl ether (1 mL). The product was then dried under vacuum to yield **1d** as a yellow powder (405 mg, 67% yield). X-ray quality crystals were obtained by vapor diffusion of pentane into a benzene solution of **1d** at room temperature. NMR spectra were collected at –15 °C to help resolve phenyl resonances. ^{1}H NMR (500 MHz,in CD_2Cl_2at –15 °C): δ 8.12-7.99 (br s, 4H), 7.60-7.49 (brs, 6H), 7.44 (t,J_{HH}= 8.8 Hz, 4H), 7.35-7.27 (multiple peaks, 2H), 7.22-7.05 (multiple peaks, 6H), 6.55-6.36 (multiple peaks, 3H), 4.45-4.33 (multiple peaks, 4H), 4.16 (s, 2H), 3.65 (s, 2H).^{19}F NMR (471 MHz, in CD_2Cl_2, –15 ºC): δ –18.84 (dd, J_{FP} = 32.0, 20.2 Hz). ^{31}P NMR (202 MHz, in CD_2Cl_2, -15 ºC): δ 22.04 (app quint, J_{PF} =J_{PP}= 32.0 Hz, 1P), 20.61 (m,1P). HRMS-electrospray (m/z): [M – F]$^+$calcd for $C_{41}H_{33}F_2P_2FeNi$, 763.1636; found, 763.1623; [M –CF_3]$^+$calcd for $C_{40}H_{33}P_2FeNi$: 713.1668; found, 713.1654.

Preparation of Zn(4-F-C_6H_4)$_2$: A 50 mL side arm Schlenk flask equipped with a magnetic stir bar was charged with anhydrous zinc chloride (273 mg, 2.0mmol, 1.0equiv) and diethyl ether(2 mL). The mixture was stirred vigorously for 1 h and then 4-fluoro-phenylmagnesium bromide (4.0 mL, 2.0equiv, 1.0 M in 2-MeTHF) was added dropwise. This mixture was stirred for 1.5h at room temperature and then 1,4-dioxane(2 mL)was added, at which time a white precipitate formed immediately. The reaction mixture was stirred for an additional 1 h and then filtered through a glass frit. The resulting light yellow solution contained the desired product. A^{19}F NMR standard (4,4'-difluorobiphenyl) was added to assess the concentration by ^{19}F NMR

spectroscopy (calculated concentration = 0.23M). The product wasstored in solution at –35°Cunder an inert atmosphere and was used within 2 days of preparation.

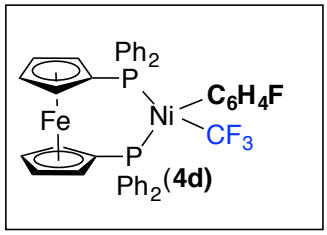

Synthesis of (dppf)Ni(CF_3)(4-F-C_6H_4) 4d A 100 mL Schlenk flask was charged with a magnetic stir bar, (dppf)Ni(CF_3)(OTFA) (640 mg, 0.80mmol, 1.0equiv), and THF (70 mL). The resulting solution was cooled to –78°C using a dry ice/acetone bath. The Zn(4-F-C_6H_4)$_2$ solution (3.5 mL, 0.81 mmol, 0.55 equiv) was added in one portion. The reaction mixture was stirred at –78 °C for 30 min andthen vacuum filtered through a 3 cm thick pad of basic alumina. The pad was washed with additional THF (10 mL). The volatiles were removed under reduced pressure to afford an orange powder. The powder was collected by vacuum filtration and washed with acetone (3x 1 mL at–35 °C)and then acetonitrile(1 mL). The resulting solids were dried under vacuum to yield(dppf)Ni(*p*-F-C_6H_4)(CF_3) as a yellow powder (509 mg, 82% yield). ^{1}H NMR (500 MHz, in CD_2Cl_2at 23 °C): δ 8.07 (s, 4H), 7.78-6.73 (multiple peaks, 16H), 6.33 (s, 2H), 4.72-3.93 (multiple peaks, 6H), 3.66 (brs, 4H). ^{19}F NMR (471 MHz, in CD_2Cl_2at 23 °C): δ –20.8 (dd, J_{FP} = 32.0, 19.0 Hz, 3F), –128.04 (s, 1F). ^{31}P NMR (202 MHz, in CD_2Cl_2at 23 °C): δ 22.40 (appquint, J_{PP} = J_{PF} =29.4 Hz, 1P), 21.35 (m, 1P). HRMS-electrospray (m/z): [M – CF_3]$^+$calcd for $C_{40}H_{32}FP_2FeNi$, 707.0666; found, 707.0640.

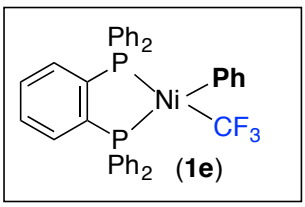

Synthesis of (dppbz)Ni(CF_3)(Ph) 1e: A 100 mLSchlenk flask was charged with a magnetic stirbar, (dppbz)Ni(CF_3)(OTFA) (275 mg, 0.40mmol, 1.0equiv) and THF (50 mL). A solution of $ZnPh_2$ (48 mg, 0.22 mmol, 0.55 equiv) in THF (4.0 mL) was added. The reaction mixture was stirred at room temperature for 20 min. The solution was then vacuum filtered through a 3 cm thickpad of basic alumina, and the pad was washed with THF (5 mL). The washes were combined and the volatiles were removed under reduced pressure. The resulting yellow powder collected by vacuum filtration and was washed with acetone (3 x 0.5 mL) and acetonitrile (2 mL). The powder was taken up in a minimum volume of THF and recrystallized by the dropwiseaddition of diethyl ether. The crystals were collected and dried under vacuum to yield **1e**as a yellow crystalline solid (141 mg, 50% yield). ^{1}H NMR (700MHz, in CD_2Cl_2at 23 °C): δ 7.67 (t, J_{HH} =9.4 Hz, 4H), 7.41-7.54 (multiple peaks, 10H), 7.38 (t, J_{HH} =7.48 Hz, 2H), 7.17-7.28 (multiple peaks, 8H), 6.98 (s, 2H), 6.62 (s, 3H). ^{19}F NMR (471 MHz, in CD_2Cl_2at 23 °C):δ –19.50 (dd, J_{FP} = 36.7, 19.0 Hz). ^{31}P NMR (283 MHz, in CD_2Cl_2at 23 °C):

δ 53.93 (qd, J_{PF}=19.0, 10.1 Hz, 1P), 52.56 (qd, J_{PF}=36.7,J_{PP}=10.1 Hz, 1P). HRMS-electrospray (m/z): [M – F]$^+$calcd for $C_{37}H_{29}F_2P_2Ni$, 631.1066; found, 631.1069.

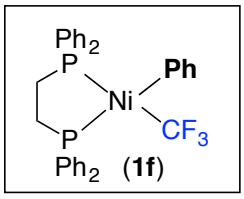

(**1f**)

Synthesis of (dppe)Ni(CF_3)(Ph) 1f: A 100 mLSchlenk flask was charged with a magneticstirbar, (dppe)Ni(CF_3)(OTFA) (255 mg, 0.4 mmol, 1.0equiv), and THF (40 mL). A solution of $ZnPh_2$ (48 mg, 0.22 mmol, 0.55 equiv) in THF (4 mL) was added. The resulting solution was stirred at room temperature for 20 min. It was then vacuum filtered through a 3 cm alumina pad. The pad was washed with 5 mL of THF,the THF washes were combined, and volatiles were removed under reduced pressure. The resulting yellow powder was collected by vacuum filtration and then washed with diethyl ether (3 x 3 mL) and acetone (1 x 0.5 mL at –35 ºC). The solid was then taken up in a minimum volume of THF and recrystallized by drop-wise addition of pentane. The crystals were separated and dried under vacuum to yield **1f** as a yellow microcrystalline solid (157mg, 75% yield). X-ray quality crystals were obtained by diffusion of pentane into a benzene solution of **1f.** ^{1}H NMR (700 MHz, in CD_2Cl_2 at 23 °C): δ 7.85 (t, J_{HH}= 8.4 Hz, 4H), 7.55 (multiple peaks, 6H), 7.44 (td, J_{HH} = 7.3, 1.7 Hz, 2H), 7.39-7.28 (multiple peaks, 8H), 7.14 (t, J_{HH} = 5.7 Hz, 2H), 6.67 (t, J_{HH}=6.8 Hz, 2H), 6.60 (t, J_{HH} = 7.2 Hz, 1H), 2.22-2.07 (multiple peaks, 4H). ^{19}F NMR (471 MHz, in CD_2Cl_2 at 23 °C): δ –17.95 (dd, J_{FP} = 35.9, 20.4 Hz). ^{31}P NMR (283 MHz, in CD_2Cl_2 at 23°C): δ 49.23 (qd, J_{PF} = 35.9, J_{PP}= 8.5 Hz, 1P), 48.92 (qd, J_{PF}= 20.4,J_{PP}=8.5 Hz, 1P). HRMS-electrospray (m/z): [M – F]$^+$calcd for $C_{33}H_{29}F_2P_2Ni$, 583.1066; found,583.1067

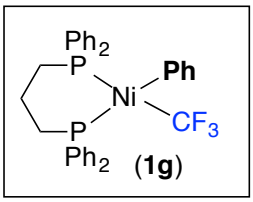

(**1g**)

Synthesis of (dpp)Ni(CF_3)(Ph) 1g: A Schlenk flask was charged with a magnetic stirbar, (dppp)Ni(CF_3)(OTFA) (261 mg, 0.4 mmol, 1.0equiv), and THF (40 mL). A solution of $ZnPh_2$ (48 mg, 0.22 mmol, 0.55 equiv) in THF (4 mL) was added. The resulting solution was stirred at room temperature for 15 min. The reaction mixture was then vacuum filtered through a 3 cm pad of basic alumina. The volatiles were removed under reduced pressure. The compound was further purified by precipitation from a minimum volume of THF by the slow addition of diethyl ether. The resulting solid was washed with diethyl ether (3 x 3 mL) and dried under vacuum to yield **1g** as a yellow powder (115 mg, 47% yield). ^{1}H NMR (700 MHz,in CD_2Cl_2 at 23°C): δ 7.83-7.77 (multiple peaks, 4H), 7.52-7.47 (multiple peaks, 6H), 7.39 (t, J_{HH}= 8.8 Hz, 4H), 7.31 (t, J_{HH}= 7.5 Hz, 2H), 7.20 (t, J_{HH} = 7.7 Hz, 4H), 7.06 (t, J_{HH} = 6.5 Hz, 2H), 6.46 (t, J_{HH}=6.9 Hz, 2H), 6.38 (t, J_{HH} = 7.1 Hz, 1H), 2.28-2.16 (multiple peaks, 4H), 1.66 (m, 2H).

^{19}F NMR (476 MHz,in CD_2Cl_2 at 23 °C): δ –19.66 (dd, J_{FP} = 33.2, 19.7 Hz). ^{31}P NMR (283 MHz,in CD_2Cl_2 at 23°C): δ 13.61 (app. quint, J_{PF}= J_{PP} = 33.2 Hz, 1P), 8.97 (m,1P). HRMS-electrospray (m/z): $[M - F]^+$calcd for $C_{34}H_{31}F_2P_2Ni$, 597.1223; found, 597.1210.

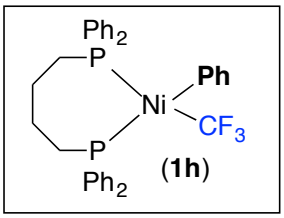

Synthesis of (dppb)Ni(CF_3)(Ph) 1h: A 20 mL vialwas charged with a stirbar, (dppb)Ni(CF_3)(OTFA) (26 mg, 0.04 mmol, 1.0equiv), andacetone-d_6 (3 mL). The resulting solution was cooled to –35 ºC. $ZnPh_2$ (4.8 mg, 0.022 mmol, 0.55 equiv) was added in one portion to the vigorously stirring solution of (dppb)Ni(CF_3)(OTFA). The resulting solution was allowed to stir at–35 ºCfor 2 minand was then filtered through a 3 cm thickpad of basic alumina prepared in a pipette. The alumina pad was washed with acetone-d_6 (0.5 mL).Thewashings were combined to afford a yellow solution of **1h**. When stored at –35 ºC under an inert atmosphere, the solution of **1h**showed no signs of decomposition over 48h. The concentration of **1h** wasdetermined to be 0.0085 M via^{19}F NMR spectroscopy using a known amount of 4,4-difluorobiphenyl as an internal standard. NMR spectra were recorded at –10 °C to improve resolution in the aromatic region. ^{1}H NMR (700 MHz, in acetone-d_6 at–10°C): δ 7.90 (m, 4H), 7.58-7.44 (multiple peaks, 8H), 7.44-7.24 (multiple peaks, 8H), 7.12 (brs, 2H), 6.37 (t, J_{HH}= 7.3 Hz, 2H), 6.32 (m, 1H), 2.51-2.37 (multiple peaks,4H), 1.79-1.54 (multiple peaks, 4H). ^{19}F NMR (471 MHz, in acetone-d_6 at–10 °C): δ –20.61 (dd, J_{FP} = 32.6, 18.8 Hz). ^{31}P NMR (283 MHz,in acetone-d_6 at–10 °C): δ 27.30 (qd, J_{PF} = 32.6,J_{PP}=19.1 Hz, 1P), 17.62 (app.pent, J_{PF} =J_{PP}= 19.1 Hz, 1P). Note*: complex**1h**is unstable upon concentration at room temperature. The complex can be isolated in the solid state by rapid precipitation from acetone solution upon the addition of 10 mL of pentane at –35 ºC. However, subsequent purification of the crude solid proved challenging. The cleanest spectra were obtained from the generation of **1h** in-situ.*

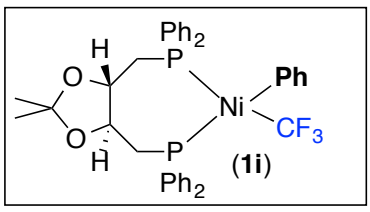

Synthesis of (diop)Ni(CF_3)(Ph) 1i:A 100 mLSchlenk flask was charged with a magnetic stir bar, (diop)Ni(CF_3)(OTFA) (186 mg, 0.25mmol, 1.0 equiv), and 20 mL of THF. The solution was cooled to –35 °C. Next, $ZnPh_2$ (31 mg, 0.14 mmol, 0.55 equiv) in 3 mL of THF was added in one portion. The solution was stirred at–35 °Cfor 4 min. The solution was then vacuum filtered through a 3 cm alumina pad. The pad was washed with additional THF (10 mL). The volatiles were removed under reduced pressure. The resulting viscous film was taken up in a minimum volume of Et_2O (2 mL). To this solution was added cold pentane (15 mL at –35 ºC). A precipitate immediately formed. The suspension was

stored at –35 °C for 2 h, and then the solids were collected on glass frit, washed with cold pentane (2 mL at –35 C) and dried under vacuum to yield compound **1i** asa khaki powder (45 mg, 26% yield). ^{1}H NMR (700 MHz, acetone-d_6 at 23 °C): δ 7.98 (t, J_{HH}=8.9 Hz, 2H), 7.92 (m, 2H), 7.69 (t, J_{HH} = 8.4 Hz, 2H), 7.59-7.38 (multiple peaks, 8H), 7.37-7.25 (multiple peaks, 4H), 7.15 (t, J_{HH} = 6.8 Hz, 2H), 6.96 (t, J_{HH} = 8.9 Hz, 2H), 6.58-6.42 (multiple peaks, 3H), 4.18 (q, J_{HH} = 9.4 Hz, 1H), 3.95 (m, 1H), 2.76-2.62 (multiple peaks, 2H), 2.56 (m,1H), 2.18 (dd, J_{HH} = 14.6, 9.1 Hz, 1H), 1.18 (s, 3H), 1.14 (s, 3H). ^{19}F NMR (471 MHz, acetone-d_6 at 23°C): δ –19.55 (dd, J_{FP} = 33.5, 18.0 Hz). ^{31}P NMR (283 MHz, acetone-d_6 at23°C): δ 13.74 (app. quint, J_{PF}= J_{PP}= 18.0 Hz, 1P), 11.88 (qd, J_{PF} =33.5, J_{PP}=18.0 Hz, 1P). HRMS-electrospray (m/z): [M-CF_3]+calcd. for $C_{37}H_{37}OP_2Ni$, 633.1622; found, 633.1604.

.

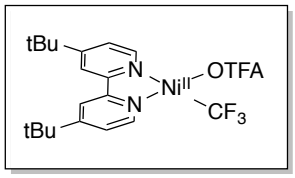

Synthesis of [(dtbpy)Ni^{II}(CF_3)(OTFA)]: Under ambient conditions, a 200 mL round bottomed flask was charged with (PPh_3)$_2$Ni(CF_3)(OTFA) (1.0 g, 1.3 mmol, 1.0 equiv) and 4,4'-di-*tert*-butylbipyridine (385 mg, 1.4 mmol, 1.1 equiv). Dry dichloromethane (50 mL) was added, and the resulting dark orange solution stirred for 5 min at room temperature. The volatiles were removed under reduced pressure, and pentane (20 mL) was added to triturate the residue. The resulting solids were collected, washed with a 10:1 solution of pentane: diethyl ether (3 x 30 mL), and dried under reduced pressure to afford (dtbpy)Ni(CF_3)(OTFA) as a yellow solid (603 mg, 91% yield). The ^{1}H and ^{13}C NMR spectra of this complex were recorded at –30 ºC to slow the fluxional processes associated with this complex.^{1}H NMR (700 MHz, CD_2Cl_2, –30 ºC): δ 8.21 (br, 1H), 7.82 (br, 2H), 7.74 (br, 1H), 7.46 (br, 1H), 7.39 (br, 1H), 1.36 (br, 18H). ^{13}C NMR (176 MHz, CD_2Cl_2, –30 ºC): δ 165.83, 165.42, 161.98, 155.35, 153.10, 152.84, 147.40, 124.26, 124.06, 118.36, 117.81, 115.08, 35.66, 35.62, 29.91, 29.85. ^{19}F NMR (471 MHz, CD_2Cl_2, 23 ºC): δ –34.40 (br, 3F, CF_3), –75.35 (br, 3F, OCOCF_3). IR (ATR, cm^{-1}): 1695 (s), 1617 (m), 1415 (m), 1195 (s).

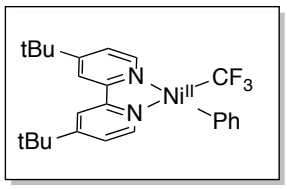

Synthesis of [(dtbpy)Ni^{II}(CF_3)(Ph)] : In the glovebox, a 150 mL round bottomed flask was charged with (dtbpy)Ni^{II}(CF_3)(OTFA) (590 mg, 1.16 mmol, 1.0 equiv), and this yellow solid was dissolved in THF (60 mL). The resulting solution was cooled to –35 ºC, and then $ZnPh_2$ (140 mg, 0.63 mmol, 0.55 equiv) in THF (5 mL) was added. The reaction mixture was allowed to warm to room temperature over approximately 5 min, during which time the

solution changed color from dark orange to dark red. The solution was then filtered through a 3 cm pad of basic alumina, and the pad was washed with THF (5 mL). The washes were combined, and the volatiles were removed under reduced pressure. The resulting dark red residue was triturated with pentane (10 mL), and the solids were collected by filtration. The solids were washed with additional pentane (40 mL) and then dried under reduced pressure to yield complex **16** as an orange solid (334 mg, 61% yield) ^{1}H NMR (700 MHz, CD_2Cl_2, 23 ºC): δ 8.78 (d, J_{HH} = 6.0 Hz, 1H), 7.90 (d, J_{HH} = 2.0 Hz, 1H), 7.84 (d, J_{HH} = 2.0 Hz, 1H), 7.65-7.61 (multiple peaks, 2H), 7.50 (dd, J_{HH} = 6.0, 2.0 Hz, 1H), 7.14 (dd, J_{HH} = 6.1, 2.0 Hz, 1H), 7.11 (d, J_{HH} = 6.0 Hz, 1H), 7.00 (multiple peaks, 2H), 6.89 (t, J_{HH} = 7.3 Hz, 1H), 1.40 (s, 9H), 1.31 (s, 9H). ^{13}C NMR (176 MHz, CD_2Cl_2, 23 ºC): δ 163.32, 163.20, 155.20, 154.05, 151.51, 151.48, 150.63, 139.31 (q, J_{CF} = 359 Hz), 135.45, 125.96, 123.73, 123.23, 122.01, 117.51, 117.22, 35.36, 35.29, 29.96, 29.88. ^{19}F NMR (377 MHz, CD_3CN, 23 ºC): δ –21.95 (s, 3 F). HRMS-electrospray (m/z): $[M - F]^+$ calcd. for $C_{25}H_{29}F_2N_2Ni$, 453.1652; found, 453.1644. Elemental Analysis calcd. for $C_{25}H_{29}F_2N_2Ni$, C: 63.45, H: 6.18, N: 5.92; found, C: 63.30, H: 6.26, N: 5.82

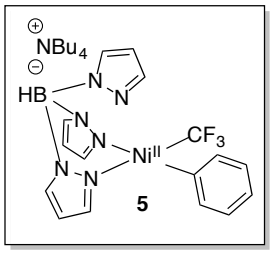

5

Synthesis of $[NMe_4(Tp)Ni^{II}(CF_3)(Ph)]$ (**5**): This procedure is based on the previous synthesis of the NBu_4 analogue. A 20 mL vial was charged with $(dtbpy)Ni^{II}(CF_3)(Ph)$ (90 mg, 0.19 mmol, 1.1 equiv), and the orange solid was dissolved in a minimal amount of acetonitrile (2 mL). A solution of NMe_4Tp (49.8 mg, 0.17 mmol, 1.0 equiv) in acetonitrile (1 mL) was added, and the resulting dark orange solution immediately changed color to yellow-brown. Over the course of approximately 10 min, 4,4'-di-tert-butylbipyridine (dtbpy) precipitated from solution in the form of a white crystalline solid. The solution was concentrated to approximately 1 mL, which led to further precipitation of dtbpy. The solution was then stored at –35 ºC for 20 min. The precipitate was collected on a paper filter and was washed with 1 mL of cold (–35 ºC) acetonitrile. The filtrate was collected and concentrated under reduced pressure to about 1.5 mL. This solution was then filtered through a pipette filter to remove additional precipitate. The filter was washed with cold acetonitrile (1 mL). The combined filtrates were reduced to a brown viscous residue. The resulting residue was suspended in 5 mL of 1:1 pentane/Et_2O. The residue was scraped with a spatula until it became a solid. The solid was collected over a frit and washed with (3 x 2 mL) and pentane (3 x 5 mL),

and the remaining solid was collected to afford complex **1e** as a light tan powder (60 mg, 71% yield).

^{1}H NMR (700 MHz, CD_3CN, 23 ºC): δ 7.90 (br, 3H), 7.44 (d, J_{HH} = 7.5 Hz, 2H), 7.29 (br, 3H) 6.77 (t, J_{HH} = 7.5 Hz, 1H), 6.67 (t, J_{HH} = 7.3 Hz, 1H), 6.15 (br, 3H), 4.66 (bq, B-***H***, 1H) 3.08 (s, 12H).^{13}C NMR (176 MHz, CD_3CN, 23 ºC): δ 164.51, 141.54, 139.82 (q, J_{CF} = 369.9 Hz), 136.45, 134.75, 120.59, 103.97, 55.05.^{11}B NMR (225 MHz, CD_3CN, 23º C): δ –2.26 (d, J_{BH} = 110 Hz, ***B***-H).^{19}F NMR (371 MHz, CD_3CN, 23 ºC): δ -21.32 (s, 3F). Elemental Analysis calcd for $C_{20}H_{27}BF_3N_7N$, C: 48.83, H: 5.53, N: 19.93; found, C: 49.02, H: 5.79, N: 19.90

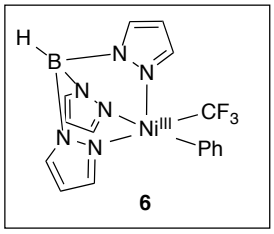

6

Synthesis of [(Tp)Ni^{III}(CF$_3$)(Ph)] (6): In the glovebox, a 20 mL vial was charged with a magnetic stirbar, NMe_4[Ni^{II}(Tp)(CF_3)(Ph)] (40 mg, 0.081 mmol, 1.0 equiv), and acetonitrile (1.5 mL). A separate 4 mL vial was charged with $AgBF_4$ (15.6 mg, 0.081 mmol, 1.0 equiv) and acetonitrile (0.5 mL). The two solutions were then cooled to –35 ºC over 20 min. To a rapidly stirring solution of **1e**, the $AgBF_4$ solution was added dropwise over 30 s. Upon the addition of $AgBF_4$ a black precipitate immediately formed. The combined solutions were then allowed to stand at –35 ºC for 2 min before they were filtered through a 2 cm cold (–35 ºC) silica pad. The orange filtrate was concentrated to near dryness as a waxy solid. This solid was taken up in a minimum (approximately 7 mL) of cold diethyl ether (–35 ºC), at which point it turned green. The ethereal solution of **2e** was filtered through an additional wet-packed (Et_2O) silica pad pre-cooled to -35 ºC. The volatiles were quickly removed under vacuum, and the solid was taken up in a minimum amount of cold diisopropyl ether (–35 ºC, approximately 2 mL). To the diisopropyl ether solution was added cold pentane (-35 ºC, ~3 mL). This solution was stored in a –35 ºC freezer for 4 d to afford green X-ray quality crystals of **2e**. The solvent was decanted, the crystals were washed with 1 mL of cold pentane (-35 ºC), and the crystals were dried under vacuum for 20 min at room temperature to give **2e** as an emerald green crystalline solid (29 mg, 87% yield).

Note: Complex **2e** decomposes to an unknown gray/green solid slowly over approximately 48 h at room temperature in the solid state. It should be kept below –15 ºC for prolonged storage. Samples of **2e** could be stored without major decomposition for over 3 months at –35 ºC. ^{11}B NMR (128 MHz, in CD_3CN): δ –5.30 (d, J_{BH}= 47 Hz, ***B***-H).Elemental Analysis calcd for

$C_{16}H_{15}BN_6F_3$, C: 45.99, H: 3.62, N: 20.11; found, C: 45.50, H: 3.43, N: 19.95. μ_{eff} (CH_3CN, 23 ºC) = 1.81

2.3.3. General Procedures for Reactivity Studies

Initial Oxidant Screen:

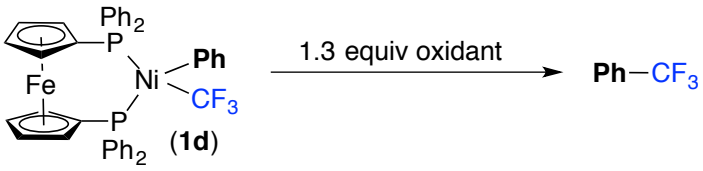

A 4 mL vial was charged with **1d** (11 mg, 0.014 mmol, 1.0equiv), 4,4' difluorobiphenyl, and acetone-d_6 (2 mL). A 0.4 mL aliquot was removed for analysis by ^{19}F NMR spectroscopy. The ratio between the standard and **1d**was determined by ^{19}F NMR integration. The NMR sample was brought back into the glovebox and recombined with the remaining solution. A separate vial was charged with the oxidant (0.018 mmol, 1.3 equiv). The solution of **1d** was added in one portion to the vial containing the oxidant. The vial was shaken vigorously for 15 s. After 10 min, the sample was analyzed by ^{19}F NMR spectroscopy to determine the yield of $PhCF_3$.

Table 2.3 Metallocene oxidant and solvent optimization

Entry	oxidant	solvent	yield Ph-CF_3
1	none	acetone-d_6	<1%
2	$FcPF_6$	acetone-d_6	77%
3	$AcFcBF_4$	acetone-d_6	71%
4	$Cp^*_2FeBF_4$	acetone-d_6	<1%
5	Cp_2CoPF_6	acetone-d_6	<1%
6	$FcBF_4$	acetone-d_6	71%
7	$FcPF_6$	THF	66%
8	$FcPF_6$	MeCN	74%

Reactivity Studies with $FcPF_6$ as the Oxidant:

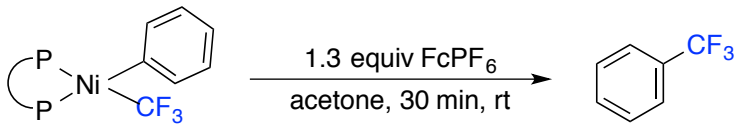

General Procedure:(P~P)Ni(CF_3)(Ph) (0.014mmol, 1.0equiv) was dissolved in acetone-d_6 (0.5 mL) to make a 0.007 M solution. 4,4'-Difluorobiphenyl was added to the solution as an internal standard. A 0.4 mL aliquot was removed for analysis by ^{19}F NMR spectroscopy. The ratio between the standard peak and (P~P)Ni(CF_3)(Ph) was determined by ^{19}F NMR integration. The NMR sample was brought back in the glovebox and recombined with the remaining solution. The combined solutions were added to a 4 mL scintillation vial containing $FcPF_6$ (6.0 mg, 1.3 equiv, 0.018 mmol). The vial was shaken vigorously for 15 s.After 30 min at room temperature, the solution was analyzed by ^{19}F NMR spectroscopy to determine the yield of $PhCF_3$. The authentic sample of the coupled product was spiked into the crude reaction mixtures, and in each case, the ^{19}F NMR resonances were coincident. Some of the non-fluorinated products, benzene and biphenyl, were identified by GCMS.

Procedure for compound 1e: The oxidation of **1e** was conducted according to the General Procedure, with the exception that a 2 : 5 mixture of $C_6D_6$to acetone-d_6 was used as the solvent because **1e** is not sufficiently soluble in acetone.

Procedure for compound 1h: A 4 mL vial was charged with 1.6 mL of the solution of **1h** in acetone and 0.4 mL of acetone. 4,4'-Difluorobiphenyl was added as an internal standard. A 0.4 mL aliquot was removed for analysis by ^{19}F NMR spectroscopy. The ratio between the standard and **1h**was measured by ^{19}F NMR spectroscopy. The NMR sample was brought back in the glovebox and recombined with the remaining solution. The combined solutions were added to a 4 mL scintillation vial containing $FcPF_6$ (6.0 mg, 1.3 equiv, 0.018 mmol). The vial was shaken vigorously for 15 s. After 30 min at room temperature, the solution was analyzed by ^{19}F NMR spectroscopy to determine the yield.
Representative ^{19}F NMR spectra are shown below

Figure 2.8. ^{19}F NMR spectra of (a) **1d** and internal standard prior to oxidation; (b) reaction mixture after treatment with 1.3 equiv of $FcPF_6$

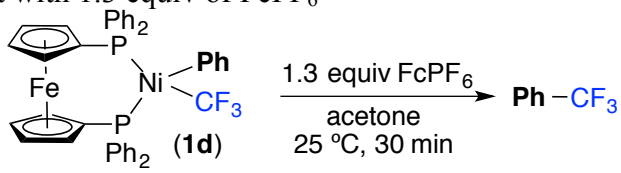

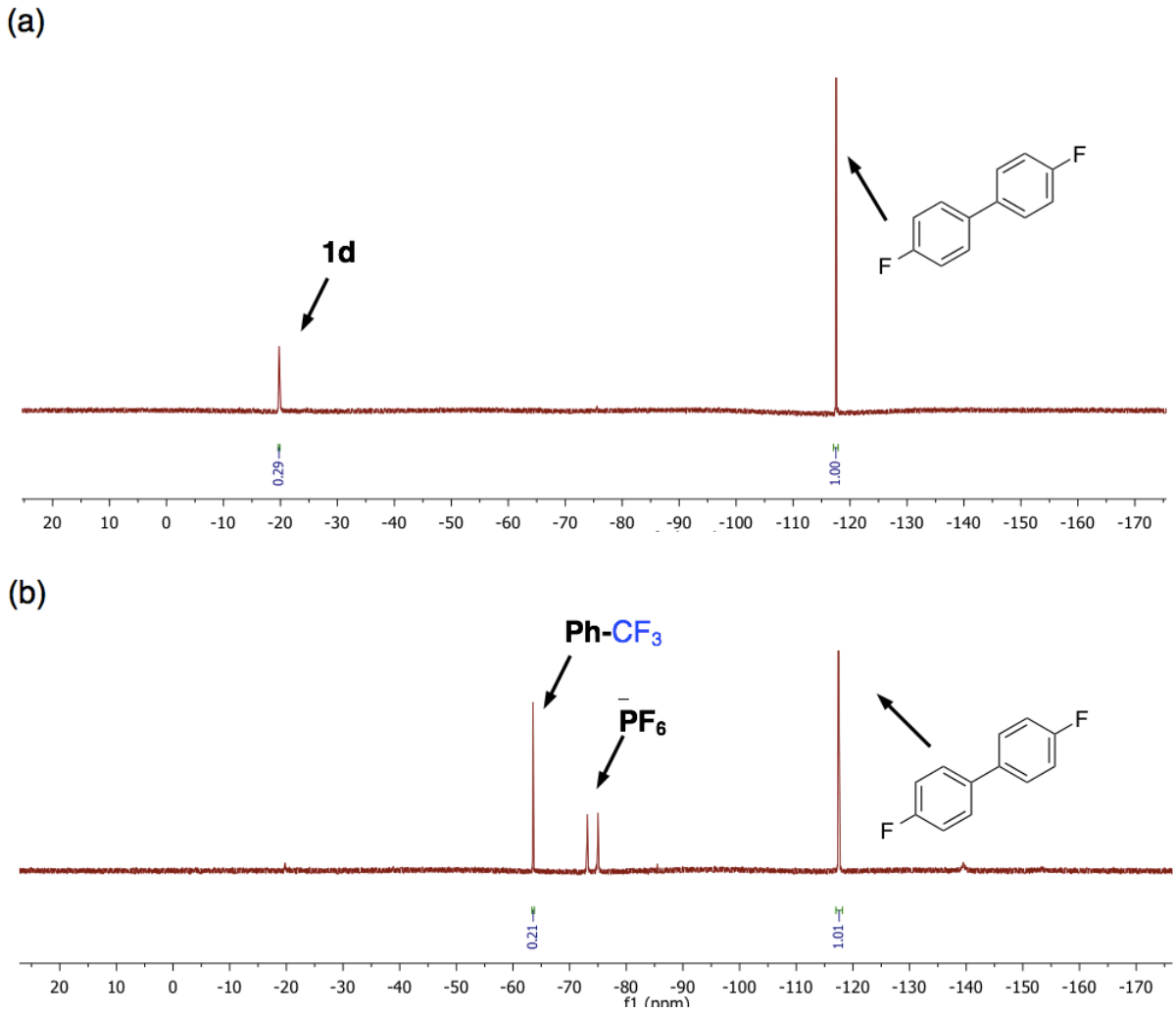

Figure 2.9. ^{19}F NMR spectra of (a) **1e** and internal standard prior to oxidation; (b) reaction mixture after treatment with 1.3 equiv of $FcPF_6$

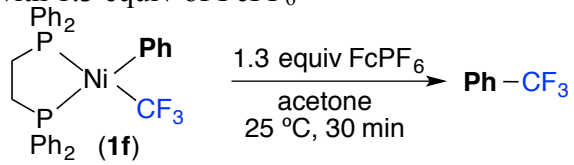

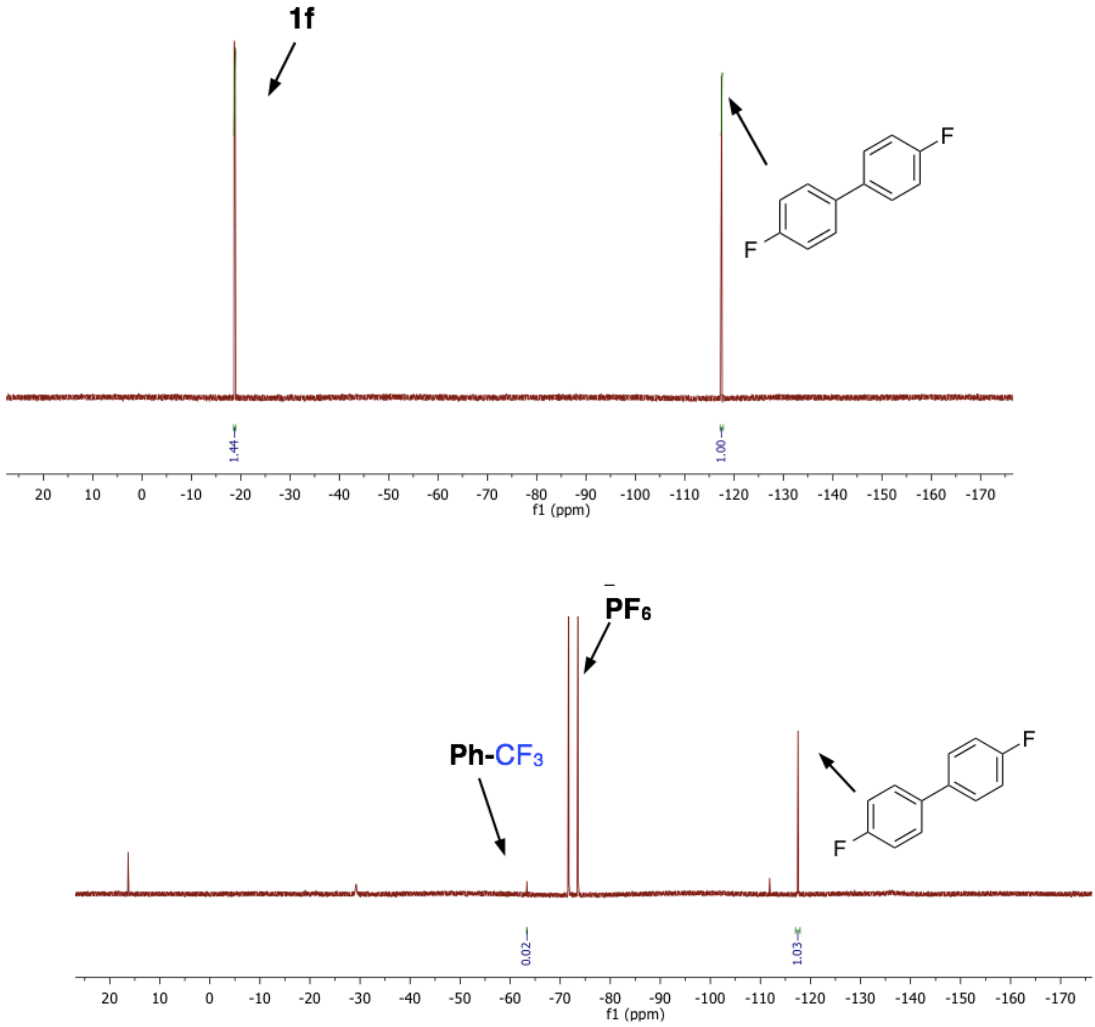

Reductive Elimination From Trispyrazolylborate Complexes

Procedure for the thermolysis of 6: A 4 mL vial was charged with **6** (3.1 mg, 0.0075 mmol) and 4,4'-difluorobiphenyl (0.5 mL in 0.023M CD_3CN, 1.5 equiv). The resulting orange solution was transferred to a teflon-lined screw cap NMR tube and removed from the glovebox. The NMR tube was heated in an oil bath at 40 ºC for 3 h or 80 ºC for 5 min. The solution was then analyzed by ^{19}F NMR spectroscopy to determine the yield of benzotrifluoride. The NMR tube was then brought back in the glove box, and NBu_4BF_4 (0.2 mL, 0.038 M in MeCN, 1.0 equiv) was added to the NMR tube as an ^{11}B NMR standard. The tube was capped, and the sample was analyzed by quantitative ^{11}B NMR spectroscopy to determine the yield of $Ni^{II}Tp_2$. Representative NMR spectra are shown in below.

Figure 2.10. A representative ^{19}F NMR spectrum of the crude reaction mixture after heating **2e** at 80 ºC for 5 min. Standard = 4,4-difluorobiphenyl.

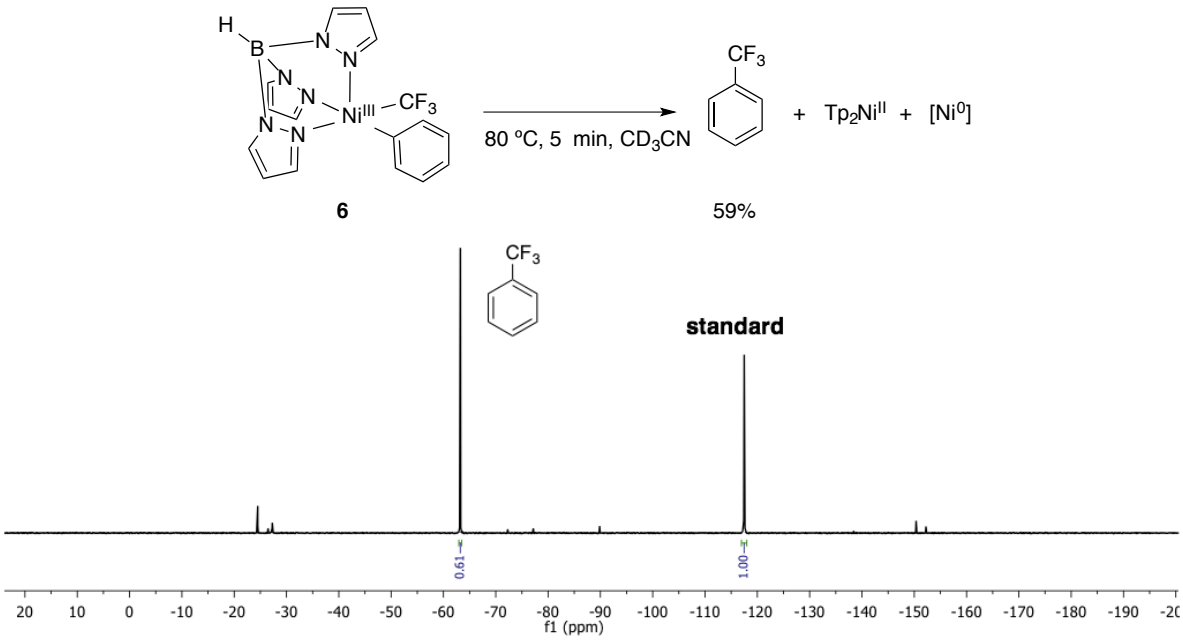

Procedure for the thermolysis of 2e in the presence of TEMPO: A 4 mL vial was charged with **6** (3.1 mg, 0.0075 mmol, 1.0 equiv), TEMPO (2.4 mg, 0.015 mmol, 2.0 equiv), and CD_3CN (0.5 mL). The resulting orange solution was transferred to a teflon-lined screw cap NMR tube and removed from the glovebox. The NMR tube was heated in an oil bath at 40 ºC for 3 h. The NMR tube was then brought back in the glove box, and the standard 4,4'-difluorobiphenyl (0.2 mL in 0.056 M MeCN, 1.5 equiv) was added to the NMR tube. The tube was capped, and the sample was analyzed by ^{19}F NMR spectroscopy to determine the yield of Ph-CF_3 (57%). Neither TEMPO-CF_3 nor CF_3H/D were detected by ^{19}F NMR spectroscopy. A representative ^{19}F NMR spectrum is shown below

Figure 2.11. ^{19}F NMR spectrum of **6** and TEMPO after heating at 40 ºC for 3 h. Standard = 4,4'-difluorobiphenyl.

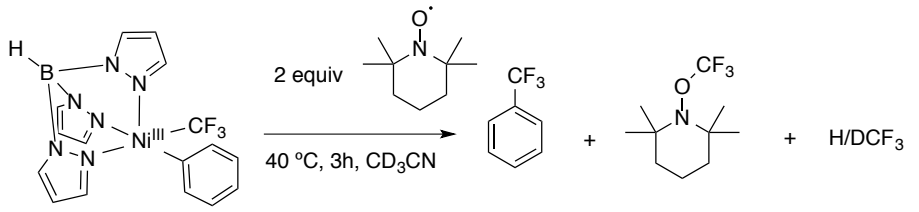

6 57% not detected not detected

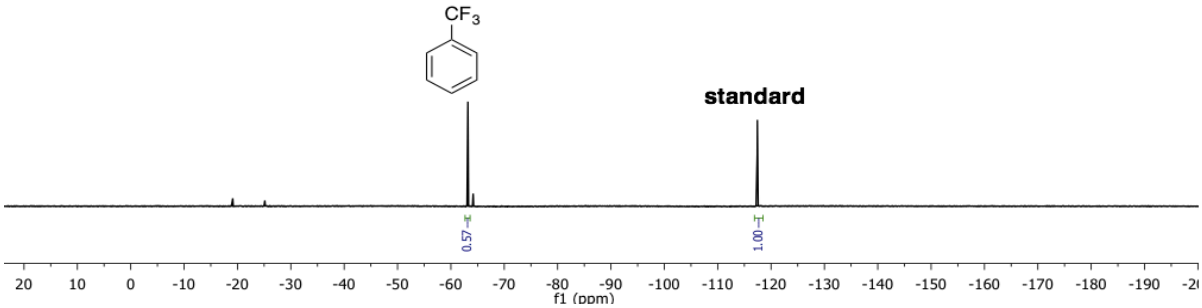

Figure 2.12. (a) ^{19}F NMR spectrum and (b) ^{1}H NMR spectrum of the crude reaction mixture after heating **6** at 40 ºC for 5 h; (c) ^{1}H NMR spectrum of authentic $C_6H_5CF_3$ in C_6D_6 for comparison.

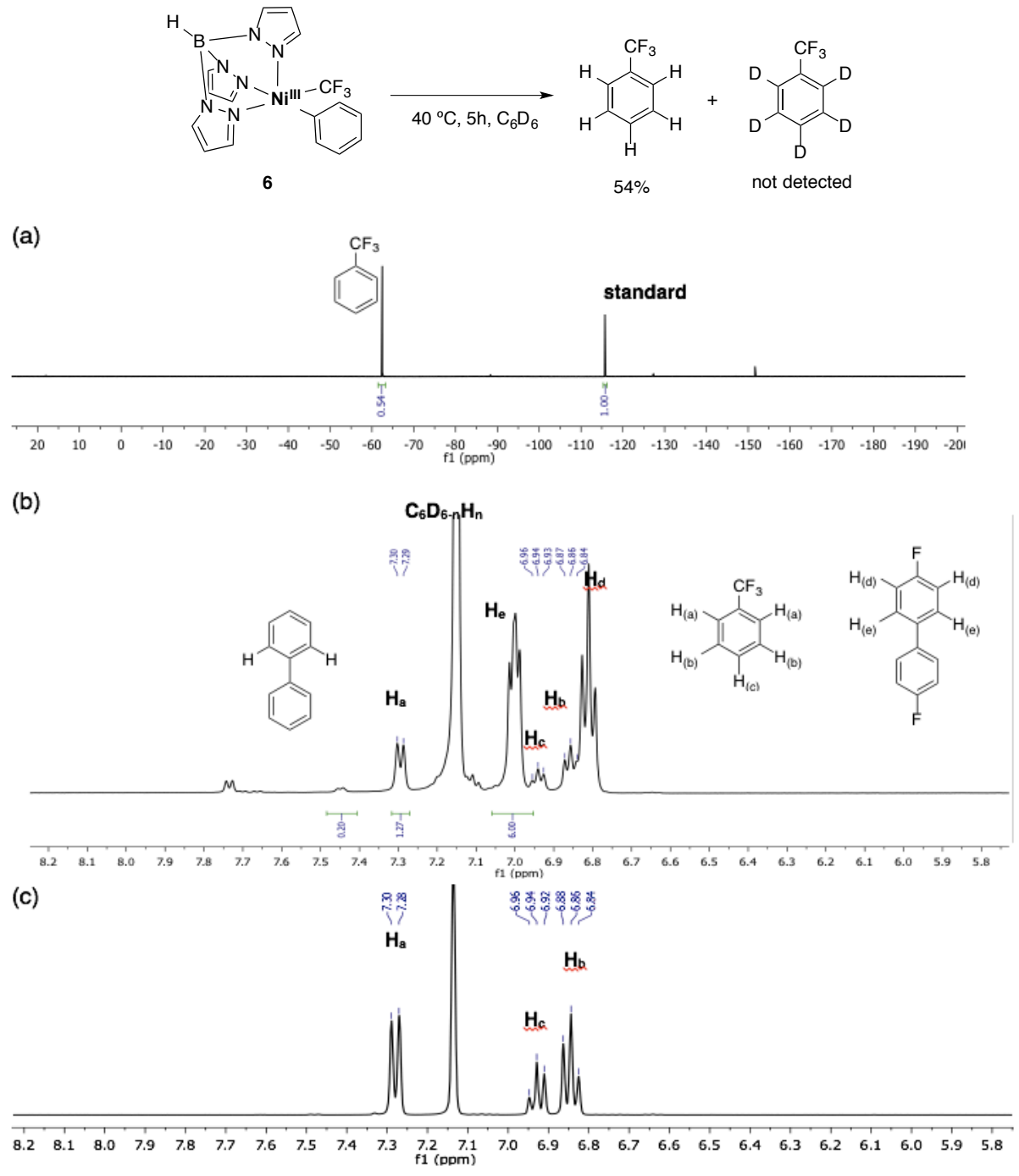

Procedure for low temperature oxidatively induced coupling from 6 with $NOBF_4$: A 4 mL vial was charged with **2e** (3.1 mg, 0.0075 mmol, 1.0 equiv) and the standard 4,4'-difluorobiphenyl (0.5 mL in 0.023 M CD_3CN, 1.5 equiv). The resulting orange solution was transferred to septum-capped NMR tube and removed from the glovebox. The NMR tube was cooled to 0 ºC in an ice bath over 5 minutes. Next, $NOBF_4$ was added via syringe as a stock solution (150 L, 0.05 M in room temperature CD_3CN, 1.0 equiv). The solution was vigorously shaken for about 3 s before it was inserted into a precooled (–30 ºC) NMR probe. A new ^{19}F NMR resonance consistent with a new diamagnetic [Ni-CF_3] complex (~31% yield) was detected at –30.85 ppm, along with benzotrifluoride (33%) .After a spectrum was collected at –30 ºC, the NMR probe was warmed to room temperature over 1 min. A second spectrum was collected approximately 2 min later to determine the yield of benzotrifluoride (50%, Figure 2.13). A final spectrum was taken 30 min later, at which point no additional benzotrifluoride was observed.

Figure 2.13. ^{19}F NMR spectrum of **6** when reacted with 1 equiv of $NOBF_4$ at (a) –30 ºC after 1 min and (b) after warming to room temperature for 2 min

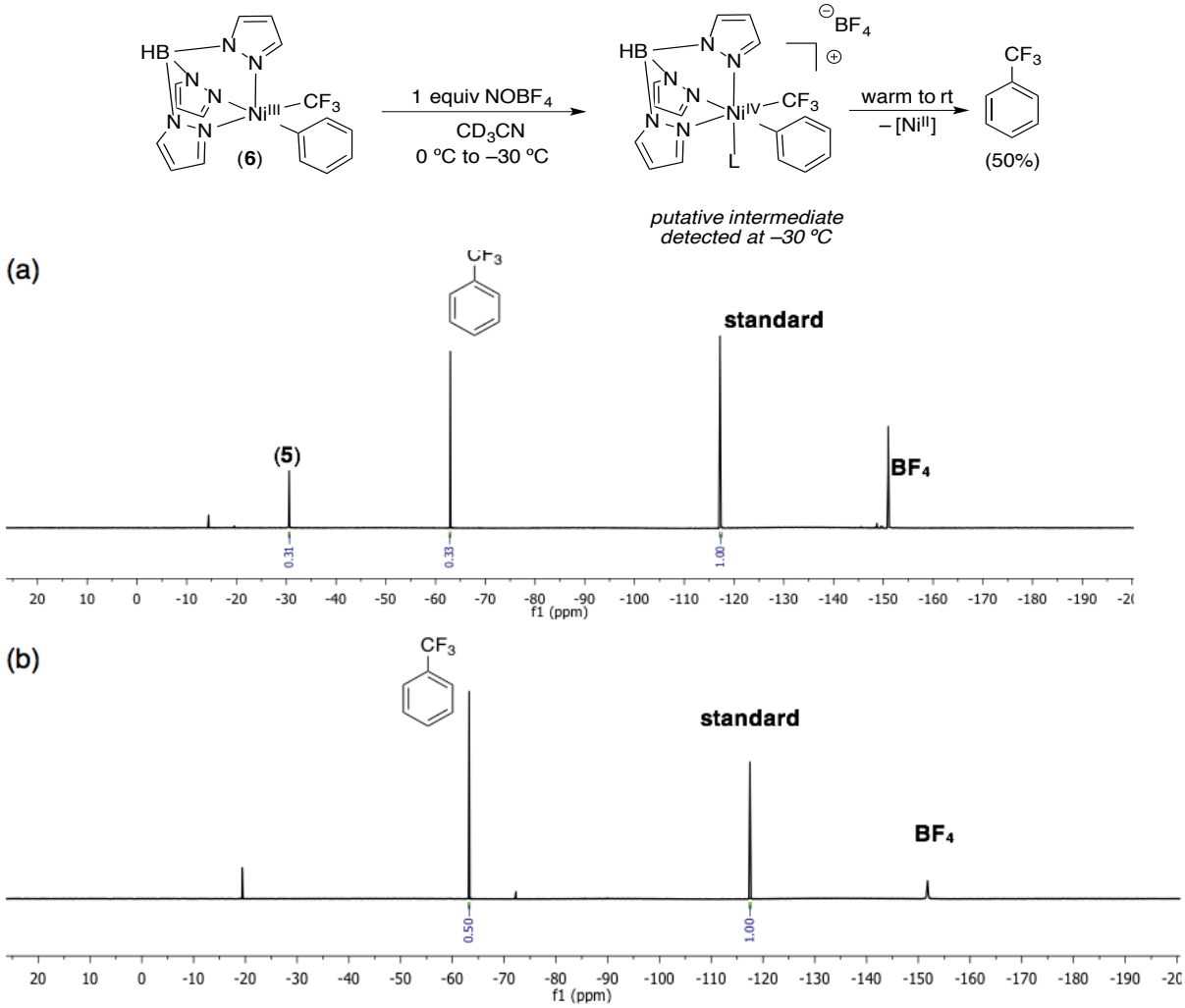

Procedure for the thermolysis of 6 with added weak oxidant: A 4 mL vial was charged with **6** (3.1 mg, 0.0075 mmol, 1.0 equiv), the standard 4,4'-difluorobiphenyl (0.5 mL in 0.023M CD_3CN, 1.5 equiv), and the corresponding amount of decamethylferrocenium tetrafluoroborate $Cp^*_2FeBF_4$. The resulting green solution was transferred to a teflon-lined screw cap NMR tube and removed from the glovebox. The NMR tube was heated in an oil bath at 40 ºC for 3 h. The solution was then analyzed by ^{19}F NMR spectroscopy to determine the yield of benzotrifluoride.

Figure 2.14. ^{19}F NMR spectrum of the crude reaction mixture after heating **6** at 40 ºC for 5 h in the presence of (a) 1 equiv of $Cp_2^*FeBF_4$ or (b) 5 equiv of $Cp_2^*FeBF_4$.

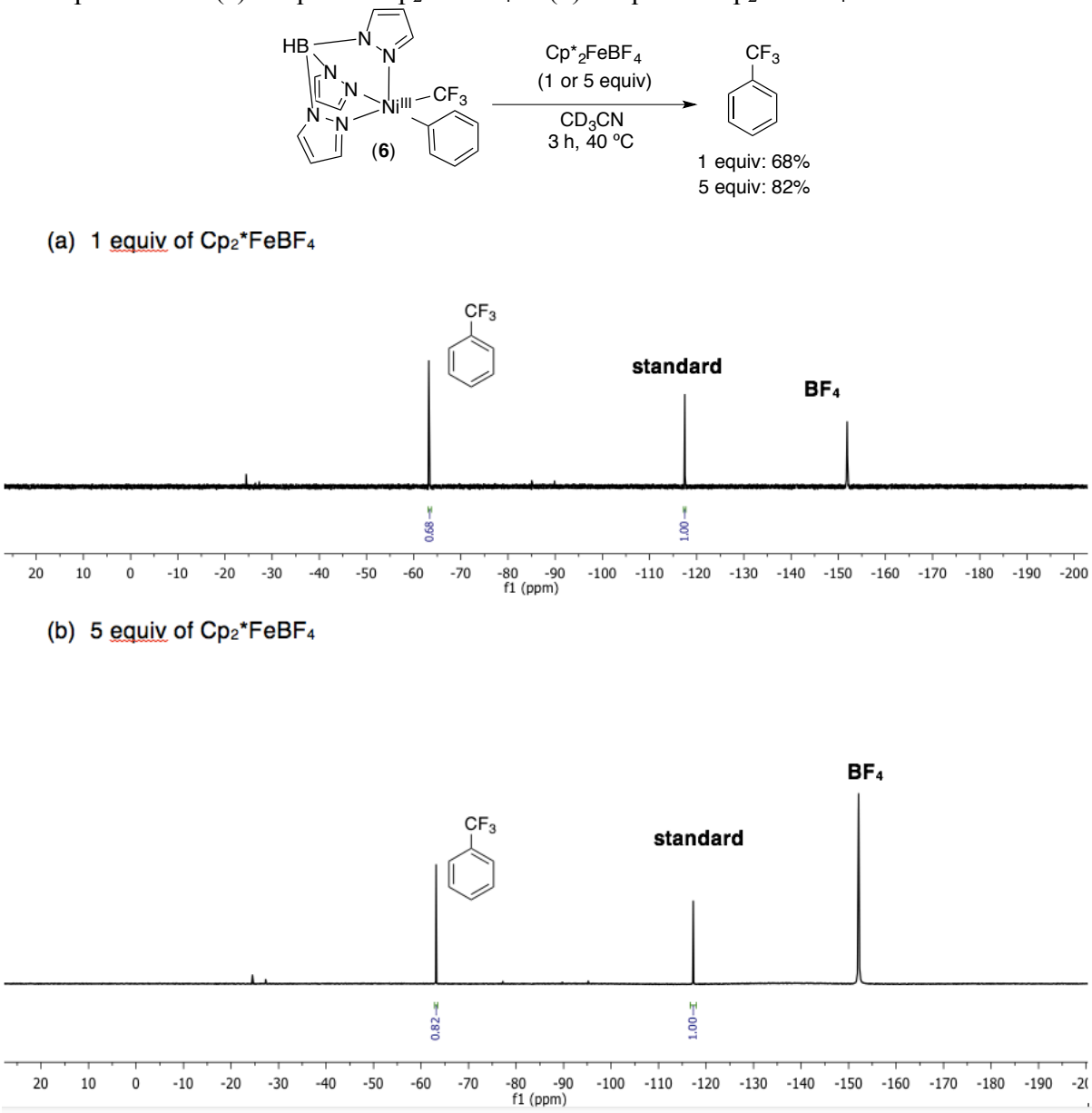

General procedure for the thermolysis of 6 in the presence of exogenous ligand: A 4 mL vial was charged with **6** (3.1 mg, 0.0075 mmol, 1.0 equiv), the standard 4,4'-difluorobiphenyl (0.5 mL in 0.023M CD_3CN, 1.5 equiv), and 3 equiv of the corresponding ligand (pyridine and PMe_3 were added from a stock solution with the internal standard, PPh_3 was added as a solid). The resulting orange (with the addition of PPh_3 and pyridine) or brown (with the addition of PMe_3) solution was transferred to a teflon-lined screw cap NMR tube and removed from the glovebox. The NMR tube was heated in an oil bath at 40 ºC for 6 h. The solution was then analyzed by ^{19}F NMR spectroscopy to determine the yield of benzotrifluoride. Representative NMR spectra are shown in below.

Figure 2.15 Thermolysis of **6** in the presence of added ligands

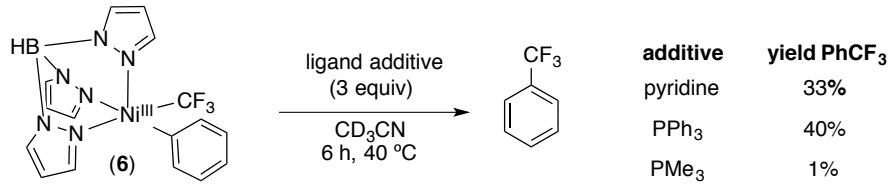

additive	yield $PhCF_3$
pyridine	33%
PPh_3	40%
PMe_3	1%

(a) 3 equiv of pyridine

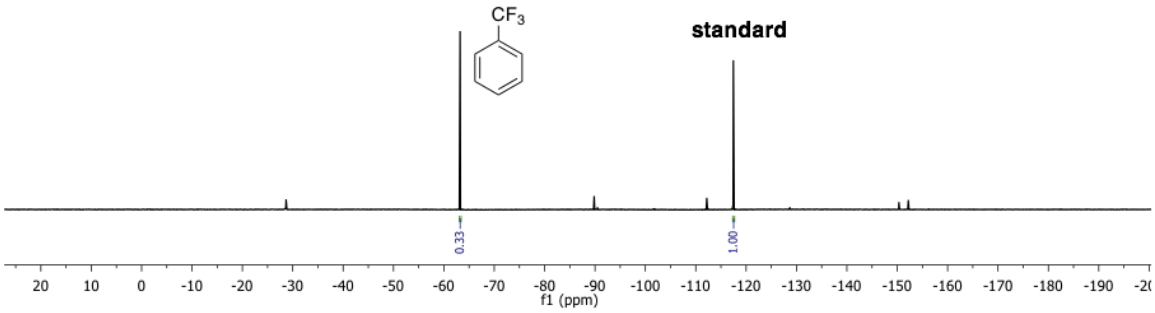

(b) 3 equiv of PPh_3

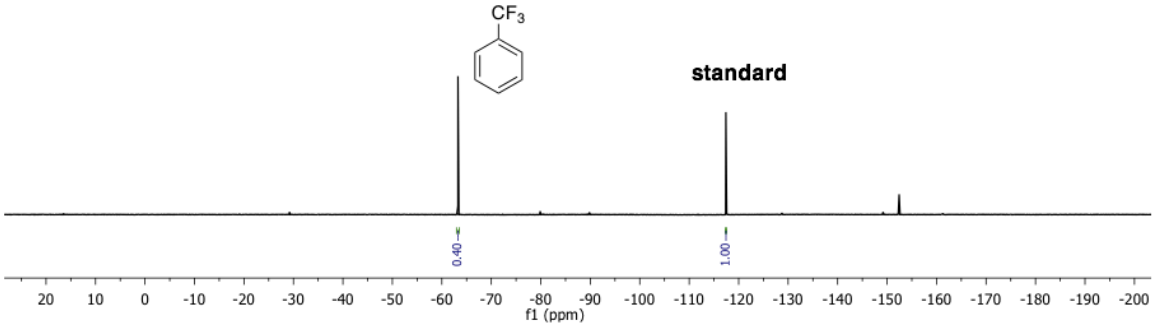

(c) 3 equiv of PMe_3

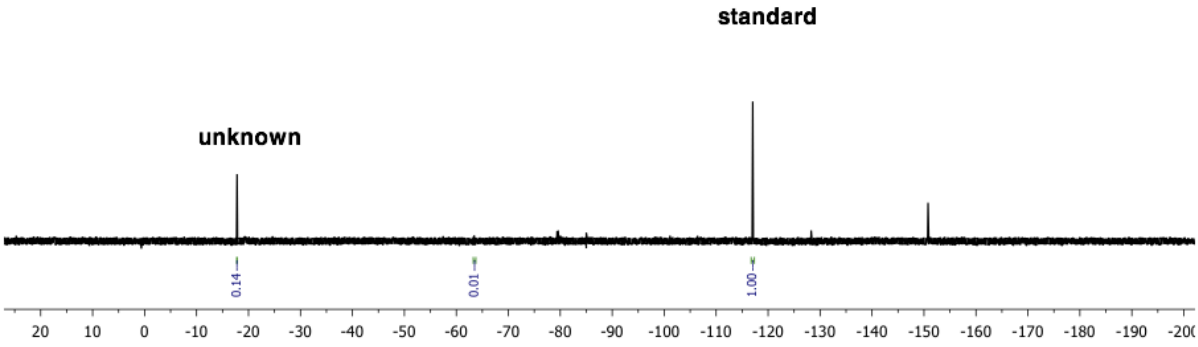

2.3.4 Cyclic Voltammetry Studies

Cyclic Voltammetry Studies of Diphosphines Complexes

Experimental Procedure: Cyclic voltammetry on complex **1d-1i** was performed in a 3-electrode cell consisting of a 3mm glassy carbon disc working electrode, a Ag/Ag^+ reference electrode with a Ag wire in a fritted chamber containing a solution of $AgBF_4$ (0.01 M) and NBu_4BF_4 (0.1 M) in acetonitrile, and a Pt wire counter electrode. A 2 mL solution of complex **1d**(0.0033 M) and NBu_4BF_4 (0.1 M) in acetonitrile was added to the electrochemical cell. Cyclic voltammetry scans were taken at 100 mV/s starting from –0.5 to +0.6 V in the positive direction.

Figure 2.16 Representative cyclic voltammogram of **1d**

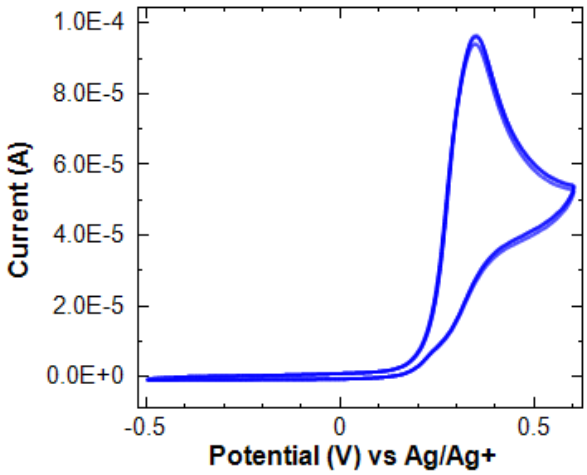

Cyclic Voltammetry Studies of Tris-pyrazolylborate Complexes

Experimental Procedure: Cyclic voltammetry on complex **5** was performed in a 3-electrode cell consisting of a 3 mm glassy carbon disc working electrode, a Ag/Ag^+ reference electrode with a Ag wire in a fritted chamber containing a solution of $AgBF_4$ (0.01 M) and NBu_4PF_6 (0.1 M) in acetonitrile, and a Pt wire counter electrode. A 2 mL solution of each complex (0.01 M) and NBu_4PF_6 (0.1 M) in acetonitrile was added to the electrochemical cell. Cyclic voltammetry scans were taken at 100 mV/s. After obtaining the CV, ferrocene was added as an internal reference.

Figure 2.17 Cylcic Voltammogram of **5**

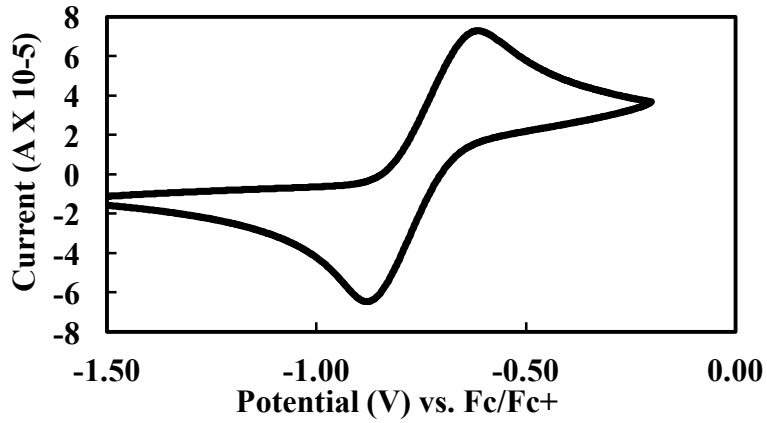

3.4.5. EPR Characterization Procedure

A 4 mL scintillation vial was charged with **5** (0.005 mmol) and acetonitrile (1 mL). A separate 4 mL vial was charged with $FcBF_4$ (0.02 mmol) and acetonitrile (1 mL). Both solutions were then cooled to –78 ºC in a glovebox cold well. After 10 min, 200 µL of the $FcBF_4$ solution (0.004 mmol, 0.8 equiv) was added in one portion via syringe to the solution of $NMe_4[Ni^{II}(Tp)(R)(R^1)]$. The vial was quickly shaken, resulting in the immediate disappearance of the blue $FcBF_4$ salt, indicating rapid consumption of the oxidant. Four drops of this solution were transferred to 300 µL of a precooled (–78 ºC) solution of 3:1 PrCN:MeCN. The sample was then flash-frozen (at –196 ºC) in a septum-capped EPR tube until analysis.

Figure 2.18. EPR spectrum of **6** (bottom/blue) and the simulated spectrum (top/red). Fit using the following parameters: $g_x = 2.18$, $g_y = 2.15$, $g_z = 2.00$, $A_N(N) = 21G$, $A_{N'}(N') = 18G$.

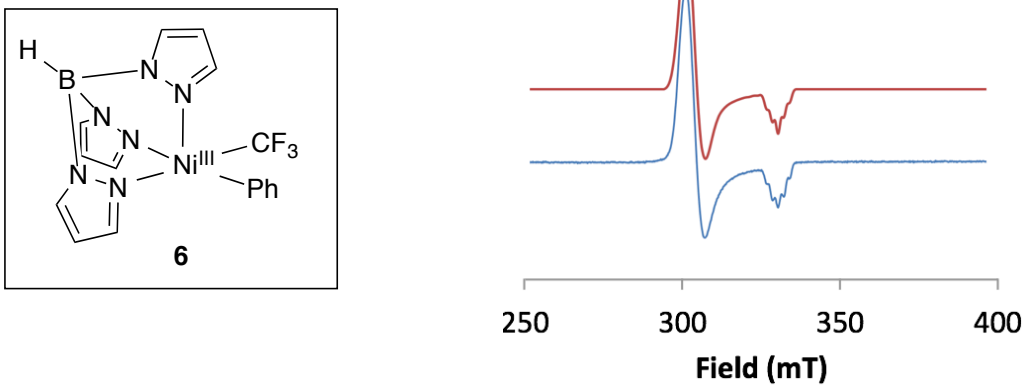

2.3.6. Determining the Order in 6 for Ar–CF_3 Coupling

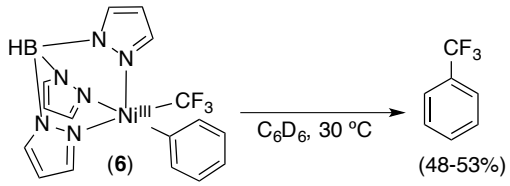

Experimental procedure: Complex **6** and 4,4'-difluorobiphenyl (1.5 equiv) were added directly to a Teflon-capped NMR tube from a freshly prepared stock solution in C_6D_6. This solution was then diluted to the appropriate concentration by the addition C_6D_6 via syringe ([**6**] = 0.01M to 0.03 M). The resulting solution was capped and brought outside of the glovebox to be flash frozen at –78 ºC until analysis. The NMR tubes were thawed at room temperature and then placed in the NMR probe pre-warmed to 30 ºC. The formation of Ph-CF_3 was monitored by ^{19}F NMR spectroscopy at this temperature. Concentration versus time data were obtained through integration of the C***F***$_3$ signals of Ph-CF_3. Initial rates were obtained from the average of two trials by taking the slopes of linear-fit lines for the first 6% of the reaction progress (Figure 2.19). When a plot of these rates was fit to $A=m[Ni]^X$ the order in nickel was found to be 0.80. *Note: Given the thermal instability of* ***6*** *even in the solid state, the stock solution of* ***6*** *and internal standard was prepared within 2 h of use and was stored as a solid at –35 ºC.*

Figure 2.19. Representative initial rates plots of concentration vs. time for reductive elimination from **2e** to form Ph-CF_3. ●= 0.03M [Ni], y= $6.42e^{-4}$+ $1.08e^{-6}$x, R^2=0.979. ●= 0.025M [Ni], y= $5.35xe^{-4}$+ $9.65e^{-7}$x, R^2=0.960. ●= 0.02M [Ni], y= $2.88e^{-4}$+ $6.82e^{-7}$x, R^2=0.978. ●= 0.015M [Ni], y= $2.07e^{-4}$+ $6.30e^{-7}$e, R^2=0.975. ●= 0.01M [Ni], y= $1.16e^{-4}$+ $4.45e^{-7}$x, R^2=0.962. ■ = 0.02 M [Ni] + 15 equiv MeCN, y= $2.88e^{-4}$ + $6.73e^{-7}$x, R^2= 0.966

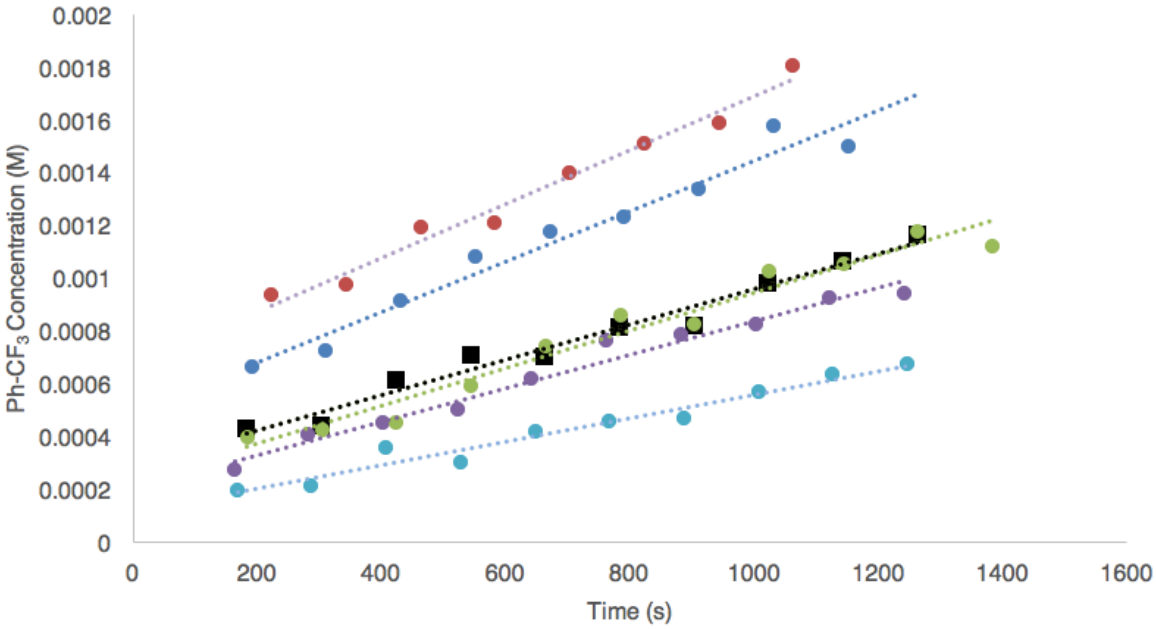

2.3.7 X-ray Structural Determination

Structure Determination of 1d

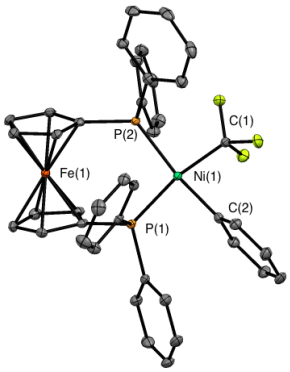

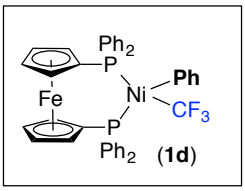

Orange prisms of **1d** were grown by diffusing pentane into a benzene solution of the compound at 22 deg. C. A crystal of dimensions 0.14 x 0.14 x 0.06 mm was mounted on a Rigaku AFC10K Saturn 944+ CCD-based X-ray diffractometer equipped with a low temperature device and Micromax-007HF Cu-target micro-focus rotating anode (= 1.54187 A) operated at 1.2 kW power (40 kV, 30 mA). The X-ray intensities were measured at 85(1) K with the detector placed at a distance 42.00 mm from the crystal. A total of 1187 images were collected with an oscillation width of 1.0 in The exposure time was 1 sec. for the low angle images, 7 sec. for high angle. The integration of the data yielded a total of 28539 reflections to a maximum 2 value of 136.48 of which 4983 were independent and 4936 were greater than 2 (I). The final cell constants (S2) were based on the xyz centroids 20327 reflections above 10 (I). Analysis of the data showed negligible decay during data collection; the data were processed with CrystalClear 2.0 and corrected for absorption. The structure was solved and refined with the Bruker SHELXTL (version 2008/4) software package, using the space group Pna2(1) with Z = 4 for the formula $C_{41}H_{33}F_3P_2FeNi$. All non-hydrogen atoms were refined anisotropically with the hydrogen atoms placed in idealized positions. Full matrix least-squares refinement based on F^2 converged at R1 = 0.0232 and wR2 = 0.0592 [based on I > 2sigma(I)], R1 = 0.0234 and wR2 = 0.0593 for all data. Additional details are presented in Table 1 and are given as Supporting Information in a CIF file. Acknowledgement is made for funding from NSF grant CHE-0840456 for X-ray instrumentation.

Table 2.4: X-ray Acquisition and Structural Parameters for 1d

Empirical Formula	$C_{41}H_{33}F_3FeNiP_2$
Formula Weight	759.17
Temperature	85(2) K
Wavelength	1.54178 A
Crystal System	Orthorhombic
Space Group	Pna2(1)
Unit Cell Dimensions	a = 17.6528(3) A alpha = 90 deg. b = 18.3170(13) A beta = 90 deg c = 10.4223(2) A gamma = 90 deg.
Volume	3370.0(3) A^3
Z	4
Calculated Density	1.496 Mg/m^3
Absorption Coefficient	5.427 mm^{-1}
F(000)	1560
Crystal Size	0.14 x 0.14 x 0.06 mm
Theta Range for Data Collection	3.48 to 68.24 deg
Limiting Indicies	$-21\leq h\leq 21$, $-22\leq k\leq 21$, $-12\leq l\leq 9$
Reflections Collected	28539
Independent Reflections	4983 [R(int) = 0.0499
Completeness to Theta	68.24 (100%)
Absorption Correction	Semi-empirical from equivalents
Max and Min Transmission	0.7366 and 0.5171
Refinement Method	Full-matrix least-squares on F^2
Data / Restraints / Parameters	4983 / 1 / 434
Goodness-of-Fit on F^2	1.014
Final R Indices [$l>2\sigma(l)$]	R1 = 0.0232, wR2 = 0.0592
R indices (all data)	R1 = 0.0234, wR2 = 0.0593
Largest Difference Peak and Hole	0.257 and -0.288 $e.A^{-3}$

Structure Determination of 1f

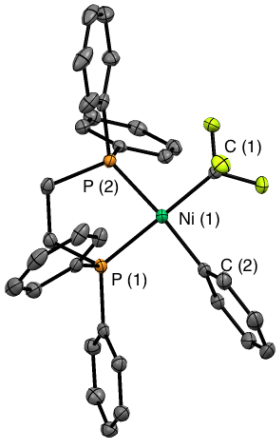

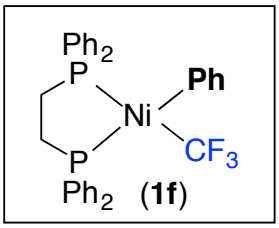

Yellow needles of **1f** were grown from a benzene/pentane solution of the compound at 22 deg. C. A crystal of dimensions 0.12 x 0.03 x 0.03 mm was mounted on a Rigaku AFC10K Saturn 944+ CCD-based X-ray diffractometer equipped with a low temperature device and Micromax-007HF Cu-target micro-focus rotating anode (= 1.54187 A) operated at 1.2 kW power (40 kV, 30 mA). The X-ray intensities were measured at 85(1) K with the detector placed at a distance 42.00 mm from the crystal. A total of 3905 images were collected with an oscillation width of 1.0 in The exposure time was 3 sec. for the low angle images, 15 sec. for high angle. The integration of the data yielded a total of 84803 reflections to a maximum 2 value of 136.48 of which 5927 were independent and 5462 were greater than 2 (I). The final cell constants (S7) were based on the xyz centroids 45870 reflections above 10 (I). Analysis of the data showed negligible decay during data collection; the data were processed with CrystalClear 2.0 and corrected for absorption. The structure was solved and refined with the Bruker SHELXTL (version 2008/4) software package, using the space group P2(1)/n with Z = 4 for the formula $C_{33}H_{29}F_3P_2Ni$, (C_6H_6). All non-hydrogen atoms were refined anisotropically with the hydrogen atoms placed in idealized positions. Full matrix least-squares refinement based on F^2 converged at R1 = 0.0380 and wR2 = 0.0969 [based on I > 2sigma(I)], R1 = 0.0403 and wR2 = 0.0982 for all data. Additional details are presented in Table 1 and are given as Supporting Information in a CIF file. Acknowledgement is made for funding from NSF grant CHE-0840456 for X-ray instrumentation.

Table 2.5: X-Ray Acquisition and Crystal Structural Parameters

Empirical Formula	$C_{39}H_{35}F_3NiP_2$
Formula Weight	681.32
Temperature	85(2) K
Wavelength	1.54178 A
Crystal System	Monoclinic
Space Group	P2(1)/n
Unit Cell Dimensions	a = 13.1224(2) A alpha = 90 deg. b = 19.8640(4) A beta = 112.916(8) deg. c = 13.4850(10) A gamma = 90 deg.
Volume	3237.6(3) A^3
Z	4
Calculated Density	1.398 Mg/m_3
Absorption Coefficient	2.167 mm^{-1}
F(000)	1416
Crystal Size	0.12 x 0.03 x 0.03 mm
Theta Range for Data Collection	3.99 to 68.24 deg
Limiting Indices	$-15\leq h\leq 15$, $-23\leq k\leq 23$, $-16\leq l\leq 16$
Reflections Collected	84803
Independent Reflections	5927 [R(int) = 0.0571]
Completeness to Theta	68.24 (100%)
Absorption Correction	Semi-empirical from equivalents
Max and Min Transmission	0.9378 and 0.7810
Refinement Method	Full-matrix least-squares on F^2
Data / Restraints / Parameters	5927 / 0 / 406
Goodness-of-Fit on F^2	1.149
Final R Indices [$l>2\sigma(l)$]	R1 = 0.0380, wR2 = 0.0969
R indices (all data)	R1 = 0.0403, wR2 = 0.0982
Largest Difference Peak and Hole	0.405 and -0.417 $e.A^{-3}$

Structure Determination of 6

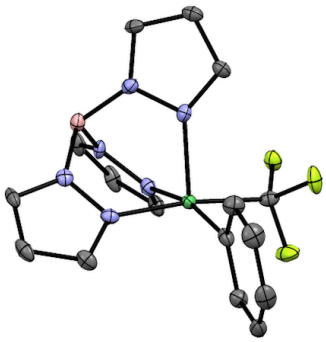

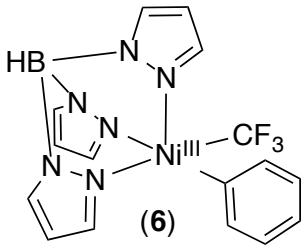

(**6**)

Green block-like crystals of **6** were grown from a diisopropyl ether/pentane solution of the compound at –35 ºC. A crystal of dimensions 0.20 x 0.18 x 0.18 mm was mounted on a Rigaku AFC10K Saturn 944+ CCD-based X-ray diffractometer equipped with a low temperature device and Micromax-007HF Cu-target micro-focus rotating anode (λ = 1.54187 A) operated at 1.2 kW power (40 kV, 30 mA). The X-ray intensities were measured at 85(1) K with the detector placed at a distance 42.00 mm from the crystal. A total of 2028 images were collected with an oscillation width of 1.0° in ω. The exposure times were 1 sec. for the low angle images, 6 sec. for high angle. The integration of the data yielded a total of 51388 reflections to a maximum 2θ value of 136.45° of which 6411 were independent and 6372 were greater than 2σ(I). The final cell constants (Table S19) were based on the xyz centroids 42847 reflections above 10σ(I). Analysis of the data showed negligible decay during data collection; the data were processed with CrystalClear 2.0 and corrected for absorption. The structure was solved and refined with the Bruker SHELXTL (version 2014/6) software package, using the space group Pca2(1) with Z = 8 for the formula $C_{16}H_{15}BN_6F_3Ni$. All non-hydrogen atoms were refined anisotropically with the hydrogen atoms placed in both idealized and refined positions. The structure was refined as a two-component inversion twin. Full matrix least-squares refinement based on F^2 converged at R1 = 0.0440 and wR2 = 0.1094 [based on I > 2sigma(I)], R1 = 0.0442 and wR2 = 0.1096 for all data. Additional details are presented in Table S18 and are given as Supporting Information in a CIF file. Acknowledgement is made for funding from NSF grant CHE-0840456 for X-ray instrumentation.

Table 2.6. Crystal Data and Structural Refinement for **6**

Empirical Formula	$C_{16}H_{15}BF_3N_6Ni$
Formula Weight	417.86
Temperature	85(2) K
Wavelength	1.54178 A
Crystal System	Orthorhombic
Space Group	PCa2(1)
Unit Cell Dimensions	a = 20.4982(1) A alpha = 90 deg. b =10.1199(13) A beta = 90 deg c = 17.0418(2) A gamma = 90 deg.
Volume	3535.1(1) A^3
Z	8
Calculated Density	1.570 Mg/m^3
Absorption Coefficient	1.987 mm^{-1}
F(000)	1704
Crystal Size	0.20 x 0.18 x 0.18 mm
Theta Range for Data Collection	4.314 to 68.223 deg
Limiting Indicies	$-24\leq h\leq 24$, $-10\leq k\leq 11$, $-20\leq l\leq 20$
Reflections Collected	51388
Independent Reflections	6411 [R(int) = 0.0463]
Completeness to Theta	67.679 /99.6
Absorption Correction	Semi-empirical from equivalents
Max and Min Transmission	0.7366 and 0.6464
Refinement Method	Full-matrix least-squares on F^2
Data / Restraints / Parameters	6411 / 1 / 497
Goodness-of-Fit on F^2	1.063
Final R Indices [$I>2\sigma(I)$]	R1 = 0.0440, wR2 = 0.1094
R indices (all data)	R1 = 0.0442, wR2 = 0.1096
Largest Difference Peak and Hole	1.550 and -0.670 $e.A^{-3}$

Structure Determination of 6–PMe_3

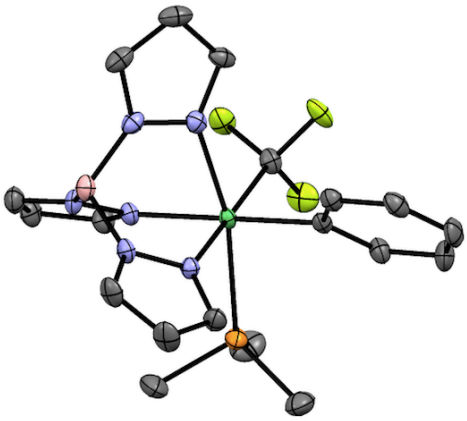

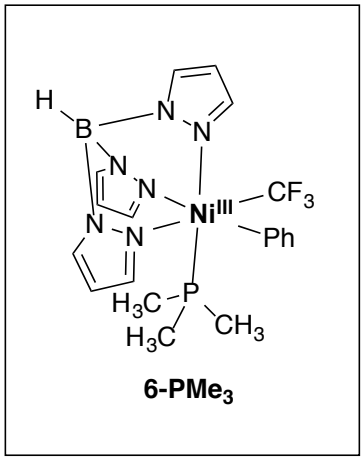

6-PMe_3

Blue needles of **6-PMe_3** were grown from a diisopropyl ether/pentane (net 0.04 M PMe_3) solution of **6** at –35 ºC. A crystal of dimensions 0.15 x 0.02 x 0.02 mm was mounted on a Rigaku AFC10K Saturn 944+ CCD-based X-ray diffractometer equipped with a low temperature device and Micromax-007HF Cu-target micro-focus rotating anode (λ = 1.54187 A) operated at 1.2 kW power (40 kV, 30 mA). The X-ray intensities were measured at 85(1) K with the detector placed at a distance 42.00 mm from the crystal. A total of 2028 images were collected with an oscillation width of 1.0 in ω The exposure times were 1 sec. for the low angle images, 8 sec. for high angle. Rigaku d*trek images were exported to CrysAlisPro for processing and corrected for absorption. The integration of the data yielded a total of 17165 reflections to a maximum 2θ value of 138.53° of which 3360 were independent and 3337 were greater than 2σ(I). The final cell constants (Table S25) were based on the xyz centroids 11867 reflections above 10σ(I). Analysis of the data showed negligible decay during data collection. The structure was solved and refined with the Bruker SHELXTL (version 2014/6) software package, using the space group Cc with Z = 4 for the formula $C_{19}H_{24}BF_3N_6PNi$. All non-hydrogen atoms were refined anisotropically with the hydrogen atoms placed in a combination of idealized and refined positions. Full matrix least-squares refinement based on F^2 converged at R1 = 0.0264 and wR2 = 0.0667 [based on I > 2sigma(I)], R1 = 0.0269 and wR2 = 0.0670 for all data. Additional details are presented in Table S25 and are given as Supporting Information in a CIF file. Acknowledgement is made for funding from NSF grant CHE-0840456 for X-ray instrumentation.

Table 2.7. Crystal Data and Structural Refinement for **6-PMe_3**

Empirical Formula	$C_{19}H_{24}BF_3N_6NiP$
Formula Weight	493.20
Temperature	85(2) K
Wavelength	1.54184 A
Crystal System	Monoclinic
Space Group	Cc
Unit Cell Dimensions	a = 8.50891(8)A alpha = 90º b =17.83577 (13) A beta = 100.4640(9)º c = 15.13048(14) A gamma = 90º
Volume	2258.06 (1) A^3
Z	4
Calculated Density	1.453 Mg/m^3
Absorption Coefficient	2.292 mm^{-1}
F(000)	1020
Crystal Size	0.15 x 0.20 x 0.20 mm
Theta Range for Data Collection	4.959 to 69.266º
Limiting Indicies	$-24\leq h\leq 24$, $-10\leq k\leq 11$, $-20\leq l\leq 20$
Reflections Collected	17165
Independent Reflections	3360[R(int) = 0.0610]
Completeness to Theta	67.684 /98.2
Absorption Correction	Semi-empirical from equivalents
Max and Min Transmission	0.7366 and 0.6464
Refinement Method	Full-matrix least-squares on F^2
Data / Restraints / Parameters	6411 / 1 / 497
Goodness-of-Fit on F^2	1.047
Final R Indices [$l>2\sigma(l)$]	R1 = 0.0264, wR2 = 0.0667
R indices (all data)	R1 = 0.0269, wR2 = 0.0670
Largest Difference Peak and Hole	0.250and -0.221A^{-3}

2.4. References and Notes

[1] a) Müller, K.; Faeh, C.; Diederich, F. *Science* **2007**, *317*, 1881. (b) Hagmann, W. K. *J. Med. Chem.* **2008**, *51*, 4359. (c) Schlosser, M. *Angew. Chem. Int. Ed.* **2006**, *45*, 5432. (d) Yale, H. L. *J. Med. Pharm. Chem*. **1958**, *1*, 121. (e) Kobyashi, Y.; Kumadaki, I. *Acc. Chem. Res.* **1978**, *11*, 197. (f) Holmes, S. A.; Thomas, T. D. *J. Am. Chem. Soc.* **1975**, *97*, 2337.

[2] (a) Tomashenko, O. A.; Grushin, V. V. *Chem. Rev.* **2011**, *111*, 4475. (b) Furuya, T.; Kamlet, A. S.; Ritter, T. *Nature* **2011**, 473, 470. (c) Grushin, V. V. *Acc. Chem. Res.* **2010**, *43*, 160. (d) Ye, Y.; Sanford, M. S. *Synlett* **2012**, *23,* 2005.

[3] Select examples: (a) Morimoto, H.; Tsubogo, T.; Litvinas, L.; Hartwig, J. F. *Angew. Chem. Int. Ed.* **2011**, *50*, 3793. (b) Novák, P.; Lishchynskyi, A.; Grushin, V. V. *Angew. Chem. Int. Ed*. **2012**, *51*, 7767. (c) Ye, Y.; Lee, S. H.; Sanford, M. S. *Org. Lett.* **2011**, *13*, 5464. (d) Shang, M.; Sun, S.-Z.; Wang, H.-L.; Laforteza, B. N.; Dai, H.-X.; Yu, J.-Q. *Angew. Chem. Int. Ed.* **2014**, *53*, 10439. (e) Winston, M. S.; Wolf, W.J.; Toste, F. D.; *J. Am. Chem. Soc.* **2014**, *136*, 7777.

[4] Grushin, V. V.; Marshall, W. J. *J. Am. Chem. Soc.* **2006**, *128*, 12644.

[5] Cho, E. J.; Senecal, T. D.; Kinzel, T.; Zhang, Y.; Watson, D. A.; Buchwald, S. L. *Science* **2010**, *328*, 1679.

[6] Nickel is approximately 1/2,000th the cost of palladium per mole: Tasker, S. Z.; Standley, E. A.; Jamison, T. F. *Nature* **2014**, *509*, 299.

[7] Montgomery, J.; Lipschutz, B. H. *Ed.* Organonickel chemistry. *Organometallics in Synthesis, Fourth Manual.* Wiley: Hoboken, NJ, 2013; pp 322-414.

[8] Dubinina, G. G.; Brennessel, W. W.; Miller, J. L.; Vicic, D. A. *Organometallics* **2008**, *27*, 3933.

[9] Jover, J.; Miloserdov, F. M.; Benet-Buchholz, J.; Grushin, V. V.; Maseras, F. *Organometallics* **2014**, *33*, 6531.

[10] Tasker, S. Z.; Standley, E. A.; Jamison T. J. *Nature* 2014, 509, 299

[11] Maleckis, A.; Sanford, M. S.; *Organometallics* **2014**, *33*, 3381.

[12] A complex mixture of inorganic products was formed, but $PhCF_3$ was not detected.

[13] Griffin, K. A.; Pua, L. A.; Piortrakowski, S.; Gabidullin, B. A.; Korobkov, I.; Hughes, R. P.; Baker, R. T *J. Am. Chem. Soc.* **2017**, *139*, 4075

[14] Similar results were obtained when the reaction was conducted in the presence of 1 equiv of exogenous Xantphos

[15] Han, R.; Hillhouse, G. L. J. Am. Chem. Soc. **1997**, *119*, 8135.

[16] Standley, E. A.; Smith, S. J.; Müeller, P.; Jamison, T. F. *Organometallics* **2014**, *33*, 2012.

[17]The *cis*-geometry predominated for **1d** in all solvents examined (C_6D_6, CD_3CN, and acetone-d_6).

[18] van Leeuwen, P. W. N. M.; Kamer, P. C. J.; Reek, J. N. H.; Dierkes, P. *Chem. Rev*. **2000**, *100*, 2741.

[19] Gramlich, V.; Consiglio, G. *Helv. Chim. Acta,* **1979,** 62, 1016

[20] Grushin, V. V.; Marshall, W. J. *J. Am. Chem. Soc.* **2006**, *128*, 12644.

[21] Zhang, C. P.; Wang, H.; Klein, A.; Biewer, C.; Stimat, K.; Yamaguchi, Y.; Xu, L.; Gomez-Benitez, V.; Vicic, D. A. *J. Am. Chem. Soc.* **2013**, *135*, 8141.

[22] Bour, J. R.; Camasso, N. M.; Meucci, E. M.; Kampf, J. W.; Canty, A. J. Sanford, M. S. *J. Am. Chem. Soc.* **2016**, *138*, 16105.

[23] Desrochers, P. J.; Corken, A. L.; Tarka, A. M.; Besel, B. M.; Mangum, E. E.; Linz, T. N *Inorganic Chemistry,* **2009***, 48*, 3535.

[24] Han, R.; Hillhouse, G. L. *J. Am. Chem. Soc.* **1997**, *119*, 8135.

[25] Alternatively, a CF_3 ligand could be transferred directly from 1 equiv of **2e** to a second equiv of **2e** to form **4**, without the intermediacy of F_3C•.
[26] Shi, G.; Shao, C.; Pan, S.; Yu, J.; Zhang, Y. *Org. Lett.* **2015**, *17*, 38.
[27] The wide peak-to-peak separation of 856 mV is likely due to an electron-transfer chemical (EC) reaction mechanism, wherein oxidation to Ni^{IV} triggers the association of a solvent molecule to form a more stable octahedral product.
[28] Notably, $NOBF_4$ was very recently used by Mirica for converting organometallic Ni^{III} complexes to their Ni^{IV} analogues see: Schultz, J. W.; Fuchigami, K.; Zheng, B.; Rath, N. P.; Mirica, L. M. *J. Am. Chem. Soc*. **2016**, *138*, 12928.
[29] The initial rates studies were conducted in benzene rather than MeCN because the reaction affords comparable yield (54%) in benzene but is cleaner (ie, affords fewer minor side products). The addition of 15 equiv of MeCN to the reaction of **6** in benzene had no discernable impact on the initial rate of this reaction (rate = $7.13x10^{-7}$ s^{-1} without MeCN and $6.73x10^{-7}$ s^{-1} with MeCN at 0.2 M concentration of **6**).
[30] We are unable to rule out a mechanism wherein a rate determining ligand dissociation precedes disproportionation. However, the >50% yield observed at high temperature and the absence of **6** in the reaction mixture are inconsistent with this pathway.
[31] (a) Mann, G.; Shelby, Q.; Roy, A. H.; Hartwig, J. F. *Organometallics* **2003**, *22*, 2775. (b) Mann, G.; Baranano, D.; Hartwig, J. F.; Rheingold, A. L.; Guzei, I. A. *J. Am. Chem. Soc.* **1998**, *120*, 9205. (c) Pérez-Temprano, M. H.; Racowski, J. M. Kampf, J. W.; Sanford, M. S. *J. Am. Chem. Soc.* **2014**, *136,* 4097. (d) Racowski, J. M.; Dick, A. R.; Sanford, M. S. *J. Am. Chem. Soc.* **2009**, *131*, 10974.
[32] Connelly, N. G.; Geiger, W. E. *Chem. Rev.* **1996**, *96*, 877

CHAPTER 3

Elementary Organometallic Reactions Relevant to Ni(II)/(IV) Catalysis

3.1. Introduction

Over the past decade, nickel-catalyzed cross-coupling has emerged as an attractive method for a variety of carbon-carbon and carbon-heteroatom bond-forming reactions.[1] The mechanisms of these transformations are generally proposed to involve sequences of $1e^-$ and $2e^-$ redox events that interconvert Ni^0, Ni^I, Ni^{II} and/or Ni^{III} intermediates.[1,2] In contrast, organometallic Ni^{IV} intermediates are rarely invoked in cross-coupling reactions. This is largely due to Kochi's pioneering mechanistic studies that implicated Ni^I and Ni^{III}-aryl intermediates in Ni-mediated carbon-carbon bond-forming processes.[2b,c]

As the field of homogeneous nickel catalysis has matured, a growing number of experimental[3] and theoretical[4] reports have concluded against Kochi-type mechanisms in favor of $Ni^{II/IV}$ redox cycling. In 2014 Chatani suggested that the Ni-catalyzed C–H arylation reactions of quinolinyl amides with diaryliodonium electrophiles proceeds via Ni^{IV}(σ-alkyl)(σ-aryl) intermediates from which $2e^-$ C–C coupling occurs (Scheme 3.1).[3a] While these putative Ni^{IV} species were not detected directly, radical trapping experiments provided evidence against the involvement of single electron pathways. This proposal was recently supported by thorough DFT analyses comparing $Ni^{I/III}$ mechanisms to $Ni^{II/IV}$ mechanisms with a variety of electrophiles.[4] Despite these extensive theoretical analyses clearly implicating Ni^{IV} intermediates, there is still little experimental precedent for the feasibility of these elementary

organometallic reactions under controlled conditions. Furthermore, the mechanistic details of these steps are essentially unknown.

Scheme 3.1 (a) General reaction scheme of the nickel catalyzed functionalization of quinolinyl amides and (b) the proposed key redox steps of this transformation

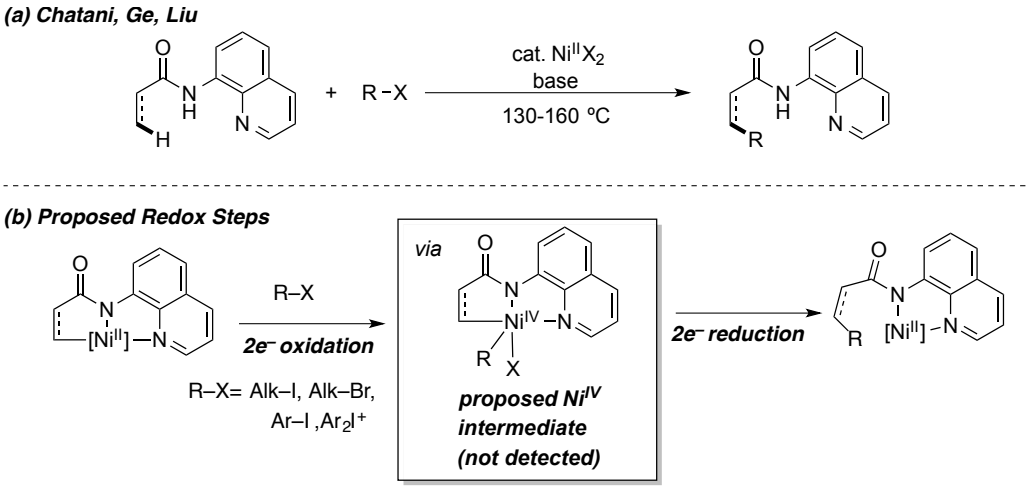

More recently, Punji and coworkers proposed that alkyl iodides react with $(N^3)Ni^{II}(Ar)$ complexes to form diorganonickel(IV) intermediates through a stepwise radical oxidative addition mechanism (Scheme 3.2).[3h] This proposal was made on the basis of radical trapping studies, stoichiometric reactions of $Ni^{II}(Ar)$ intermediates, and DFT studies. Though C–C coupling from organonicke(III) intermediates was not explicitly ruled out, the DFT studies support the kinetic feasibility of this $Ni^{II/III/IV}$ oxidation. However, like Chatani's report, the proposed Ni^{IV} intermediates proved too fleeting for detailed studies or even detection.

Scheme 3.2 (a) The nickel catalyzed alkylation of benzothiazoles (b) the proposed oxidation mechanism for the formation of Ni^{IV}

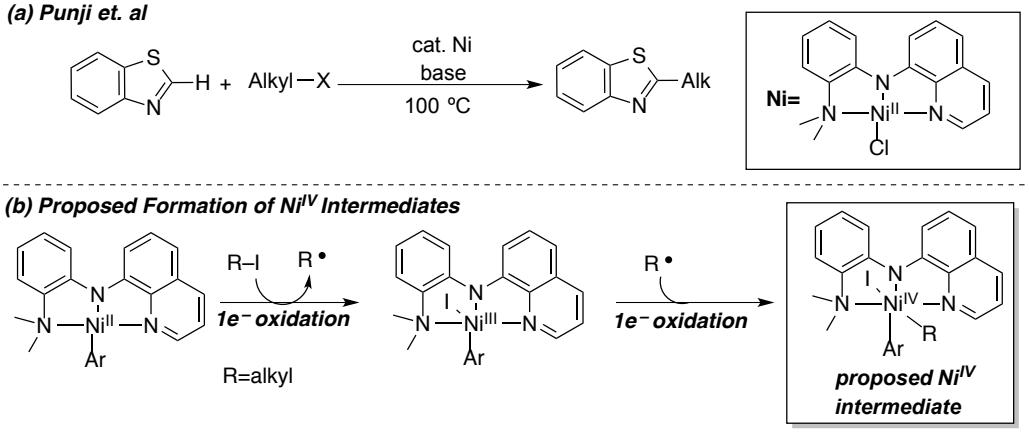

These proposals raise questions about reactions leading to the formation of and subsequent reactivity of Ni^{IV} intermediates in catalytic transformations. Importantly, if such Ni^{IV} intermediates are accessible, then they are likely to exhibit complementary reactivity profiles compared to their lower valent Ni counterparts.[5] A detailed understanding of the conditions for the generation and bond-forming reactivity of Ni^{IV} is therefore imperative for the hypothesis-driven development of new catalytic methods. This chapter describes the design and reactivity of model systems to explore the feasibility and mechanisms elementary reactions relevant to $Ni^{II/IV}$ catalysis. Specifically, we study the (1) net $2e^-$ oxidation of Ni^{II} to Ni^{IV} with carbon-based electrophiles and (2) the bond-forming $2e^-$ reduction of the resultant Ni^{IV} centers.

3.2. Results and Discussion

3.2.1. Model System Design Considerations

Our initial studies focused on designing an organometallic model system that would enable us to answer two key questions: (1) Can carbon-based electrophiles effect the $2e^-$ oxidation (excluding CF_3^+ reagents) of Ni^{II} precursors to Ni^{IV} products? and (2) What is the bond-forming reactivity of the putative Ni^{IV}(alkyl/aryl) complexes? To address these questions, we sought to identify an organometallic Ni^{II} precursor that would yield a detectable and ideally isolable Ni^{IV}(alkyl/aryl) species following a reaction with an alkyl/aryl electrophile. A recent report from our group has shown that organometallic Ni^{IV} complexes can be prepared by the oxidation of Ni^{II} starting materials with electrophilic trifluoromethylating reagents (CF_3^+ in Scheme 3.3a).[6] Both the facial tridentate ligand trispyrazolylborate (Tp) and the trifluoromethyl ligand were found to stabilize the Ni^{IV} product **1**. Notably, under no circumstances was the CF_3 ligand found to participate in C–C coupling; instead, completely selective elimination of 2,2-dimethylbenzocyclobutane was observed. The high selectivity for C(sp3)–C(sp2) coupling to generate a four-membered ring over C($sp^{2/3}$)–CF_3 elimination

suggests that CF_3 ligands are slow to participate in reductive elimination reactions . We hypothesized that we could leverage this sluggish reactivity to attenuate the traditionally fast reductive decomposition of organonickel(IV) complexes. Thus, in the current study we targeted Ni^{IV}-(alkyl/aryl) complexes of general form $TpNi^{IV}(CF_3)_2$(alky/aryl) (2) through the reaction of a carbon-based electrophile with $TpNi^{II}(CF_3)_2$ (3) (Scheme 3.3b). These stable non-cyclometalated Ni^{IV} complexes provide an excellent platform to study challenging C–C and C–X coupling reactions.

Scheme 3.3 (a) Camasso and Sanford's CF_3-stabilized nickelacycleneophyl Ni^{IV} complex[6] (b) a new model system to enable the proposed studies.

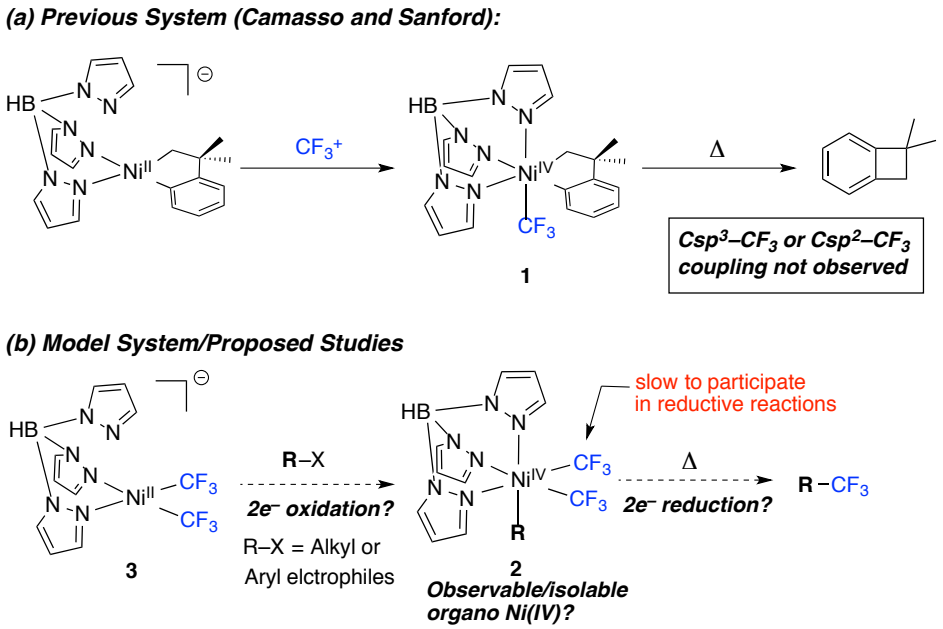

3.2.2. Net $2e^-$ oxidation of Ni^{II} to Ni^{IV} with Carbon-Based Electrophiles

Oxidation with Aryl Electrophiles

The Ni^{II} starting material $NBu_4[TpNi^{II}(CF_3)_2]$ **(3)**[7] was prepared in 94% isolated yield by the reaction of NBu_4Tp with $(MeCN)_2Ni^{II}(CF_3)_2$. No reaction was observed upon the treatment of **3** with phenyl iodide, phenyl bromide, or phenyl triflate, even after heating at 70 ºC for 12 h. When heated under more forcing conditions (12h at 120 ºC), **3** decomposed with no evidence for the formation of a Ni^{IV} intermediate. However, **3** rapidly reacted with the more electrophilic arylating reagents Ph_2IBF_4 and PhN_2BF_4 to yield a new diamagnetic complex

consistent with a [Ni^{IV}–CF_3] species in 77% and 42% respectively (Scheme 3.4). Purification of the crude residue by silica column chromatography and characterization by NMR spectroscopy, elemental analysis and single crystal X-ray diffraction confirmed the suspected formal $2e^-$ oxidation product $TpNi^{IV}(CF_3)_2Ph$ (**2a**). Notably, Ph_2IBF_4 and PhN_2BF_4 reacted with **3** at or below room temperature and is stable up to 45ºC, at which point it slowly eliminates Ph–CF_3. This reaction is discussed in greater detail below. These results demonstrate for the first time that $Ni^{II/IV}$ manifolds are accessible under thermally mild conditions with strong aryl electrophiles. Mechanistic details of this transformation will be discussed later.

Scheme 3.4 Electrophile scope in the $2e^-$ Oxidation of **3** to **2a**

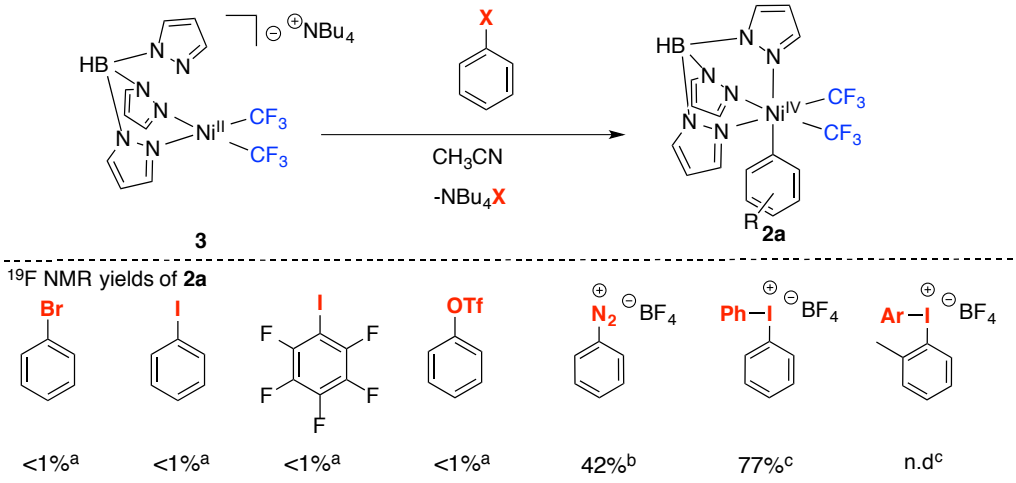

Figure 3.1 X-ray crystal structure of **2a**. Thermal ellipsoids are drawn at 50% probability. The hydrogen atoms and rotational disorder of the CF_3 ligands have been removed for clarity.

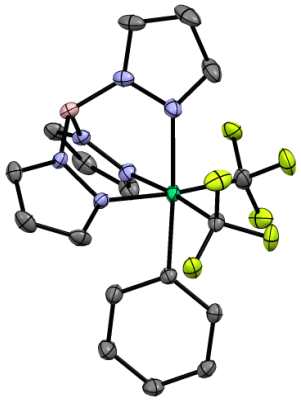

We next sought to address the missing 23-58% nickel mass balance in the reaction of **3** with Ph_2IBF_4 or PhN_2BF_4. Analysis of the crude reaction mixture by ^1H and ^{19}F NMR of **3**

with Ph_2IBF_4 showed relatively clean formation of **2a** with no evidence for significant quantities of other diamagnetic nickel complexes. The ^{11}B NMR, however, showed the formation of **2a** and an unknown compound, presumably a paramagnetic [TpNi] complex. Purification of this compound by silica column chromatography and subsequent characterization by EPR, elemental analysis, and single crystal X-ray diffraction revealed the unknown to be $TpNi^{III}(CF_3)_2(MeCN)$ (**4**, 15-30% isolated) (Scheme 3.2a).

Figure 3.2 (a) Experimental (bottom/blue) and simulated (top/red) EPR spectrum of **4** fit using the following parameters G_x=2.18, G_y=2.15, G_z= 2.00 A_N(N)= 21G, $A_{N'}$(N')= 18G. (b) X-ray crystal structure of **4**. The thermal ellipsoids are drawn at 50% probability and the hydrogens have been omitted for clarity.

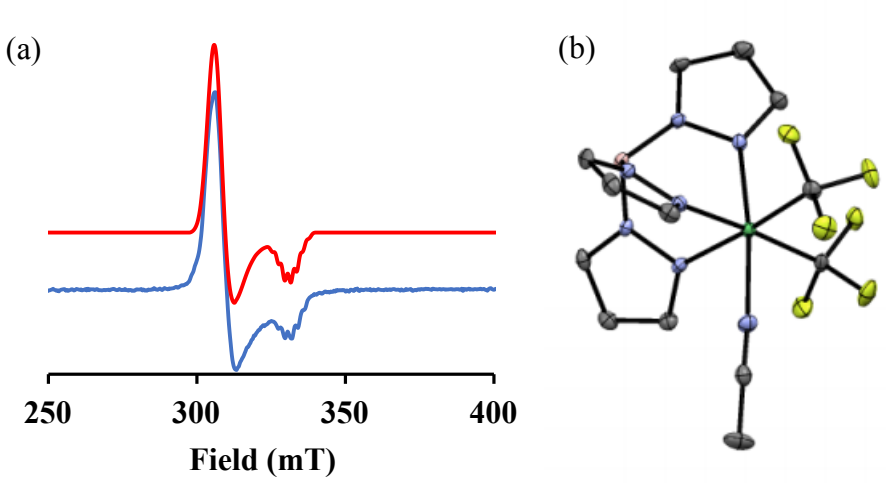

Mechanistic Aspects of the 2e Oxidation of 3 to 2a with Ph_2IBF_4 and PhN_2BF_4

The above results initially seem to provide experimental support Chatani's proposed concerted $2e^-$ oxidation of Ni^{II} with diaryliodonium salts. However, the formation a Ni^{III} complex as a significant side product in both reactions raises questions about oxidation mechanism leading to the formation of **2a**. Namely, it is unclear if **4** is formed through a mechanistically unrelated side reaction, or if it is an arrested intermediate in the formation of **2a**. Moreover, it is well-established that diaryliodoniums can act as 1 or $2e^-$ electron oxidants.[8] Thus the formation of **2a** may be more complicated than the concerted $2e^-$ Chatani-type oxidation. Scheme 3.6 shows two potential mechanisms that could lead to **2a** from **3**. In

mechanism A, **2a** is generated through the concerted $2e^-$ oxidation of **3**. The formation of the observed Ni^{III} product (**4**) would therefore be mechanistically unrelated to the generation of **2a**. Mechanism B depicts an initial single electron transfer from nickel to the oxidant, fragmentation to generate an aryl radical, which then combines with the resultant Ni^{III} center. In this regime, inefficient radical capture by a nickel center would explain the significant quantities of **4**.

Scheme 3.5 Potential oxidation mechanisms for the formation of **2a**

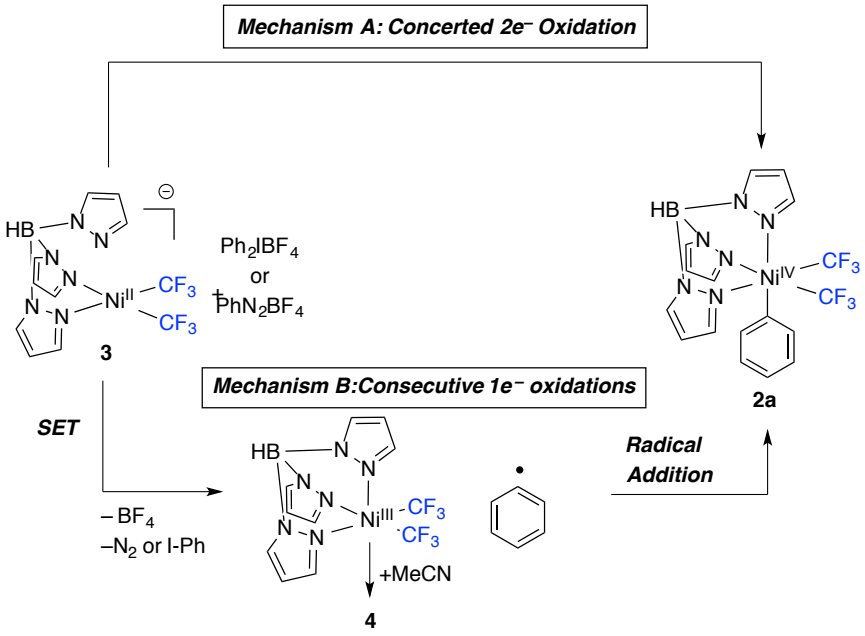

A key distinguishing feature between Mechanisms A and B is the presence of free carbon-centered radicals. Thus the detection of aryl radical would strongly implicated Mechanism B. Treatment of **3** with $(4\text{-F-Ph})_2IBF_4$ (for convenient monitoring by ^{19}F NMR) in the presence of 3 equivalents of (2,2,6,6-tetramethylpiperidinyl-yl)oxyl free radical (TEMPO) resulted in significantly lower yields relative to the analogous reactions run in the absence of a radical trap (Scheme 3.7) Importantly, TEMPO does not observably react with the oxidants or the nickel complex on the time scale of the reaction.

Scheme 3.6 Radical trapping experiments in the oxidation of **3** with an Ar_2IBF_4 Salt

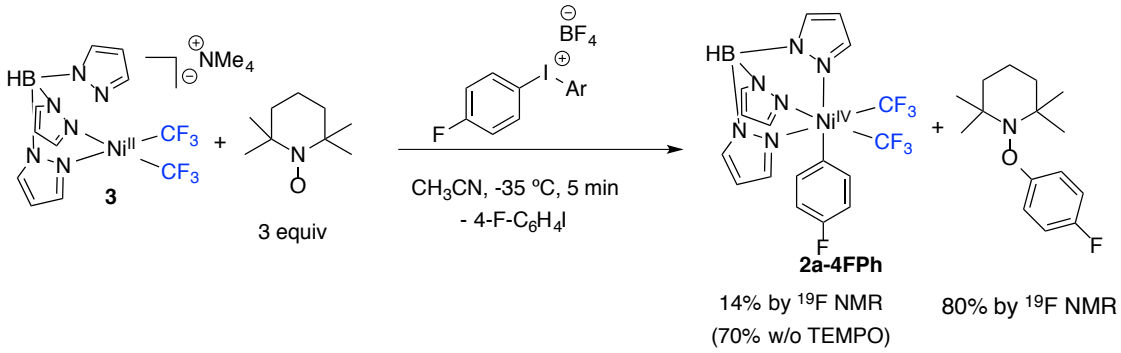

To further corroborate the intermediacy of aryl radicals, we next conducted the oxidation reactions in neat THF. Aryl radicals are known to efficiently abstract H atoms from THF at rates upwards of 10^6 $M^{-1}s^{-1}$. In this way THF could serve as an aryl radical trap that is otherwise unlikely to interfere with other intermediates generated in the course of the reactions. Indeed the reaction of **3** with $(4\text{-F-Ph})_2IBF_4$ or $(4\text{-F-Ph})N_2BF_4$ in THF did not yield detectable quantities of the Ni(IV) product (**2a-4FPh**) despite the full consumption of the starting material (Scheme 3.8). Instead, the product of H atom abstraction, Ph–F ,was observed in ~70% yield by ^{19}F NMR. We note that the successful formation of **2a** is not exclusive to CH_3CN. High yields of **2a** were also noted in CD_3NO_2. When taken together with the TEMPO radical trapping experiments, these results strongly implicate the intermediacy of aryl radicals in this reaction and thus Mechanism B.

Scheme 3.7. Radical trapping experiment in the oxidation of **3** with an Ar_2IBF_4 Salt in THF

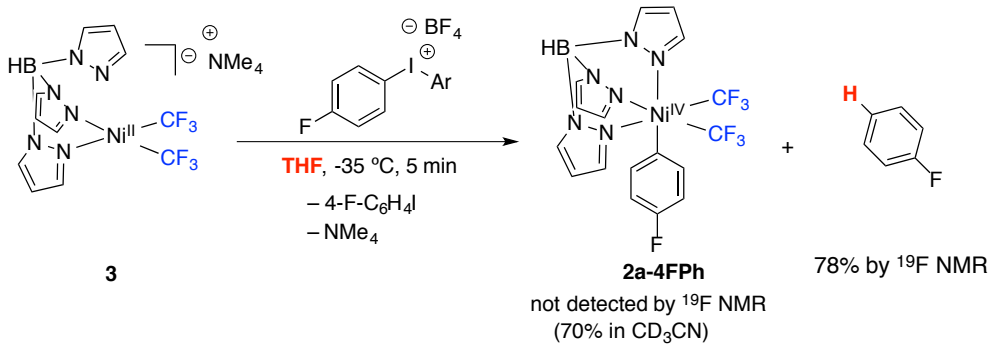

Extension to a Catalytically Relevant Ligand

In a final set of experiments, we examined whether the observed net $2e^-$ oxidation is limited to Tp-ligated complexes or if these results could be extended to ligands more commonly employed in catalysis. We chose the bidentate ligand 4,4'-di-*tert*-butylbipyridine (dtbpy) for these studies due to its abundant use in C–C and C–heteroatom coupling reactions. When dtbpy-supported Ni^{II} complex **5** was mixed with 1.5 equiv of Ph_2IBF_4 no reaction was observed over the course of 24 h. However, when **5** was stirred with the stronger aryl electrophile, PhN_2BF_4, benzotrifluoride was observed in 67% yield after 10 minutes as determined by ^{19}F NMR spectroscopy (Scheme 3.9a). Monitoring this reaction by ^{19}F NMR spectroscopy at –25 ºC showed the presence of a transient diamagnetic [Ni–CF_3] complex.[9] The ^{19}F NMR resonances associated with this intermediate (a pair of quartets at –19.8 and –23.8 ppm, J_{FF} = 7.9 Hz; Scheme 3.10) are consistent with an unsymmetrical Ni^{IV} bis-trifluoromethyl complex of general structure **6**. The decay of intermediate **6** was accompanied by growth of the resonance associated with benzotrifluoride. As further support of the proposed structure, the same intermediate was observed upon treatment of (dtbpy)Ni(CF_3)(Ph) (**7**) with the CF_3^+ reagent TDTT (Scheme 3.9b). Overall, these results strongly suggest that even with electron withdrawing CF_3 ligands, organometallic Ni^{IV} complexes are accessible under mild conditions using catalytically relevant bidentate nitrogen donor ligands.

Scheme 3.8. In-situ generation of **6** from (dtbpy)Ni^{II} Precursors (**5** and **7**) at low temperature

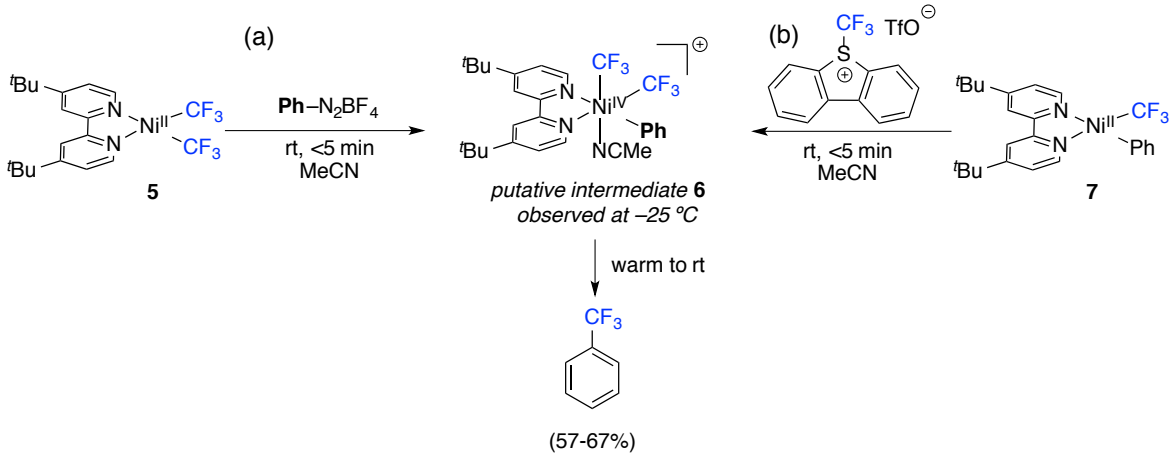

Scheme 3.9 ^{19}F NMR spectrum of **6** at -25 ºC showing non-equivalent CF_3 resonances

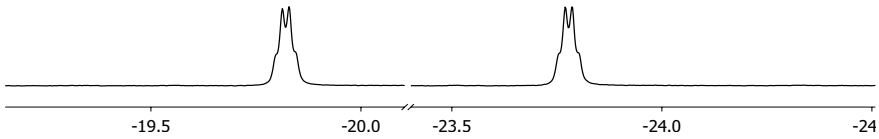

Oxidation with Alkyl Electrophiles

In parallel with our studies of the $2e^-$ oxidation of **3** with aryl electrophiles we also investigated analogous reactivity with alkyl electrophiles. These investigations also targeted compounds of general structure $TpNi(CF_3)_2(alkyl)$ (**2**) due to the anticipated stability of the oxidation products. Well-defined examples $C(sp^3)–CF_3$ of reductive elimination from low or high-valent metal centers are exceedingly rare. The ostensibly high kinetic barrier to this process is accordingly expected to stabilize the oxidation products of these reactions. We next sought to probe the feasibility of the $2e^-$ oxidation of **3** with alkyl electrophiles.

Our initial experiments focused on the oxidation of **3** with methyl electrophiles because they are among the most electrophilic carbon electrophiles, have minimal steric bulk, and the resulting $Ni^{IV}–CH_3$ complex would be inert to complications associated with β-eliminations. To this end, **3** was treated with 5 equiv of Me–I in CD_3CN at room temperature. After 30 minutes the reaction had yielded partial conversion (~10%) of the Ni^{II} starting material to a mixture of compounds most consistent with other $[Ni^{II}(CF_3)_2]$ complexes as determined by ^{19}F NMR spectroscopy. Additional heating at 50 ºC resulted in complex decomposition and the formation of insoluble particulates. During the course of this reaction no detectable Ni^{IV} intermediates were observed.

Scheme 3.10 Reactivity of **3** with methyl electrophiles

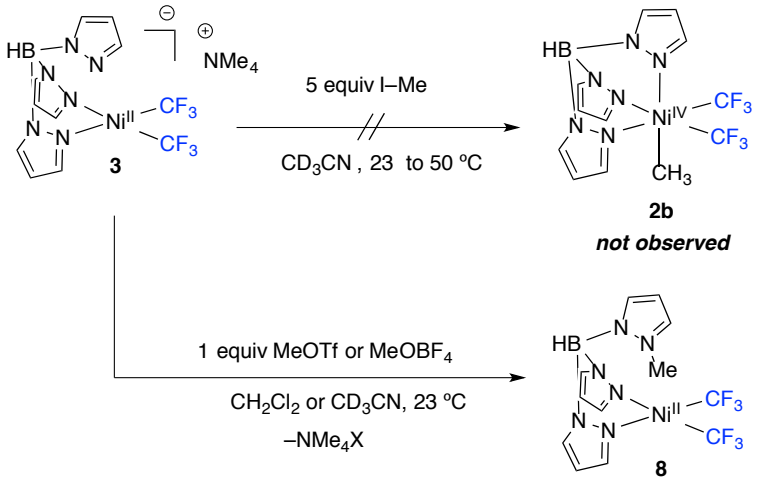

The CH_3 ligand on the product Ni^{IV} complex $TpNi^{IV}(CF_3)_2(CH_3)$ is expected to be highly electrophilic; thus the oxidation using Me–I may therefore be thermodynamically unfavorable. The addition of the stronger methylating agents, MeOTf or Me_3OBF_4, to **3** in CH_3CN resulted in the immediate formation of a new diamagnetic nickel complex with full consumption of both starting materials. However, the ^{19}F NMR spectrum of this compound was inconsistent with a Ni^{IV} complex. Additional long-range $^{13}C/^{19}F$ correlational experiments confirmed that the methylation did not occur at nickel, rather the free pyrazole arm of the Tp ligand was methylated to yield Ni^{II} complex **8**.

Radical Relay Oxidation of Ni^{II} to Ni^{IV}

The unexpectedly sluggish and poorly selective reactivity of Me–I, an otherwise highly reactive electrophile, with **3** was an unanticipated challenge in our studies. We had originally hypothesized that the largest barrier facing the unambiguous observation of a Ni^{II} to Ni^{IV} oxidation would be the stability of the Ni^{IV} product rather than the reactivity of the Ni^{II} starting material. As such, our initial design focused on the generation of product Ni^{IV} complexes bearing CF_3 ligands which are inductively withdrawing but reductively inert(thus stabilizing oxidized metal centers). However, our oxidation studies also suggest that this key design element comes at a steep cost; the electronic withdrawing nature of these ligands renders the

$[Ni^{II}(CF_3)_2]$ starting complexes inert to all but the strongest carbon-based electrophiles (i.e. Ph_2I^+ and ArN_2^+) at room temperature. This does not necessarily imply that **3** is any less reducing than Ni^{II} intermediates formed in catalysis.[10] Catalytic reactions proposed to go through $Ni^{II/IV}$ redox cycles are almost categorically performed at high temperatures. Thus it may very well be the case, if not likely, that alkyl iodides react with **3** to generate high-valent nickel products at temperatures more compatible with catalysis (+100 ºC). However, reactions at these temperatures are unlikely to yield detectable Ni^{IV} intermediates and are therefore of limited relevance to the objectives of this study.

To circumvent the vast temperature differential between conditions compatible with the Ni^{IV} product complexes and catalysis, we targeted a strategy wherein alkyl radicals could be generated using redox activation rather than thermal activation. Specifically, we hypothesized that the aryl radicals generated in the reaction of **3** with ArN_2^+ salts could be intercepted by alkyl iodides to generate alkyl radicals through transiodination (Scheme 3.12). Aryl radicals are well established to rapidly abstract iodine atoms from alkyl iodides to cleanly yield aryl iodides and alkyl radicals.[11] Thus the strong driving force for the reduction of an aryl diazonium could replace the high temperatures required to initiate the initial C–I cleavage during the radical oxidative addition of an alkyl iodide.

Scheme 3.11 Proposed radical relay to generate alkyl radicals from aryl radicals

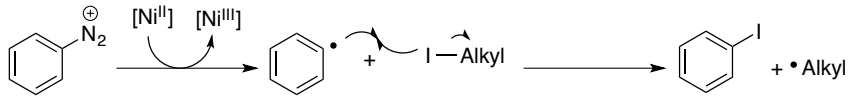

To test this hypothesis, a sterically hindered diazonium (to slow or prevent addition to the hindered nickel center) was added to a prestirred solution of **3** and excess Me–I. Upon addition of the diazonium, the reaction immediately evolved a gas and underwent a distinct color change. Analysis of the crude NMR spectrum revealed the presence of a new diamagnetic nickel complex consistent with $TpNi^{IV}(CF_3)_2(CH_3)$.

Scheme 3.12 Radical relay oxidation of **3** to generate **7**

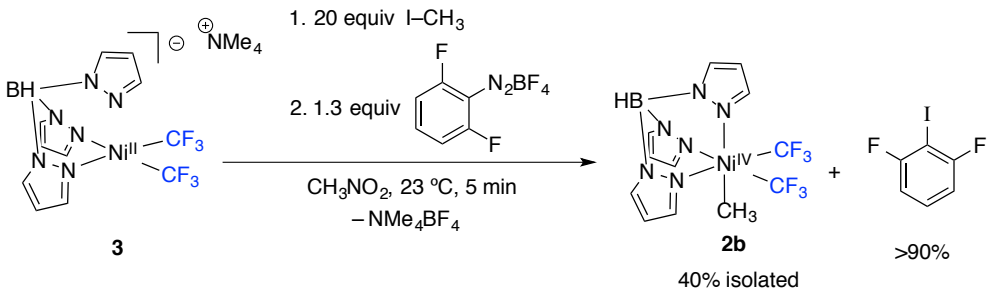

Complex **2b** was characterized by elemental analysis and ^{1}H, ^{11}B, ^{13}C, and ^{19}F NMR spectroscopy. The ^{13}C NMR and ^{13}C/^{19}F HMBC spectra confirm the proposed methylation at nickel. As seen in Figure 3.3 the ^{13}C NMR spectrum displays a distinct ^{13}**C**H$_3$–^{19}**F** coupling ($^{3}J_{CF}$ 4.7Hz) which is further confirmed to be CF coupling in the ^{13}C/^{19}F HMBC spectrum (Figure 3.3b). These through-bond correlations are not expected if methylation occurred at the free pyrazole arm.

Figure 3.3 (a) ^{13}C NMR Spectrum of **7** showing $^{3}J_{CF}$ coupling and (b) ^{13}C/^{19}F HMBC spectrum showing a through-bond ^{13}C/^{19}F correlation of the CH$_3$ and CF$_3$ ligands

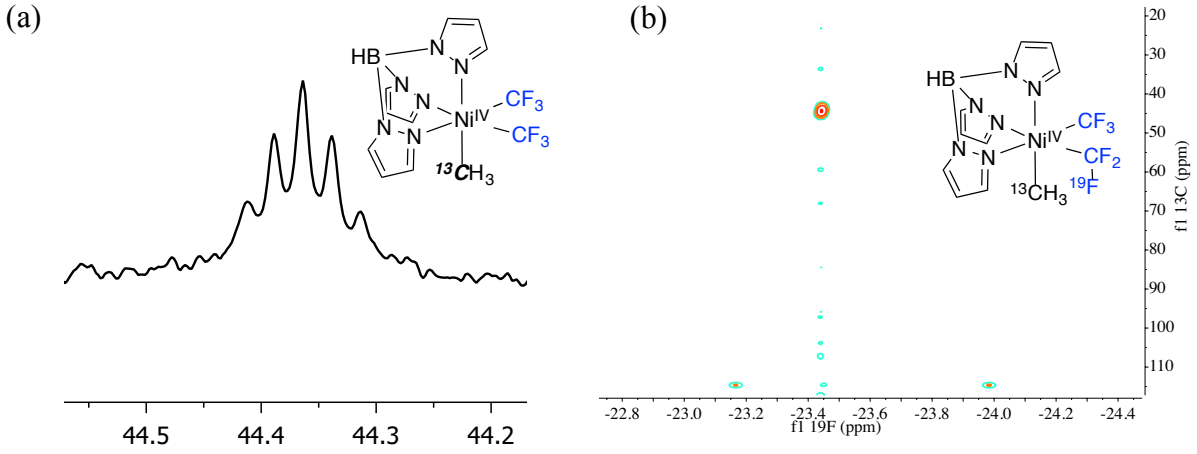

numerous attempts to structurally characterize **2b** were unsuccessful due to poor crystal quality. However, we were able to obtain high quality crystals of the isobutyl analog of **2b** (**2c**) which was synthesized through an identical protocol. As seen in Figure 3.4, the X-ray structure confirms the proposed connectivity. Compounds **2b** and **2c** are extremely rare examples of non-cyclometallated Ni^{IV}–(alkyl) complexes.

Figure 3.4 X-ray crystal structure of **2c**. The thermal ellipsoids are drawn at 50% probability and the hydrogen atoms have been omitted for clarity.

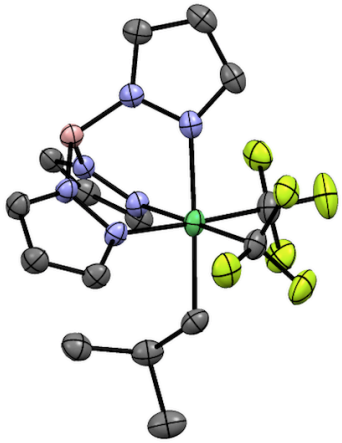

We propose that **2b** is formed through initial reduction of the aryl diazonium by **3**, iodine atom abstraction by the resultant aryl radical, and methyl radical addition to the newly formed Ni^{III} complex to yield a **2b** complex (Scheme 3.14). Thus the generation of **2b** is mechanistically similar to the radical oxidative addition of an alkyl/aryl iodide to a low-valent group 10 metal: radical reduction/fragmentation of a C–X bond by M, followed by subsequent alkyl radical capture yielding $M^{n+2}(X)(R)$. These data partially support Punji's proposed radical oxidative additions in high-valent manifolds insofar as alkyl radical generation can lead to organonickel(IV) complexes. Ongoing studies in this area are focused on better model systems that more closely match catalytically relevant intermediates and reagents.

Scheme 3.13. Mechanistic Proposal for the radical relay oxidation of **3**

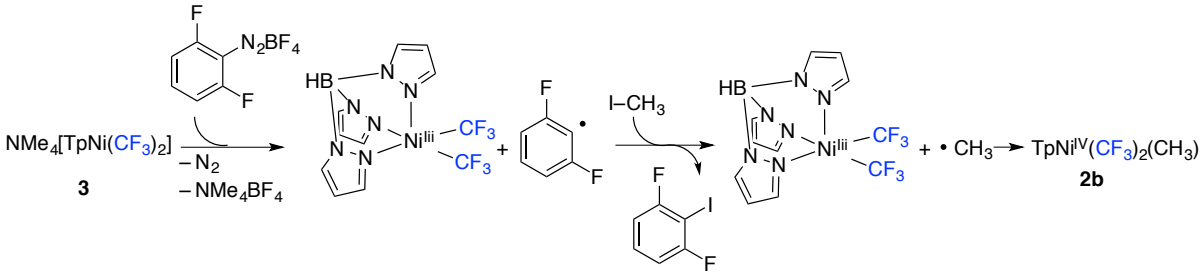

Oxidation of $[Ni^{II}(CH_3)_2]$ Complexes with Alkyl Iodides

The previous section describes the oxidation of Ni^{II} to Ni^{IV} using the irreversible reduction of an aryldiazonium to drive the low temperature activation of methyl iodide. The

aryldiazonium was required to bridge the mismatched oxidation/reduction potentials of Me–I and **3**. Alternatively, exchange of the CF_3 ligands for more donating methyl ligands is expected to expand the scope of reactive electrophiles at the cost of product Ni^{IV} complex stability. However, given the greater than expected stability of our $[TpNi^{IV}(CF_3)_2(alkyl/aryl)]$ compounds, we hypothesized that the $TpNi^{IV}(alkyl)_3$ products may still be detectable or isolable at low temperatures.

Scheme 3.14 Structural comparisons of Ni^{II} complexes **3** and **9**

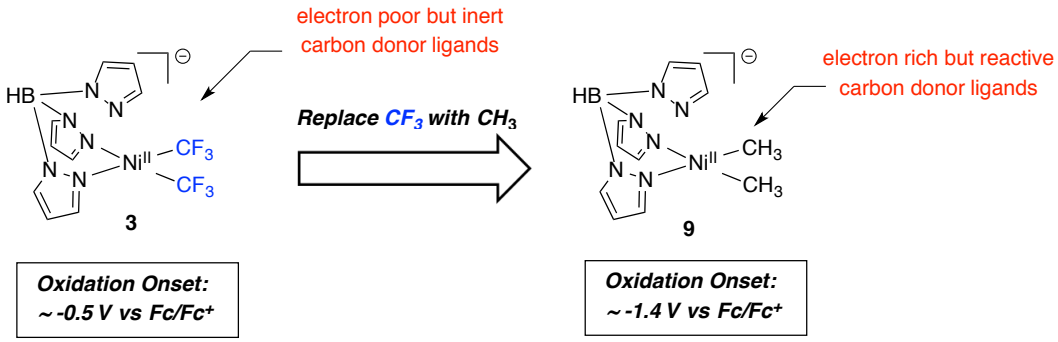

Figure 3.5 (a) Cyclic voltammogram of complex **3** with 0.1 M NBu_4PF_6 in CH_3CN at a scan rate of 100 mV/s. (b) Cyclic voltammogram of complex **9** with 0.1 M NBu_4PF_6 in CH_3CN at a scan rate of 100 mV/s.

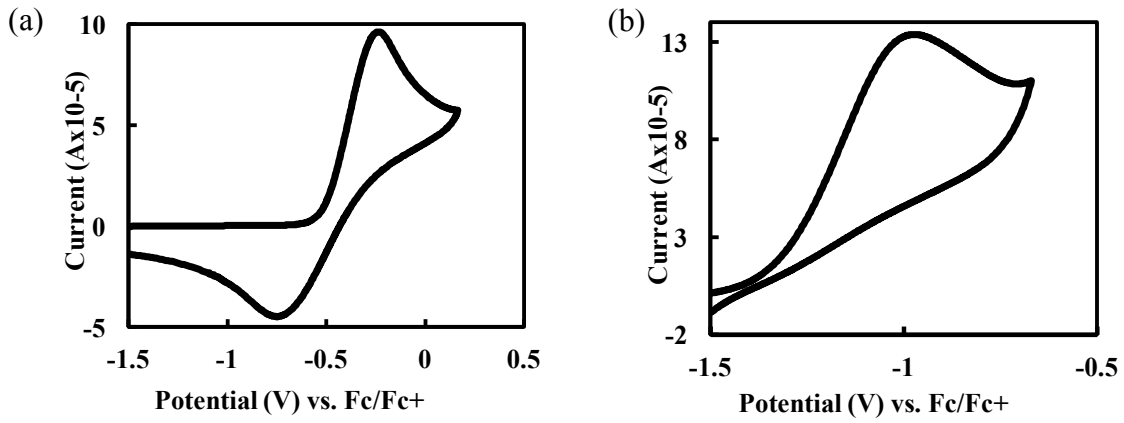

The methyl analog of **3** can be conveniently prepared through the ligand exchange of $(Py)_2Ni(CH_3)_2$ with NMe_4Tp in CH_3CN under dynamic vacuum to remove pyridine. Characterization of $NMe_4[TpNi^{II}(CH_3)_2]$ (**9**) by cyclic voltammetry confirms the anticipated cathodic shift of the $Ni^{II/III}$ couple relative to **3**. As it can be seen in Figure 3.5, the onset of

oxidation occurs approximately 900 mV lower than **3**. These data suggest that **9** should be significantly more reactive to weaker electrophiles than its CF_3 congener. However, the highly irreversible oxidation shown in Scheme 3.5b may reflect the comparatively reactive nature of the CH_3 ligands relative to CF_3 ligands. Although, chemical reversibility by CV is not always representative of a compound's stability following bond-forming oxidation.

Consistent with the cyclic voltammograms, **9** was found to be much more reactive to Me–I than **3**. Whereas, **3** was found to decompose slowly in the presence of 5 equivalents of Me–I at 23 ºC, treatment of **9** with one equivalent of Me–I at –35 ºC resulted in a rapid color change from yellow to colorless with concomittant precipitation of NMe_4I. Analysis of the crude reaction mixture by ^{1}H NMR revealed the formation of a new diamagnetic complex of C_{3v} symmetry in 70% NMR yield. The observed C_{3V} symmetry is consistent with a nickel-based rather than a ligand-based methylation to yield $TpNi^{IV}(CH_3)_3$ (**10**). Alkylation of the pyrazole army is expected to to yield a C_{1V}-symmetric compound. More extensive characterization was not possible as **9** was found to eliminate ethane in ~70% yield over the course of 3 h at room temperature.[12] Importantly, Me–I has been proposed to act as a $2e^-$ oxidant in $Ni^{II/IV}$ catalytic reactions. This is, to our knowledge the first unambigous example of an Ni^{II}(alkyl) to Ni^{IV}(alkyl) oxidation complex using an alkyl halide.

Scheme 3.15 Syntheis of **9** and subsequent oxidation to **10** with Me–I

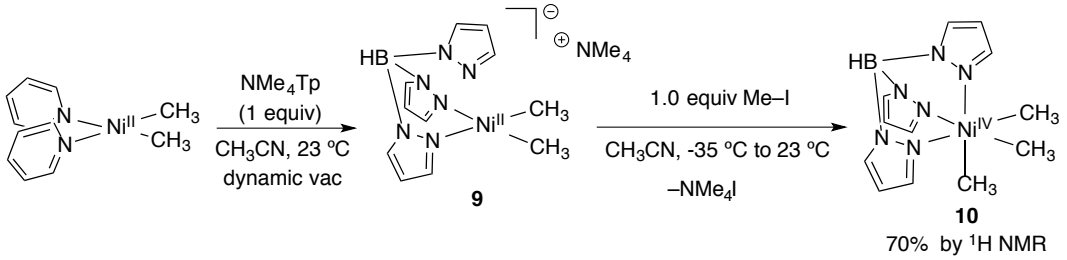

Figure 3.6 The ^{1}H NMR NMR spectrum (a) ^{1}H NMR Spectrum of **9** Immediately Prior to Oxidation with Me–I at -35 ºC and (b) 5 minutes after the addition of Me–I.

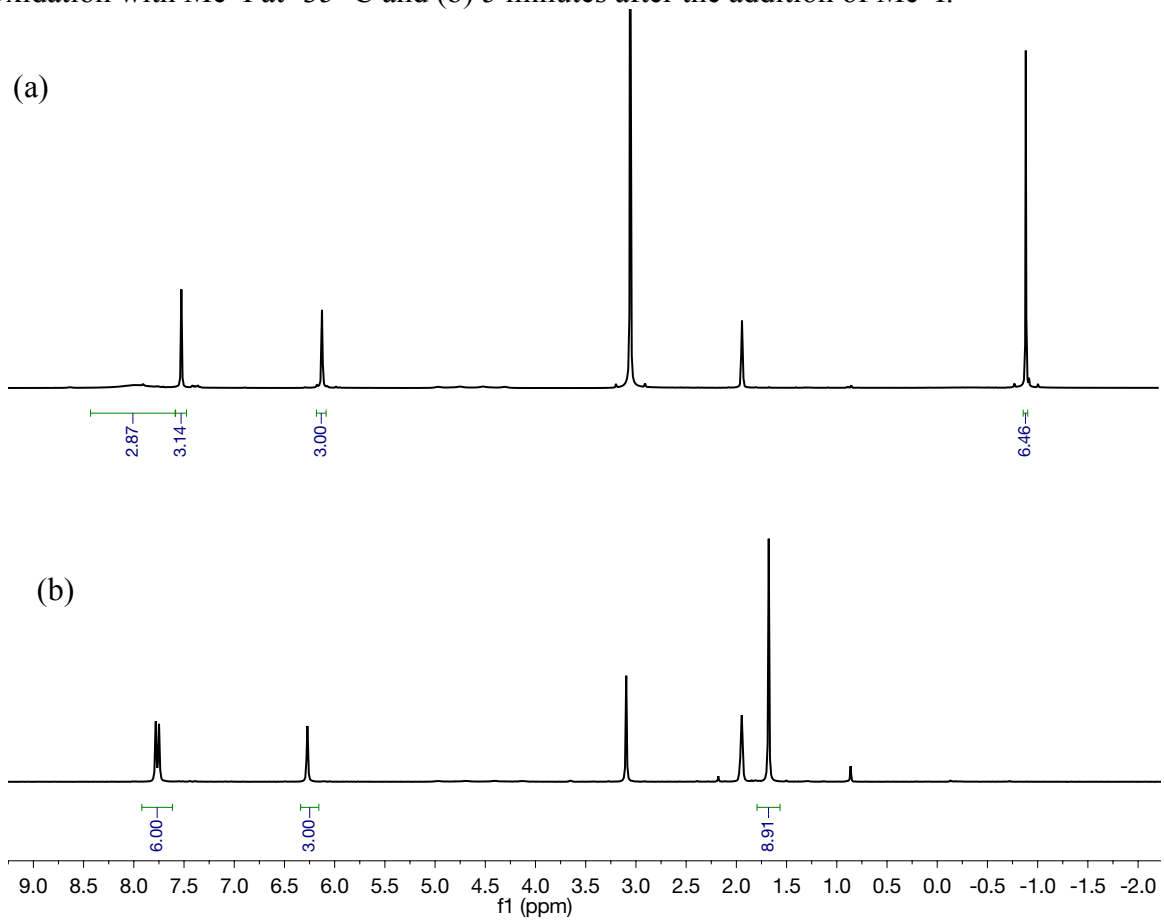

The clean oxidation of **9** by Me–I may not be generally representative of other alkyl iodides; methyl iodide is significantly more electrophilic than even primary alkyl iodides. In a final set of experiments, we next examined the reactivity of a more substituted, and presumably less electrophilic alkyl iodide. Treatment of **3** with 1 equivalent of ^{n}Bu–I at room temperature did not result in an immediate formation of a detectable Ni^{IV} complex. Instead the Ni^{II} starting material slowly decomposed to yield n-pentane in 14% yield. No diamagnetic intermediates consistent with a Ni^{IV} complex were detected in the course of this reaction. Notably, ethane was not detected by ^{1}H NMR. On the basis of the sluggish reactivity of **3** with ^{n}Bu–I , we tentatively propose that the observed formation of $TpNi^{IV}(CH_3)_3$ complex (**10)** is through an S_N2–type oxidative addition, as radical mechanisms are anticipated to be faster with ^{n}Bu–I than

Me–I. Additional experiments aimed at the detection of carbon-centered radicals will be necessary to confirm this proposal.

Scheme 3.16 Oxidation of **9** with ^{n}Bu–I at Room Temperature

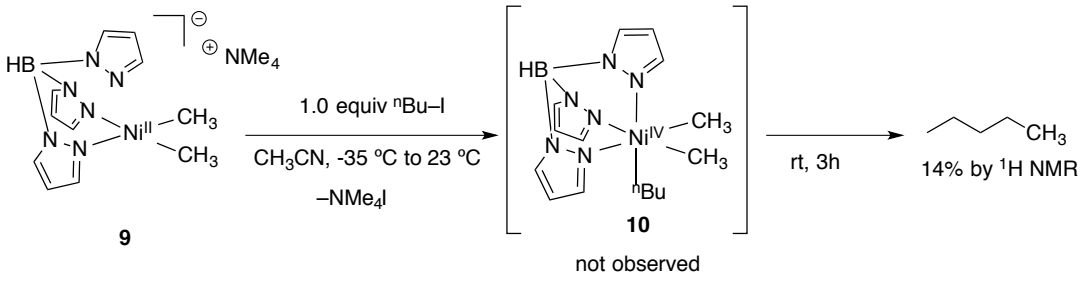

3.2.3 Aspects of Bond-Forming Reductive Elimination from Fluoroalkyl Ni^{IV}(alkyl/aryl) Complexes

The previous two sections describe the design and reactivity of model nickel complexes to examine the feasibility of the $2e^-$ oxidation of organometallic Ni^{II} with carbon-based electrophiles. On the basis of their excellent stability the product Ni^{IV} complexes should also be well suited to study the other key redox reaction in $Ni^{II/IV}$ catalysis: $2e^-$ C–C or C–X bond-forming reductive elimination. Indeed, this step has significant precedent from model organonickel(IV) complexes. However, at the time of our studies, published model systems were generally stabilized with cyclometallated carbon donor ligands.[6,13] Competitive decomposition reactions, such as Ni–C reductive homolysis are far less likely with these scaffolds and thus limit the generality of these studies. The $TpNi^{IV}(CF_3)_2$(alkyl/aryl) complexes synthesized in the previous section are more representative of catalytic intermediates in that none of the carbon donor ligands are tethered together. We next investigated the scope and mechanism of bond forming elimination reactions to better understand the key product release step of $Ni^{II/IV}$ catalysis.

C–C Bond-Forming Reactivity of 2a

We first investigated the reactivity of the Ni^{IV} product **2a**. Upon heating at 55 ºC for 15 h in CD_3CN, **2a** underwent clean C(sp^2)-CF_3 bond-forming reductive elimination to afford

benzotrifluoride in 76% yield as determined by ^{19}F NMR spectroscopy (Scheme 3.18). The Ni^{II} byproducts of the reaction are $Ni^{II}Tp_2$ (26% yield) and $(CD_3CN)_2Ni^{II}(CF_3)_2$ (29% yield) both of which can be formed in a maximum of 50% yield. These are presumably generated via ligand exchange from the initial reductive elimination product, $TpNi^{II}CF_3$. The reaction represents the first reported example of C–C coupling from a non-cyclometallated and well-defined Ni^{IV} complex.

Scheme 3.17 Thermally induced Ph–CF_3 Coupling from **2a**

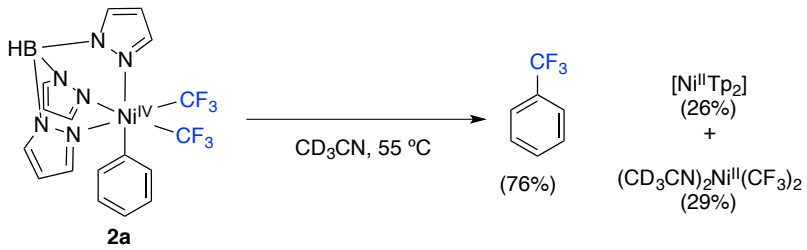

Mechanistic Considerations Ar–CF_3 Coupling from 2a[cite Nicole]

As discussed in Chapter 2, we have already established that a closely related Ni^{III} complex , $TpNi^{III}(CF_3)(Ph)$, also mediates the formation of Ar–CF_3 bonds. As such, we next sought to probe the mechanism of the coupling step to determine if Ni^{III} intermediates are involved in the formation of Ph–CF_3 from **2a**. Scheme 3.19 shows two potential mechanisms for the formation of Ni^{III} intermediates in the course of the thermolysis of **2a**. In mechanism A, homolytic cleavage of a Ni–CF_3 bond would yield $TpNi(CF_3)(Ph)$ (**11**) , from which Ar–CF_3 coupling is known to occur. We note that Ni–CF_3 homolytic cleavage has been observed from other high-valent nickel complexes. The second pathway, Mechanism B, shows a radical chain mechanism wherein small quantities of a reductant (generated through decomposition of **2a**) initiates chain reductive decomposition through the Ar–CF_3 coupling from a triorganonickel(III) complex (**12**).

Figure 3.18 Potential Ph–CF_3 Coupling Mechanisms from **2a** Involving Ni^{III}

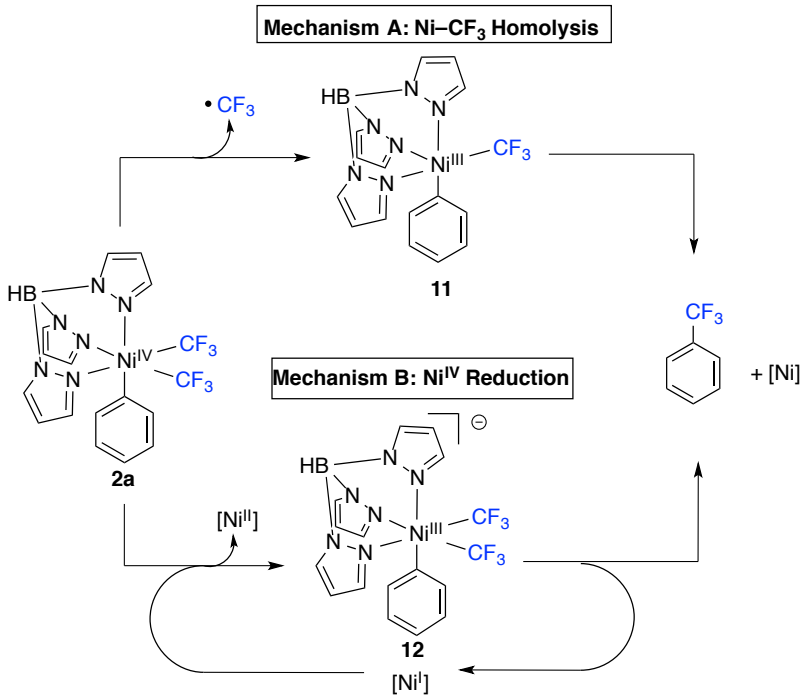

Mechanism A was first interrogated by conducting the thermolysis of **2a** in the presence of the radical trap TEMPO. TEMPO has been shown to efficiently scavenge free trifluoromethyl radicals from solution to form TEMPO–CF_3 which can be conveniently detected by ^{19}F NMR spectroscopy.[14] Not only was TEMPO–CF_3 not detected upon heating **2a** at 55 ºC with 2 equivalents of TEMPO, but the Ar–CF_3 coupling yield was essentially unchanged (79% vs 76%). These observations are inconsistent with the *in-situ* generation **11** through reductive homolysis of a Ni–CF_3 bond.

Scheme 3.19 Radical trapping experiments in the thermolysis of **2a**

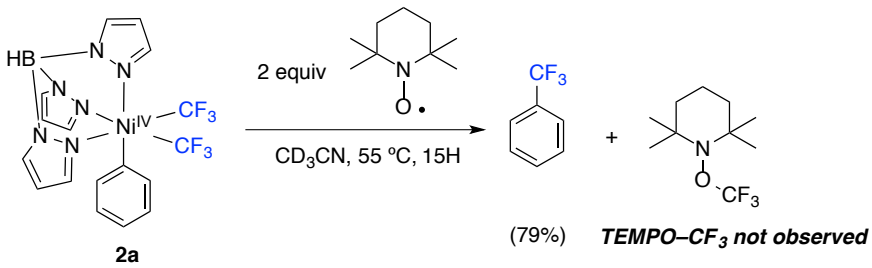

We next sought to determine if Ar–CF_3 coupling from tri-organoNi(III) complex (**12**) (the key intermediate in mechanism B) is feasible through independent synthesis and reactivity

studies of **12**. We first attempted to synthesize $[TpNi^{III}(CF_3)_2(Ph)]^-$ through the $1e^-$ reduction of **2a**. Addition of 1 equivalent of Cp_2Co^{II} to a cooled solution of **2a** in CD_3CN resulted in a rapid color change to orange which partially faded upon warming to room temperature. Analysis of the crude reaction mixture by ^{19}F NMR showed the formation of a complicated mixture of diamagnetic $[Ni^{II}(CF_3)]$ complexes (Scheme 3.21). The targeted Ni^{III} complex proved to be quite unstable under these conditions; additional attempts to observe the Ni^{III} intermediate by ^{11}B NMR spectroscopy were unsuccessful at -35 ºC. To ensure that the observed result was not an artifact of an unknown complication associated with the chosen reductant, we targeted an alternate synthesis involving addition of a nucleophilic Ph equivalent to $TpNi^{III}(CF_3)_2(MeCN)$ (**4**) Upon treatment of **4** with 0.55 equivalents of $ZnPh_2$ the solution immediately changed from purple to orange. The crude ^{19}F NMR spectrum showed a similar product distribution as the reduction of **2a** with Cp_2Co^{II}. Taken together, these results suggest that Ar–CF_3 coupling from trioganonickel(III) complex **12** is slow relative to non-productive decomposition. Under no circumstances was Ph–CF_3 observed to form as determined by ^{19}F NMR spectroscopy. We tentatively propose that $1e^-$ reduction of **2a** yields the $[TpNi(CF_3)_2(Ph)]^-$ which rapidly decomposes through homolytic cleavage of Ni–C bond. Evidence for both CF_3 and Ph homolysis was observed I the ^{19}F NMR. Similar reactivity has been noted in the $1e^-$ reduction of related octahedral Co^{III} organometallic complexes such as methylcobalamin. Ultimately these results suggest that Mechanism B is unlikely and that Ar–CF_3 coupling occurs directly from **2a**.

Scheme 3.21 Attempted synthesis of triorgano Ni^{III} complex **12** via (*i*) the $1e^-$ reduction of **2a** by Cp_2CO and (*ii*) transmetallation at Ni^{III} with $ZnPh_2$.

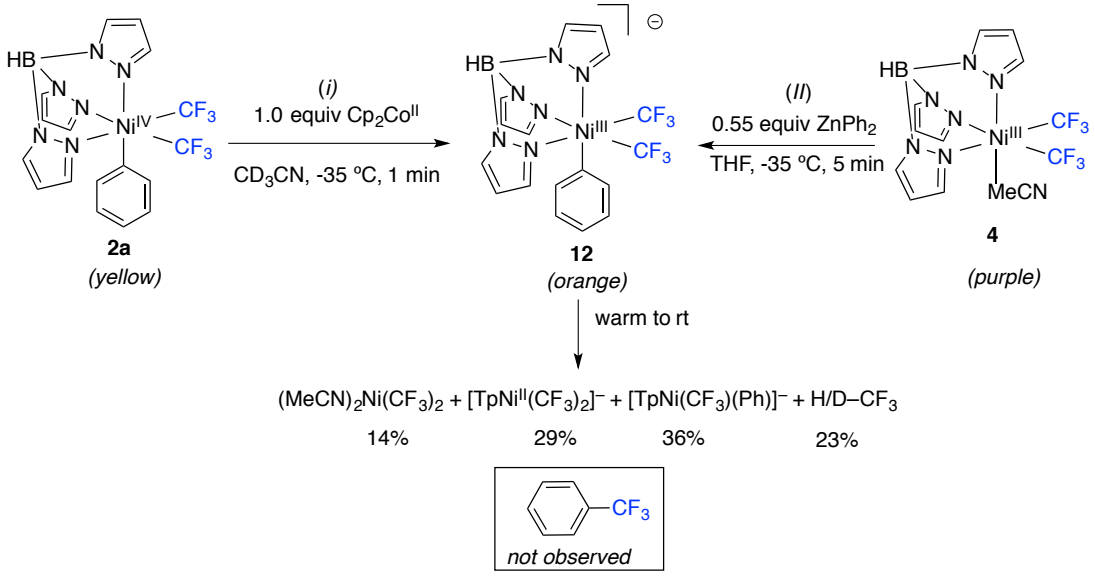

Having firmly established that the Ar–CF_3 coupling occurs from discrete Ni^{IV} complex, we next investigated electronic effects on the aryl-CF_3 coupling step. A series of substitutionally varied complexes were synthesized via the treatment of **3** with the appropriate Ar_2IBF_4 reagents. Heating the substituted Ni^{IV} complexes at 55 °C in CD_3CN for 4-18 h afforded the corresponding benzotrifluorides in 70-95% yield as determined by ^{19}F NMR spectroscopy. No obvious correlation between yield and electron donating or withdrawing nature of the substituent was observed (Table 1).

Table 3.1 Ar–CF_3 coupling from substituted Ni^{IV} complexes

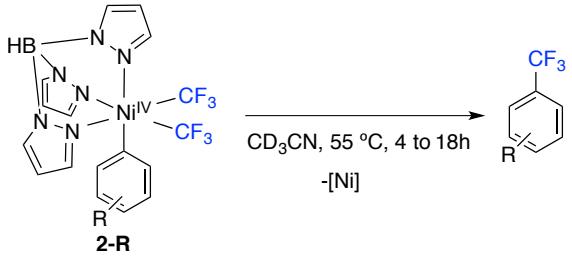

Complex (2–2/3/4-R)	Time (h)	σ =	%Ar-CF_3 (^{19}F NMR)
2-4OMe	4	-0.27	95
2-4Me	15	-0.14	71
2-4H (2a)	15	0	76
2-4Br	16	0.26	81
2-3CO_2Me	18	0.36	70

The rate constant (k_{obs}) for reductive elimination from each complex at 55 ºC was obtained by monitoring the reactions by ^{19}F NMR spectroscopy. A Hammett plot of the resulting data is shown in Figure 3.7. This plot shows a ρ-value of –0.91, indicating that reductive elimination is accelerated by electron-releasing substituents on the aromatic ring. This effect mirrors the trend reported for aryl-CF_3 bond-forming reductive elimination from related Pd^{IV}(aryl)(CF_3) complexes.[15]

Figure 3.7 Hammett plot of the reductive elimination from compound **2-R**

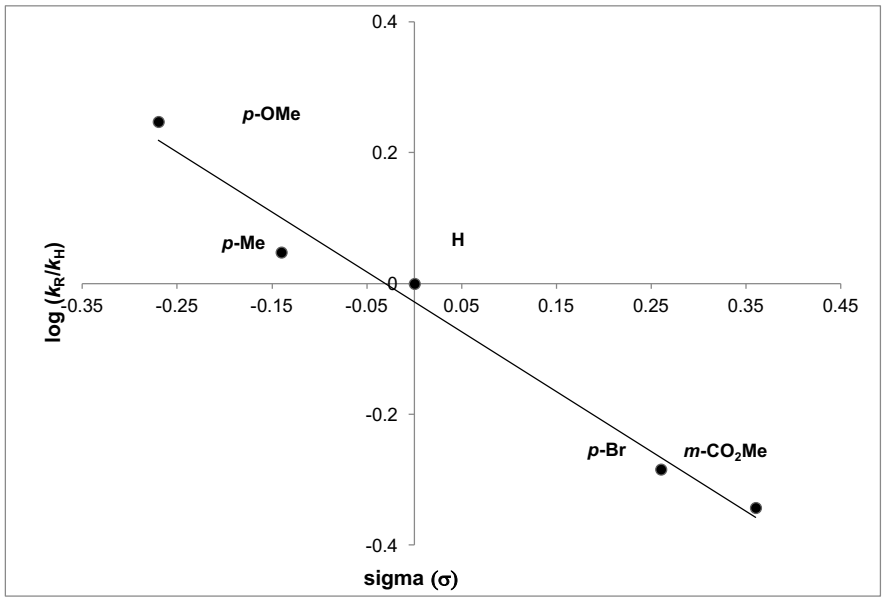

The electronic effect can be rationalized in two ways: (a) the larger trans-effect of electron-rich σ-aryl groups facilitates faster ligand dissociation to generate a reactive five-coordinate Ni^{IV} intermediate from which reductive elimination occurs and/or (b) the electron donor substituents accelerate a nucleophilic attack by the σ-aryl ligand onto the electrophilic CF_3 group in the transition state (Scheme 3.22).

Scheme 3.21 (a) Potential role of aryl substitution on Ar–CF_3 coupling through the trans Effect and (b) rationalizing the observed effect through the nucleophilic role of the aryl ligand

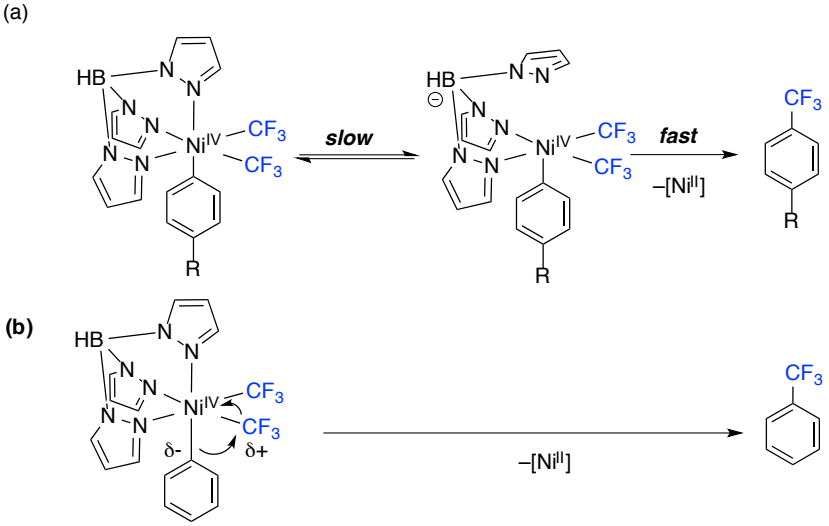

Density functional theory calculations were performed by professor Allan Canty at the University of Tasmania to better understand the role of the arene electronics on the Ar–CF_3 coupling step. Figure 3.8 shows DFT energy profiles of Ar–CF_3 coupling from **2a**. These calculations suggest that coupling is expected to occur from an octahedral nickel center as opposed to a square pyramidal complex formed through pyrazole dissociation. The observed negative ρ value is therefore not due to the stronger trans effect and thus faster formation of potentially more reactive 5-coordinate complex. Rather, we proposed that the arene should be considered as the nucleophile and the trifluoromethyl ligand as the electrophile in the transition state. Interestingly, the nucleophilic role of the aryl ligand is inverted relative to more common C–C and C–X coupling reactions at low oxidation states of group 10 metals. In these low-valent regimes, the arene is generally considered the electrophilic partner in the transition state.

Figure 3.8 The calculated potential energy profile of Ph–CF_3 coupling from **2a**. Single point calculations were performed in CH_3CN (PCM) at the M06//def2-QZVP//6-311G(2d,p) level of theory and geometry optimizations were performed at using B3LYP//SDD//6-31G(d) in CH_3CN (PCM).

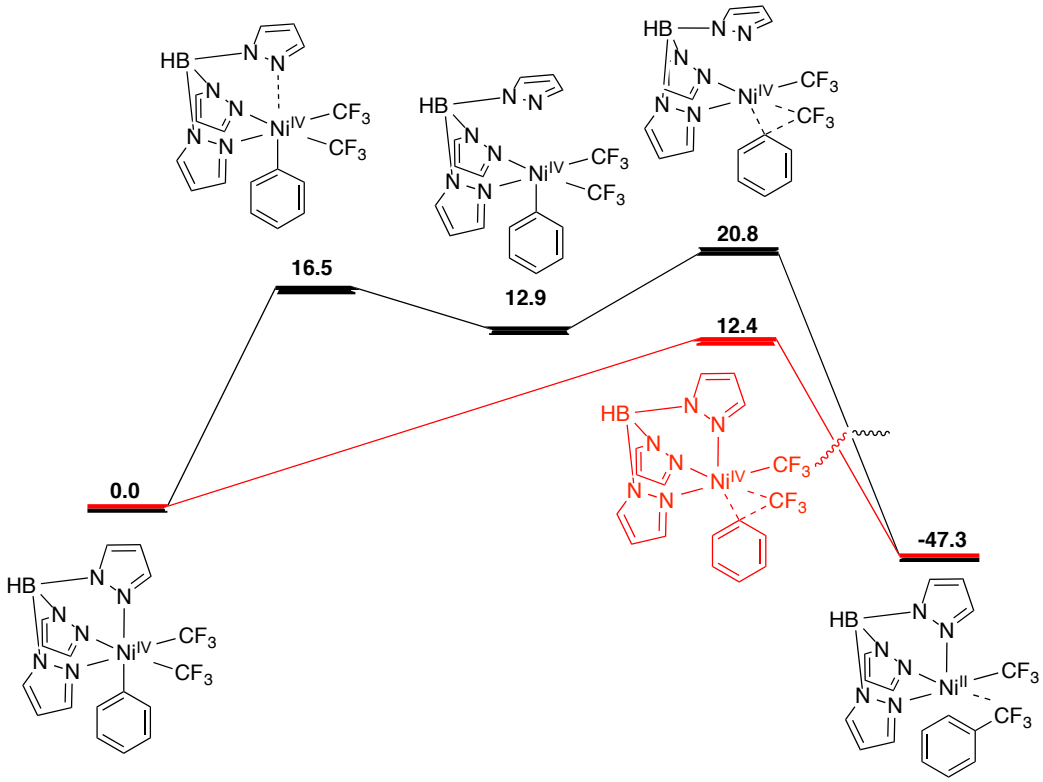

Attempted C(sp^3)–CF_3 Coupling from 2b

Well-defined and high-yielding examples of C(sp^3)–CF_3 coupling from an isolated metal complex are exceedingly rare. Not only has this transformation received far less attention than C(sp^2)–CF_3 coupling, it is generally regarded to have an even higher kinetic barrier. Encouraged by the thermally mild and clean Ar–CF_3 coupling from **2a**, we next investigated thermally induced H_3C–CF_3 elimination from **2b**.

Scheme 3.22 Attempted Thermal Elimination of H_3C–CF_3 from **2b**

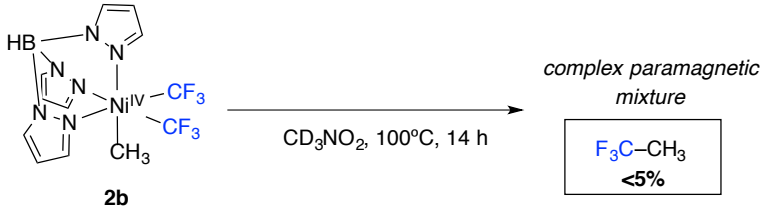

Complex **2b** proved to be remarkably stable under thermolytic conditions. Heating solution of **2b** in CD_3NO_2 for 1 hour at 90 ºC resulted in less than 10% decomposition of the original starting material as determined by ^{19}F NMR spectroscopy. Additional heating at 100 ºC for 14 h resulted in complete decomposition of the complex into a complicated paramagnetic mixture. Small quantities of ethane were detected (~15%) but less than 5% yield of 1,1,1 trifluoroethane was observed by ^{19}F NMR spectroscopy. For comparison, its phenyl analog fully decomposed into Ph–CF_3 after 1 hour at 90 ºC in CD_3CN.

DFT calculations corroborate the comparatively low barrier to Ph–CF_3 coupling from these Ni^{IV} complexes. As it can be seen in Scheme 3.25, the calculated barrier to inner-sphere H_3C–CF_3 elimination (right) is approximately 10 kcal/mol higher than Ph–CF_3 reductive elimination (left). Taken together with the excellent thermal stability of **2b**, these experiments suggest that the failure to observe C(sp^3)–CF_3 coupling is due to a high barrier to elimination rather than low barriers to competitive decomposition.

Figure 3.9 Comparative Calculated Potential Energy Profiles for R–CF_3 Coupling from **2a** (left) and **2b**(right0 Single Point Calculations were performed in CH_3CN (PCM) at the M06//def2-QZVP//6-311G(2d,p) level of theory and geometry optimizations were performed at using B3LYP//SDD//6-31G(d) in CH_3CN (PCM).

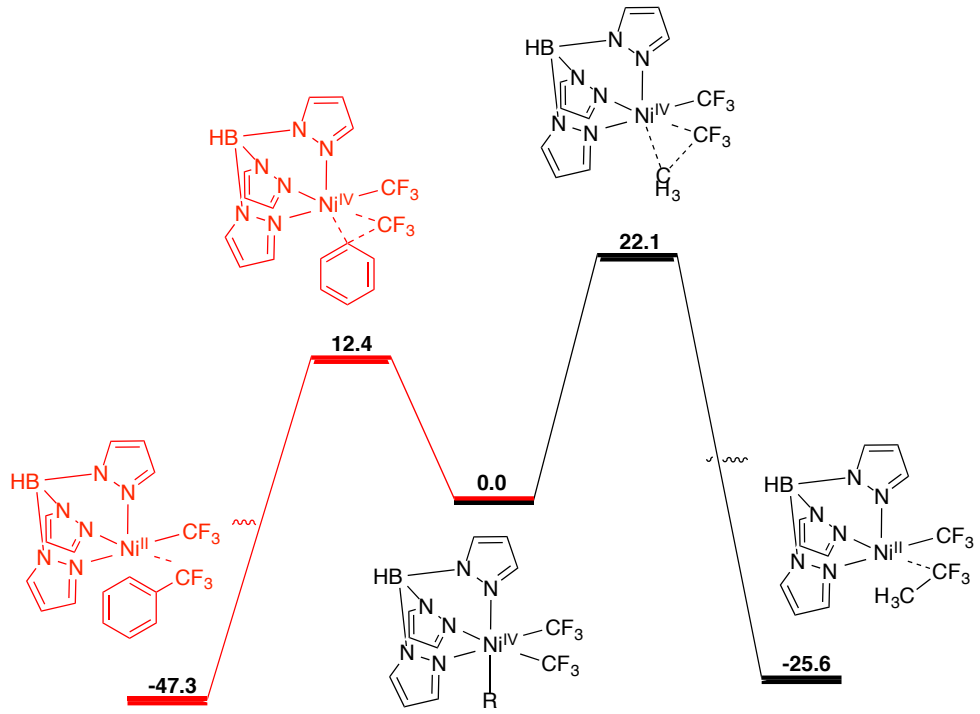

Overall, the combined experimental and theoretical studies in this section highlight the remarkable challenge of $C(sp^3)$–CF_3 coupling from a Ni^{IV} center. Even highly stabilized organonickel(IV) complexes are known to mediate the formation of traditionally challenging bonds such as those in four-membered rings. Yet no evidence for concerted elimination from **2b** was detected under our conditions. More generally, these data confirm a previous proposal that a paradigm shift away from canonical cross-coupling strategies may be necessary for the catalytic formation of $C(sp^3)$–CF_3. To date, no catalytic examples of this transformation have been reported, though the challenges of this reaction have captured the attention of organometallic and synthetic chemists alike.

C–X Coupling from 2b

We hypothesized that the failure of **2b** to efficiently undergo C–C reductive elimination is not reflective its high general stability, but rather the remarkable resistance of CF_3 ligands to reductive elimination reactions. To test this proposal, we next investigated the reactions of **2b** to with carbon and heteroatom nucleophiles. As illustrated in Scheme 3.26, treatment of **2b** with alkyl ammonium salts of CN^-, OAc^- , and I^-resulted in rapid $2e^-$ reduction of the metal through the formation of C–C and C–X bonds. Most notably, **2b** underwent rapid C–I bond formation to yield Me–I in near quantitative yield. This observation insinuates that the failure of **3** to undergo oxidation with Me–I in section 3.2.2 may be a thermodynamic rather than kinetic limitation. These reactions also confirm the anticipated strong driving force for reduction of **2b** and thus highlight the extraordinary difficulty of $C(sp^3)$–CF_3 reductive elimination. Perhaps most importantly, these reactions corroborate and expand of Camasso and Sanford's previous Ni^{IV} C–X coupling studies that identify Ni^{IV} intermediates as promising targets for the catalytic coupling of weak nucleophiles.

Scheme 3.23 Reactions of nucleophiles with compound **3**. Yields of the methylated products were determined by ^{1}H NMR and the yield of the nickel-containing product was determined by ^{19}F NMR.

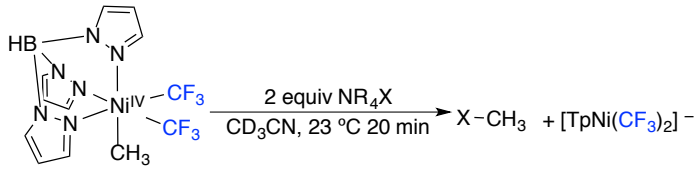

2b **3**

X=	NMR Yield (X–CH_3 / **3**)
CN^-	77%/ 94[b]%
OAc^-	98%/ 94 %
I^-	> 98%/ >98 %

Conclusions

In conclusion, this chapter describes our studies of elementary organometallic reactions pertinent to $Ni^{II/IV}$ catalysis. These investigations were ultimately enabled through the identification of a suitable model system that does not rely on cyclometallated carbon donor ligands to yield stable Ni^{IV} complexes. Specifically, utilization of trifluoromethyl ligands was found to afford sufficiently stable Ni^{IV} complexes for detailed studies of carbon-based electrophile-mediated $2e^-$ oxidations and bond-forming elimination reactions of the resultant Ni^{IV} complexes.

In section 3.2.2 we examined the feasibility and mechanisms of the net $2e^-$ oxidation of Ni^{II} to Ni^{IV} with carbon-based electrophiles. Our studies show that strong aryl electrophiles can effect the net $2e^-$ oxidation of Ni^{II} through apparent consecutive $1e^-$ oxidations. This observation contrasts Chatani's proposed concerted $2e^-$ oxidation with diaryliodonoium electrophiles, though it is currently unclear if the observed $1e^-$ reactivity is unique to our model system. At a minimum, these observations suggest that $1e^-$ redox events should always be considered when Ni^{IV} intermediates are suspected. This radical reactivity was then leveraged to initiate radical oxidative addition mechanisms of alkyl iodides at temperatures compatible with the Ni^{IV} product compounds. Notably, these results provide preliminary experimental validation of literature proposals of radical oxidative additions of Ni^{II} with alkyl iodides to yield Ni^{IV}. Finally, we examined the reactivity of a highly reducing dimethyl nickel compound with alkyl iodides. Our initial observations suggest alkyl iodides may indeed oxidize these

electron rich nickel centers by two electrons, though more stabilizing ancillary ligands and additional mechanistic studies are needed to fully understand the details this reaction.

In section 3.2.3 we investigated the bond-forming reactivity of the product TpNi(CF_3)$_2$(alkyl/aryl) complexes from section 3.2.2. The stability of these compounds allowed us to directly interrogate the potential intermediacy of organonickel(III) intermediates as well as the electronic character of each ligand in the course of the Ar–CF_3 elimination. These mechanistic studies confirmed the proposed elimination from a discrete Ni^{IV} complex and implicate a nucleophilic role for the arene in the elimination. The high yielding and relatively clean Ar–CF_3 elimination observed in this system starkly contrasts our studies of C(sp^3)–CF_3 coupling from Ni^{IV}. Non-descript decomposition of TpNi(IV)(CF_3)$_2$(CH_3) **2b** was found to predominate over H_3C–CF_3 reductive elimination. This complex, was however, highly reactive to outer-sphere C–X coupling reactions. High-yielding C–C, C–O, and C–I elimination was observed at room temperature on the minute timescale.

Overall these studies support the catalytic relevance of organonickel(IV) by confirming proposed mechanisms of its formation as well as confirming and expanding the scope of known bond-forming reactions. We anticipate that these elementary reactions outlined in this chapter will help aid in the mechanistic interpretation of nickel catalysis under oxidizing conditions. Future studies in this area are aimed at translating these results to new catalytic methods with a focus on transformations challenging or impossible through more traditional low-valent manifolds (e.g. Ar–CF_3 coupling).

3.3. Experimental Procedures and Characterization of Compounds

3.3.1. General Procedures and Materials and Methods

General Procedures

All manipulations were performed inside an N2 filled glovebox unless otherwise noted. NMR spectra were obtained on a Varian VNMR 700 (699.76 MHz for ^{1}H; 175.95 MHz for ^{13}C) or a

Varian VNMR 500 (500.09 MHz for ^{1}H; 470.56 MHz for ^{19}F; 125.75 MHz for ^{13}C; 225 or 128 MHz for ^{11}B) spectrometer. ^{1}H and ^{13}C NMR chemical shifts are reported in parts per million (ppm) relative to TMS, with the residual solvent peak used as an internal reference. 19F NMR chemical shifts are reported in ppm relative to CCl_3F. 11B NMR spectra are referenced to BF3!Et2O. Abbreviations used in the NMR data are as follows: s, singlet; d, doublet; t, triplet; q, quartet; m, multiplet; bq, broad quartet; br, broad signal; quint, quintet. Due to significant peak overlap of the diphosphine complexes and extensive ^{13}C-^{31}P and ^{13}C-^{19}F coupling, ^{13}C shifts are not reported as a list. Yields of reactions that generate fluorinated products were determined by ^{19}F NMR analysis using a relaxation delay of 12 s. Quantitative 11B NMR were recorded according to the literature1 at a 90º pulse angle with a 125 s relaxation delay (longest T_1 = 23 s) and a 10 s acquisition period and were checked against a calibration curve. Magnetic susceptibilities were determined by the Evans method in CH_3CN at 23 ºC on a 700 MHz spectrometer.2 Mass spectral data were obtained on a Micromass Magnetic Sector Mass Spectrometer in electrospray ionization mode. Elemental analyses were conducted by Midwest Microlabs. Cyclic voltammetry was performed using a CHI600C potentiostat from CH Instruments. EPR spectra were collected at –176 ºC using a Bruker EMX ESR Spectrometer with a nitrogen-cooled cryostat. X-ray crystallographic data were collected on a Rigaku AFC10K Saturn 944+ CCD-based X-ray diffractometer. Flash chromatography was performed using a Biotage Isolera One system with cartridges containing high performance silica gel.

Materials and Methods

The following compounds were prepared via literature procedures: $(PPh_3)2Ni(CF_3)(OTFA)$, [3] $(dtbpy)Ni(CF_3)(Ph)$, $AcFcBF_4$, $Cp^*_2FeBF_4$, Ph_2IBF_4,[16] $(4\text{-}MeOC_6H_4)_2IBF_4$,[17] $(4\text{-}Br\text{-}C_6H_4)(Mes)IBF_4$,[18] $(3\text{-}CO_2MeC_6H_4)(Mes)IBF_4$,[4] and $(dtbpy)Ni(CF_3)_2$[19] were prepared according to literature procedures. Ni(COD)2, biphenylene, $NOBF_4$, $AgBF_4$, and Ph_2Zn were purchased from Strem Chemicals. 4,4'-di-tert-butylbipyridine (dtbpy), Cp_2FePF_6, PPh_3, dppe, dppbz, (–)-diop, and dppp and were purchased from Aldrich. 4,4'-difluorobiphenyl was purchased from Oakwood Chemicals. Xantphos, dppf, and dppb were purchased from ArkPharm. KTp was purchased from Alfa Aesar. Dichloromethane (Fisher), pentane (Fisher), diethyl ether (EMD), toluene (Fisher), and tetrahydrofuran (Fisher) were deaerated via a N2 sparge and were purified by a solvent purification system. Acetonitrile (Acros) and benzonitrile (Acros), diisopropyl ether (Acros) were sparged and used without further purification. CD_2Cl_2, $C6D_6$, CD_3CN, and acetone-d^6 were obtained from Cambridge Isotopes Laboratories and were stored over activated 4 Å molecular sieves (EMD Millipore). Basic alumina (Aldrich) was

dried for 48 h under vacuum at 210 °C. Celite was dried for 12 h under vacuum at 100 °C. Unless otherwise noted, all glassware was dried overnight in an oven at 150 °C and cooled under an inert atmosphere before use. All commercial reagents were used without further purification/drying unless explicitly stated in the experimental section. Unless otherwise noted, all manipulations were performed under an inert atmosphere in a N_2 glovebox.

3.3.2 Synthesis and Characterization of Compounds

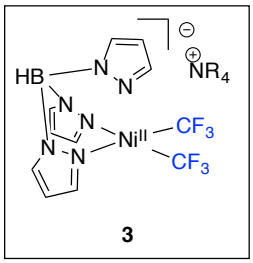

3

Synthesis of [NBu_4(Tp)Ni(CF_3)$_2$] (3): The following procedure is for the NBu_4 counterion, this procedure works for the NMe_4 example as well. In the glovebox, a 20 mL vial was charged with $(MeCN)_2Ni(CF_3)_2$ (178 mg, 0.62 mmol, 1.0 equiv), NBu_4Tp (242 mg, 0.62 mmol, 1.0 equiv), and acetonitrile (10 mL). The solution was stirred for 1 min before the volatiles were removed under reduced pressure. Pentane (5 mL) was added to the resulting viscous residue. The mixture was allowed to stand at –35 ºC for 6 h, during which time colorless crystals formed. The solution was decanted away from the crystals, and the crystals were washed with pentane (2 x 3 mL) and then dried under vacuum to afford **3** as a light yellow solid (380 mg, 94% yield). ^{1}H NMR (498 MHz, $(CD_3)_2CO$, 23 ºC): δ 7.77-7.66 (overlapping peaks, 6H), 6.16 (br signal, 3H), 5.09 (br, B-*H*), 3.14-3.06 (m, 8H), 1.62 (m, 8H), 1.38 (h, J_{HH} = 7.4 Hz, 8H), 0.99 (t, J_{HH} = 7.4 Hz, 12H).^{13}C NMR (176 MHz, $(CD_3)_2CO$, 23 ºC): δ 141.29, 134.16, 103.31, 23.41, 19.34, 12.84. ^{11}B NMR (225 MHz, $(CD_3)_2CO$, 23 ºC): δ –2.65 (d, J_{BH} = 113 Hz). ^{19}F NMR (471 MHz, $(CD_3)_2CO$, 23 ºC): δ –25.76 (s, 6F)

Synthesis of [(Tp)Ni^{IV}(CF_3)$_2$(Ph)] (2-H):

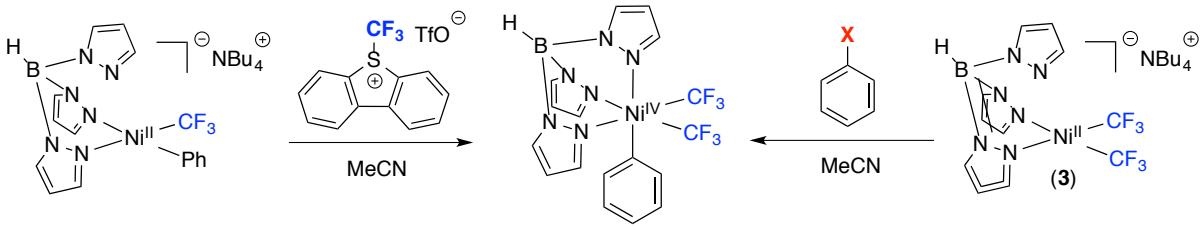

2a

Procedure A: [NBu_4(Tp)Ni^{II}(CF_3)(Ph)] (**1**) (120 mg, 0.18 mmol, 1.0 equiv) and *S*-(trifluoromethyl)dibenzothiophenium triflate (95 mg, 0.24 mmol, 1.3 equiv) were combined in a 20 mL vial under an inert atmosphere. Acetonitrile (8 mL) was added, and the resulting yellow solution was allowed to stand for 1 min at room temperature. The vial was then removed from the glovebox and concentrated under reduced pressure. The resulting yellow-brown

residue was purified by silica gel chromatography (mobile phase: hexanes/ethyl acetate with a gradient from 100:1 to 60:40). Complex **2-H** was isolated as a yellow solid (79 mg, 90% yield).

Procedure B: Under an inert atmosphere, a 20 mL vial was charged with **3** (230 mg, 0.35 mmol, 1.0 equiv) and acetonitrile (17 mL). The resulting yellow-orange solution was then cooled to –35 °C. After equilibrating for 10 min at this temperature, Ph_2IBF_4 was added to the solution of **3**. The vial was shaken vigorously for 10 s, at which point the reaction mixture immediately turned brown. After 3 min at –35 °C the solution was warmed to room temperature. The reaction was removed from the drybox and filtered through a 2 cm thick pad of silica on the benchtop. The pad was washed with THF (5 mL), and the combined filtrates were concentrated to dryness under reduced pressure. The crude solid was further purified by flash chromatography (mobile phase: hexanes/ethyl acetate with a gradient from 100:1 to 90:10). The product was obtained as a bright yellow solid (89 mg, 52% yield). Samples for elemental analysis were obtained by an additional crystallization from a minimum amount of methanol by the slow addition of water. ^{1}H NMR (700 MHz, CD_3CN, 23 ºC): δ 8.05 (s, 1H), 7.94 (d, J_{HH} = 2.3 Hz, 1H), 7.91 (d, J_{HH} = 2.3 Hz, 2H), 7.31 (d, J_{HH} = 2.3 Hz, 2H), 7.14 (t, J_{HH} = 7.0 Hz, 1H), 6.97 (t, J_{HH} = 7.7 Hz, 2H), 6.72 (s, 2H), 6.43 (t, J_{HH} = 2.2 Hz, 1H), 6.27 (t, J_{HH} = 2.2 Hz, 2H), 4.69 (br, B-***H***). ^{13}C NMR (176 MHz, CD_3CN, 23 ºC): δ 158.54, 143.53, 143.18, 136.60, 135.98, 135.15, 127.46, 126.69, 112.44 (q, J_{CF} = 383 Hz), 106.28, 105.97. ^{11}B NMR (225 MHz, CD_3CN, 23 ºC): δ –4.22 (d, J_{BH} = 117.7 Hz). ^{19}F NMR (379 MHz, CD_3CN, 23 ºC): δ –19.38 (s, 6F). Elemental Analysis calcd. for $C_{17}H_{15}BF_6N_6Ni$, C: 41.94, H: 3.11, N: 17.26; found, C: 41.59, H: 2.95, N: 17.37

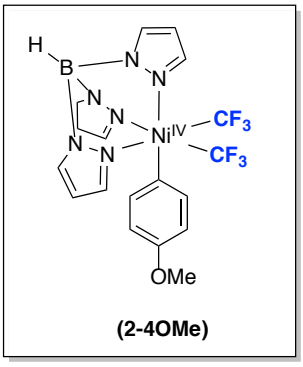

(2-4OMe)

Synthesis of [(Tp)Ni^{IV}(CF$_3$)$_2$(4-MeO-C$_6$H$_4$)] (2-4OMe): Under an inert atmosphere, a 20 mL vial was charged with $(MeCN)_2Ni(CF_3)_2$ (100 mg, 0.35 mmol, 1 equiv), KTp (91 mg, 0.35 mmol, 1.0 equiv), and MeCN (20 mL). The vial was shaken for 10 s until all of the solids had dissolved. Next, $(4\text{-}OMe\text{-}C_6H_4)_2I(BF_4)$ (144 mg, 0.39 mmol, 1.1 equiv) was added. The vial was shaken vigorously for 10 s at which point the yellow solution turned orange-red. The resulting solution was allowed to stand at 0 °C for 60 min under an inert atmosphere. The reaction mixture was then removed from the drybox and was filtered through a 3 cm thick pad of silica on the benchtop. The pad was washed with THF (15 mL), and the combined filtrates were concentrated to dryness under reduced pressure. The crude solid was purified further by flash

chromatography on silica gel (mobile phase: hexanes/ethyl acetate with a gradient from 100:1 to 90:10). The product was obtained as an orange solid (50 mg, 28% yield).

Note: The title compound undergoes slow reductive elimination at room temperature in MeCN. As such, expeditious handling of the crude mixture at room temperature is required. The NMR spectra were prepared and recorded at –10 ºC to avoid decomposition. Complex **2-4MeO** was found to decompose upon standing in the solid state. Accordingly, all reactivity investigations were performed using freshly prepared samples of **2-4MeO.** ^{1}H NMR (700 MHz, CD_3CN, –10 ºC): δ 8.05 (s, 1H), 7.94 (d, J_{HH} = 2.2 Hz, 1H), 7.91 (d, J_{HH} = 2.2 Hz, 2H), 7.33 (s, 2H), 6.59 (multiple peaks, 4H), 6.43 (t, J_{HH} = 2.2 Hz, 1H), 6.27 (t, J_{HH} = 2.2 Hz, 2H), 4.68 (br, B-***H***), 3.78 (s, 3H). ^{13}C NMR (176 MHz, CD_3CN, –10 ºC): δ 158.69, 148.69, 144.04, 143.78, 137.17, 136.56, 135.80, 113.27 (q, J_{CF} = 391 Hz), 112.67, 106.86, 106.57, 55.53. ^{11}B NMR (225 MHz, CD_3CN, –10 ºC): δ –4.22 (d, J_{BH} = 117.9 Hz). ^{19}F NMR (470 MHz, CD_3CN, –10 ºC): δ –19.14 (s, 6F).

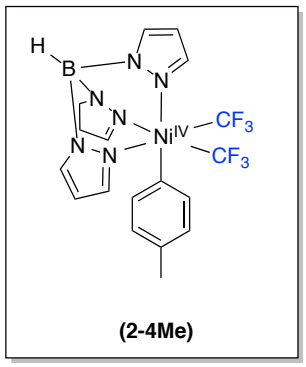

(2-4Me)

Synthesis of [(Tp)Ni^{IV}(CF$_3$)$_2$(4-Me-C$_6$H$_4$)] (2-4Me): Under an inert atmosphere, a 20 mL vial was charged with complex **2** (229 mg, 0.35 mmol, 1.0 equiv) and MeCN (17 mL). (4-Me-C_6H_4)$_2$IPF$_6$ (144 mg, 0.39 mmol, 1.1 equiv) was added to the solution of **3**. The vial was shaken vigorously for 10 s at which point the reaction immediately turned brown. The resulting solution was allowed to stand for 15 min at room temperature under an inert atmosphere. The reaction mixture was then removed from the drybox and was filtered through a 3 cm thick pad of silica on the benchtop. The pad was washed with THF (5 mL), and the combined filtrates were concentrated to dryness under reduced pressure. The crude solid was purified further by flash chromatography on silica gel (mobile phase: hexanes/ethyl acetate with a gradient from 100:1 to 90:10). The product was obtained as a yellow solid (84 mg, 48% yield).

Complex **2-4Me** was found to decompose upon standing in both the solid state and in solution. As such, all reactivity investigations were performed using freshly prepared samples of **2-4Me.** ^{1}H NMR (700 MHz, CD_3CN, 23 ºC): δ 8.04 (s, 1H), 7.93 (d, J_{HH} = 2.2 Hz, 1H), 7.91 (s, 2H), 7.31 (d, J_{HH} = 2.2 Hz, 2H), 6.81 (d, J_{HH} = 8.4 Hz, 2H), 6.58 (s, 2H), 6.43 (t, J_{HH} = 2.3 Hz, 1H), 6.26 (t, J_{HH} = 2.3 Hz, 2H), 4.68 (br, B-***H***). ^{13}C NMR (176 MHz, CD_3CN 23 ºC): δ 155.61, 143.47, 143.18, 136.38, 136.16, 136.01, 135.22, 128.00, 112.77 (q, J_{CF} = 391.6 Hz), 106.32,

106.02, 19.23. ^{11}B NMR (225 MHz, 23 ºC): δ –4.28 (d, J_{BH} = 117.7 Hz). ^{19}F NMR (470 MHz, CD_3CN, 23 ºC): δ –19.35 (s, 6F). Elemental Analysis calcd. for $C_{18}H_{17}BF_6N_6Ni$, C: 43.16, H: 3.42, N: 16.78; found, C: 43.27, H: 3.48, N: 17.75

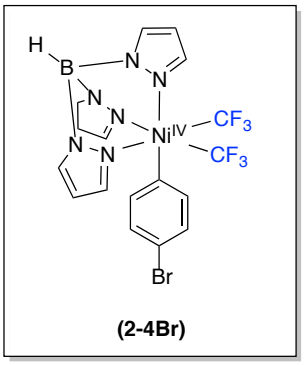

(2-4Br)

Synthesis of [(Tp)Ni^{IV}(CF$_3$)$_2$(4-Br-C$_6$H$_4$)] (2-4Br): Under an inert atmosphere, a 20 mL vial was charged with $(MeCN)_2Ni(CF_3)_2$ (51 mg, 0.18 mmol, 1.0 equiv), KTp (47 mg, 0.18 mmol, 1 equiv), and MeCN (15 mL). The solution was cooled to –35 °C. [Mes-I-4-Br-C_6H_4](BF$_4$) (95 mg, 0.26 mmol, 1.1 equiv) was added to the solution of **2**. The vial was shaken vigorously for 10 s at which point the reaction immediately turned purple. The resulting solution was allowed to stand for 5 min at –35 °C under an inert atmosphere before it was warmed to room temperature. The reaction was then removed from the drybox and was filtered through a 3 cm thick pad of silica on the benchtop. The pad was washed with THF (10 mL), and the combined filtrates were concentrated to dryness under reduced pressure. The crude solid was purified further by flash chromatography on silica gel (mobile phase: hexanes/ethyl acetate with a gradient from 100:1 to 90:10). The product was obtained as a yellow solid (36 mg, 34% yield).

Complex **2-4Br** was found to decompose upon standing in both the solid state and in solution. As such, all reactivity investigations were performed using freshly prepared samples of **2-4Br.**

^{1}H NMR (700 MHz, CD_3CN, 23 ºC): δ 8.05 (s, 1H), 7.95 (d, J_{HH} = 2.3 Hz, 1H), 7.92 (d, J_{HH} = 2.3 Hz, 2H), 7.33 (d, J_{HH} = 2.3 Hz, 2H), 7.17 (d, J_{HH} = 8.6 Hz, 2H), 6.67 (s, 2H), 6.44 (t, J_{HH} = 2.3 Hz, 1H), 6.28 (t, J_{HH} = 2.3 Hz, 2H), 4.68 (br, B-***H***). ^{13}C NMR (176 MHz, CD_3CN, 23 ºC): δ 156.52, 143.99, 143.74, 138.75, 136.74, 135.92, 120.78, 112.87 (q, J_{CF} = 392), 107.07, 106.72 ^{11}B NMR (225 MHz, CD_3CN, 23 ºC): δ –4.26 (d, J_{BH} = 118.0 Hz). ^{19}F NMR (470 MHz, CD_3CN, 23 ºC): δ –18.91 (s, 6F). Elemental Analysis calcd. for $C_{17}H_{14}BF_6N_6NiBr$, C: 36.09, H: 2.49, N: 14.86; found, C:36.05, H: 2.60, N: 15.91

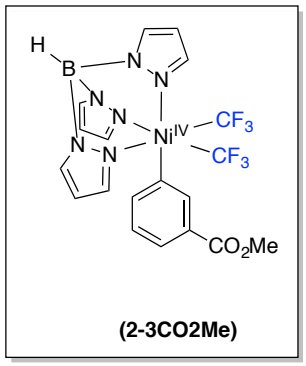

(2-3CO2Me)

Synthesis of [(Tp)Ni^{IV}(CF$_3$)$_2$(3-CO$_2$Me-C$_6$H$_4$)] (2-3CO$_2$Me): Under an inert atmosphere, a 20 mL vial was charged with (MeCN)$_2$Ni(CF$_3$)$_2$ (72 mg, 0.26 mmol, 1 equiv), KTp (65 mg, 0.26 mmol, 1.0 equiv), and MeCN (20 mL). The solution was cooled to –35 °C. [Mes-I-CO$_2$Me-C$_6$H$_4$](BF$_4$) (133 mg, 0.29 mmol, 1.1 equiv) was added to the solution of **3**. The vial was shaken vigorously for 10 s, at which point the reaction turned purple. The resulting solution was allowed to stand at –35 °C for 5 min under an inert atmosphere before it was warmed to room temperature. The reaction was removed from the drybox and was filtered through a 3 cm thick pad of silica on the benchtop. The pad was washed with THF (10 mL), and the combined filtrates were concentrated to dryness under reduced pressure. The crude solid was purified further by flash chromatography on silica gel (mobile phase: hexanes/ethyl acetate with a gradient from 100:1 to 90:10). The product was obtained as a yellow solid (34 mg, 24% yield).

^{1}H NMR (700 MHz, CD$_3$CN, 23 °C): δ 8.06 (s, 1H), 7.96 (s, 1H), 7.94 (d, J_{HH} = 3.1 Hz, 2H), 7.79 (d, J_{HH} = 7.8 Hz, 1H), 7.29 (br, 1H), 7.09 (t, J_{HH} = 7.8 Hz, 1H), 6.45 (s, 1H), 6.28 (d, J_{HH} = 3.1 Hz, 2H), 4.71 (br, B-***H***), 3.83 (s, 3H). ^{13}C NMR (176 MHz, CD$_3$CN, 23 °C): δ 166.74, 157.53, 144.20, 143.99, 142.03, 137.89, 136.99, 136.15, 129.83, 128.32, 127.98, 113.13 (q, J_{CF} = 392 Hz), 107.30, 106.95, 52.72. ^{11}B NMR (225 MHz, CD$_3$CN, 23 °C): δ –4.24 (d, J_{BH} = 117.7 Hz). ^{19}F NMR (470 MHz, CD$_3$CN, 23 °C): δ –19.15 (s, 6F). Elemental Analysis calcd. for C$_{19}$H$_{17}$BF$_6$N$_6$NiO$_2$, C: 41.88, H: 3.14, N: 15.42; found, C: 41.61, H: 3.00, N: 15.32

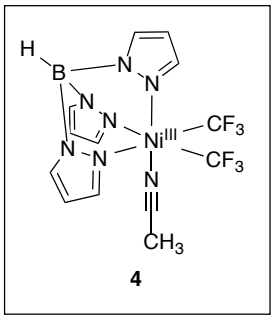

4

Synthesis of [(Tp)Ni^{III}(CF$_3$)$_2$(MeCN)] (4) As authentic standard for comparison to **4** isolated from the crude oxidation of **3** to **2a.** In the glovebox, a 20 mL vial was charged with (MeCN)$_2$Ni^{II}(CF$_3$)$_2$ (150 mg, 0.54 mmol, 1.0 equiv). The solid was dissolved in acetonitrile (8 mL). A solution of NMe$_4$Tp (163 mg, 0.57 mmol, 1.05 equiv) in acetonitrile (3 mL) was added, and the yellow-brown solution immediately turned orange-brown. A solution of AgBF$_4$ (105 mg, 0.54 mmol, 1.0 equiv) in acetonitrile (2 mL) was then added to the reaction mixture at –35 ºC. The orange-brown reaction mixture immediately changed color to purple, with concomitant formation of a Ag mirror. The crude reaction mixture was removed from the glovebox and filtered through a celite plug. The celite plug was washed with acetonitrile (10 mL), and the combined filtrates were concentrated to dryness under reduced pressure. The crude purple-brown solid was purified further by flash

chromatography on silica gel (mobile phase: hexanes/ethyl acetate with a gradient from 90:10 to 80:20). Compound **2c** was obtained as a purple solid (132 mg, 54% yield). ^{11}B NMR (225 MHz, CD_3CN, 23 ºC): δ –14.03 (br). Elemental Analysis calcd for $C_{13}H_{13}BF_6N_7Ni$, C: 34.64, H: 2.91, N: 21.75; found, C: 34.80, H: 2.98, N: 21.77. μ_{eff}(CH_3CN, 23 ºC) = 1.75.

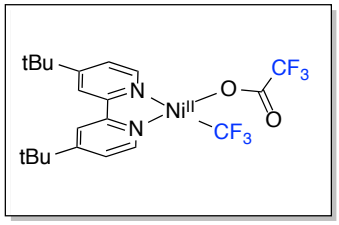

Synthesis of [(dtbpy)Ni^{II}(CF$_3$)(OTFA)]: Under ambient conditions, a 200 mL round bottomed flask was charged with $(PPh_3)_2Ni(CF_3)(OTFA)$[1] (1.0 g, 1.3 mmol, 1.0 equiv) and 4,4'-di-*tert*-butylbipyridine (385 mg, 1.4 mmol, 1.1 equiv). Dry dichloromethane (50 mL) was added, and the resulting dark orange solution stirred for 5 min at room temperature. The volatiles were removed under reduced pressure, and pentane (20 mL) was added to triturate the residue. The resulting solids were collected, washed with a 10:1 solution of pentane: diethyl ether (3 x 30 mL), and dried under reduced pressure to afford (dtbpy)Ni(CF_3)(OTFA) as a yellow solid (603 mg, 91% yield). The ^{1}H and ^{13}C NMR spectra of S1 were recorded at –30 ºC to slow the fluxional processes associated with this complex ^{1}H NMR (700 MHz, CD_2Cl_2, –30 ºC): δ 8.21 (br, 1H), 7.82 (br, 2H), 7.74 (br, 1H), 7.46 (br, 1H), 7.39 (br, 1H), 1.36 (br, 18H). ^{13}C NMR (176 MHz, CD_2Cl_2, –30 ºC): δ 165.83, 165.42, 161.98, 155.35, 153.10, 152.84, 147.40, 124.26, 124.06, 118.36, 117.81, 115.08, 35.66, 35.62, 29.91, 29.85. ^{19}F NMR (471 MHz, CD_2Cl_2, 23 ºC): δ –34.40 (br, 3F, C*F*$_3$), –75.35 (br, 3F, OCOC*F*$_3$). IR (ATR, cm^{-1}): 1695 (s), 1617 (m), 1415 (m), 1195 (s).

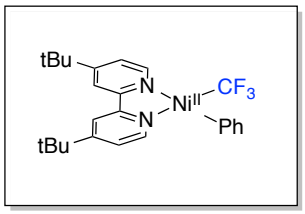

Synthesis of [(dtbpy)Ni^{II}(CF$_3$)(Ph)]: In the glovebox, a 150 mL round bottomed flask was charged with (dtbpy)Ni^{II}(CF_3)(OTFA) (590 mg, 1.16 mmol, 1.0 equiv), and this yellow solid was dissolved in THF (60 mL). The resulting solution was cooled to –35 ºC, and then $ZnPh_2$ (140 mg, 0.63 mmol, 0.55 equiv) in THF (5 mL) was added. The reaction mixture was allowed to warm to room temperature over approximately 5 min, during which time the solution changed color from dark orange to dark red. The solution was then filtered through a 3 cm pad of basic alumina, and the pad was washed with THF (5 mL). The washes were combined, and the volatiles were removed under reduced pressure. The resulting dark red residue was triturated with pentane (10 mL), and the solids were collected by filtration. The solids were washed with additional pentane (40 mL) and then dried under reduced pressure to

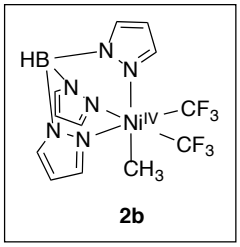

2b

yield complex 4 as an orange solid (334 mg, 61% yield). ^{1}H NMR (700 MHz, CD_2Cl_2, 23 ºC): δ 8.78 (d, J_{HH} = 6.0 Hz, 1H), 7.90 (d, J_{HH} = 2.0 Hz, 1H), 7.84 (d, J_{HH} = 2.0 Hz, 1H), 7.65-7.61 (multiple peaks, 2H), 7.50 (dd, J_{HH} = 6.0, 2.0 Hz, 1H), 7.14 (dd, J_{HH} = 6.1, 2.0 Hz, 1H), 7.11 (d, J_{HH} = 6.0 Hz, 1H), 7.00 (multiple peaks, 2H), 6.89 (t, J_{HH} = 7.3 Hz, 1H), 1.40 (s, 9H), 1.31 (s, 9H). ^{13}C NMR (176 MHz, CD_2Cl_2, 23 ºC): δ 163.32, 163.20, 155.20, 154.05, 151.51, 151.48, 150.63, 139.31 (q, J_{CF} = 359 Hz), 135.45, 125.96, 123.73, 123.23, 122.01, 117.51, 117.22, 35.36, 35.29, 29.96, 29.88. ^{19}F NMR (377 MHz, CD_3CN, 23 ºC): δ –21.95 (s, 3 F). HRMS-electrospray (m/z): $[M - F]^+$ calcd. for $C_{25}H_{29}F_2N_2Ni$, 453.1652; found, 453.1644. Elemental Analysis calcd. for $C_{25}H_{29}F_2N_2Ni$, C: 63.45, H: 6.18, N: 5.92; found, C: 63.30, H: 6.26, N: 5.82.

Synthesis of TpNi^{IV}(CF$_3$)$_2$(CH$_3$) (2b): Note: **2b** is mildly light sensitive and should be stored in a dark place. Extended manipulations in direct light can result in slightly diminished yields. A 20 mL vial was charged with NMe_4Tp (258 mg, 0.9 mmol, 1 equiv.), $(MeCN)_2Ni(CF_3)_2$ [6] (250 mg, 0.90 mmol, 1 equiv), 4 mL of anhydrous CH_3NO_2 and a magnetic stir bar. The resultant solution was stirred for 1 minute before 1.1 mL of I–CH3 (18 mmol, 20 equivalents) was added in one portion. A separate vial, 2,6-difluorobenzenediazonium tetrafluoroborate (1.2 mmol, 1.3 equiv) and a minimum of CH_3NO_2 (~1.5 mL). Upon addition, the combined solutions immediately bubbled vigorously and turned dark brown. The vial was then removed from the box and the volatiles were removed under a gentle stream of N_2. The resultant residue was then stirred over 2 mL of 1:1 hexanes: ethyl acetate for 20 minutes. This solution was loaded directly on to a silica column and was purified using a gradient from pure hexane to 95:5 hexane:ethyl acetate. The product was collected and the volatiles were removed to yield **7** as an off white powder (153mg, 40%). ^{1}H NMR (700 MHz, Acetonitrile-d_3) δ 8.09 (s, 1H), 7.93 (s, 1H), 7.88 (s, 2H), 7.83 (s, 2H), 6.41 (s, 1H), 6.35 (s, 2H), 3.68 (s, 3H). ^{13}C NMR (176 MHz, Acetonitrile-d_3) δ 143.81, 141.79, 136.11, 135.92, 114.57 (q, J=386Hz) 106.34, 105.87, 44.37 (sept, J= 5.4Hz) ^{11}B NMR (225 MHz, Acetonitrile-d_3) δ -4.52 (d, J=113.9 Hz).^{19}F NMR (471 MHz, Acetonitrile-d_3) δ -23.44. Elemental analysis: calculated for $C_{12}H_{13}N_6BF_6Ni$, C: 33.93, H: 3.08, N: 19.79; Found: C: 34.28, H: 3.55, N: 19.66.

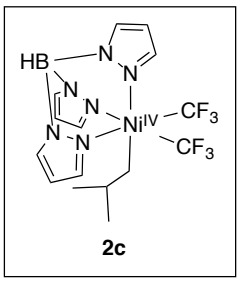

2c

Synthesis of $TpNi^{IV}(CF_3)_2(CH_3)$ (7): Note: **2c** is highly light and thermally sensitive. It should be stored in a dark place. Extended manipulations in direct light can result in diminished yields. A 20 mL vial was charged with NMe_4Tp (65 mg, 0.9 mmol, 1 equiv.), $(MeCN)_2Ni(CF_3)_2$ [6] (63 mg, 0.22 mmol, 1 equiv), 1 mL of anhydrous CH_3NO_2 and a magnetic stir bar. The resultant solution was stirred for 1 minute before 0.250 mL of I–CH3 (4.5 mmol, 20 equivalents) was added in one portion. A separate vial, 2,6-difluorobenzenediazonium tetrafluoroborate (XXmg, 0.30 mmol, 1.3 equiv) and a minimum of CH_3NO_2 (~0.5 mL). Upon addition, the combined solutions immediately bubbled vigorously and turned dark brown. The vial was then wrapped in aluminum foil, removed from the box, and the volatiles were removed under a gentle stream of N_2. The resultant residue was then stirred over 1 mL of 1:1 hexanes: ethyl acetate for 5 minutes. This solution was loaded directly on to a silica column and was purified using a gradient from pure hexane to 95:5 hexane:ethyl acetate. The product was collected and the volatiles were removed under reduced pressure in the dark to yield **7** as a white microcrystalline powder (9.5 mg, 9%). NMR spectra were recorded at -25 ºC to reduce decomposition ^{1}H NMR (700 MHz, CD_3CN) δ 8.02 (s, 2H), 7.97 (s, 1H), 7.87 (s, 1H), 7.84 (s, 1H), 6.34 (d, J = 2.5 Hz, 2H), 6.31 (s, 1H), 4.89-4.24 (multiple peaks, 3H), 2.14 (m, 1H), 0.33 (d, J = 6.6 Hz, 6H). ^{11}B NMR (225 MHz, CD_3CN) δ -4.46 (d, J = 116.4 Hz).^{13}C NMR (176 MHz, CD_3CN)) δ 143.59, 143.17, 136.22, 135.49, 114.15 (q, J= 388 Hz), 105.89, 105.47, 76.72 (m) 34.89, 19.52. ^{19}F NMR (377 MHz, CD_3CN) δ -23.92.

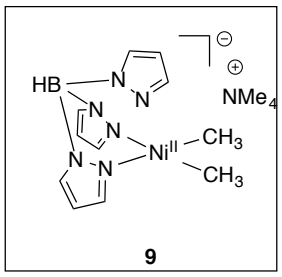

9

Synthesis of [NMe_4(Tp)Ni(CH_3)$_2$] (3): In the glovebox, a 20 mL vial was charged with $(Py)_2Ni(CH_3)_2$ (50, 0.20 mmol, 1.0 equiv), NMe_4Tp (57 mg, 0.20 mmol, 1.0 equiv), and acetonitrile (5 mL). The solution was stirred for 1 min before the volatiles were removed under reduced pressure. An additional 5 mL of acetonitrile were added and subsequently removed to dryness under vacuum. The resultant cream solid was triturated with pentane (5 mL) and dried under vacuum to yield (380 mg, 94% yield). ^{1}H NMR (498 MHz, $(CD_3)_2CO$, 23 ºC): δ 8.13 (bs, 3H), 7.42 (s, 3H), 6.28 (s, 3H), 3.01 (s, 12H) -0.85 (s, 6H). ^{11}B NMR (225 MHz, δ -2.52 (d, 1H). Elemental analysis: calculated for $C_{15}H_{28}N_6BNi$, C: 47.92, H: 7.51, N: 26.08 Found: C: 47.66, H: 7.45, N: 25.89.

3.3.3 NMR Scale Oxidation Studies

$2e^-$ Oxidation of 3 with Aryl Electrophiles

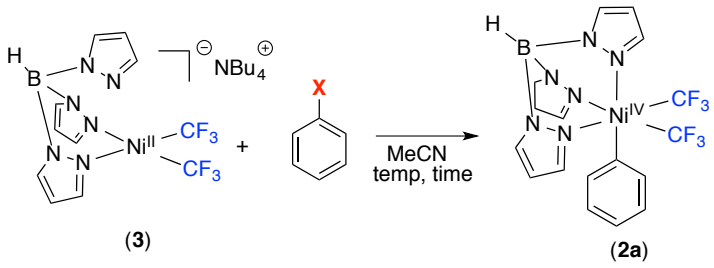

(3) (2a)

A screw cap NMR tube was charged with complex **3** (6.0 mg, 0.0092 mmol, 1.0 equiv), the internal standard 4,4'-difluorobiphenyl (~2 mg), and CD_3CN (0.5 mL) and TEMPO during radical detection studies. The ratio between the standard and **3** was determined by ^{19}F NMR integration.The NMR sample was taken back into the glovebox, and the appropriate aryl electrophile and additive, if present, were added. After heating at the appropriate temperature, the yield of Ni^{IV} complex **2a** was determined by ^{19}F NMR spectroscopy . Representitive NMR are shown below.

Table 3.2. Summary of Ph-X oxidation attempts. NR = no reaction. [a] Unidentified decomposition of the starting materials was observed, but Ph-CF_3 was not detected. [b]A purple paramagnetic mixture of products consistent with the generation of **4** was observed by ^1H and ^{19}F NMR spectroscopy.

Ar-X	Time	Temp (°C)	Ar-X Equiv	Additive	^{19}F NMR Yield of 2 (%)
PhN_2BF_4	10 min	23	1.1	none	42
Ph_2IBF_4	10 min	–35	1.1	none	77
PhI	12 h	70	1.1	none	NR
PhI	12 h	135	500 (neat)	none	<1[a]
PhI	12 h	23	2	2 equiv AgOAc	<1[b]
PhI	12 h	23	2	2 equiv $AgBF_4$	<1[b]
PhI	12 h	23	2	2 equiv $TlPF_6$	<1[a]
PhOTf	12 h	70	10	none	NR
PhBr	12 h	70	10	none	NR
IC_6F_5	12 h	70	10	none	NR
3,5-CF_3-IC_6H_3	12 h	70	10	none	NR
3,5-CF_3-IC_6H_3	12 h	23	2	2 equiv AgOAc	<1[b]

Radical Trapping Experiments in the Oxidation of 3 to 2a

Figure 3.10. ^{19}F NMR spectra of: (top) **3,** TEMPO and the internal standard at room temperature prior to oxidation; (bottom) reaction mixture after treatment with 1.1 equiv of N_2PhBF_4.

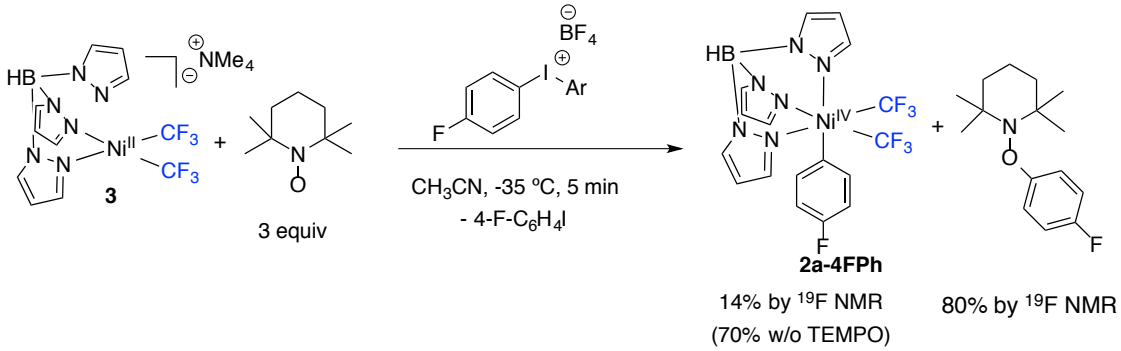

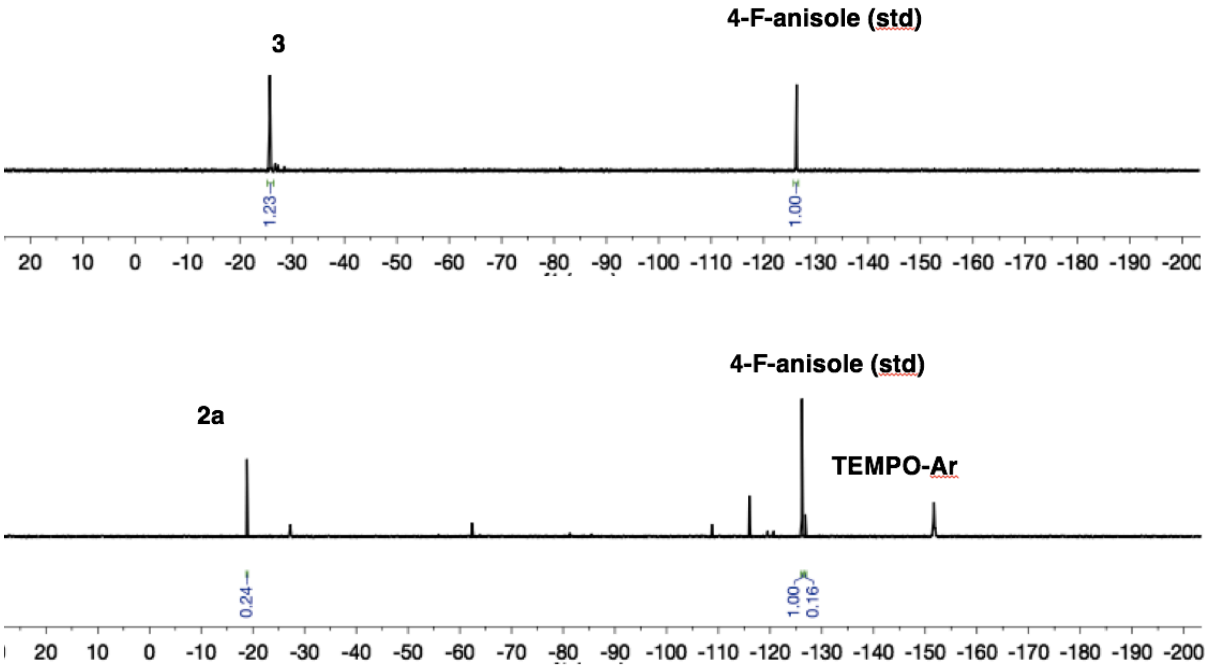

Radical Relay Oxidation Study

7 is mildly light sensitive and should be stored in a dark place. Extended manipulations in direct light can result in slightly diminished yields. A 4 mL vial was charged with NMe_4Tp (51 mg, 0.18mmol, 1 equiv.), $(MeCN)_2Ni(CF_3)_2$ [6] (50 mg, 0.18 mmol, 1 equiv), 1 mL of anhydrous CH_3NO_2 and a magnetic stir bar. The resultant solution was stirred for 1 minute

before I–CH_3 (2 mmol, 20 equivalents) was added in one portion as a 0.1M stock solution in CH_3NO_2. A separate vial, 2,6-difluorobenzenediazonium tetrafluoroborate (55 mg, 0.25 mmol, 1.3 equiv) and 1 mL of CH_3NO_2 (~1.5 mL). Upon addition, the combined solutions immediately bubbled vigorously and turned dark brown. The solution was stirred for a minute before it was removed from the glovebox and 3 equivalents of 1,4 difluorobenzene were added as an internal standard. The solution was then analyzed by ^{19}F NMR to determine the yield of

Figure 3.11 ^{19}F NMR spectra of the products of radical relay oxidation. The internal standard 1,4 difluorobenzene can be seen at -120 ppm and **2b** is seen at -23 ppm

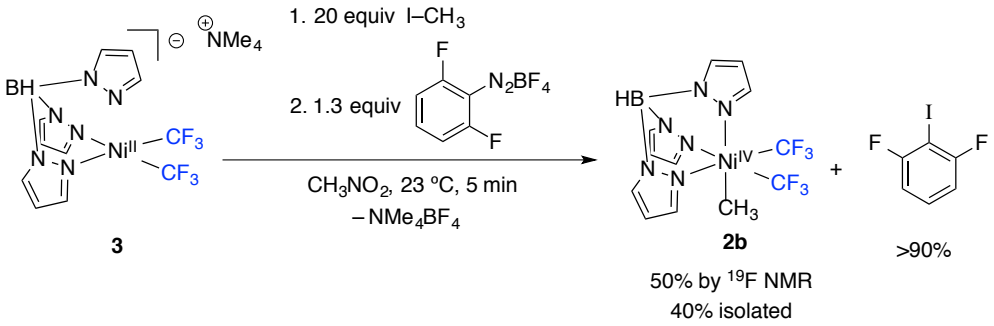

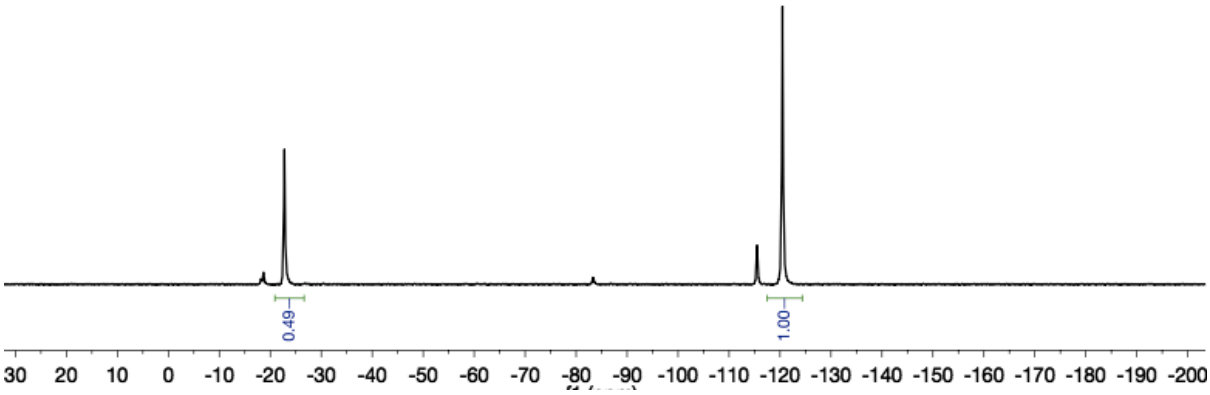

Oxidation of (dtbpy)Ni(CF_3) Complexes to 6

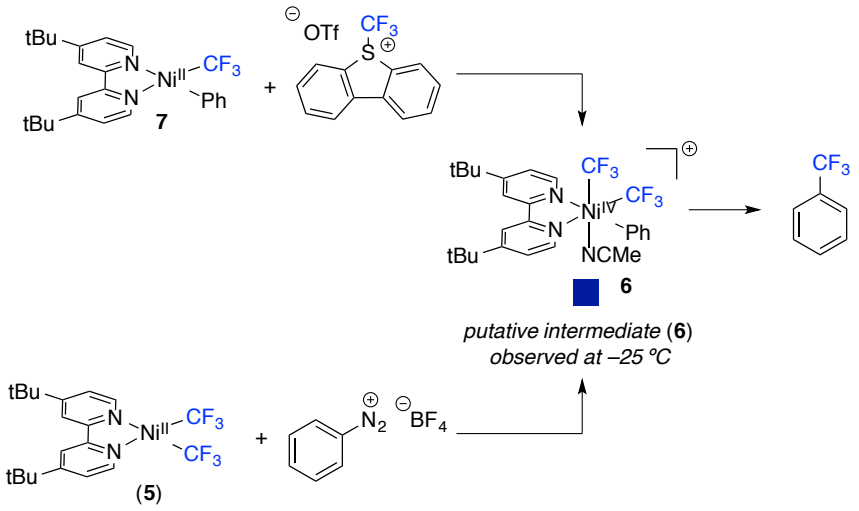

Pathway A (top): A 4 mL vial was charged with complex **7** (8.0 mg, 0.017 mmol, 1.0 equiv), tetrabutylammonium triflate (19 mg, 0.051 mmol, 3.0 equiv), and 4,4'-difluorobiphenyl. Acetonitrile-d_3 (0.5 mL) was added, and the resulting solution was transferred to an NMR tube. The sample was removed from the glovebox and placed in an NMR spectrometer pre-cooled to –25 ºC. The ratio between the standard and **4** was determined by ^{19}F NMR integration at this temperature. The sample was removed from the spectrometer, and a solution of *S*-(trifluoromethyl)dibenzothiophenium triflate (10 mg, 0.026 mmol, 1.5 equiv) in acetonitrile-d_3 (0.2 mL) was added under a N_2 atmosphere. The NMR tube was shaken vigorously and then placed back into the NMR spectrometer at –25 ºC. After 1 min at this temperature, two new ^{19}F resonances (which we attribute to the formation of **6**) were observed in 21% yield along with 27% of the reductive elimination product (–19.8 ppm, J_{FF} = 7.9 Hz, –24.8 ppm, J_{FF} = 7.9 Hz; Figure S17b). After 30 min at room temperature, the sample was analyzed by ^{19}F NMR spectroscopy and full consumption of putative intermediate **6** was observed along with 63% of benzotrifluoride .

Pathway B (b): A 4 mL vial was charged with complex **5** (4 mg, 0.0086 mmol, 1.0 equiv), tetrabutylammonium triflate (10 mg, 0.0025 mmol, 3.0 equiv), and the internal standard 4,4'-difluorobiphenyl. Acetonitrile-d_3 (0.5 mL) was added, and the resulting solution was transferred to an NMR tube. The sample was removed from the glovebox and placed in an NMR spectrometer pre-cooled to –25 ºC. The ratio between the standard and **5** was determined by ^{19}F NMR integration at this temperature. The sample was removed from the spectrometer

and allowed to warm to room temperature, and a solution of PhN_2BF_4 (1.8 mg, 0.0095 mmol, 1.1 equiv) in acetonitrile-d_3 (0.15 mL) was added under a N_2 atmosphere. The NMR tube was shaken vigorously for 15 s and then placed back into the NMR spectrometer at –25 ºC. After 1 min at this temperature, two new ^{19}F resonances (–19.8 ppm, J_{FF} = 7.9 Hz, –24.8 ppm, J_{FF} = 7.9 Hz) were observed in 28% yield along with 14% of the reductive elimination product, and 24% of unreacted **5** as determined by ^{19}F NMR integration against the standard (Figure S18b). After 60 min at room temperature, the sample was analyzed by ^{19}F NMR spectroscopy and full consumption of intermediate **6** was observed along with 43% yield of benzotrifluoride (Figure3.12)

Figure 3.12. ^{19}F NMR spectra of the reaction of 4 and 1.5 equiv of PhN_2BF_4 at: (a) –25 ºC prior to oxidation; (b) –25 ºC, 1 min after treatment with PhN_2BF_4; (c) room temperature, 60 min after oxidation.

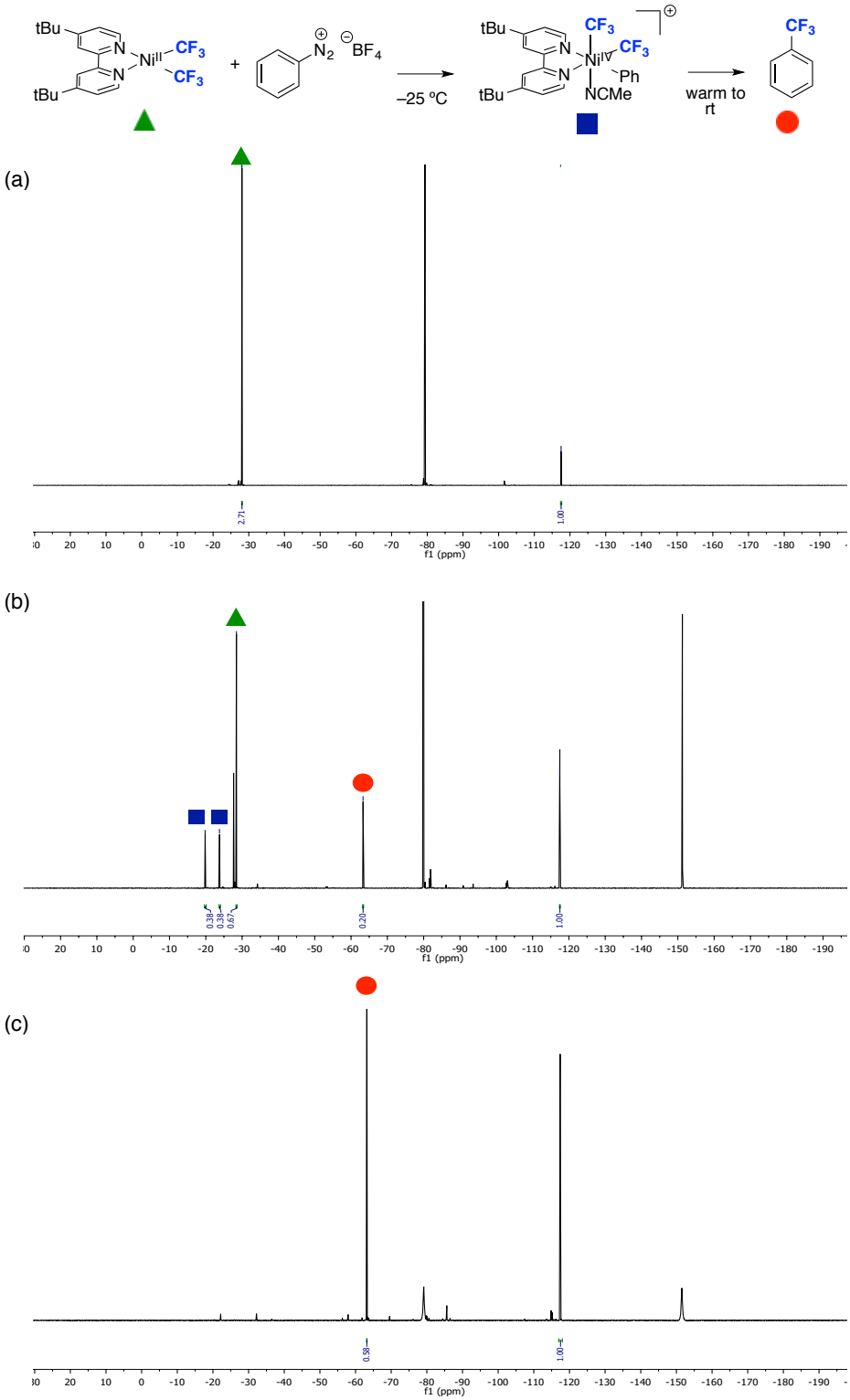

3.4.4. Reductive Elimination Studies

Ar–CF_3 Coupling from 2–R

Procedure: A 4 mL vial was charged with the appropriate Ni^{IV} complex **2** (R = *p*-OMe, *p*-Me, H, *p*-Br, *m*-CO_2Me) (0.010 mmol), 4,4'-difluorobiphenyl, and acetonitrile-d_3 (0.5 mL). The resulting yellow solution was transferred to a Teflon-lined screw cap NMR tube and removed from the glovebox. The ratio between the standard and **2** was determined by ^{19}F NMR integration at room temperature. The NMR tube was heated in an oil bath at 55 ºC for 4 to 18 h, during which time the solution changed color from yellow to colorless. The solutions were then analyzed by ^{19}F NMR spectroscopy to determine the yields of the corresponding benzotrifluorides (70-95%, Table XX). After each reaction, an authentic sample of the appropriate aryl–CF_3 product was added to the crude reaction mixture. In each case, the ^{19}F NMR resonances were coincident.

The main Ni^{II} byproducts of the reaction were determined to be $Ni^{II}Tp_2$ and $(CD_3CN)_2Ni^{II}(CF_3)_2$.[20] These are presumably generated via ligand disproportionation from the initial reductive elimination product, $TpNi^{II}CF_3$. $(CD_3CN)_2Ni(CF_3)_2$ was formed in 29% yield as determined by ^{19}F NMR spectroscopy (Figure S3b). $NiTp_2$ precipitated from the crude reaction mixture as purple crystals and was isolated in 26% yield (0.031 mmol reaction scale).[21] The spectra of these compounds were compared to those reported in the literature to confirm their identities.[19,20] Unidentified paramagnetic species (likely Ni^{III} compounds) were also detected by ^{1}H NMR spectroscopic analysis following the thermolysis of **2**. The origin of these species is not well-understood and will require further detailed investigation. However, we have conducted a number of preliminary experiments to test whether these are generated via radical processes and/or whether reductive elimination is proceeding from Ni^{III} intermediates rather than Ni^{IV}. As described below, radical trapping experiments and single electron reduction of **2-Me** are both inconsistent with the involvement of Ni^{III} intermediates in aryl–CF_3 bond-forming reductive elimination.

Table 3.3. Reductive elimination from Ni^{IV} complexes **2-R** at 55 ºC. Yields of Ar-CF_3 are determined by ^{19}F NMR integration against the fluorine standard 4,4'-difluorobiphenyl.

Complex	Time (h)	Ar-CF_3 ^{19}F NMR Yield (%)
2-H	15	76
2-OMe	4	95
2-Me	15	71
2-Br	16	81
2-CO_2Me	18	70

Radical Trapping Studies

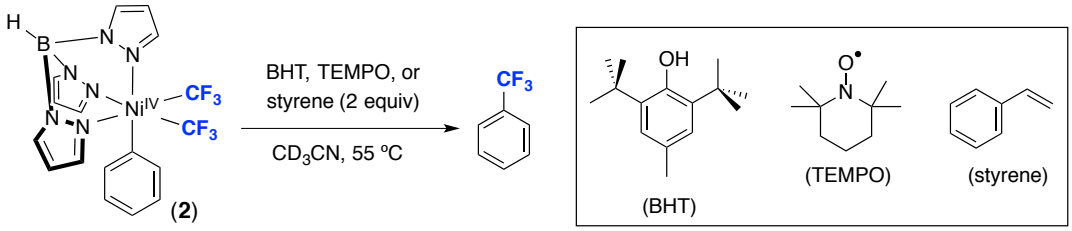

Procedure: A 4 mL vial was charged with Ni^{IV} complex **2** (4.0 mg, 0.0083 mmol, 1.0 equiv) and the respective radical trap (0.016 mmol, 2.0 equiv). 4,4'-Difluorobiphenyl was added as an internal standard. Acetonitrile-d_3 (0.5 mL) was added, and the resulting yellow solution was transferred to a Teflon-lined screw cap NMR tube and removed from the glovebox. The ratio between the standard and **2** was determined by ^{19}F NMR integration at room temperature. The NMR tube was heated in an oil bath at 55 ºC for 18 h. After the reaction reached completion, the solution was analyzed by ^{19}F NMR spectroscopy to determine the yield of benzotrifluoride. In all cases, the yield of $PhCF_3$ was not affected by the presence of radical traps, suggesting that the reductive elimination process does not proceed via a radical hemolysis pathway.

Table 3.4 Effect of various common radical traps on the yield of Ph–CF_3 from **2a**

Radical Trap	^{19}F NMR Yield of Ar-CF_3 (%)
None	76%
BHT	76%
TEMPO	79%
styrene	70%

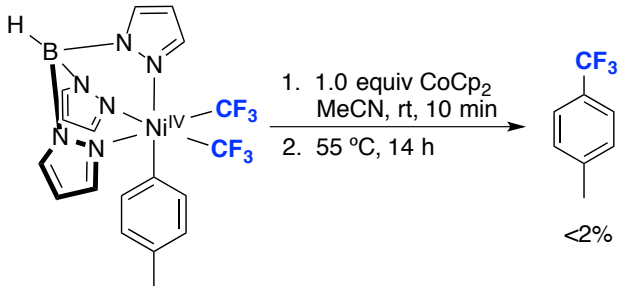

To investigate the possibility for reductive elimination from Ni^{III} species generated *in situ*, **2-Me** was reacted with 1 equiv of the single electron reductant, $CoCp_2$. The procedure and supporting spectra can be found below.

Procedure: A 4 mL vial was charged with Ni^{IV} complex **2-Me** (4.1 mg, 0.0083 mmol, 1.0 equiv), acetonitrile-d_3 (0.4 mL) and 4,4'-difluorobiphenyl as an internal standard. The solution was transferred to a Teflon-lined screw cap NMR tube, and the tube was removed from the glove box. The ratio between the standard and **2-Me** was determined by ^{19}F NMR integration at room temperature. The sample was brought back into the glove box. A separate 4 mL vial was charged with $CoCp_2$ (15.5 mg, 0.082 mmol) and acetonitrile-d_3 (1 mL). Next, $CoCp_2$ from the stock solution (100 µL, 1.0 equiv) was added to the solution of **2-Me** via syringe. The reaction mixture was shaken vigorously for 5 s. Over 1 min, the solution turned green and then orange. After 10 min, the sample was then analyzed by ^{19}F NMR spectroscopy. A mixture of compounds consistent with the formation $[Ni^{II}(CF_3)_n]$ complexes was observed. The diamagnetic compounds in this reaction are likely formed via the radical homolysis of transient $TpNi^{III}(CF_3)_2(4\text{-}MeC_6H_4)$ (formed from the initial $1e^-$ reduction of **2-Me** by $CoCp_2$). Both $CHCF_3$ and $CDCF_3$ were observed in the crude reaction mixture. The NMR tube was then heated in an oil bath at 55 ºC for 14 h. The solution was analyzed by ^{19}F NMR spectroscopy to determine the yield of 4-Me-benzotrifluoride.

3.4.5. Reaction Kinetics

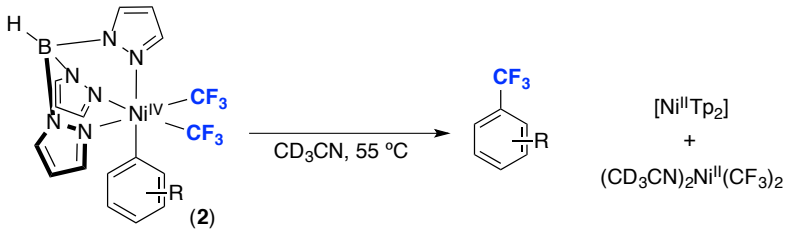

R = *p*-OMe, *p*-Me, H, *p*-Br, *m*-CO_2Me

Procedure: A Teflon-lined screw cap NMR tube was charged with the respective Ni^{IV} complex **2-R** (R = *p*-OMe, *p*-Me, H, *p*-Br, *m*-CO_2Me) (0.010 mmol). 4,4'-Difluorobiphenyl (0.010 mmol, 1.0 equiv) was added as an internal standard. Dry acetonitrile-d_3 (0.5 mL) was added, and the NMR sample was removed from the glove box and placed in the NMR spectrometer with the temperature pre-set to 55 ºC. The rates of reductive elimination from complexes **2-R** to form the corresponding benzotrifluoride products were obtained by monitoring the reactions by ^{19}F NMR spectroscopy at this temperature. Concentration versus time data was acquired from the integration of the ^{19}F NMR signals of **2-R** and the substituted benzotrifluoride (**Ar-CF_3**) versus the internal standard. The rate constant for each experiment was determined by fitting the decay of **2-R** and the growth of the coupled product (**Ar-CF_3**) to single exponentials (Figures S9-S13; Table S4). A plot of the Hammett value,[22] , versus log (k_R/k_H) showed a linear correlation (R^2 = 0.98) with a negative slope, = –0.91 (Figure S8, solid line). Rate constants obtained from the growth of the Ar-CF_3 reductive elimination product gave a similar trend (Figure S8, dotted line; = –1.05, R^2 = 0.99).

Table 3.5. Relevant kinetic parameters and data from the thermolysis of **2-R**

Substituent (R)	Hammett Value (σ)	Ni^{IV} decay k_{obs} (x10^{-4} s^{-1})	Ar-CF_3 growth k_{obs} (x10^{-4} s^{-1})
p-OMe	–0.27	4.6	3.5
p-Me	–0.14	2.9	2.2
H	0	2.6	2.0
p-Br	0.26	1.4	1.0
m-CO_2Me	0.36	1.1	0.74

3.4.6. Cyclic Voltammetry Studies

Experimental Procedure: Cyclic voltammetry on complexes **3** and **5** was performed in a 3-electrode cell consisting of a 3 mm glassy carbon disc working electrode, a Ag/Ag^+ reference electrode with a Ag wire in a fritted chamber containing a solution of $AgBF_4$ (0.01 M) and NBu_4PF_6 (0.1 M) in acetonitrile, and a Pt wire counter electrode. A 2 mL solution of each complex (0.01 M) and NBu_4PF_6 (0.1 M) in acetonitrile was added to the electrochemical cell. Cyclic voltammetry scans were taken at 100 mV/s. After obtaining the CV, ferrocene was added as an internal reference.

Figure 3.13 Cyclic Voltammograms of complexes **3** (a) and **9** (b)

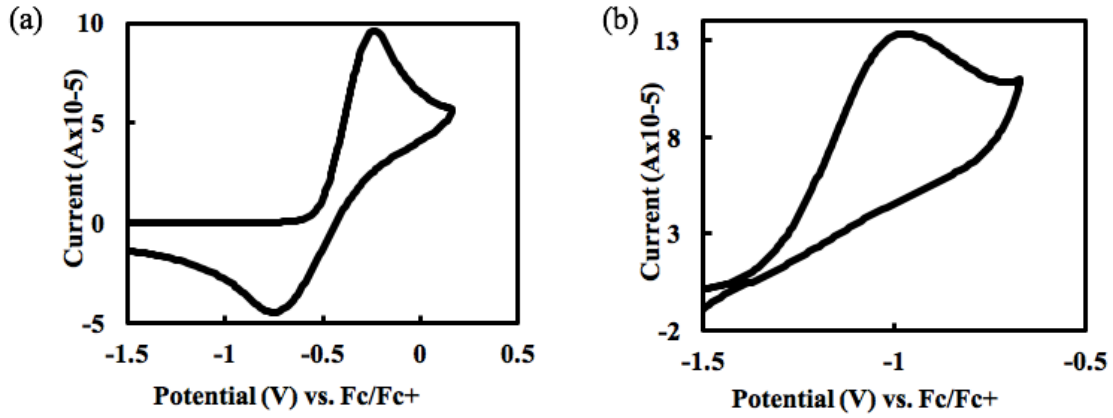

4. Computational Methodology

Gaussian 09[23] was used for DFT calculations at the B3LYP level for optimization, using the Stuttgart/Dresden ECP (SDD) basis set for Ni and the 6-31G(d) basis set for other atoms Single-point calculations were performed at the M06 level, utilizing the quadruple-ξ valence polarized def2-QZVPbasis set on Ni along with the corresponding ECP and the 6-311+G(2d,p) basis set on other atoms All calculations were carried out for acetonitrile as solvent with the IEFPCM (SCRF) model. All thermodynamic data were calculated at the standard state (298.15 K and 1 atm), and entropy calculations were adjusted by the method proposed by Okuno.(33f) All transition structures contained one imaginary frequency, exhibiting atom displacements consistent with the anticipated reaction pathway. The nature of transition structures was confirmed by intrinsic reaction coordinate (IRC) searches, vibrational frequency calculations, and potential energy surface scans.

3.3.7. X-ray Structural Determination

Structure Determination of 2a

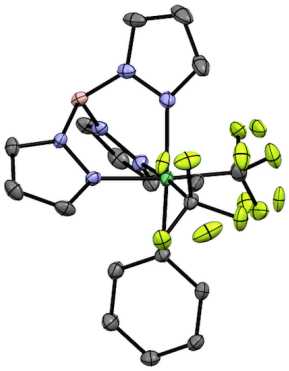

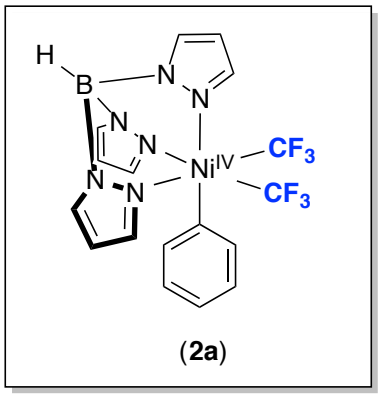

(**2a**)

Yellow plates of **2a** were grown by slow evaporation of methanol/acetonitrile solution of the compound at 23 ºC. A crystal of dimensions 0.16 x 0.12 x 0.04 mm was mounted on a Rigaku AFC10K Saturn 944+ CCD-based X-ray diffractometer equipped with a low temperature device and Micromax-007HF Cu-target micro-focus rotating anode (= 1.54187 A) operated at 1.2 kW power (40 kV, 30 mA). The X-ray intensities were measured at 85(1) K with the detector placed at a distance 42.00 mm from the crystal. A total of 3672 images were collected with an oscillation width of 1.0 in The exposure times were 5 sec. for the low angle images, 25 sec. for high angle. The integration of the data yielded a total of 24282 reflections to a maximum 2 value of 136.42 of which 3407 were independent and 3277 were greater than 2 (I). The final cell constants were based on the xyz centroids 15729 reflections above 10 (I). Analysis of the data showed negligible decay during data collection; the data were processed with CrystalClear 2.0 and corrected for absorption. The structure was solved and refined with the Bruker SHELXTL (version 2008/4) software package, using the space group P1bar with Z = 2 for the formula $C_{17}H_{15}BN_6F_6Ni$. All non-hydrogen atoms were refined anisotropically with the hydrogen atoms placed in idealized positions. Both trifluoromethyl ligands are rotationally disordered. Full matrix least-squares refinement based on F^2 converged at R1 = 0.0283 and wR2 = 0.0697 [based on I > 2sigma(I)], R1 = 0.0291 and wR2 = 0.0702 for all data. Additional details are presented in Table S5 and are given as Supporting Information in a CIF file. Acknowledgement is made for funding from NSF grant CHE-0840456 for X-ray instrumentation.

Table 3.6 Acquisition and refinement parameters for the structure determination of **2a**

Empirical Formula	$C_{17}H_{15}BN_6F_6Ni$
Formula Weight	486.87
Temperature	85 (1) K
Wavelength	1.54178 A
Crystal System	triclinic
Space Group	P-1
Unit Cell Dimensions	a= 7.73560(10) Å α= 98.463(7) b = 8.7328(2) Å β= 96.208(7) c = 14.9794(11) Å γ= 107.975(8)
Volume	939.27(7) A^3
Z	2
Calculated Density	1.721 Mg/m^3
Absorption Coefficient	2.207 mm^{-1}
F(000)	492
Crystal Size	0.16x0.12x.04 mm
Theta Range for Data Collection	3.04 to 68.21
Limiting Indices	$-9\leq h\leq 9$, $-10\leq k\leq 10$, $-18\leq l\leq 17$
Reflections Collected	24282
Independent Reflections	3407
Completeness to Theta	98.8%
Absorption Correction	Semi-empirical from equivalents
Max and Min Transmission	0.9169 to 0.7190
Refinement Method	Full-matrix least-squares on F^2
Data / Restraints / Parameters	3407 / 7 / 345
Goodness-of-Fit on F^2	1.042
Final R Indices [$I>2\sigma(I)$]	R1 = 0.0283, wR2 = 0.0697
R indices (all data)	R1 = 0.0291, wR2 = 0.0702
Largest Difference Peak and Hole	0.271 and -0.316 A^{-3}

Structure Determination of 4

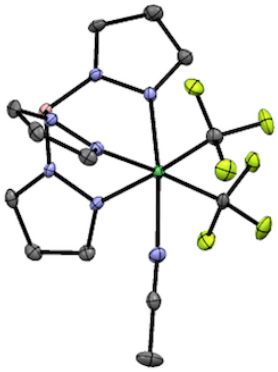

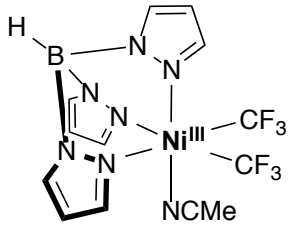

4

Purple plates of **2c** were grown from a pentane/diethyl ether (containing a 1 drop of acetonitrile) solution of the compound at 23 ºC. A crystal of dimensions 0.14 x 0.12 x 0.12 mm was mounted on a Rigaku AFC10K Saturn 944+ CCD-based X-ray diffractometer equipped with a low temperature device and Micromax-007HF Cu-target micro-focus rotating anode (λ = 1.54187 A) operated at 1.2 kW power (40 kV, 30 mA). The X-ray intensities were measured at 85(1) K with the detector placed at a distance 42.00 mm from the crystal. A total of 2028 images were collected with an oscillation width of 1.0° in ω. The exposure times were 1 sec. for the low angle images, 6 sec. for high angle. The integration of the data yielded a total of 24861 reflections to a maximum 2θ value of 136.46° of which 3099 were independent and 3064 were greater than 2σ(I). The final cell constants were based on the xyz centroids 16173 reflections above 10σ(I). Analysis of the data showed negligible decay during data collection; the data were processed with CrystalClear 2.0 and corrected for absorption. The structure was solved and refined with the Bruker SHELXTL (version 2008/4) software package, using the space group Pna2(1) with Z = 4 for the formula $C_{13}H_{13}BN_7F_6Ni$. All non-hydrogen atoms were refined anisotropically with the hydrogen atoms placed in a combination of idealized and refined positions. Full matrix least-squares refinement based on F^2 converged at R1 = 0.0263 and wR2 = 0.0636 [based on I > 2sigma(I)], R1 = 0.0266 and wR2 = 0.0638 for all data. Additional details are presented in Table S13 and are given as Supporting Information in a CIF file. Acknowledgement is made for funding from NSF grant CHE-0840456 for X-ray instrumentation.

Table 3.7. Acquisition and refinement parameters for the structure determination of **4**

Empirical Formula	$C_{13}H_{13}BF_6N_7Ni$
Formula Weight	450.82
Temperature	85(2) K
Wavelength	1.54178 A
Crystal System	Orthorhombic
Space Group	Pna2(1)
Unit Cell Dimensions	a = 17.0516(1) A alpha = 90 deg. b =7.53680(13) A beta = 90 deg c = 13.2536(2) A gamma = 90 deg.
Volume	1703.28(1) A^3
Z	4
Calculated Density	1.758 mg/m^3
Absorption Coefficient	2.390 mm^{-1}
F(000)	908
Crystal Size	0.20 x 0.14 x 0.12 mm
Theta Range for Data Collection	5.19 to 68.23 deg
Limiting Indicies	$-20\leq h\leq 20$, $-9\leq k\leq 9$, $-15\leq l\leq 15$
Reflections Collected	24861
Independent Reflections	3099 [R(int) = 0.0499]
Completeness to Theta	68.23 (100%)
Absorption Correction	Semi-empirical from equivalents
Max and Min Transmission	0.7366 and 0.6464
Refinement Method	Full-matrix least-squares on F^2
Data / Restraints / Parameters	3099 / 1 / 259
Goodness-of-Fit on F^2	1.183
Final R Indices [$I>2\sigma(I)$]	R1 = 0.0262, wR2 = 0.0636
R indices (all data)	R1 = 0.0266, wR2 = 0.0638
Largest Difference Peak and Hole	0.260 and -0.240 $e.A^{-3}$

Structure Determination of 2c

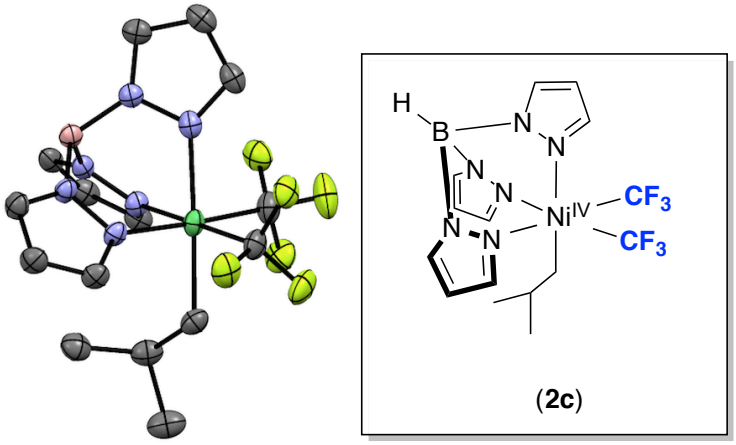

Light yellow plates of **2c** were grown from a pentane/ethyl acetate solution of the compound at 23 deg. C. A crystal of dimensions 0.08 x 0.04 x 0.02 mm was mounted on a Rigaku AFC10K Saturn 944+ CCD-based X-ray diffractometer equipped with a low temperature device and Micromax-007HF Cu-target micro-focus rotating anode (λ = 1.54187 A) operated at 1.2 kW power (40 kV, 30 mA). The X-ray intensities were measured at 85(1) K with the detector placed at a distance 42.00 mm from the crystal. A total of 2028 images were collected with an oscillation width of 1.0° in ω. The exposure times were 1 sec. for the low angle images, 5 sec. for high angle. Rigaku d*trek images were exported to CrysAlisPro for processing and corrected for absorption. The integration of the data yielded a total of 56880 reflections to a maximum 2θ value of 138.46° of which 6973 were independent and 6561 were greater than 2σ(I). The final cell constants (Table 1) were based on the xyz centroids of 26888 reflections above 10σ(I). Analysis of the data showed negligible decay during data collection. The structure was solved and refined with the Bruker SHELXTL (version 2016/6) software package, using the space group P2(1)/n with Z = 8 for the formula $C_{15}H_{19}BN_6F_6Ni$. All non-hydrogen atoms were refined anisotropically with the hydrogen atoms placed in idealized positions. Full matrix least-squares refinement based on F^2 converged at R1 = 0.0441 and wR2 = 0.1136 [based on I > 2sigma(I)], R1 = 0.0463 and wR2 = 0.1157 for all data. Additional details are presented in Table 1 and are given as Supporting Information in a CIF file. Acknowledgement is made for funding from NSF grant CHE-0840456 for X-ray instrumentation.

Table 3.8. Acquisition and refinement parameters for the structural refinement of **2c**

Empirical Formula	$C_{13}H_{13}BF_6N_7Ni$
Formula Weight	450.82
Temperature	85(2) K
Wavelength	1.54178 A
Crystal System	Orthorhombic
Space Group	Pna2(1)
Unit Cell Dimensions	a = 17.0516(1) A alpha = 90 deg. b =7.53680(13) A beta = 90 deg c = 13.2536(2) A gamma = 90 deg.
Volume	1703.28(1) A^3
Z	4
Calculated Density	1.758 mg/m^3
Absorption Coefficient	2.390 mm^{-1}
F(000)	908
Crystal Size	0.20 x 0.14 x 0.12 mm
Theta Range for Data Collection	5.19 to 68.23 deg
Limiting Indicies	$-20\leq h\leq 20$, $-9\leq k\leq 9$, $-15\leq l\leq 15$
Reflections Collected	24861
Independent Reflections	3099 [R(int) = 0.0499]
Completeness to Theta	68.23 (100%)
Absorption Correction	Semi-empirical from equivalents
Max and Min Transmission	0.7366 and 0.6464
Refinement Method	Full-matrix least-squares on F^2
Data / Restraints / Parameters	3099 / 1 / 259
Goodness-of-Fit on F^2	1.183
Final R Indices [$I>2\sigma(I)$]	R1 = 0.0262, wR2 = 0.0636
R indices (all data)	R1 = 0.0266, wR2 = 0.0638
Largest Difference Peak and Hole	0.260 and -0.240 $e.A^{-3}$

3.4. References and Notes

[1] Hu, X. *Chem. Sci.* **2011**, *2*, 1867. (b) Rosen, B. M.; Quasdorf, K. W.; Wilson, D. A.; Zhang, N.; Resmerita, A-M.; Garg, N. K.; Percec, V. *Chem Rev.* **2011**, *111*, 1346. (c) Montgomery, J. "Organonickel Chemistry" in *Organometallics in Synthesis: Fourth Manual* Lipshutz, B. H. (Ed.) Wiley, Hoboken, N.J., **2013**, pp. 319-428. (d) Tasker, S. Z.; Standley, E. A.; Jamison, T. F. *Nature* **2014**, *509*, 299. (e) Everson, D. A.; Weix, D. J. *J. Org. Chem.* **2014**, *79,* 4793.

[2] For examples of stoichiometric C–heteroatom and C–C reductive elimination from Ni^{III}, see: (a) Burk, P.; Liu, M.; Miyashita, A.; Grubbs, R.H. *J. Am. Chem. Soc.* **1978**, *100,* 2418. (b) Tsou, T. T.; Kochi, J. K. *J. Am. Chem. Soc*. **1978**, *100*, 1634. (c) Tsou, T. T.; Kochi, J. K. *J. Am. Chem. Soc.* **1979**, *101*, 7547. (d) Amatore, C.; Jutand, A. *Organometallics* **1988**, *7*, 2203. (e) Matsunaga, P. T.; Hillhouse, G. L.; Rheingold, A. L. *J. Am. Chem. Soc.* **1993**, *115*, 2075. (f) Koo, K.; Hillhouse, G. L. *Organometallics* **1995**, *14*, 4421. (g) Koo, K.; Hillhouse, G. L. *Organometallics* **1996**, *15*, 2669. (h) Jones, G. D.; McFarland, C.; Anderson, T. J.; Vicic, D. A. *Chem. Commun.* **2005**, 4211. (i) Lin, X. F.; Phillips, D. L. *J. Org. Chem*. **2008**, *73*, 3680. (j) Higgs, A. T.; Zinn, P. J.; Sanford, M. S. *Organometallics* **2009**, *28*, 6142. (k) Breitenfeld, J.; Woodrich, M.; Hu, X. *Organometallics* **2014**, *33*, 5708. (l) Zheng, B.; Tang, F.; Luo, J.; Schultz, J. W.; Rath, N. P.; Mirica, L. M. *J. Am. Chem. Soc.* **2014**, *136*, 6499. (m) Cloutier, J-P.; Vabre, B.; Moungang-Soumé, B.; Zargarian, D. *Organometallics* **2014**, *34*, 133

[3] (a) Aihara, Y.; Chatani, N. *J. Am. Chem. Soc.* **2013**, *136,* 898. (b) Iyanaga, M.; Aihara, Y.; Chatani, N. *J. Org. Chem.* **2014**, *79*, 11933. **(c)** Wu, X.; Zhao, Y.; Ge, H. *J. Am. Chem. Soc.* **2014**, *136*, 1789. (d) Yan, S.-Y.; Liu, Y.-J.; Liu, B.; Liu, Y.-H.; Zhang, Z.-Z.; Shi, B.-F. *Chem. Commun*. **2015**, *51*, 734. (e). Terao, J.; Kambe, N. *Acc. Chem. Res.* **2008**, *41*, 1545. (f) Soni, V.; Jagtap, R.; Gonnade, *J. Am. Chem. Soc.* **137**, 16064.; Punji, P.; *ACS Catalysis.* **2016**, *6*, 5666. (g) Soni, V.; Khake, S. M.; Punji, B. *ACS Catalysis* **2016,** *6*, 4202**.** (h) Patel, U.; Jain, S.; Pandey, D.; Gonnade, R. G.; Vanka, K.; Punji, B. *Organometallics* **2018**, ASAP DOI: 10.1021/acs.organomet.8b00025

[4] (a) Omer, H. M.; Liu, P. *J. Am. Chem. Soc.* **2017,** *139*, 9909**.** (b) Singh, S.; K. S.; Sunoj, R.; *J. Org. Chem.* **2017**, *82,* 9619. (c) Li, Y.; Zou, L.; Bai, R.; Lan, Y. *Org. Chem. Front.* **2018** *5*, 615.

[5] For reviews discussing the complementary reactivity of Pd^{II} versus Pd^{IV} in catalysis, see: (a) Muñiz, K. *Angew. Chem. Int. Ed.* **2009**, *48*, 9412. (b) Canty, A. J. *Dalton Trans*. **2009**, 10409. (b) Xu, L.-M.; Li, B.-J.; Yang, Z.; Shi, Z.-J. *Chem. Soc. Rev.* **2010**, *39*, 712. (c) Sehnal, P.; Taylor, R. J. K.; Fairlamb, I. J. S. *Chem. Rev.* **2010**, *110*, 824. (d) Racowski, J. M.; Sanford, M. S. *Top. Organomet. Chem.* **2011**, *35*, 61. (e) Hickman, A. J.; Sanford, M. S. *Nature* **2012**, *484*, 177.

[6] Camasso, N. M.; Sanford, M. S. *Science* **2015**, *347*, 1218

[7] The identity alkylammonium counterion was not found to affect reactivity of the Ni^{II} thus all Tp complexes with varying alkylammonium ions are labeled with the same compound number.

[8] (a) Neufeldt, S.; Sanford, M. S. *Adv. Synth. Catal.* **2012**, *354,* 3517. (b) Wang, L.; Liu, J. *Eur. J. Org. Chem.* **2016**, 1813.

[9] The reaction of complex **5** with PhN_2BF_4 was conducted at 23 ºC and then rapidly cooled down to –25 ºC to resolve J_{FF} coupling.

[10] Unpublished results from our lab actually suggest that the $Ni^{II/III}$ redox potential of **3** is actually *lower* than the $Ni^{II/III}$ oxidation potential of the Ni^{II} intermediates formed in Chatani's quinolinyl amide-direct C–H functionalization reactions.

[11] Danen, W. C.; Winter, R. *J. Am. Chem. Soc.* **1971**, *93*, 716.

[12] The crude reaction mixture following ethane elimination was highily paramagnetic. Quantification by ^{1}H NMR was complicated by the broad signals.

[13] H.-F. Klein, A. Bickelhaupt, T. Jung, G. Cordier *Organometallics* **1994**, *13*, 2557 (b) Carnes, M.; Buccella, D.; Chen, J. Y. C.; Ramirez, A. P.; Turro, N. J.; Nuckolls, C.; Steigerwald, M. *Angew. Chem., Int. Ed.* **2009**, *48*, 290.
[14] Zhang, C.-P.; Wang, H.; Klein, A.; Biewer, C.; Stirnat, K.; Yamaguchi, Y.; Xu, L.; Gomez-Benitez, V.; Vicic, D. A. *J. Am. Chem. Soc*. **2013** , *135*, 8141.
[15] Ball, N. D.; Gary, J. B.; Ye, Y.; Sanford M. S. *J. Am. Chem. Soc.* **2011**, *133*, 7577.
[16] Chen, D.; Ochiai, M. *J. Org. Chem.* **1999**, *64*, 6804.
[17] Bielawski, M.; Aili, D.; Olofsson, B. *J. Org. Chem.* **2008**, *73*, 4602.
[18] Ichiishi, N.; Canty, A. J.; Yates, B. F.; Sanford, M. S. Org. *Lett.* **2013**, *15*, 5134.
[19] Zhang, C.-P.; Wang, H., Klein, A.; Biewer, C.; Stirnat, K.; Yamaguchi, Y.; Xu, L..; Gomez-Benitez, V.; Vicic, D. A. *J. Am. Chem. Soc.* **2013**, *135*, 8141.
[20] Camasso, N. M.; Sanford, M. S. *Science* **2015**, *347*, 1218.
[21] The maximum yield of $(CD_3CN)_2Ni(CF_3)_2$ and $NiTp_2$ are both 50% respectively.
[22] Ritchie, C. D., Sager, W. F. *Prog. Phys. Org. Chem.* **1964**, *2*, 323.
[23] Frisch, M. J.; Trucks, G. W.; Schlegel, H. B.; Scuseria, G. E.; Robb, M. A.; Cheeseman, J. R.;Scalmani, G.; Barone, V.; Mennucci, B.; Petersson, G. A.; Nakatsuji, H.; Caricato, M.; Li, X.;Hratchian, H. P.; Izmaylov, A. F.; Bloino, J.; Zheng, G.; Sonnenberg, J. L.; Hada, M.; Ehara, M.; Toyota, K.;Fukuda, R.; Hasegawa, J.; Ishida, M.; Nakajima, T.; Hon da, Y.; Kitao, O.; Nakai, H.; Vreven, T.; Montgomery, J. A., Jr.; Peralta, J. E.; Ogliaro, F.; Bearpark, M.; Heyd, J. J.; Brothers, E.; Kudin, K. N.; Staroverov, V. N.;Kobayashi, R.; Normand, J.; Raghavachari, K.; Rendell, A.; Burant, J. C.; Iyengar, S. S.; Tomasi, J.;Cossi, M.; Rega, N.; Millam, J. M.; Klene, M.; Knox, J. E.; Cross, J. B.; Bakken, V.; Adamo, C.; Jaramillo, J.;Gomperts, R.; Stratmann, R. E.; Yazyev, O.; Austin, A. J.; Cammi, R.; Pomelli, C.; Ochterski, J. W.;Martin, R. L.; Morokuma, K.; Zakrzewski, V. G.; Voth, G. A.; Salvador, P.; Dannenberg, J. J.; Dapprich, S.;Daniels, A. D.; Farkas, O.; Foresman, J. B.; Ortiz, J. V.; Cioslowski, J.; Fox, D. J. Gaussian 09, revision A.02; Gaussian, Inc., Wallingford, CT, **2009**.

CHAPTER 4

Connecting Organometallic Ni(III) and Ni(IV): Reactions of Carbon-Centered Radicals with High-Valent Organonickel Complexes

4.1. Introduction

Nickel-catalyzed cross coupling reactions have emerged as powerful synthetic methods for the mild and selective construction of C–C and C–X bonds.[1] Mechanistic studies of these transformations suggest that nickel engages many organic substrates via radical chain reactions involving carbon-centered radicals (CCRs).[2] These radicals are most commonly proposed to add to organonickel(II) complexes to generate diorganonickel(III) intermediates (*e.g.,* conversion of **A** to **B** in Scheme 4.1). These transient Ni^{III} intermediates are then proposed to undergo inner-sphere $2e^-$ carbon-carbon or carbon-heteroatom coupling to release organic products.

Scheme 4.1 Commonly proposed interactions of CCRs with nickel catalysts

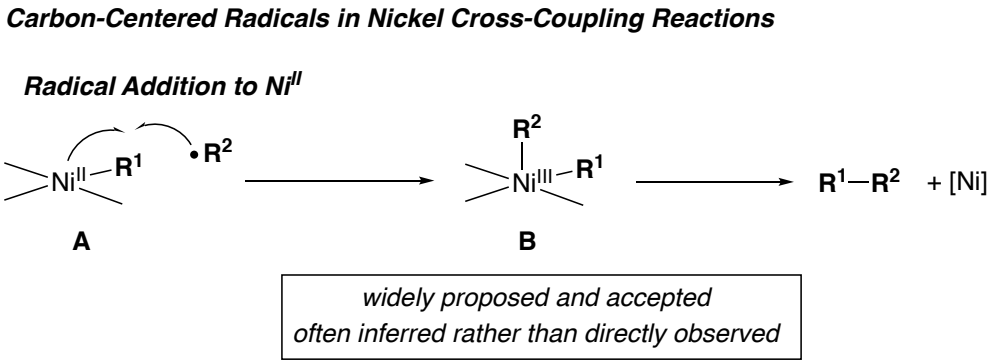

We noted that there are several other rarely considered ways that organo-Ni intermediates could engage with CCRs. For instance, Ni^{III} intermediate **B** could participate in

a second CCR capture reaction to generate an organo-Ni^{IV} intermediate of general structure **C** (Scheme 4.2a). Alternatively, either Ni^{III} complex **B** or Ni^{IV} species **C** could react with a CCR via an outer-sphere $1e^-$ radical coupling process to release an organic product (example reaction shown in Scheme 4.2b). These types of elementary steps are rarely considered, let alone directly interrogated in mechanistic studies. These omissions are particularly noteworthy given the precedent for these transformations in other organometallic systems. [3] Perhaps most notably, methylcorrin cofactors and other B_{12} derivatives are proposed to participate in a variety of outer sphere radical coupling reactions in biosynthetic methylation pathways.[3a-c] Overall, little is known about the reactions of high oxidation state organonickel complexes with CCRs despite their ubiquity in nickel catalysis.

Scheme 4.2 Elementary organometallic reactions studied in this chapter

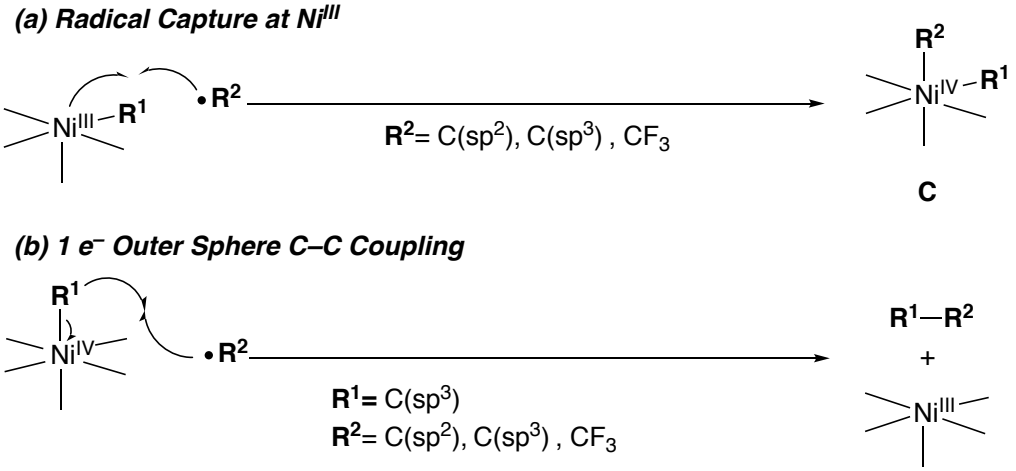

As experimental and theoretical support for the catalytic relevance of Ni^{IV} complexes grows,[4,5] so does the need for detailed descriptions of their formation and bond-forming reactions. This chapter describes the development and reactivity of model organometallic Ni^{III} and Ni^{IV} complexes with carbon centered radicals under controlled conditions. Using tris-pyrazolylborate-stabilized fluoroalkyl Ni^{III} and Ni^{IV} complexes, we demonstrate herein that both radical capture by organo-Ni^{III} complexes (Scheme 4.2a) and outer-sphere $1e^-$ C–C coupling reactions at organo-Ni^{IV} intermediates (Scheme 4.2b) can occur under mild

conditions. Furthermore, we show that these pathways open up previously unprecedented types of reactivity, including mild C–C coupling to form $H_3C–CF_3$, a reaction found to be highly challenging through traditional inner-sphere coupling.[6] We anticipate that these results will have broader implications on the development of new nickel-catalyzed cross-coupling reactions and the interpretation of high-valent nickel catalysis mechanisms.

4.2. Results and Discussion

4.2.1 Carbon-Centered Radical Addition to Organonickel(III) Complexes

We first sought to develop a model system to probe the reactivity of organo-Ni^{III} complexes with CCRs. There are two key challenges for directly studying this transformation. First, it is essential to identify a sufficiently stable organometallic Ni complex where both the Ni^{III} starting material and Ni^{IV} product of CCR capture are detectable and preferably isolable. Second, the CCRs used for this reaction must be generated under conditions that are compatible with the Ni^{III} starting material and the Ni^{IV} product. The most common CCR-forming reactions involve thermolytic, photolytic, oxidative, or reductive generation of the free radical. However, most high valent Ni complexes decompose rapidly at high temperatures, as well as in the present of light and/or reductants.

Scheme 4.3 Proposed model system for studies of CCR addition to organonickel(III)

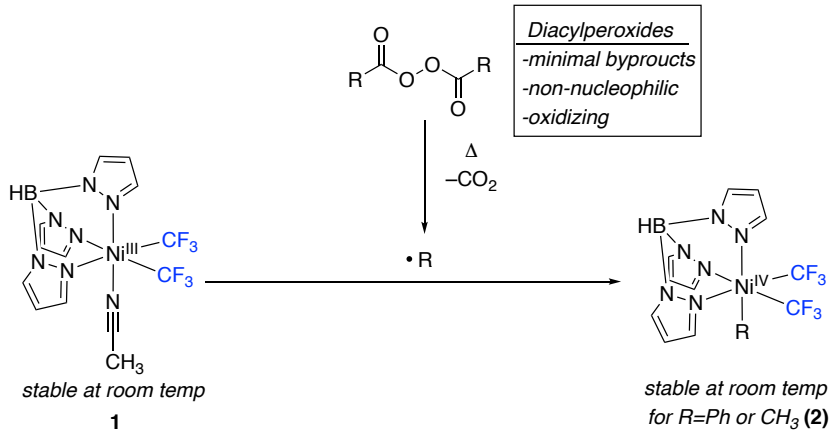

On the basis of these two key considerations, we initially selected the Ni^{III} complex $TpNi^{III}(CF_3)_2(CH_3CN)$ (**1**) as a model system for studying this transformation. Our previous work has shown that **1** can be formed and isolated via the $1e^-$ oxidation of $[TpNi^{II}(CF_3)_2]$.[7] Furthermore, the related Ni^{IV} complex $TpNi^{IV}(CF_3)_2(Ph)$ (**2**) has also been independently formed from the reaction of $[TpNi^{II}(CF_3)_2]^-$ with aryl electrophiles (Chapter 3). Lastly, diacyl peroxides $[(RCOO)_2]$ were chosen as the CCR source for these reactions. These are well-suited for this study because they are strong oxidants that generate CCRs upon relatively mild conditions (heating above ~75ºC) without the requirement for light and/or reductants.[8]

We initially explored the reaction of **1** with bis-(4-fluorobenzoyl)peroxide (4-F-BPO) in CD_3NO_2. Importantly, the $t_{1/2}$ for 4-F-BPO is 1h at ~90 ºC.[8] Over 12 h at 25 ºC, no reaction was observed by ^1H, ^{11}B, or ^{19}F NMR spectroscopy, consistent with the high stability of 4-F-BPO at room temperature. However, heating this reaction at 95 ºC for 15 min resulted in the complete consumption of **1**, as determined ^{11}B NMR spectroscopic analysis of the crude reaction mixture. Encouragingly, this was accompanied by the formation of small quantities (~2% yield) of **2**, suggesting the feasibility of the proposed CCR radical addition pathway. However, attempts to improve the yield by variation of the temperature, concentration, or solvent manipulation were unsuccessful. Independent thermolysis of **1** in the absence of aroyl peroxide resulted in full conversion to a complex mixture of products including Tp_2Ni and HCF_3.[9] This experiments suggested that the low yield of **2** was likely due to the instability of **1** rather than inefficient radical capture.

Scheme 4.4 Initial attempts at aryl radical addition to complex **1**

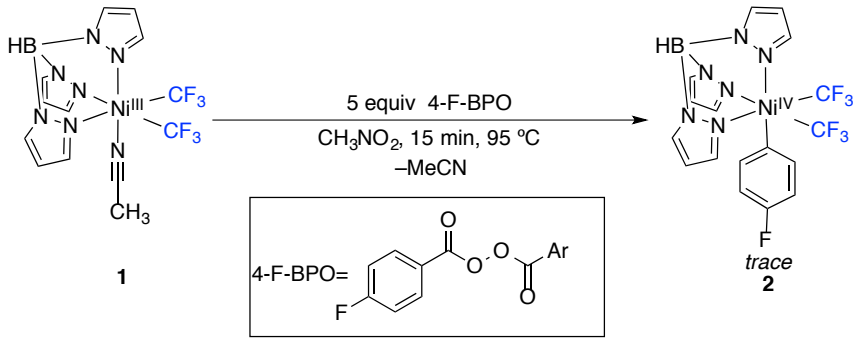

Based on this hypothesis, we next pursued the synthesis of a more stable organo-Ni^{III} starting material. A recent report by Vicic demonstrated that Ni^{III} complexes bearing perfluoronickelocyclopentane ligands exhibit dramatically enhanced thermal stability relative to their trifluoromethyl analogues.[10] The perfluoronickelocyclopentane Ni^{III} complex **3** was synthesized via the $1e^-$ oxidation of $NMe_4[TpNi(C_4F_8)]$ by $AgBF_4$ in THF (Figure 4.1a). Complex **3** was isolated in 57% yield after purification by column chromatography on silica gel. In contrast to **1**, elemental analysis and X-ray crystallography suggest that compound **3** is a 5-coordinate Ni^{III} complex, without a solvent ligand coordinated in the sixth site at the Ni center. This observation is further confirmed by EPR spectroscopic analysis in toluene glass at 100K. The EPR spectrum of **3** displays hyperfine coupling to one nitrogen atom in the z axis rather than the two that would be expected upon coordination of a nitrile ligand to the open coordination site (Chapter 3, Figure 3.2).

Figure 4.1 (a) Synthesis of nickelocyclopentane complex **3**. (b) X-ray crystal structure of **3**. Thermal ellipsoids are drawn at 50% probability. (c) Experimental (blue) and simulated (red) EPR spectrum of **3**. Gx=2.28 Gy=2.22 Gz=2.01 A_N(N)=22 G.

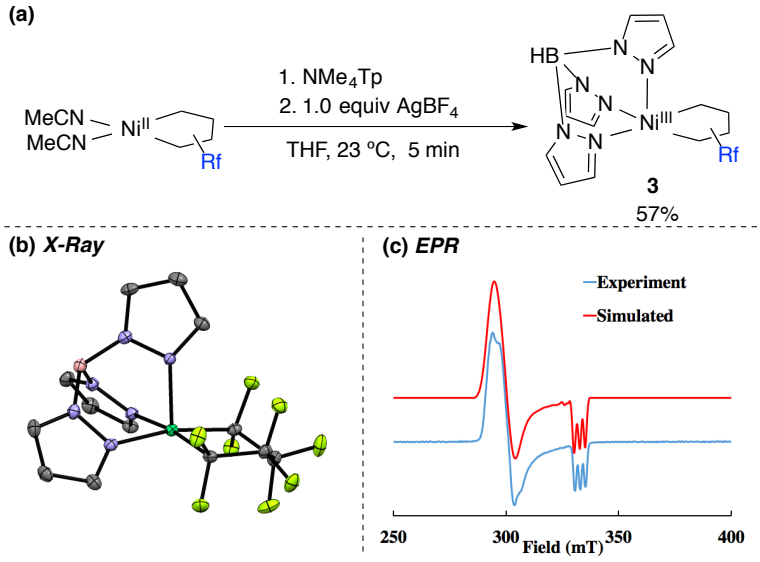

As predicted, complex **3** exhibits significantly enhanced thermal stability compared to **1**. Heating a CD_3NO_2 solution of **3** at 95 ºC for 15 min resulted in minimal decomposition, as determined by ^{1}H, ^{19}F, or ^{11}B NMR spectroscopy.[11] This suggests that **3** should be compatible with the thermolytic conditions required for radical generation from 4-F-BPO. Indeed, the treatment of **3** with 5 equiv of 4-F-BPO at 95 ºC for 17 min produced $TpNi^{IV}(C_4F_8)(4\text{-F-}C_6H_4)$ (**5**) in 40% yield, as determined by ^{19}F NMR spectroscopy (Scheme 4.5). However, monitoring this reaction showed that product **5** decomposes under these conditions at a rate that is competitive with its formation. We hypothesized that this issue could be addressed by increasing the equivalents of 4-F-BPO, which should accelerate the rate of formation of **5**. Indeed, the use of 10 or 18 equiv of 4-F-BPO under otherwise identical conditions increased the yield of **5** to 53 and 61%, respectively.[12] Product **5** was purified by column chromatography on silica gel and was isolated in 31% yield as an analytically pure yellow-orange solid. This octahedral Ni^{IV} product of CCR capture was characterized by X-ray crystallography (Figure 4.2), elemental analysis as well as by ^{1}H, ^{19}F, and ^{13}C NMR spectroscopy.

Scheme 4.5 Aryl radical addition to stabilized Ni^{III} complex **3**

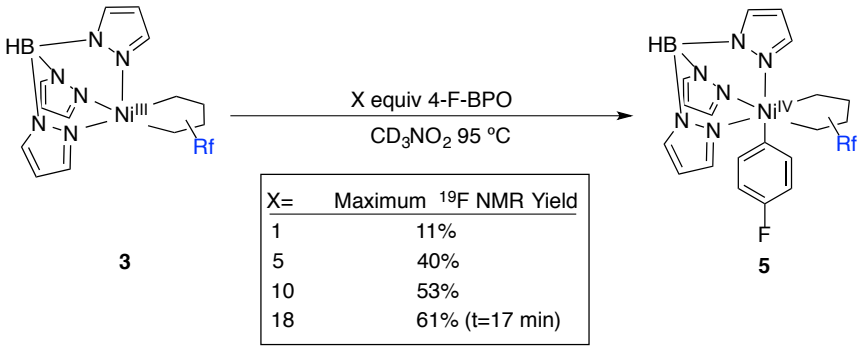

3

X=	Maximum ^{19}F NMR Yield
1	11%
5	40%
10	53%
18	61% (t=17 min)

5

Figure 4.2 X-ray crystal structure of **5**. Thermal ellipsoids are drawn at 50% probability level and hydrogen atoms have been omitted for clarity.

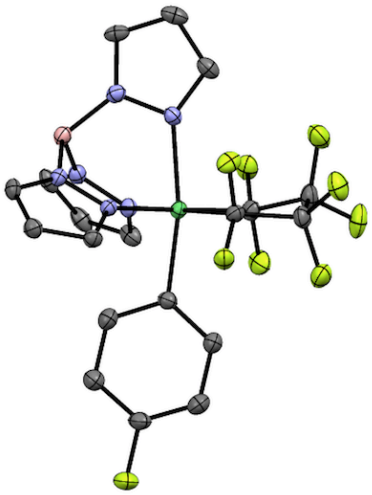

We next investigated analogous alkyl radical capture reactions using the alkyl peroxide bis-(4-phenylbutyryl)peroxide (4-Ph-BuPO). Notably, alkyl radicals are among the most commonly proposed CCR intermediates in Ni-catalyzed cross coupling reactions.[2] Indeed, the reaction of **3** with 10 equiv of 4-Ph-BuPO at 85 ºC for 6 min afforded $TpNi^{IV}(C_4F_8)(CH_2CH_2CH_2Ph)$ (**6**) in 49% yield by ^{19}F NMR spectroscopy (Scheme 4.6). Once again, the yield is moderate because the decomposition rate of **6** is competitive with that of its formation at 85 ºC.[13] Nonetheless, **6** could be isolated as a yellow-orange solid in 17% yield via column chromatography on silica gel. This product was characterized via ^{1}H, ^{11}B, ^{13}C , and ^{19}F NMR spectroscopy, as well as by X-ray crystallographic analysis (Figure 4.3).[14]

Scheme 4.6 Alkyl radical addition to stabilized Ni^{III} complex **3**

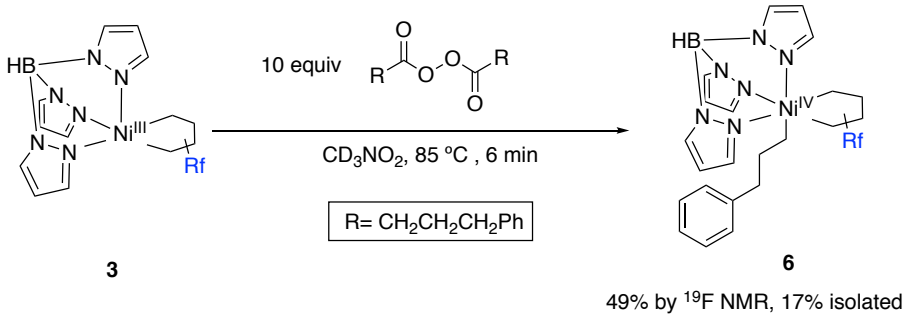

Figure 4.3 X-ray crystal structure of **5**. Thermal ellipsoids are drawn at 50% probability level and hydrogen atoms have been omitted for clarity.

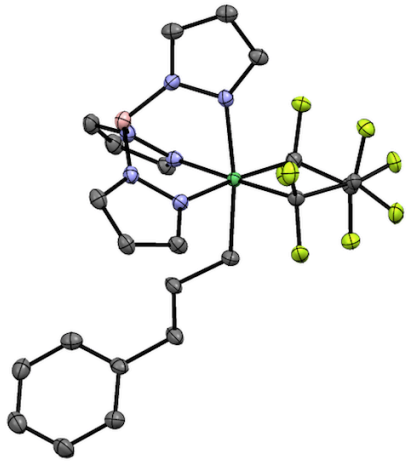

To gain more insights on the mechanisms of these transformations, we next conducted the reactions of **3** with diacylperoxides in the presence of the oxidatively stable radical traps β-nitrostyrene and cinnamonitrile.[15] Notably, we first confirmed that these additives do not react with Ni^{III} complex **3** over the timescale of these experiments. As summarized in Table 4.1, the addition of 1 equiv of either of these radical traps relative to the diacyl peroxide led to major decreases in the yield of **5** and **6**. This provides evidence supporting the intermediacy of CCRs in the conversion of **3** to **4** and **5**. Overall, we propose that these reactions proceed via the mechanism outlined in Scheme 4.7, in which initial O–O bond cleavage generates a carboxyl radical, which then undergoes radical decarboxylation, followed finally by capture of **3** to form Ni^{IV} species **5** or **6**. This transformation is a rare example of radical addition to a metal compound to furnish a stable organometallic complex.

Table 4.1 Effects of radical traps on the formation of **5** and **6**

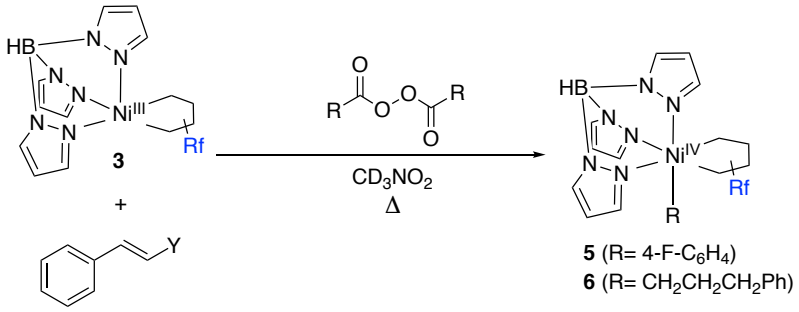

Entry	R=	Y=	Yield[a]
1	4-F-C_6H_4[b]	NO_2	17
2		CN	19
3		no trap	61
4	$CH_2CH_2CH_2Ph$[c]	NO_2	14
5		CN	10
6		no trap	49

[a]Yields determined by ^{19}F NMR spectroscopy against an internal standard [b]Conditions: [Ni]=1.5 mM, [PhC_2H_2Y]= 30 mM, [4-F-BPO]= 30mM at 95 ºC, 15 min. [c][Ni]= 1.5 mM, [PhC_2H_2Y]= 15 mM, [4-F-BPO]= 15 mM at 85 ºC, 6 min.

Scheme 4.7 Proposed mechanism for the formation of **5** and **6** from **3** and diacylperoxides

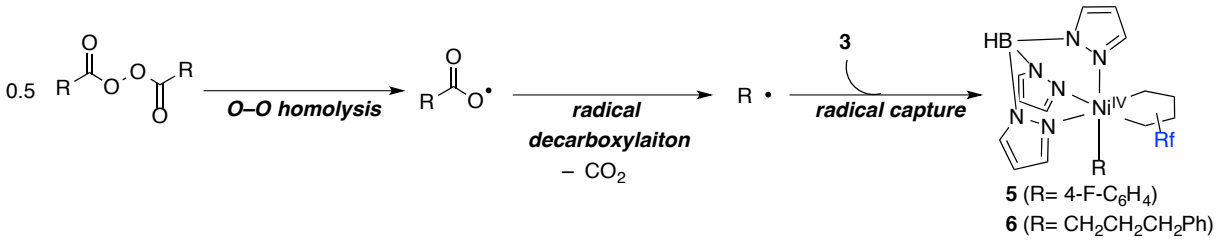

4.2.2. Outer sphere C–C coupling reactions of Ni^{IV} alkyl complexes with R•.

Though less common, carbon centered radicals have also been proposed to interact with metal complexes through an outer-sphere process involving homolytic abstraction of a M–C bond or M–X bond. These transformations have been proposed in a variety of systems, including iron catalyzed C–C coupling or C–O bond formation.[16] However, this mechanistic pathway for C–C coupling has rarely been experimentally validated for two reasons. First, the identification/isolation of discrete organometallic complexes with sufficiently reactive M–C bonds remain challenging. Second, for complexes bearing open sites at the metal center, it is

challenging to differentiate a direct outer sphere radical C–C coupling mechanism from a sequential inner sphere CCR addition/reductive elimination pathway. As previously mentioned, one of the best characterized examples of this type of process involves the reactions of alkyl radicals with methylcobalamin-type cofactors (Scheme 4.8). In this system, the accessibility of a stable, coordinatively saturated Co^{III}–methyl complex bearing a weak Co–C bond (36 kcal/mol) makes the outer-sphere nature of this transformation unambiguous.[17]

Scheme 4.8 Outer sphere radical coupling reaction of methylcobalamin.[3a]

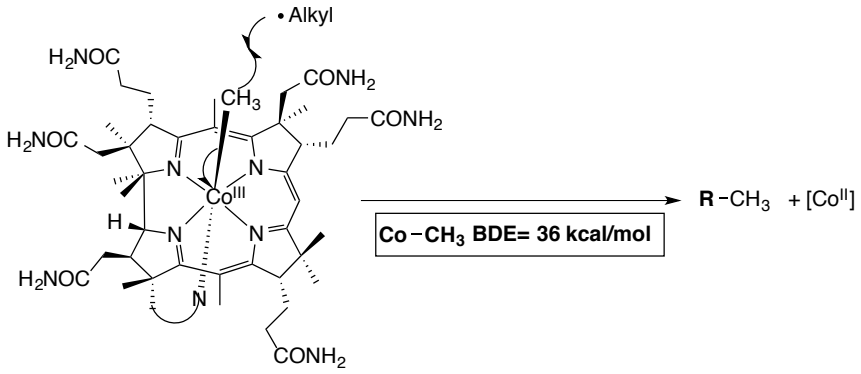

Preliminary DFT calculations suggest that the newly formed Ni^{IV}–C bonds in complexes **5** and **6** are relatively weak (with bond dissociation enthalpies of 35 and 32 kcal/mol, respectively, using the M06 functional and 6-31G(d,p) basis set). These data implied that a less sterically hindered derivatives of **6** may be susceptible to outer sphere radical coupling reactions. As such, we hypothesized that coordinatively saturated Ni^{IV} complexes of general structure $TpNi^{IV}(R_F)_2$(alkyl) (R_F = fluoroalkyl) would be an ideal system to test the feasibility of outer sphere radical coupling. For initial studies, we sought a derivative that was synthetically accessible and thermally stable (such that it would be compatible with thermal radical generation from diacylperoxides). These criteria led us to target $TpNi^{IV}(CF_3)_2(CH_3)$ (**7**). As established in Chapter 3, **7** can be conveniently prepared in 40% yield via the reaction of $NMe_4[TpNi^{II}(CF_3)_2]$ with excess methyl iodide and 1.3 equiv of 2,6-difluorobenzendiazonium tetrafluoroborate (Scheme 4.9). Importantly, our previous studies of this molecule suggest that the CF_3 ligands are largely inert even at high temperatures. We attribute the high thermal

stability to the apparent high barrier for CH_3–CF_3 coupling via inner-sphere reductive elimination.

Scheme 4.9 Synthesis and thermal stability of complex **7**

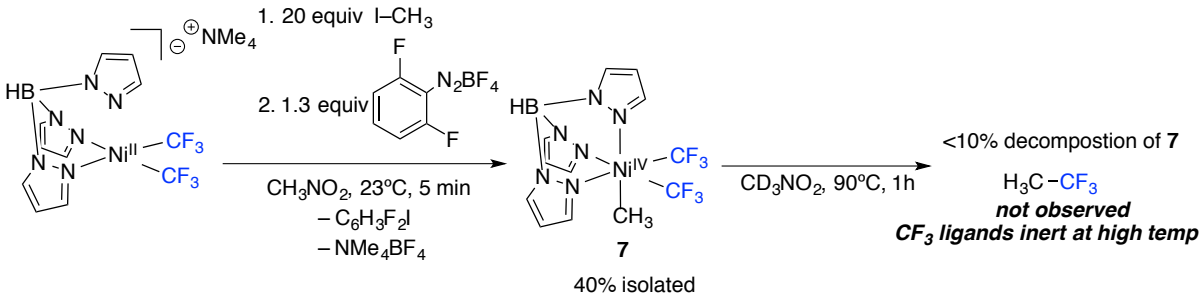

We next probed the feasibility of outer sphere C–C coupling reactions between complex **7** and CCRs generated from aryl and alkyl diacylperoxides. Heating a solution of **7** with 3 equiv of the aryl radical source 4-F-BPO at 90 ºC for 1 h resulted in the formation of the C–C coupled product 4-fluorotoluene in 60% yield as determined by ^{19}F NMR spectroscopic analysis.[18] Similarly, the reaction of **7** with 3 equiv of the alkyl radical source 4-Ph-BuPO at 80 ºC for 1 h afforded *n*-butyl benzene in 78% yield.

Scheme 4.10 Reaction of **7** with carbon-centered radicals generated from diacylperoxides

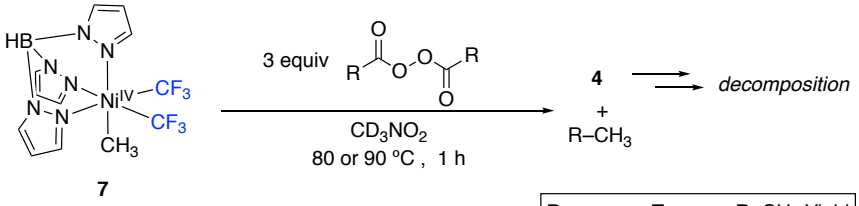

R =	Temp	R–CH_3 Yield
4-F-C_6H_4	90	60
^{n}C_3H_6Ph	80	78

We next sought to examine whether this approach could be used to forge bonds that are challenging to form via more traditional inner sphere 2e^- pathways. Specifically, we focused on C(sp^3)–CF_3 couplings, which are known to be extremely challenging at most metal centers. This is exemplified in Scheme 4.9 for complex **7**, where prolonged heating leads to decomposition of the $Ni^{IV}(CF_3)_2(CH_3)$, without the observed formation of CH_3CF_3. In contrast, heating a solution of **7** with bis(trifluoroacetyl)peroxide at 45 ºC for 90 min resulted in the

rapid decay of the Ni^{IV} starting material along with concomitant formation of trifluoroethane in 74% yield, as determined by ^{19}F NMR spectroscopy (Scheme 4.11). Importantly, control reactions show that CH_3CF_3 is not formed in significant yields unless both **7** and bis(trifluoroacetyl)peroxide are present in the reaction. As such, this represents an extremely rare example of metal-mediated $C(sp^3)$–CF_3 coupling, which appears to be enabled by the accessibility of a $1e^-$ outer sphere pathway.

Scheme 4.11 Radical outer sphere C–CF_3 coupling from **7** and formation of $TpNi^{IV}(CF_3)_3$

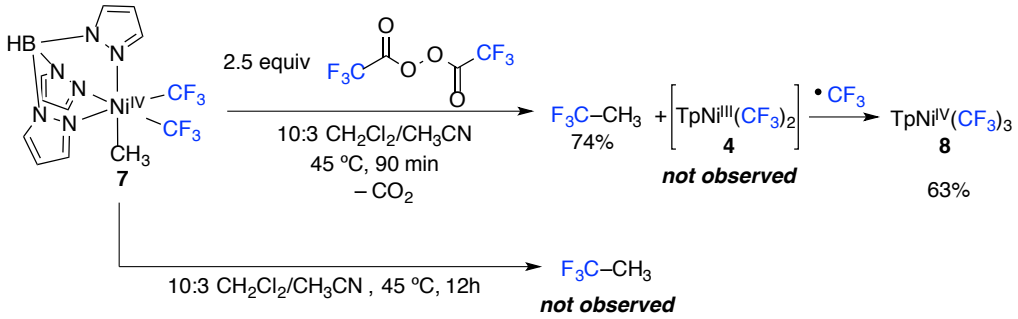

One important uncertainty in these $1e^-$ outer sphere radical coupling pathways is the nature of the Ni byproducts. While the initial Ni product in all three reactions is expected to be the Ni^{III} complex $TpNi^{III}(CF_3)_2$ (**4**), we have shown that **4** is extremely unstable at temperatures >70 ° C (Scheme 4.11). As such, a complex mixture of unidentified Ni-containing products including $NiTp_2$ was formed in the reactions with 4-F-BPO (conducted at 90 ºC) and 4-Ph-BuPO (conducted at 80 ºC).[19] In contrast, the reaction with bis(trifluoroacetyl)peroxide proceeded under significantly milder conditions (45 ºC) and afforded $TpNi^{IV}(CF_3)_3$ (**8**) as the main Ni-containing product in 63% yield, as determined by ^{19}F NMR spectroscopic analysis (X-ray characterization, Figure 4.4).[20] We hypothesize that this product is formed via the reaction of the initial Ni^{III} product **4** with an equivalent of •CF_3 formed from radical decarboxylation of bis-trifluoroacetylperoxide.

Figure 4.4 X-ray crystal structure of **8**. Thermal ellipsoids drawn at 50% probability level and the hydrogen atoms have been omitted for clarity.

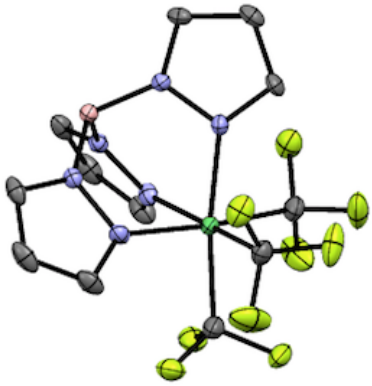

Mechanistic Insights on Outer Sphere Radical Coupling from 7

We next sought to preliminarily probe alternate mechanistic possibilities that could also account for the formation of the C–C coupled products. Scheme 4.12 illustrates three reasonable reaction mechanisms that could account for the observed products. In mechanism A, liberation of a coordination site through Ni^{IV}–CF_3 homolysis and subsequent CCR addition generates a new Ni^{IV} complex **10**, from which rapid $C(sp^{2/3})$–$C(sp^3)$ coupling is expected to occur. The second pathway (mechanism B) depicts the proposed outer sphere radical coupling through direct CH_3 abstraction from **7**. Finally, mechanism C depicts radical heterodimerization of CCRs with methyl radicals formed through Ni^{IV}–CH_3 homolysis.

Scheme 4.12 Potential mechanisms for C–C coupling from **7** in the presence of CCRs

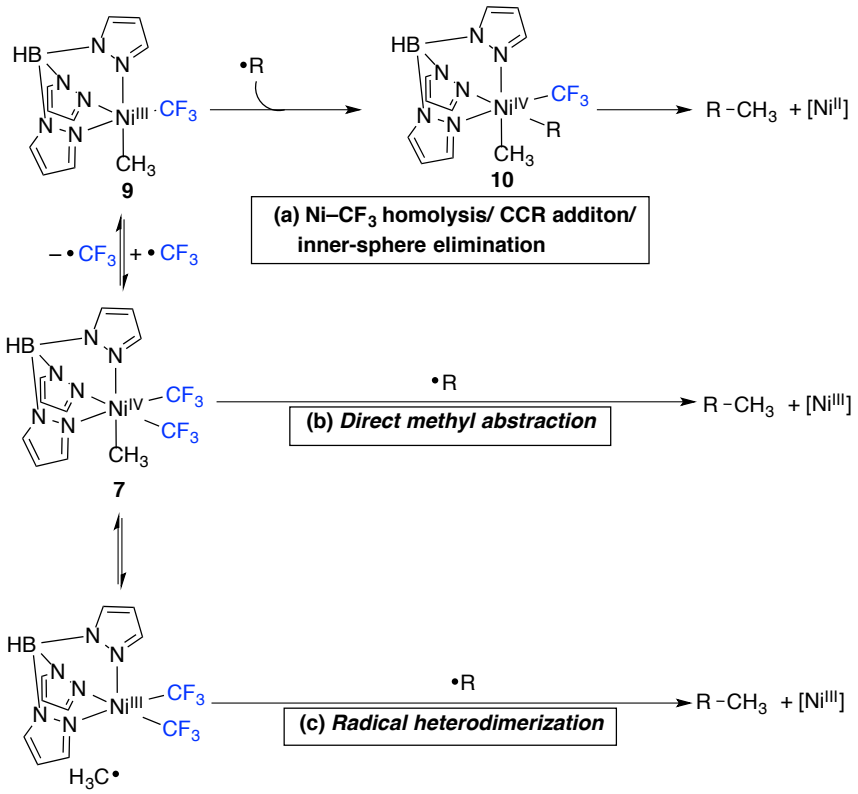

Two observations make mechanism A unlikely. First, our previous studies of C–C coupling demonstrate that $TpNi^{III}(CF_3)(CH_3)$ (**9**) is highly reactive. Our attempts to isolate **9** were unsuccessful and stability studies later demonstrated that it decomposes into ethane and a complex mixture of nickel-containing products within seconds at –35 ºC. Because diacylperoxides slowly release CCRs at elevated temperatures, the lifetime of **9** at 90 ºC is unlikely to be sufficient under the reaction conditions. Secondly, mechanism A does not account for the observed $C(sp^3)$–CF_3 coupling. When R = CF_3, mechanism A depicts a degenerate CF_3 exchange where intermediate **10** would be identical to **7.** Complex **7** is quite stable at 45 ºC and does not afford high yields of trifluoroethane even when subjected to forcing conditions. Taken together, these experiments suggest that product formation through a more traditional inner sphere reductive elimination mechanism is unlikely.

To distinguish between the possibility of mechanisms B and C, we next examined the stability of **7** in the presence of radical traps. If mechanism B were operating, **7** is expected be

stable in the presence of radical traps. If **7** simply serves as a latent source of methyl radicals (mechanism C) then it should rapidly decompose when heated at the reaction temperature. As seen in Figure 4.5, heating a solution of **7** in the presence of radical traps did not significantly affect the rate of decomposition. In contrast, treatment of **7** with 4-F-BPO or 4-Ph-BuPO resulted in rapid decomposition of **7**. Importantly, the CCR capture studies described above (Table 4.1) show that β-nitrostyrene and cinnamonitrile are suitable CCR scavengers in these reactions. These data suggest that C–C coupling does not occur through heterodimerization of free methyl radicals. Rather, the observed outcomes are most consistent with mechanism B: CCR-mediated homolytic Ni–CH_3 bond cleavage.

Figure 4.5. (a)Time study of thermal decomposition of **7** in the presence of various additives and (b) Figure key ✖= 1,4-dinitrobenzene (0.075M, 5 equiv), ▲= None ([Ni]= 0.015), ◆= b-nitrostyrene (0.075M, 5 equiv), ●= Cinnamonitrile (0.075M, 5 equiv), ■= 4-F-BPO (0.045M, 3 equiv), ▬= 4-Ph-BuPO 7yu7(0.045M, 3 equiv)

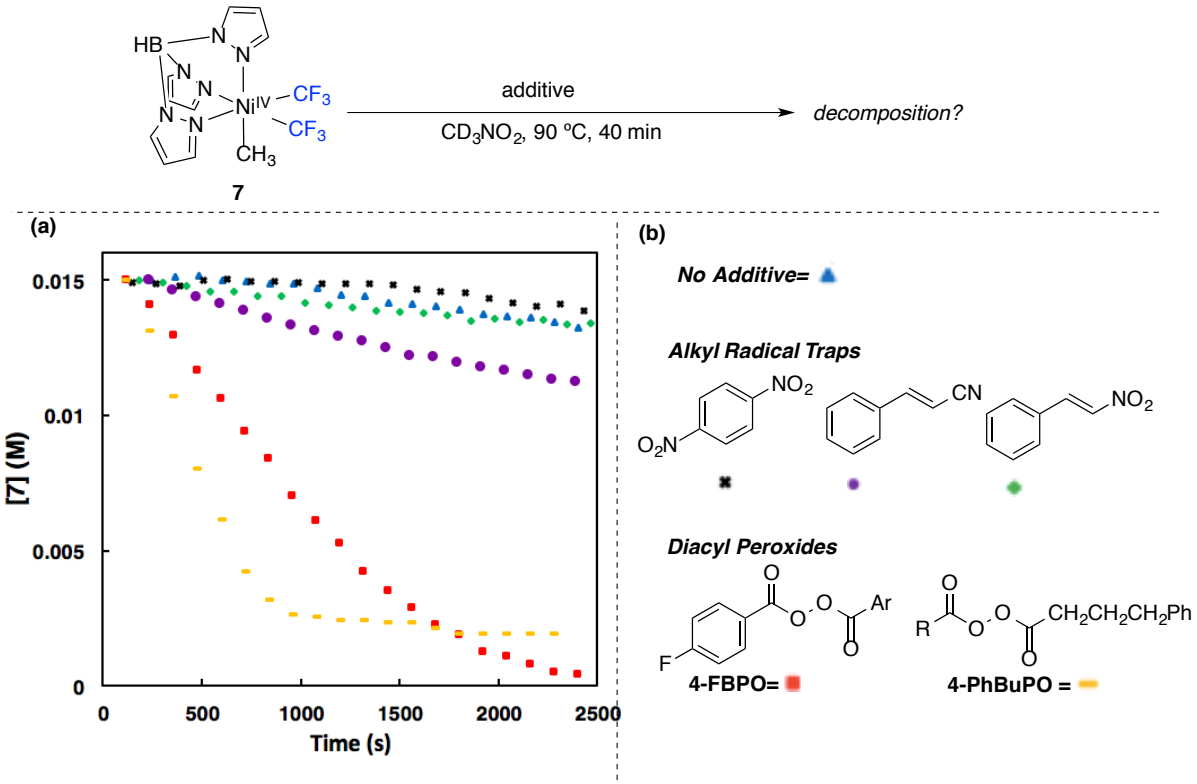

Comparisons to Related Reactions at Palladium

Although significant progress has been made in recent years, high-oxidation state organonickel chemistry is still in its infancy relative to high-valent palladium chemistry. The majority of reports on organonickel(III/IV) have focused largely on the same bond-forming reactions and ligand scaffolds for which there is a direct analogy or precedent with Pd^{IV} (C–C/C–X coupling, C–H activation, etc.). Our studies of outer-sphere radical coupling, however, have no direct analogy in Pd^{IV}. Though it is widely recognized that organopalladium(IV) generally participates in clean $2e^-$ reductions, its reactivity with carbon centered radicals is essentially unknown. Given the remarkable reactivity of CCRs and the weak (relative to C–C and C–H bonds) Pd–C bonds, we next explored the possibility of outer sphere radical C–C coupling from Pd^{IV}.

We began our studies with the synthesis of $TpPd^{IV}(CF_3)_2(CH_3)$ (**11**). Initial attempts to prepare **11** through direct analogy to its nickel analog, **7,** were unsuccessful. The low-valent ligand exchange chemistry of $(CH_3CN)_2Pd^{II}(CF_3)_2$ proved to be far more complicated than with nickel. All attempts to generate $[TpPd(CF_3)_2]^-$ complexes led to complicated mixtures of [Pd–CF_3] compounds and subsequent oxidations of the crude mixtures to Pd^{IV} complexes were unsuccessful. As such, an alternate strategy involving the synthesis of $[(N\sim N)Pd(CF_3)(CH_3)]$, where N~N=1,2-dipiperidinoethane (DPE), was developed. Our group has previously determined that DPE offers an excellent balance between stability and lability when ligated to organometallic palladium. The key $[(N\sim N)Pd(CF_3)(CH_3)]$ complex was synthesized in two steps from the previously reported $(DPE)Pd(CF_3)(Ph)$ complex. Exchange of DPE for KTp and oxidation of the crude product by a CF_3^+ oxidant furnished a complex mixture of Pd^{IV} compounds and organics. However, the desired product could be purified by silica column

chromatography and was isolated in 12% overall yield. Characterization by X-ray crystallography as well as ^{1}H, ^{11}B, ^{13}C, and ^{19}F NMR confirmed the proposed structure.

Scheme 4.13 Synthesis of **11** from (DPE)Pd(CF_3)(Ph)

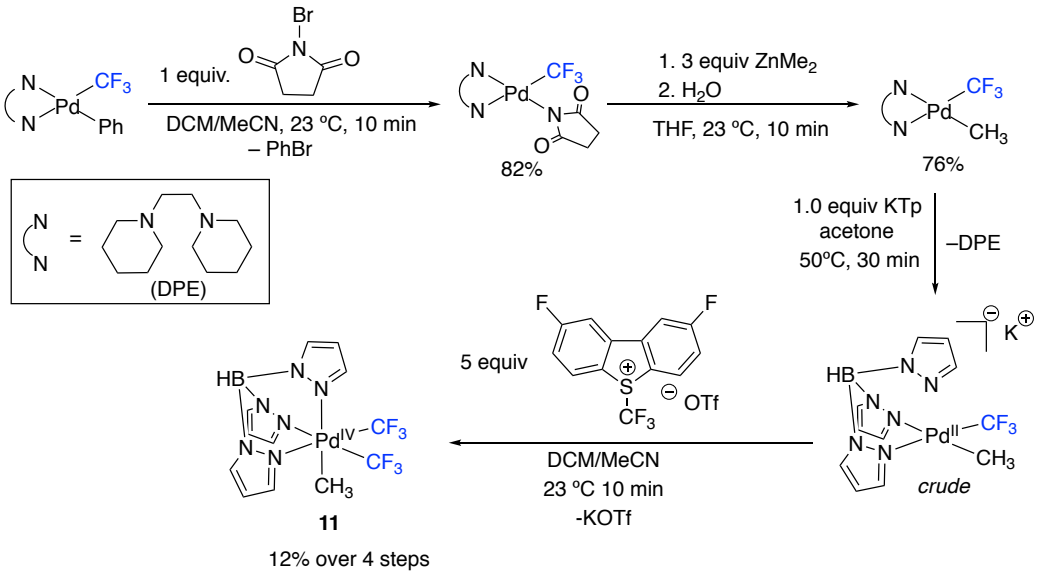

Figure 4.6 X-ray crystal structure of **11**. Thermal ellipsoids drawn at 50% probability and the hydrogen atoms have been omitted for clarity.

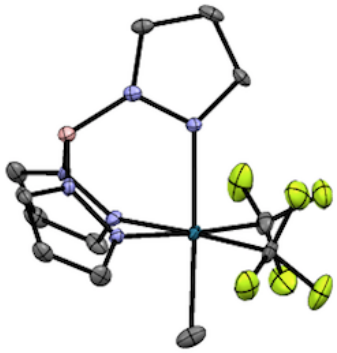

With the desired Pd complex in hand, its reactivity with carbon centered radicals was examined. Heating a solution of **11** with 3 equiv of 4-F-PBO or 4-PhBuPO did not result in detectable quantities of methylated organic products despite approximately 80% conversion of the diacyl peroxides. Importantly, Pd^{IV} complex **11** was stable under the reaction conditions; over 98% of the initial complex remained intact at the end of the reaction.

Scheme 4.14 Reaction of **11** with CCRs generated from diacylperoxides

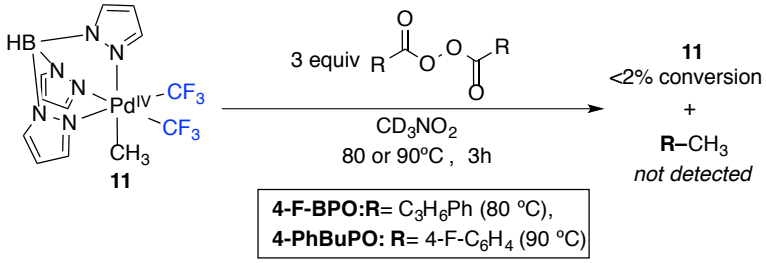

Tp-ligated Pd^{IV} complexes are notoriously unreactive and the failure of **11** to participate in radical coupling may not be reflective of Pd in general, but rather the overall stability of **11.** In other words, we next considered if our model system was globally inert or if it is selectively activated to *heterolytic* Pd–C bond-breaking reactions and deactivated to *homolytic* Pd–C bond-breaking reactions. This possibility would starkly contrast the reactivity of its nickel analog (**7**), which was found to readily engage in both $2e^-$ *and* $1e^-$ Ni^{IV}–C bond cleavage reactions (Chapter 3). To evaluate the heterolytic bond-breaking reactivity of **11,** we next investigated its reduction through an S_N2-type reductive elimination with a weak nucleophile.[21] Treatment of **11** with 2 equiv of NMe_4OAc in CD_3CN resulted in full conversion of **11** to $[TpPd^{II}(CF_3)_2]^-$ and the S_N2 organic reductive elimination product, H_3C–OAc, in 92% yield by ^1H NMR spectroscopy. Rapid reduction of **11** by a weak oxygen nucleophile suggests that the Pd^{IV} center is indeed highly electrophilic and the failure of **11** to react in with CCRs is not reflective of the compound's global stability. We propose that it is instead representative of palladium's resistance to single electron redox events. Overall, these experiments confirm that the radical outer sphere C–C coupling observed with **7** is due, at least in part, to the relative accessibility of $1e^-$ reactions. More importantly, these experiments clearly identify palladium, and perhaps more generally second and third row transition metals, as poor catalyst choices for the implementation of $1e^-$ outer sphere coupling in catalysis.

Scheme 4.15 Reaction of **11** with NMe_4OAc

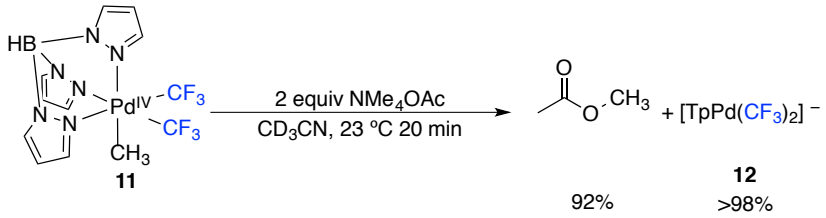

Conclusions

In summary, this chapter describes the reactions of carbon centered radicals with model high-valent organonickel complexes. Careful choice of supporting ligands and radical source ultimately allowed the detailed investigation of CCR addition to unsaturated high-valent nickel compounds and the bond-forming reactions of organonickel(IV) with CCRs.

Our studies of CCR capture at Ni^{III} demonstrate that Ni^{IV} compounds can be generated by carbon-centered radicals and Ni^{III} complexes. Key to the unambiguous detection of this transformation? was the development of an appropriate model system where radical generation is unlikely to generate reduced nickel species. These results have broader implications for the interpretation of nickel-catalyzed cross coupling reactions. First, it partially erodes the strong association between the detection of carbon-centered radicals and mechanisms involving C–C or potentially C–X coupling from Ni^{III}. These results suggest that consideration of coupling events from saturated Ni^{IV} is warranted when carbon-centered radicals are detected. Secondly, CCR addition to Ni^{III} may be mechanistically pertinent to the formation of side products in nickel-cross coupling reactions. For example, common side reactions such as electrophile homo-coupling could be rationalized through consecutive additions of CCRs to a Ni^{II} center culminating in unselective C–C elimination from a Ni^{IV} intermediate. Ultimately, these results raise new questions about the mechanistic role of CCRs and organonickel(IV) intermediates in catalysis.

Our investigations also reveal that CCRs can mediate the formal reduction of a Ni^{IV} center and C-C bond formation through homolytic cleavage of a Ni^{IV}–C bond. Preliminary mechanistic evidence suggests that this process occurs through direct abstraction of a nickel-bound carbon ligand rather than through more conventional inner-sphere coupling or radical heterodimerzation reactions. This unconventional C–C coupling paradigm was found to enable $C(sp^3)$–CF_3 coupling, a reaction that is highly challenging through traditional reductive elimination from high or low valent metal centers.

In a final set of experiments, we examined the feasibility of radical outer sphere C–C coupling from an alkyl Pd^{IV} complex. Consistent with well-established trends in organometallic reactivity, the palladium complexes were inert to the formal $1e^-$ reduction of the metal center through CCR-mediated homolytic Pd–C cleavage. The complex was not, however, inert to a more traditional $2e^-$ S_N2 type reductive elimination. It was found to cleanly react with an acetate nucleophile to yield H_3C–OAc under mild conditions. Ultimately these studies confirm the unique nature of first row transition metals to engage in $1e^-$ redox events.

Overall, these studies provide a fundamental framework through which the $1e^-$ Ni–C bond forming and breaking interconversions of organometallic Ni^{III} and Ni^{IV} can be understood. We are currently engaged in electronic structure studies to better understand the observed reactivity and identify appropriate ligand scaffolds for translation of these unusual reactions into synthetically meaningful catalytic methods.

4.3. Experimental Procedures and Characterization of Compounds

4.3.1 General Procedures and Methods

All manipulations were performed inside an N_2 filled glovebox unless otherwise noted. NMR spectra were obtained on a Varian VNMR 700 (699.76 MHz for ^1H; 175.95 MHz for ^{13}C), Varian VNMR 500 (500.09 MHz for ^1H; 470.56 MHz for ^{19}F; 125.75 MHz for ^{13}C), or Varian VNMR 400 (401 MHz for ^1H; 376 MHz for ^{19}F; 123 MHz for ^{13}C) spectrometer. ^1H

and ^{13}C NMR chemical shifts are reported in parts per million (ppm) relative to TMS, with the residual solvent peak used as an internal reference. ^{19}F NMR chemical shifts are reported in ppm and are referenced to fluorobenzene (–113.52 ppm). The ^{11}B NMR spectra are referenced to $BF_3 \bullet Et_2O$. Abbreviations used in the NMR data are as follows: s, singlet; d, doublet; t, triplet; q, quartet; m, multiplet; bq, broad quartet; br, broad signal; quint, quintet. Yields of reactions that generate fluorinated products were determined by ^{19}F NMR spectroscopic analysis using a relaxation delay of 25 s with at 90º pulse angle. Determination of yields by ^{1}H NMR were measured against $C_2H_2Cl_4$ with a relaxation delay of 25 s and a pulse angle of 90º. Mass spectral data were obtained on a Micromass Magnetic Sector Mass Spectrometer in electrospray ionization mode. Elemental analyses were conducted by Midwest Microlabs. X-ray crystallographic data were collected on a Rigaku AFC10K Saturn 944+ CCD-based X-ray diffractometer. EPR spectra were collected at –176 ºC using a Bruker EMX ESR Spectrometer with a nitrogen-cooled cryostat. Flash chromatography was performed using a Biotage Isolera One system with cartridges containing high performance silica gel.

Materials and Methods

The following compounds were prepared according to the literature procedures: NMe_4Tp,[22], $(MeCN)_2Ni(C_4F_8)$,[23] $NMe_4[TpNi(CF_3)_2]$,[1] $TpNi(CF_3)_2(MeCN)$,[1] Bis-(4-fluorophenybenzoyl)peroxide,[24] Bis-(4-Phenylbutryl)peroxide,[25] 2,6-difluorobenzenedizaonium tetrafluoroborate[26], Bis-(trifluoroacetyl)peroxide,[27] and $(DPE)Pd(CF_3)(Ph)$[28] $(MeCN)Ni(CF_3)_2$ [29] was made through a modified version of Vicic's procedure where the AgBr was separated through centrifugation under N_2 and decanted. Unless otherwise noted, all commercial compounds were used as received. S-trifluoromethyldibenzothiophenium, dicyclohexylcarbodimide, tetrafluoroborate and 1,4-dinitobenzene were purchased from Acros. Cinnamonnitrile and -nitrostyrene were purchased from Alfa Aesar. When not in use, the cinnamonnitrile was stored at -20 ºC. 2,6-difluoroaniline, and 4-phenylbutyric acid were purchased from Sigma Aldrich. Sodium Nitrite was purchased from Sigma Aldrich and was stored in a dessicator when not in use. Iodomethane and isobutyl iodide were purchased from Sigma Aldrich and dearated through a standard freeze-pump thaw procedure before use. CD_2Cl_2, $CDCl_3$, C_6D_6, and CD_3CN were obtained from Cambridge Isotopes Laboratories and were stored over activated 3 Å molecular sieves (EMD Millipore) or basic alumina. CD_3NO_2 was purchased from Cambridge isotope labs or Sigma Aldrich. Anhydrous nitromethane was purchased from Sigma Aldrich.

Trifluoroacetic anhydride was purchased from Alfa Aesar and was dearated with three careful free/pump/thaw cycles. Sodium peroxide was purchased from Acros and was always stored in an inert atmosphere glove box. Basic alumina (Aldrich) was dried for two days under vacuum at 210 °C. Silica gel was dried under vacuum at 130 ºC for one day. Celite was dried for 12 h under vacuum at 100 °C. Molecular sieves were dried under vacuum at 180 ºC for 3 d. Unless otherwise noted, all glassware and magnetic stir bars were dried overnight in an oven at 200 °C and cooled under an inert atmosphere before use. All commercial reagents were used without further purification/drying unless explicitly stated in the experimental section.

4.3.2 Synthesis of Nickel Complexes

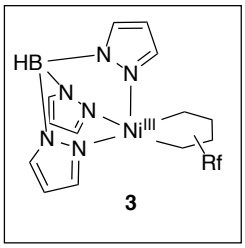

3

Synthesis of $TpNi^{III}(C_4F_8)$ (3): A 20 mL vial was charged with NMe_4Tp[22] (144 mg, 0.5 mmol, 1 equiv.), $(MeCN)_2Ni(C_4F_8)$[23] (150 mg, 0.5 mmol, 1 equiv.) and a magnetic stir bar. The solution was stirred in 10 mL of THF for 1 hour. The volatiles were removed to dryness. Next, the solid was then resuspended in 15 mL of THF under vigorous stirring. In a separate 4 mL vial, $AgBF_4$ (99 mg, 0.51 mmol, 1.02 equiv) was dissolved in a minimum of THF (~2 mL). This solution was then added in one portion to the vigorously stirring solution of $(MeCN)_2Ni(C_4F_8)/NMe_4Tp$. Upon addition of the Ag solution, the mixture went from a yellow-orange suspension to an orange solution with a gray Ag^0/ NMe_4BF_4 precipitate. The solution was stirred for 5 minutes before the vial was removed from the glove box, and filtered through a glass frit into a 50 mL round bottom flask. The frit was washed with 2 mL of Et_2O. The combined filtrates were reduced to dryness under reduced pressure. The solid was dissolved in 2 mL of CH_2Cl_2 and subsequently purified by silica column chromatography using a 5:1 hexane: ethyl acetate mobile phase. The product was collected, reduced to an oily red residue and taken up in 5 mL of anhydrous benzene. The volatiles of the yellow-green solution were removed under reduced pressure. The resulting dark green solid was brought into the glovebox where it was further lyophilized from 2 mL anhydrous benzene to yield **3** as a bright green solid (135 mg, 57%).[11]B NMR (225 MHz, Nitromethane) δ -3.26 (s) Elemental analysis: calculated for $C_{13}H_{10}N_6BF_9Ni$, C: 33.10, H: 2.14, N: 17.81; Found: C: 33.34, H: 2.31, N: 18.01. *u_{eff}=1.84 (Evans method).*

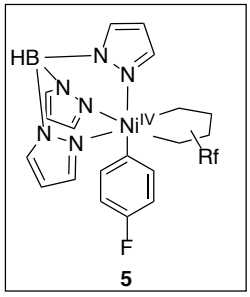

Isolation of $TpNi^{IV}(C_4F_8)(4\text{-}F\text{-}C_6H_4)$ (5): A 20 mL vial was charged with $TpNi(C_4F_8)$ (20 mg, 0.042 mmol, 1 equiv) and Bis-(4-fluorobenzoyl)peroxide (213mg, 0.77 mmol, 18 equiv). The solids were then dissolved in 2.7 mL of anhydrous CH_3NO_2. The vial was capped with a Teflon cap, removed from the glovebox, and heated at 95 ºC for 15 minutes. Over the course of the reaction the solution changed from a bright green to yellow/brown. Note: A yellow or red solution before heating indicates the presence of a lewis basic impurity, usually water. After heating, the vial was let stand at room temperature for 20 minutes before it was uncapped and the volatiles were removed under a gentle stream of N_2. The vial was charged with a magnetic stir bar and sticky solid was stirred with 1.5 mL of 1:1 hexane: ethyl acetate. After 30 min the suspension was loaded directly on to a silica column and was purified using a 98:2 hexanes:Ethyl acetate mobile phase. The title compound was isolated as a light yellow-orange powder in 31% yield (7.6 mg). *Note: **5** is mildly light sensitive. Though no precautions were taken to exclude light during the synthesis, it is best stored in a cold and dark place.* ^{1}H NMR (500 MHz, CD_3NO_2,) δ 7.77 (d, *J* = 2.2 Hz, 2H), 7.61 (d, *J* = 2.1 Hz, 1H), 7.55 (t, *J* = 2.2 Hz, 1H), 7.27 (d, *J* = 2.1 Hz, 2H), 6.38 – 6.22 (t, J= 9Hz, 2H), 6.10 (q, *J* = 2.2 Hz, 1H), 6.06 (t, *J* = 2.2 Hz, 1H), 5.76 (bs, 2H) 4.72-4.21 (br, 1 H) ^{11}B NMR (128 MHz, CD_3NO_2) δ -4.32 (d, *J* = 115.5 Hz). ^{13}C NMR (126 MHz, CD_3NO_2) δ 160.89 (d, *J* = 243.5 Hz), 143.19 (d, J=8.3 Hz), 142.99 (t, *J* = 10.5 Hz), 136.44, 135.7-135.3(multiple peaks, 2C), 112.85, 112.68, 106.96, 105.66. ^{19}F NMR (471 MHz, CD_3NO_2) δ -71.16 (d, *J* = 165.5, 9 Hz, 2F), -78.40 (dd, *J* = 165.2, 8.6 Hz, 2F), -118.33 (d, J=259 Hz, 2F), -120.46 (d, 259 Hz, 2F), -120.96. Elemental analysis: calculated for $C_{19}H_{14}N_6BF_9Ni$, C: 40.26, H: 2.49, N: 14.83; Found: C: 40.40, H: 2.53, N: 14.83

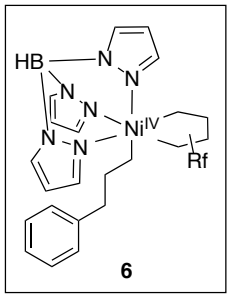

Isolation of $TpNi^{IV}(C_4F_8)(CH_2CH_2CH_2Ph)$ (6): *Note: **6** is light sensitive and precautions should be taken at each step to avoid light.* A 20 mL vial was charged with $TpNi(C_4F_8)$ (40 mg, 0.084 mmol, 1 equiv) and Bis-(4-phenylbutryle)peroxide (277mg, 0.85 mmol, 10 equiv). The solids were then dissolved in 5 mL of anhydrous CH_3NO_2. The vial was capped with a Teflon cap, wrapped in aluminum foil, and removed from the glovebox, and heated at 85 ºC for 6 minutes. Over the course of the reaction the solution changed from a bright green to orange/brown. Note: A yellow or red solution before heating indicates the presence of a lewis basic impurity, usually water. After heating, the vial was quickly dipped into ice water for 5 minutes. With the vial still wrapped in aluminum foil, the cap was removed

and the volatiles were removed under a gentle stream of N_2. The vial was then charged with a magnetic stir bar and the residue was stirred with 1.5 mL of 3:1 hexane: ethyl acetate. After 10 min the solution was loaded directly on to a silica column and was purified using a 99:1 hexanes: ethyl acetate mobile phase. The title compound was isolated as a light orange powder in 17% yield (8.4 mg). We attribute the low yield to challenges associated with separating the large quantities of Bis-(4-phenylbutyryl)peroxide, which was found to have a similar retention time as **6**. ^{1}H NMR (700 MHz, CD_3CN) δ 7.95 (d, *J* = 2.3 Hz, 2H), 7.88 (d, *J* = 2.3 Hz, 2H), 7.73 (d, *J* = 2.3 Hz, 1H), 7.68 (d, *J* = 2.5 Hz, 1H), 7.20 (t, *J* = 7.6 Hz, 2H), 7.15 (t, *J* = 7.3 Hz, 1H), 6.91 – 6.85 (m, 2H), 6.38 (t, *J* = 2.4 Hz, 2H), 6.20 (t, *J* = 2.3 Hz, 1H), 4.78-4.26 (multiple peaks, 3H), 2.34 (t, *J* = 7.7 Hz, 2H), 0.58 (apparent p, *J* = 7.8 Hz, 2H). ^{11}B NMR (225 MHz, Acetonitrile-d_3) δ -4.27. ^{13}C NMR (176 MHz, Acetonitrile-d_3):δ 145.71, 144.76, 144.68, 143.20, 139.29, 137.66, 130.98, 128.73, 109.52, 107.98, 73.28-73.56 (m), 40.81, 35.63. ^{9}F NMR (471 MHz, Nitromethane) δ -84.72 (d, *J* = 181.2 Hz), -94.26 (d, *J* = 181.6 Hz), -131.82 (d, J= 252 Hz), -133.25 (d, *J* = 252 Hz).

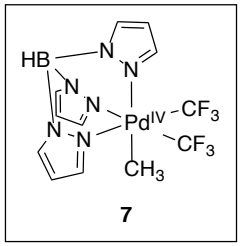

7

Synthesis of TpPd(CF$_3$)$_2$(CH$_3$): Step 1: A 20 mL vial was charged with (DPE)Pd(CF_3)(Ph)[13] (100 mg, 0.22 mmol, 1 equiv) a magnetic stir bar, and CH_2Cl_2 (~ 2 mL). In a separate 4 mL vial 40 mg of N-bromosuccinimide were dissolved in 1 mL of MeCN. The NBS solution was added dropwise to the vigorously stirring solution of (DPE)Pd(CF_3)(Ph) over the course of 30 s. The solution slowly chaged from colorless to orange over the timescale of the reaction. The vial was then removed from the glovebox and the volatiles were removed under reduced pressure. The resultant white solid was washed on a glass frit with 2 mL of -20 ºC THF . The white solid was then collected and dried under vacuum to yield 88 mg of (DPE)Pd(CF_3)($C_4H_4NO_2$) as a crude solid (82%) . This material was directly carried over to the next step. **Step 2:** Inside the glovebox a 20 mL vial was charged with 82 mg of (DPE)Pd(CF_3)($C_4H_4NO_2$), a magnetic stir bar and 6 mL of THF. The suspension was vigorously stirred for 1 minute before $ZnMe_2$ was added via syrnige as a 1.2 M soluiton in toluene (0.30 mL, 2 equiv). The vial was capped with a septum and removed from the box. Over the course of approximately 10 minutes the suspension slowly dissolved and turned brown. Once all of the solid had dissolved, the septum was removed and 0.1 mL of H_2O was added in one portion. The solution was stirred for another 5 minutes before another 0.1 mL of H_2O was added. After stirring for 15 minutes at room temperature, the solution was filtered through a 1 cm thick pad of silica which was washed with an additional 5 mL of Et_2O. The

filtrates were combined and the volatiles were removed under a gentle stream of N_2. The resultant white solid was triturated with 2 mL-20 ºC pentane, and dried under vacuum to yield (DPE)Pd(CF_3)(CH_3) as a crude off-white solid (55 mg, 76%). This solid was carried over directly to the next step. **Step 3:** In the glovebox , a 20 mL vial was charged with (DPE)Pd(CF_3)(CH_3) (55 mg, 0.14 mmol, 1 equiv), KTp (38 mg, 0.55mmol, 1.1 equiv) and 1.5 mL of anhydrous acetone. The vial was capped, removed from the glovebos, heated at 50 ºC for 30 minutes and brought back into the glovebox. Approximately half of the solvent was removed under vacuum and 1 mL of Et_2O followed by 10 mL of pentane were added. After addition of the pentane a cloudy white suspension formed which eventually oiled out on the bootom of the vial. The vial was capped, removed from the glovebox and sonicated for 30 minutes. During sonication the a white solid formed at the bottom of the vial where the oil had previously been. The vial was brought back in the glovebox where the solvent was carefully decanted. The resultant powder was dissolved in 2 mL of MeCN. A separate vial was charged with2,8-Difluoro-5-(trifluoromethyl)-5*H*-dibenzo[*b*,*d*]thiophen-5-ium Trifluoromethanesulfonate (310 mg, 5 equivalenets), a magnetic stir bar and 3 mL of MeCN. The solution of the K[TpPd(CF_3)(CH_3)] was added dropwise to the rapidly stirring solution of the S-trifluoromethylthiphenium salt. Note: order of addition is critically important for this step. The vial was removed from the glovebox and the volatiles were removed under a gentle stream of N_2. The crude residue was extracted with 1.5 mL of 1:1 Hexane:EtOAc by stirring this solvent mixture over the crude residue for 30 minutes. The resultant solution was loaded directly on to a wet silica column (10:1 Hexane:EtOAc) and was purified using a constant gradient. The product Pd complex was isolated in variable yield 4-12% overall. ^{1}H NMR (700 MHz, Chloroform-*d*) δ 7.90 (s, 1H), 7.72 (d, *J* = 2.3 Hz, 1H), 7.70 – 7.64 (multiple peaks, 4H), 6.29 (st, *J* = 2.1 Hz, 1H), 6.26 (s, 1H), 2.65 (s, 3H). ^{11}B NMR (225 MHz, Chloroform-*d*) δ -3.67 (d, *J* = 111.9 Hz). ^{13}C NMR (176 MHz, Chloroform-*d*) δ 142.22, 140.41, 135.51, 135.35, 105.80, 105.44, 30.74 – 27.15 (m). ^{19}F NMR (471 MHz, Chloroform-*d*) δ -24.52.

4.3.3. Radical Capture at Ni^{III} Experiments

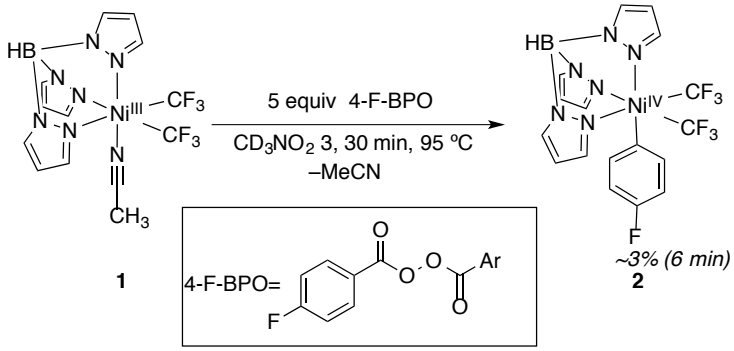

Attempted Aryl Radical Capture at 1: A 4 mL vial was charged with **1** (4.8 mg, 0.011 mmol, 1.0 equiv) with Bis-(4-fluorobenzoyl)peroxide (14.6 mg, 0.05 mmol, 5 equiv) and C_6F_6 as a stock solution in CD_3NO_2 (0.015M, 0.7 mL, 1 equiv). The vial was capped and lightly shaken to mix the contents. Once homogeneous, the solution was transferred to a J-young tube, capped and removed from the glovebox. The sample was inserted into a preheated (95 ºC) NMR spectrometer and the formation of **2** was monitored by ^{19}F NMR for 30 minutes. The yield peaked at ~3% after 8 minutes. After which point the concentration of **2** rapidly decreased until it was not detectable. We attribute the low yield to the competitive decomposition of the **1** and the product **2**.

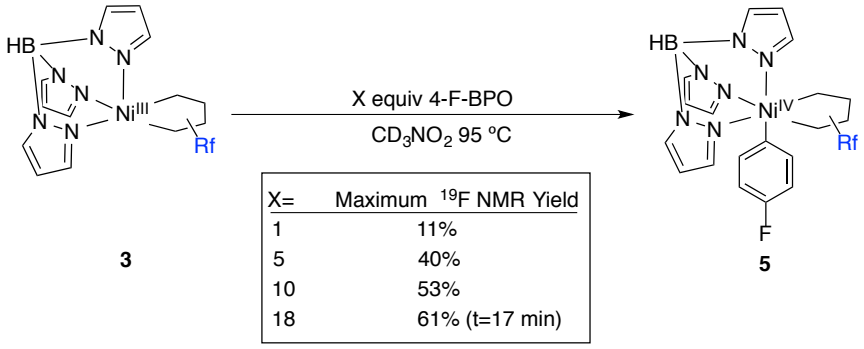

X=	Maximum ^{19}F NMR Yield
1	11%
5	40%
10	53%
18	61% (t=17 min)

Aryl Radical Capture at 3: A 4 mL vial was charged with **3** (5.0 mg, 0.010 mmol, 1.0 equiv) with the appropriate amount of Bis-(4-fluorobenzoyl)peroxide and C_6F_6 as a stock solution in CD_3NO_2 (0.014M, 0.7 mL, 1 equiv, 6F). This solution was capped, shaken and transferred into a thick-walled J-Young tube. The sample was inserted into a preheated (95 ºC) NMR spectrometer and the formation of **5** was monitored by ^{19}F NMR for ~35 minutes. As it ca be seen in figure SX, increased equivalents of 4-F-BPO resulted in higher yields. Additional heating eventually decomposed 5 into a complex mixture of nickel-containing product

Figure 4.7. Time study showing the formation and decay of **5** with 1, 5, 10 18 equiv 4-FBPO

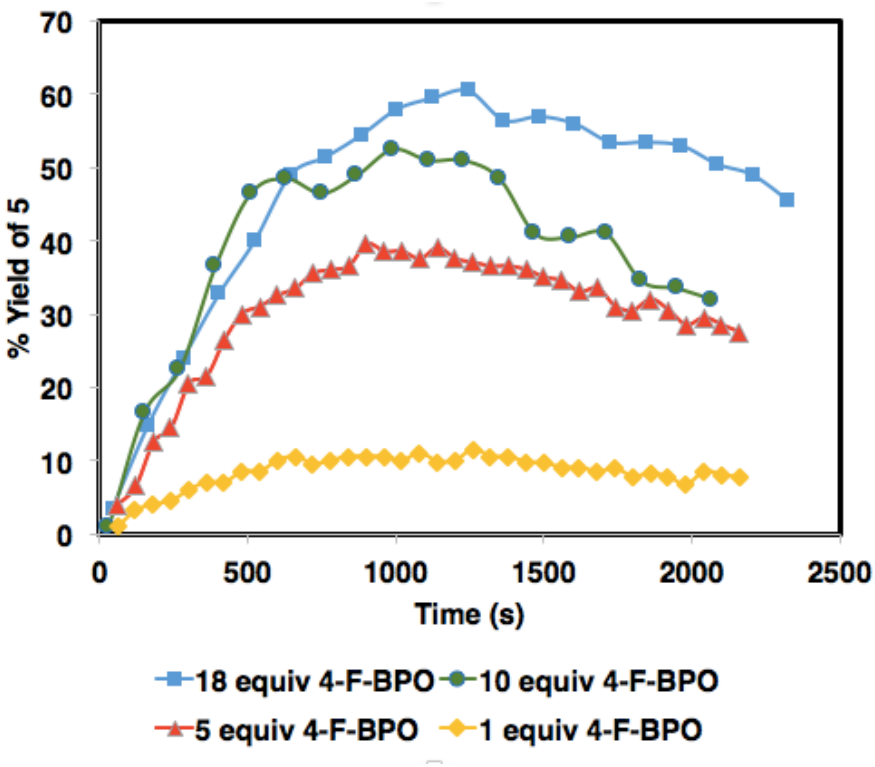

Figure 4.8. ^{19}F NMR spectrum shoing a mixture of **3**, 4-FBPO and C_6F_6 (a) prior to hearing (b) after heating and (c) after isolation of **5**.

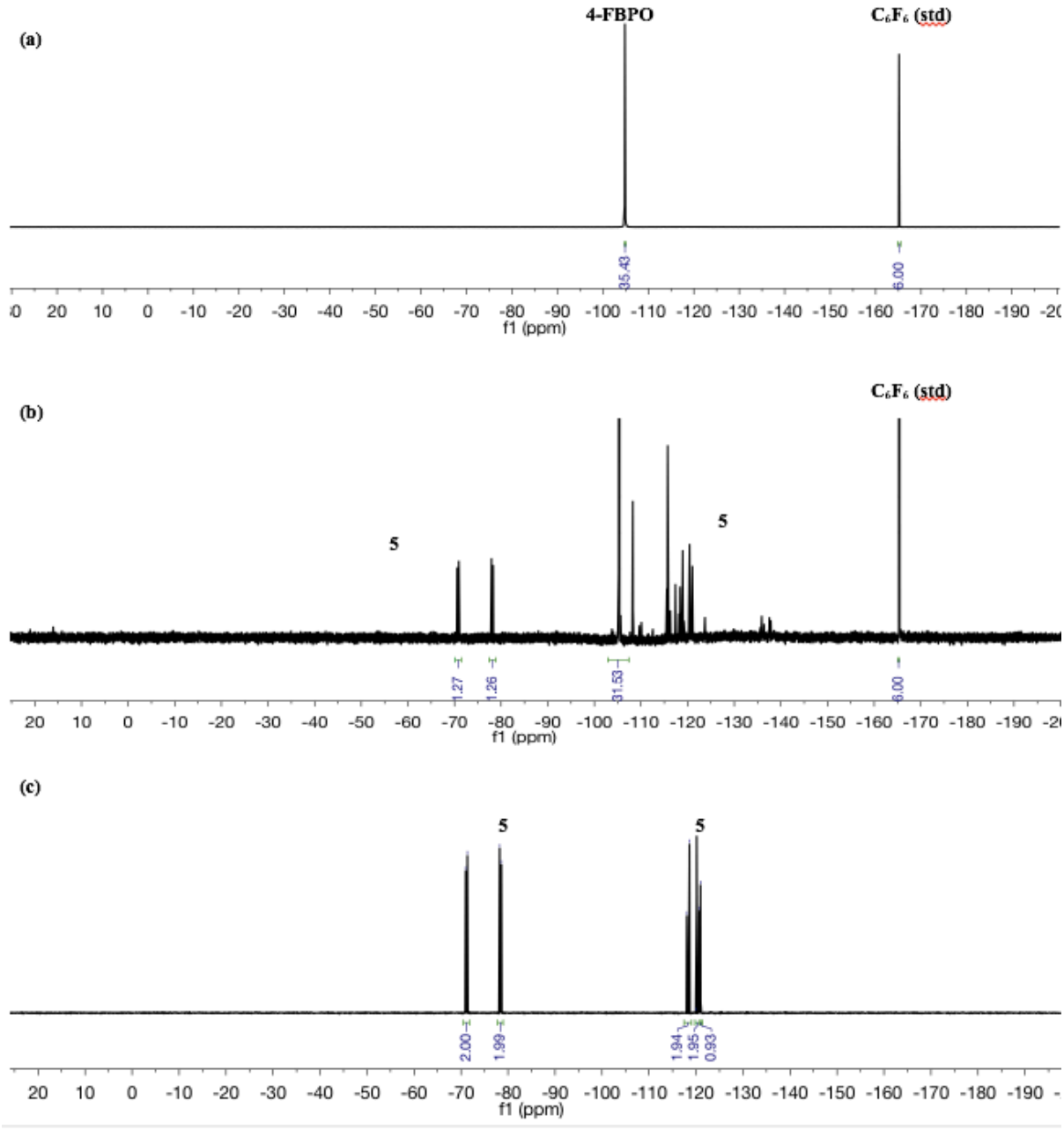

Alkyl Radical Capture at 3

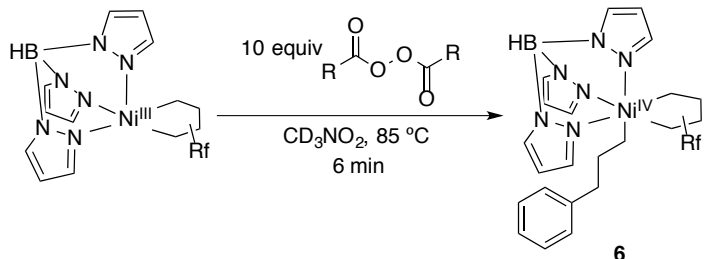

3 **6**

49% by ^{19}F NMR, 17% isolated)

Akyl Radical Capture at 3: A 4 mL vial was charged with **3** (5.0 mg, 0.011 mmol, 1.0 equiv) with Bis-(4-phenylbutryl)peroxide (and C_6F_6 as a stock solution in CD_3NO_2 (0.015M, 0.7 mL, 1 equiv, 6F). This solution was capped, shaken and transferred into a thick-walled J-Young tube. The sample was inserted into a preheated (85 ºC) NMR spectrometer and the formation of **5** was monitored by ^{19}F NMR for 30 minutes. A maximum yield was observed at 6 minutes, after which point the resonances associated with **6** decreased. A representative NMR spectrum is shown below.

Figure 4.9. ^{19}F NMR spectrum shoing a mixture of **3**, 4-PhBuPO and C_6F_6 (a) after heating for 6 minutes and (b) after isolation of **6**.

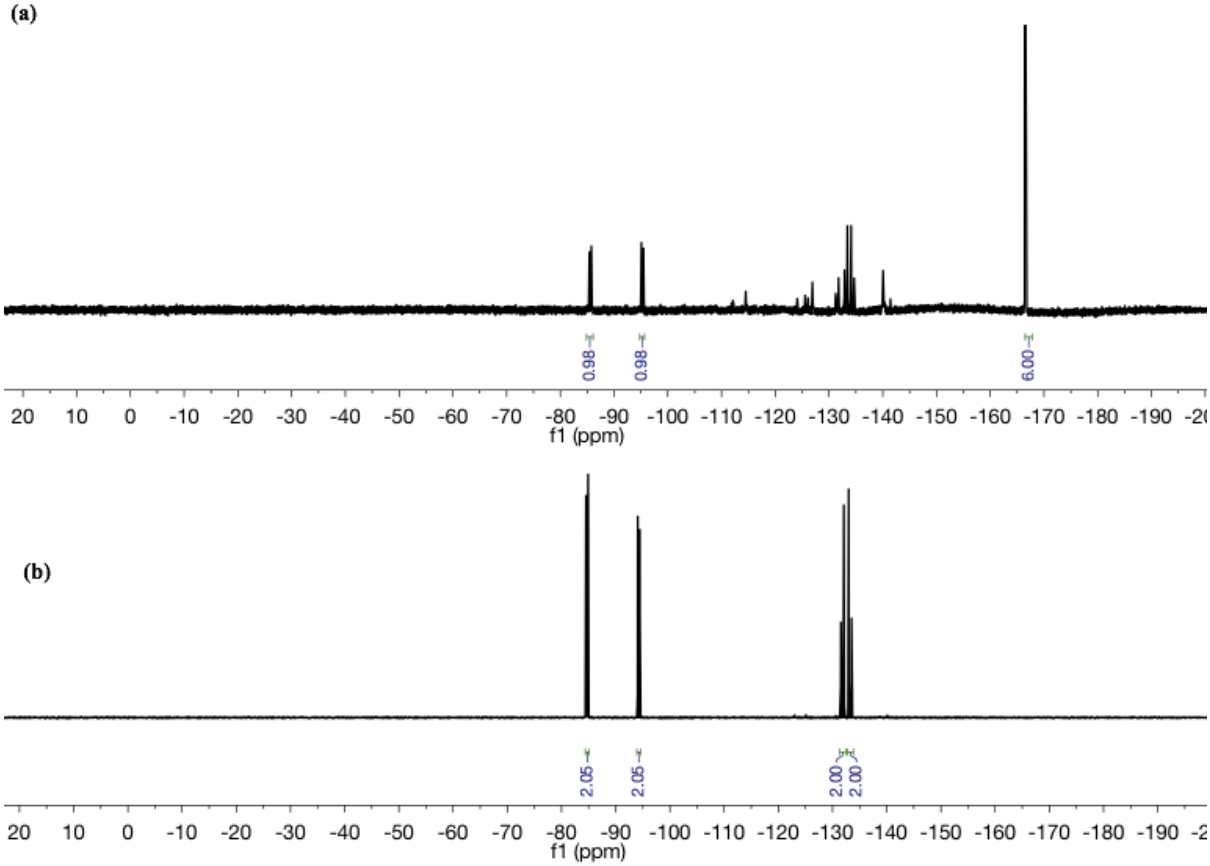

4.4.4. Outer Sphere C–C Coupling Studies

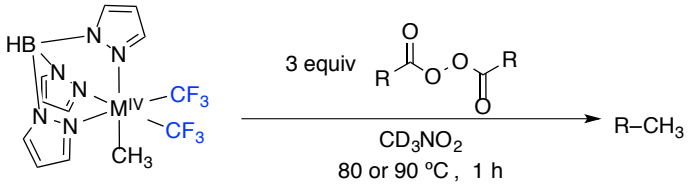

7 or 11

R =	Temp	R–CH_3 Yield
4-F-C_6H_4	90	60
$^nC_3H_6Ph$	80	78

Aryl and Alkyl Outer Sphere C-C coupling with 7 or 11: A 4 mL vial was charged with the appropriate $TpM^{IV}(CF_3)_2(CH_3)$ complex (0.011 mmol, 1 equiv) the appropriate diacylperoixde (3 equiv) and 0.7 mL of CD_3NO_2 containing C_6F_6 as an internal standard and the vial was capped and shaken. The solution was then transferred to a J-Young tube with a pipette, capped, and removed from the glovebox for analysis. In the case of aryl radical coupling an ^{19}F NMR spectrum was recorded to determine the ratio between the metal complex and internal standard. The J-Young tube was then placed in a preheated oil bath at the appropriate temperature (80 ºC or 90ºC). At this point the reaction as cooled and was analyzed by ^{19}F NMR. IN the case of alkyl radical outer sphere C-C coupling a ^1H NMR standard ($Cl_2HCCHCl_2$ or 1,3,5-trimethoxybenzene) was added as a stock solution in CD_3NO_2 after heating. Representative NMR spectra are shown below.

Figure 4.10 ^{19}F NMR spectrum of **7**, 4-FBPO and C_6F_6 in CD_3NO_2 (a) before heating and (b) after heating for 60 minutes. The C–C coupled product 4-fluorotoluene (1 F)can be seen at -122 ppm.

(a)

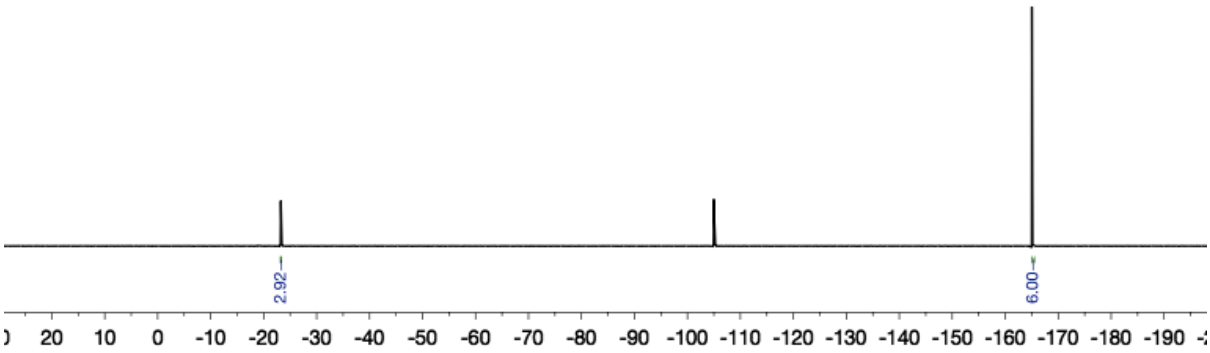

(b)

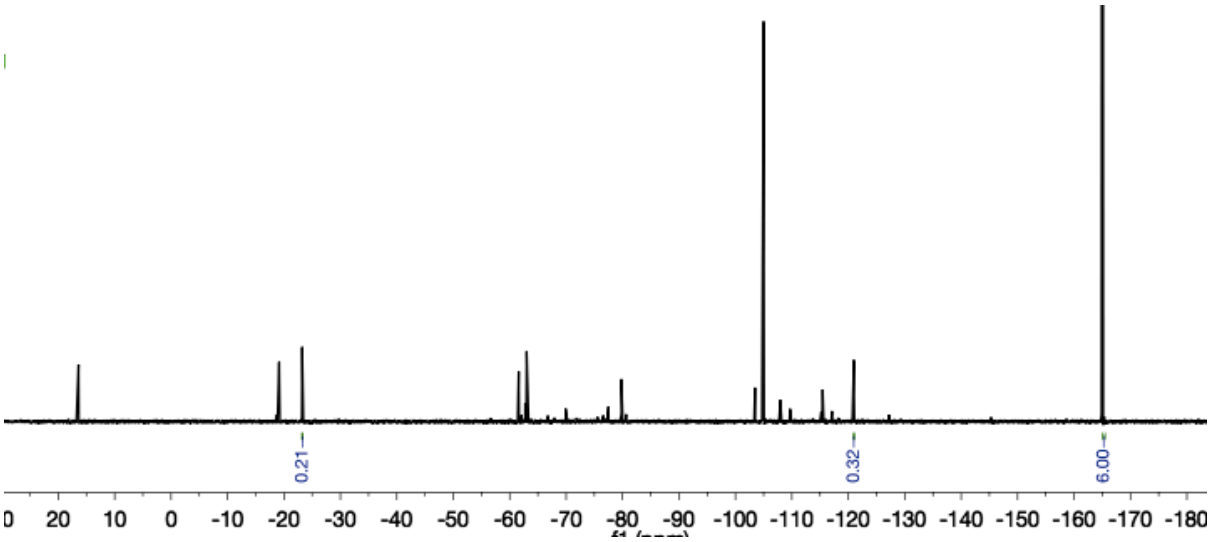

S_N2 reductive elimination study of Complex 11

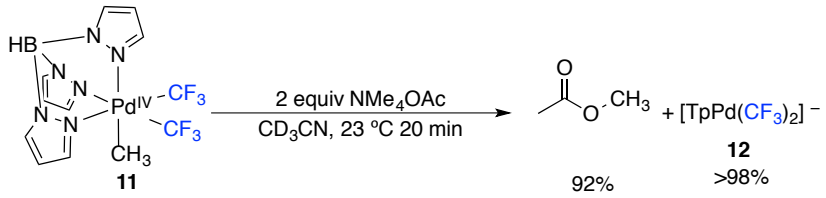

A 4 mL vial was charged with $TpM^{IV}(CF_3)_2(CH_3)$ **11** (6.5 mg, 0.011 mmol, 1 equiv), NMe_4OAc (2.9 mg, 0.022 mmol, 2 equiv) and 0.7 mL of CD_3CN containing trimethoxybenzene and C_6F_6 as an internal standard (0.015M, 1 equiv). The solution wa then transferred to a J-Young tube and was analyzed after 20 minutes. The ^1H and ^{19}F NMR spectra showed complete conversion to a new complex consistent with $[TpPd(CF_3)_2$ and MeOAc. The identity of the palladium product was further confirmed by HRMS which showed the presence of the proposed molecule. HRMS (ESI^-) Calc for $C_{11}H_{10}N_6BF_6Pd$: 457.0005; found, 457.0009.

4.3.4. X-ray Structure Determination

Structure Determination of 3

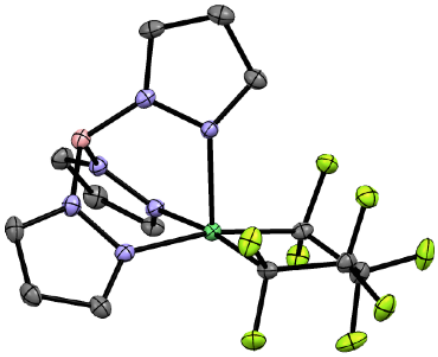

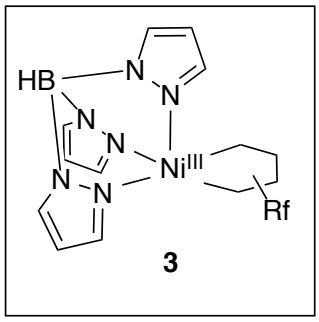

3

Green needles of **3** were grown from a diethyl ether/pentane solution of the compound at 22 deg. C. A crystal of dimensions 0.17 x 0.05 x 0.01 mm was mounted on a Rigaku AFC10K Saturn 944+ CCD-based X-ray diffractometer equipped with a low temperature device and Micromax-007HF Cu-target micro-focus rotating anode (λ = 1.54187 A) operated at 1.2 kW power (40 kV, 30 mA). The X-ray intensities were measured at 85(1) K with the detector placed at a distance 42.00 mm from the crystal. A total of 2028 images were collected with an oscillation width of 1.0° in ω. The exposure times were 1 sec. for the low angle images, 4 sec. for high angle. Rigaku d*trek images were exported to CrysAlisPro for processing and corrected for absorption. The integration of the data yielded a total of 50543 reflections to a maximum 2θ value of 138.59° of which 6266 were independent and 6073 were greater than 2σ(I). The final cell constants (Table 1) were based on the xyz centroids 33012 reflections above 10σ(I). Analysis of the data showed negligible decay during data collection. The structure was solved and refined with the Bruker SHELXTL (version 2014/6) software package, using the space group P2(1)/c with Z = 8 for the formula $C_{13}H_{10}BN_6F_8Ni$. All non-hydrogen atoms were refined anisotropically with the hydrogen atoms placed in idealized positions. Full matrix least-squares refinement based on F^2 converged at R1 = 0.0294 and wR2 = 0.0807 [based on I > 2sigma(I)], R1 = 0.0301 and wR2 = 0.0815 for all data. Additional details are presented in Table 1 and are given as Supporting Information in a CIF file. Acknowledgement is made for funding from NSF grant CHE-0840456 for X-ray.

Table 4.2. Acquisition and refinement parameters for 3

Empirical Formula	$C_{13}H_{10}BF_8N_6BNi$
Formula Weight	472.29
Temperature	85(2) K
Wavelength	1.54178 A
Crystal System	Orthorhombic
Space Group	Pna2(1)
Unit Cell Dimensions	a = 7.74730(10A alpha = 90 deg. b =12.80320(10)A beta = 90 deg c = 16.63240(10) A gamma = 90 deg.
Volume	1649.77(3)A^3
Z	4
Calculated Density	1.902 mg/m^3
Absorption Coefficient	9.784mm^{-1}
F(000)	928
Crystal Size	0.130 x 0.120 x 0.10mm
Theta Range for Data Collection	4.358 to 69.185 deg.deg
Limiting Indicies	-9<=h<=9, -15<=k<=13, -20<=l<=20
Reflections Collected	24722
Independent Reflections	3062 [R(int) = 0.0503]
Completeness to Theta	67.684 (100%)
Absorption Correction	Semi-empirical from equivalents
Max and Min Transmission	0.7366 and 0.6464
Refinement Method	Full-matrix least-squares on F^2
Data / Restraints / Parameters	3099 / 1 / 259
Goodness-of-Fit on F^2	1.109
Final R Indices [l>2σ(l)]	R1 = 0.0363, wR2 = 0.0982
R indices (all data)	R1 = 0.0363, wR2 = 0.0982
Largest Difference Peak and Hole	1.663 and -0.759 e.A^-3

Structure Determination of 5

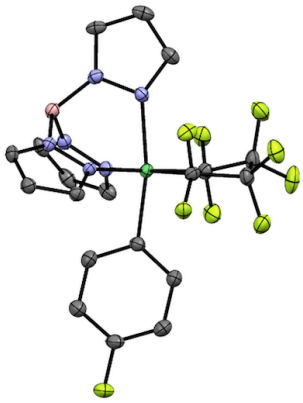

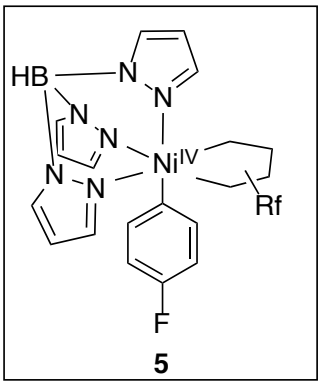

5

Orange plates of **5** were grown from a pentane solution of the compound at -20 deg. C. A crystal of dimensions 0.06 x 0.06 x 0.03 mm was mounted on a Rigaku AFC10K Saturn 944+ CCD-based X-ray diffractometer equipped with a low temperature device and Micromax-007HF Cu-target micro-focus rotating anode (λ = 1.54187 A) operated at 1.2 kW power (40 kV, 30 mA). The X-ray intensities were measured at 85(1) K with the detector placed at a distance 42.00 mm from the crystal. A total of 2028 images were collected with an oscillation width of 1.0° in ω. The exposure times were 1 sec. for the low angle images, 4 sec. for high angle. Rigaku d*trek images were exported to CrysAlisPro for processing and corrected for absorption. The integration of the data yielded a total of 16508 reflections to a maximum 2θ value of 138.42° of which 3901 were independent and 3716 were greater than 2σ(I). The final cell constants (Table 1) were based on the xyz centroids of 9288 reflections above 10σ(I). Analysis of the data showed negligible decay during data collection. The structure was solved and refined with the Bruker SHELXTL (version 2016/6) software package, using the space group P1bar with Z = 2 for the formula $C_{19}H_{14}BN_6F_9Ni$. All non-hydrogen atoms were refined anisotropically with the hydrogen atoms placed in idealized positions. Full matrix least-squares refinement based on F^2 converged at R1 = 0.0439 and wR2 = 0.1189 [based on I > 2sigma(I)], R1 = 0.0457 and wR2 = 0.1214 for all data. Additional details are presented in Table 1 and are given as Supporting Information in a CIF file. Acknowledgement is made for funding from NSF grant CHE-0840456 for X-ray instrumentation.

Table 4.3. Structure Determination of **5**

Empirical Formula	$C_{22}H_{13}BF_9N_6BNi$
Formula Weight	472.29
Temperature	85(2) K
Wavelength	1.54178 A
Crystal System	Orthorhombic
Space Group	Pna2(1)
Unit Cell Dimensions	a = 7.74730(10A alpha = 90 deg. b =12.80320(10)A beta = 90 deg c = 16.63240(10) A gamma = 90 deg.
Volume	1649.77(3)A^3
Z	4
Calculated Density	1.902 mg/m^3
Absorption Coefficient	9.784mm^{-1}
F(000)	928
Crystal Size	0.130 x 0.120 x 0.10mm
Theta Range for Data Collection	4.358 to 69.185 deg.deg
Limiting Indicies	-9<=h<=9, -15<=k<=13, -20<=l<=20
Reflections Collected	24722
Independent Reflections	3062 [R(int) = 0.0503]
Completeness to Theta	67.684 (100%)
Absorption Correction	Semi-empirical from equivalents
Max and Min Transmission	0.7366 and 0.6464
Refinement Method	Full-matrix least-squares on F^2
Data / Restraints / Parameters	3099 / 1 / 259
Goodness-of-Fit on F^2	1.109
Final R Indices [l>2σ(l)]	R1 = 0.0363, wR2 = 0.0982
R indices (all data)	R1 = 0.0363, wR2 = 0.0982
Largest Difference Peak and Hole	1.663 and -0.759 e.A^-3

Structure Determination of 6

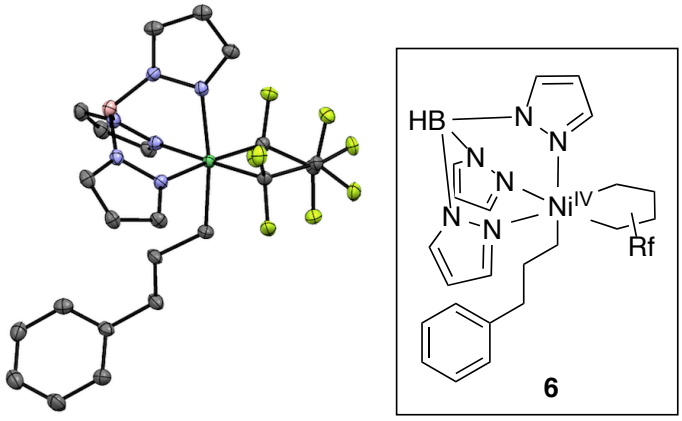

Yellow prisms of **6** were grown from a pentane solution of the compound at -22 deg. C. A crystal of dimensions 0.15 x 0.09 x 0.09 mm was mounted on a Rigaku AFC10K Saturn 944+ CCD-based X-ray diffractometer equipped with a low temperature device and Micromax-007HF Cu-target micro-focus rotating anode (= 1.54187 A) operated at 1.2 kW power (40 kV, 30 mA). The X-ray intensities were measured at 85(1) K with the detector placed at a distance 42.00 mm from the crystal. A total of 2028 images were collected with an oscillation width of 1.0 in The exposure times were 1 sec. for the low angle images, 3 sec. for high angle. Rigaku d*trek images were exported to CrysAlisPro for processing and corrected for absorption. The integration of the data yielded a total of 36328 reflections to a maximum 2 value of 138.56 of which 4509 were independent and 4444 were greater than 2 (I). The final cell constants (Table 1) were based on the xyz centroids 27038 reflections above 10 (I). Analysis of the data showed negligible decay during data collection. The structure was solved and refined with the Bruker SHELXTL (version 2016/6) software package, using the space group P2(1)/n with Z = 4 for the formula $C_{22}H_{21}BN_6F_6Ni$. All non-hydrogen atoms were refined anisotropically with the hydrogen atoms placed in idealized positions. Full matrix least-squares refinement based on F^2 converged at R1 = 0.0332 and wR2 = 0.0862 [based on I > 2sigma(I)], R1 = 0.0336 and wR2 = 0.0865 for all data. Additional details are presented in Table 1 and are given as Supporting Information in a CIF file. Acknowledgement is made for funding from NSF grant CHE-0840456 for X-ray instrumentation.

Table 4.4. Acquisition and Refinement parameters for 6

Empirical Formula	$C_{12}H_{13}BF_8N_6BNi$
Formula Weight	472.29
Temperature	85(2) K
Wavelength	1.54178 A
Crystal System	Orthorhombic
Space Group	Pna2(1)
Unit Cell Dimensions	a = 7.74730(10A alpha = 90 deg. b =12.80320(10)A beta = 90 deg c = 16.63240(10) A gamma = 90 deg.
Volume	1649.77(3)A^3
Z	4
Calculated Density	1.902 mg/m^3
Absorption Coefficient	9.784mm^{-1}
F(000)	928
Crystal Size	0.130 x 0.120 x 0.10mm
Theta Range for Data Collection	4.358 to 69.185 deg.deg
Limiting Indicies	-9<=h<=9, -15<=k<=13, -20<=l<=20
Reflections Collected	24722
Independent Reflections	3062 [R(int) = 0.0503]
Completeness to Theta	67.684 (100%)
Absorption Correction	Semi-empirical from equivalents
Max and Min Transmission	0.7366 and 0.6464
Refinement Method	Full-matrix least-squares on F^2
Data / Restraints / Parameters	3099 / 1 / 259
Goodness-of-Fit on F^2	1.109
Final R Indices [l>2σ(l)]	R1 = 0.0363, wR2 = 0.0982
R indices (all data)	R1 = 0.0363, wR2 = 0.0982
Largest Difference Peak and Hole	1.663 and -0.759 e.A^-3

Structure Determination of 11

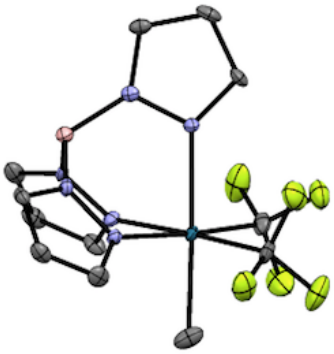

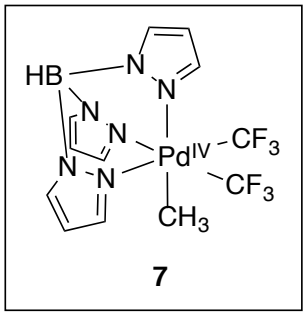

7

Colorless plates of **11** were grown from a methanol solution of the compound at 23 deg. C. A crystal of dimensions 0.13 x 0.12 x 0.10 mm was mounted on a Rigaku AFC10K Saturn 944+ CCD-based X-ray diffractometer equipped with a low temperature device and Micromax-007HF Cu-target micro-focus rotating anode (= 1.54187 A) operated at 1.2 kW power (40 kV, 30 mA). The X-ray intensities were measured at 85(1) K with the detector placed at a distance 42.00 mm from the crystal. A total of 2028 images were collected with an oscillation width of 1.0 in The exposure times were 1 sec. for the low angle images, 3 sec. for high angle. Rigaku d*trek images were exported to CrysAlisPro for processing and corrected for absorption. The integration of the data yielded a total of 24722 reflections to a maximum 2 value of 138.37 of which 3062 were independent and 3060 were greater than 2 (I). The final cell constants (Table 1) were based on the xyz centroids of 21979 reflections above 10 (I). Analysis of the data showed negligible decay during data collection. The structure was solved and refined with the Bruker SHELXTL (version 2016/6) software package, using the space group P2(1)2(1)2(1) with Z = 4 for the formula $C_{12}H_{13}BN_6F_6Pd$. All non-hydrogen atoms were refined anisotropically with the hydrogen atoms placed in idealized positions. The structure was refined as a two-component inversion twin. Full matrix least-squares refinement based on F^2 converged at R1 = 0.0363 and wR2 = 0.0982 [based on I > 2sigma(I)], R1 = 0.0363 and wR2 = 0.0982 for all data. Additional details are presented in Table 1 and are given as Supporting Information in a CIF file. Acknowledgement is made for funding from NSF grant

CHE-0840456 for X-ray instrumentation.

Table 4.5 Acquisition and refinement parameters for **11**

Empirical Formula	$C_{12}H_{13}BF_6N_6BPd$
Formula Weight	472.29
Temperature	85(2) K
Wavelength	1.54178 A
Crystal System	Orthorhombic
Space Group	Pna2(1)
Unit Cell Dimensions	a = 7.74730(10A alpha = 90 deg. b =12.80320(10)A beta = 90 deg c = 16.63240(10) A gamma = 90 deg.
Volume	$1649.77(3)A^3$
Z	4
Calculated Density	$1.902\ mg/m^3$
Absorption Coefficient	$9.784mm^{-1}$
F(000)	928
Crystal Size	0.130 x 0.120 x 0.10mm
Theta Range for Data Collection	4.358 to 69.185 deg.deg
Limiting Indicies	-9<=h<=9, -15<=k<=13, -20<=l<=20
Reflections Collected	24722
Independent Reflections	3062 [R(int) = 0.0503]
Completeness to Theta	67.684 (100%)
Absorption Correction	Semi-empirical from equivalents
Max and Min Transmission	0.7366 and 0.6464
Refinement Method	Full-matrix least-squares on F^2
Data / Restraints / Parameters	3099 / 1 / 259
Goodness-of-Fit on F^2	1.109
Final R Indices [l>2σ(l)]	R1 = 0.0363, wR2 = 0.0982
R indices (all data)	R1 = 0.0363, wR2 = 0.0982
Largest Difference Peak and Hole	1.663 and -0.759 e.A^-3

4.4. References

[1] Hu, X. *Chem. Sci.* **2011**, *2*, 1867. (b) Rosen, B. M.; Quasdorf, K. W.; Wilson, D. A.; Zhang, N.; Resmerita, A-M.; Garg, N. K.; Percec, V. *Chem Rev.* **2011**, *111*, 1346. (c) Montgomery, J. "Organonickel Chemistry" in *Organometallics in Synthesis: Fourth Manual* Lipshutz, B. H. (Ed.) Wiley, Hoboken, N.J., **2013**, pp. 319-428. (d) Tasker, S. Z.; Standley, E. A.; Jamison, T. F. *Nature* **2014**, *509*, 299. Gianatassio, R.; Schmidt, M. A.; Eastgate, M. D.; Baran, P. S. *J. Am. Chem. Soc.* **2016**, 138, 2174.

[2] Tsou, T. T.; Kochi, J. K. *J. Am. Chem. Soc.* **1979**, *101*, 7547. (b) Hu, X. *Chem. Sci.* **2011**, 2, 1867. (c) Lipschutz, M. I.; Tilley, T. D. *Angew. Chem., Int. Ed*. **2014,** *53*, 7290. (d) Everson, D. A.; Weix, D. J. *J. Org. Chem.* **2014**, *79,* 4793. (e) Tellis, J. C.; Primer, D. N.; Molander, G. A. *Science* **2014**, *345*, 433. (f) Zuo, Z.; Ahneman, D. T.; Chu, L.; Terrett, J. A.; Doyle, A. G.; MacMillan, D. W. C. *Science* **2014**, 345, 437. (g) Cornella, J.; Edwards, J. T.; Qin, T.; Kawamura, S.; Wang, J.; Pan, C.-M.;

[3] Mosiman, H.; Krautler, B. *Angew Chem. Int. Ed.* **2000**, *39*, 393. (b) D. R. Houck, K. Kobayashi, J. M. Williamson, H. G. Floss *J. Am. Chem. Soc.* **1986**, *108*, 5365; (c) P. Zhou, D. O'Hagan, U. Mocek, Z. Zeng, L.-D. Yuen, T. Frenzel, C. J. Unkefer, J. M. Beale, H. G. Floss, *J. Am. Chem. Soc.* **1989**, 111, 7274. (d) Fryberg, M.; Meyerstein, D.; J. C. S. Faraday I, **1980**, *76,* 1825. (e) MacLeod, K.; Conway, J. L.; Patrick, B.O.; Smith, K. *J. Am. Chem. Soc.* **2010**, *132*, 17325.

[4] For experimental proposals of Ni^{IV} see: Aihara, Y.; Chatani, N. *J. Am. Chem. Soc.* **2013**, *136,* 898. (b) Iyanaga, M.; Aihara, Y.; Chatani, N. *J. Org. Chem.* **2014**, *79*, 11933. (c) Wu, X.; Zhao, Y.; Ge, H. *J. Am. Chem. Soc*. **2014**, *136*, 1789. (d) Yan, S.-Y.; Liu, Y.-J.; Liu, B.; Liu, Y.-H.; Zhang, Z.-Z.; Shi, B.-F. *Chem. Commun*. **2015**, *51*, 734. (e). Terao, J.; Kambe, N. *Acc. Chem. Res.* **2008**, *41*, 1545. (f) Soni, V.; Jagtap, R.; Gonnade, R.; Punji, P.; *ACS Catalysis.* **2016**, *6*, 5666. (g) Soni, V.; Khake, S. M.; Punji, B. *ACS Catalysis* **2016,** *6*, 4202**.** (h) Patel, U.; Jain, S.; Pandey, D.; Gonnade, R. G.; Vanka, K.; Punji, B. *Organometallics* **2018**, ASAP DOI: 10.1021/acs.organomet.8b00025

[5] For theoretical investigations see: (a) Omer, H. M.; Liu, P. *J. Am. Chem. Soc.* **2017,** *139*, 9909**.** (b) Singh, S.; K. S.; Sunoj, R.; *J. Org. Chem.* **2017**, *82,* 9619. (c) Li, Y.; Zou, L.; Bai, R.; Lan, Y. *Org. Chem. Front.* **2018** *5*, 615.

[6] Levin, M. D.; Chen, T. Q.; Neubig, M. E.; Hong, C. M.; Theuller, C. A.; Kobylianski, I. J.; Janabi, M.; O'Neil, J. M.; Toste, F. D. *Science* **2017,** 356.

[7] Bour, J. R.; Camasso, N. M.; Sanford, M. S. *J. Am. Chem. Soc.* **2015**

[8] Swain, G. C.; Schaad, L. J.; Kresge, J. *J. Am. Chem. Soc.* **1958**, *80*, 5313.

[9] Bour, J. R.; Camasso, N. M.; Meucci, E. M.; Kampf, J. W.; Canty, A. J.; Sanford, M. S. *J. Am. Chem. Soc.* **2016,** *138*, 16105.

[10] Yu, S.; Dudkina, Y.; Wang, H.; Kholin, K. V.; Kadirov, M. K.; Budnikova, Y. H.; Vicic, D. A. *Dalton Trans.* **2015** , *44*, 19443.

[11] With additional heating **3** ultimately decomposes into a mixture of nickel-containing products including $Ni(Tp)_2$.

[12] Analysis of the crude reaction mixture revealed that 11% (~1.8 equiv relative to Ni) of the initial 4-F BPO was consumed at the time of maximum Ni^{IV} yield. The remaining mass balance of the reaction was fluorobenzene and 4-fluorobenzoic acid, presumably formed through H-atom abstraction from the solvent (see Figure SX). A common decomposition product of [TpNi] complexes, $NiTp_2$ was also detected by ^{11}B NMR spectroscopy.

[13] Analysis of the crude reaction mixture by ^{1}H NMR spectroscopy and GCMS revealed the formation of *n*-propylbenzene, 1,6-diphenyl hexane, and allyl benzene. The allylbenzene is

formed during the thermal decomposition of **6** via through an apparent net -hydride elimination.

[14] Diacyl peroxides are potentially explosive compounds and their handling on large scales is not recommended. As such, 6 was isolated in 17% yield through the reaction of 3 with 5 equivalents of 5 at 85 ºC for 6 minutes.

[15] Heinrich, M. R.; Wetzel, A.; Kirchenstein, M. *Org. Lett.* **2007***, 9,* 3834. (b) Barton, D. H. R.; Togo, H.; Zard, Z. S. *Tetrahedron* **1985,** *41*, 5507.

[16] Lee, W.; Guiterrez, O. *J. Am. Chem. Soc.* **2017**, *139*, 16126. (b) Sharma, A. K.; Sameera, W. M. C.; Jin, M.; Adak, L.; Okuzono, C.; Iwamoto, T.; Kato, M.; Nakamura, M.; Morokuma, K. *J. Am. Chem. Soc.* **2017**, *139*, 16117. (c) Zaragoza, J. P.; Yosca, T. H.; Siegler, M. A.; Moenne-Loccoz, P.;¨Green, M. T.; Goldberg, D. P. Direct Observation of Oxygen Rebound with an Iron-Hydroxide Complex. *J. Am. Chem. Soc.* **2017**, *139*, 13640. (e) Huang, X.; Zhuang, T.; Kates, P. A.; Gao, H.; Chen, X.; Groves, J. T. *J. Am. Chem. Soc.* **2017**, *139,* 15407.

[17] Martin, B. D.; Finke, R. G. *J. Am. Chem. Soc.* **1992**, *114*, 585. (b) Hung, R. R.; Grabowski, J. J. *J. Am. Chem. Soc.* **1999**, *121*, 1359. (c)Kozolowski, P.; Kumar, M. *J. Chem. Theory. Comput.* **2012**, *6*, 1870.

[18] A similar yield (59%) was obtained based on ^{1}H NMR spectroscopic analysis of the crude reaction mixture, suggesting that the methyl is not solvent-derived. Additionally, no fluorotoluene products were observed when the nickel compound was omitted from the reaction conditions.

[19] Attempts to isolate Ni-containing products from the crude reaction mixtures with 4-F-BPO and 4-Ph-BuPO (by silica column chromatography or recrystallization) were unsuccessful. EPR spectroscopic analysis of the crude reaction mixtures showed no signals consistent with the presence of S = $^{1}/_{2}$ Ni^{III} products.

[20] Due to the hazards associated with scaling this reaction, we did not pursue the isolation of this complex from the reaction mixture. However, an independent synthesis of $TpNi^{IV}(CF_3)_3$ confirmed the identity of this product.

[21] Camasso, N. M.; Perez-Temprano, M. H.; Sanford, M. S. *J. Am. Chem. Soc.* **2014,** *136*, 12771.

[22] Bour, J. R.; Camasso, N. M.; Meucci, E. A.; Kampf, J. W.; Canty, A. J.; Sanford, M. S. *J. Am. Chem. Soc.* **2016** *138,* 16105.

[23] Yu, S.; Dudkina, Y.; Wang, H.; Kholin, K. V.; Kadirov, M. K.; Budnikova, Y. H.; Vicic, D. A. *Dalton Trans.* **2015** *44*, 19443.

[24] Y, W-Y.; Sit, W. N.; Zhou, Z.; Chan, A. S-C *Org. Lett.* **2009**, *11*, 3174.

[25] Raveendra, K.; Zhu, N.; Bao, H. *Org. Lett.* **2017**, *19*, 46.

[26] Hansen, M. J.; Lerch, M. M.; Szymanski, W.; Feringa, B. L. *Angew. Chem. Int. Ed.* **2016** *55*, 13514.

[27] Hayakawa, Y.; Terasawa, N.; Sawada, H. *Polymer*, **2001,** *9*, 4801.

[28] Ball, N. D. Gary, J. B.; Sanford, M. S. *J. Am. Chem. Soc.* **2011,** *133*, 7577.

[29] Zhang, C. P.; Wang, H.; Klein, A.; Biewer, C.; Stirnat, K.; Yamaguchi, Y.; Xu, L.; Gomez-Benitez, Vicic, D. A. *J. Am. Chem. Soc.* **2013**, *135*, 8141.

CHAPTER 5

Synthesis, Reactivity, and Catalytic Applications of Isolable (NHC)Cu–CHF_2 Complexes.[1]

5.1. Introduction

Difluoromethyl substituents are increasingly common components of pharmaceuticals and agrochemicals.[1] As such, there is significant demand for synthetic methods that enable the formation of carbon–CHF_2 bonds. Recent reports have described Pd,[2] Ni,[3] and Cu-catalyzed[4] and/or mediated[5,6] processes for the cross-coupling of aryl electrophiles with nucleophilic "CHF_2" reagents. The Cu-based systems are the oldest and arguably most common of these methods, yet little is known about the organometallic chemistry of the intermediates formed in these reactions. These transformations are believed to proceed via the initial formation of a (L)Cu(CHF_2) intermediate **A** (Scheme 5.1, *i*), followed by the reaction of this (L)Cu(CHF_2) species with an aryl electrophile (Scheme 5.1, *ii*).

Scheme 5.1 General catalytic cycle for the Cu-catalyzed difluoromethylation of aryl halides

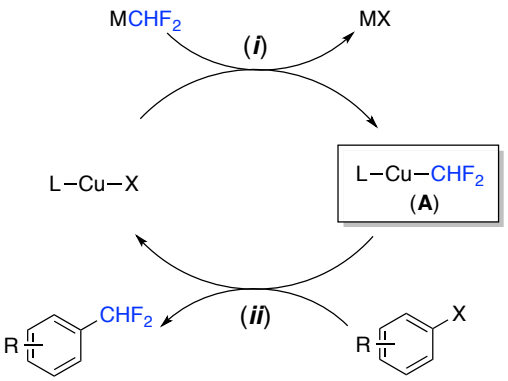

[1] Portions of this study were done in collaboration with Stavros Kariofillis. He focused on catalysis optimization and I contributed the synthesis of the complexes and catalysis scope.

Despite the importance of intermediate **A** in this catalytic cycle, little is known about the fundamental chemistry of [Cu(CHF_2)] complexes. Early reports by Burton[7a,c] and later Brauer[7b] showed that the reaction of Cd(X)(CHF_2) with CuI affords a [Cu(CHF_2)] species that can be detected by ^{19}F NMR spectroscopy at –50 ºC. However, this [Cu(CHF_2)] complex decomposes rapidly at temperatures above –30 ºC to generate a mixture of tetrafluoroethane and *cis*-difluoroethylene. These by-products implicate a bimolecular decomposition pathway, which could potentially be mitigated by the incorporation of sterically bulky ligands such as *N*-heterocyclic carbenes (NHCs). Notably, Vicic has used an analogous approach to stabilize and isolate related (NHC)Cu(CF_3) complexes.[8]

Scheme 5.2 (a)Generation and observed instability of Cu(CHF_2) at low temperatures and (b) strategy for stabilization of key CuCHF_2 intermediate for catalytic applicaitons

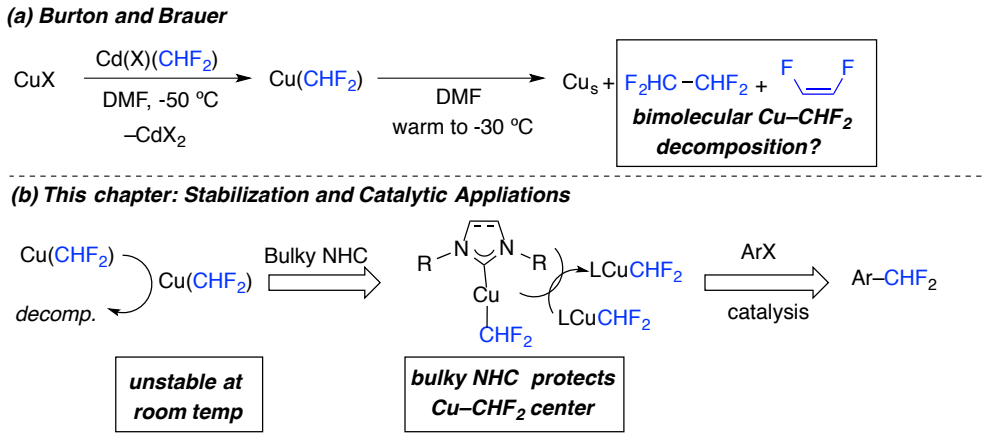

We report herein the synthesis of the first examples of isolable (NHC)Cu(CHF_2) complexes. We show that with appropriate choice of NHC, these complexes are stable for at least 24 h in solution at room temperature, suggesting that bimolecular decomposition pathways are relatively slow. Furthermore, we demonstrate that these complexes react stoichiometrically with a variety of electrophiles including diaryliodonium salts and aryl iodides to afford difluoromethylated aromatics. These stoichiometric studies are then used as

a foundation for the development of an (NHC)CuX-catalyzed cross-coupling of aryl iodides with (difluoromethyl)trimethylsilane ($TMSCHF_2$).

5.2. Results and Discussion

We initially targeted the preparation of a series of (NHC)Cu(CHF_2) complexes bearing different NHC ligands. Our synthetic procedure was borrowed from Shen's approach to related (NHC)Ag(CHF_2) compounds.[5e] The appropriate (NHC)CuCl[9] precursor was dissolved in THF, followed by the sequential addition of 2 equiv of NaO^{t}Bu and then 2.1 equiv of $TMSCHF_2$ (Scheme 5.3). With the relatively small NHC ligand ^{i}Pr (1,3-diisopropylimidazol-2-ylidene),[10] this sequence resulted in the rapid formation of *cis*-difluoroethylene and tetrafluoroethane. No ^{19}F NMR signals consistent with (^{i}Pr)Cu(CHF_2) (**2-^{i}Pr**) were detected. We hypothesize that **2-^{i}Pr** forms transiently under these conditions, but undergoes rapid bimolecular decomposition by analogy to Burton's compounds.[7, 11]

Scheme 5.3. General synthetic procedure for (NHC)Cu(CHF_2) complexes

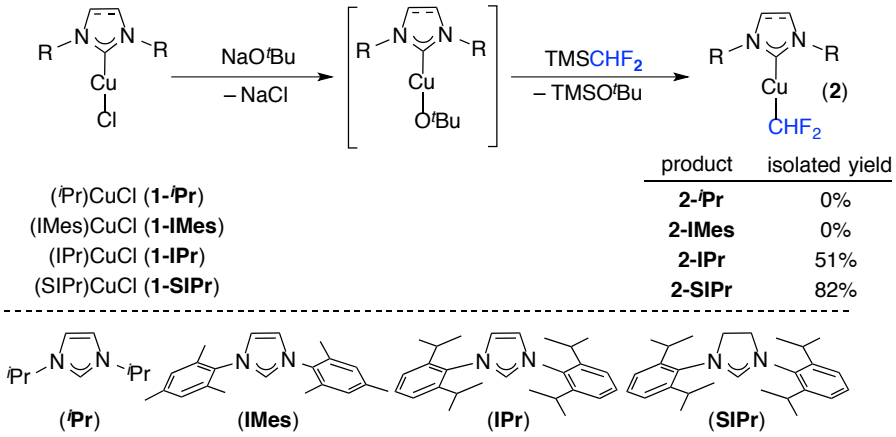

To address this issue, we next utilized the larger NHC ligand IMes (IMes = 1,3-bis(2,4,6-trimethylphenyl)imidazol-2-ylidene).[10] Subjecting (IMes)CuCl (**1-IMes**) to the reaction conditions resulted in the appearance of a ^{19}F NMR resonance at –121 ppm, which is consistent with the formation of (IMes)Cu(CHF_2) (**2-IMes**). However, the ^{19}F NMR yield of this species never exceeded 10%, and significant decomposition was observed over the course of the reaction. As such, we were unable to isolate pure samples of **2-IMes**.

However, subjecting (IPr)CuCl (**1-IPr**), which contains the even larger IPr [1,3-bis(2,6-diisopropylphenyl)-1,3-dihydro-2*H*-imidazol-2-ylidene] ligand,[10] to the same conditions resulted in the formation of a new ^{19}F NMR resonance at –119 ppm. This resonance is consistent with that expected for (IPr)Cu(CHF_2) (**2-IPr)**, and this species was stable in solution over at least 24 h at room temperature. Complex **2-IPr** was isolated in 51% yield via filtration of the reaction mixture and subsequent precipitation from a minimum volume of THF. The closely related complex (SIPr)Cu(CHF_2) (**2-SIPr**) (SIPr = 1,3-bis(2,6,-diisopropylphenyl)imidazolidin-2-ylidene)[10] was prepared and isolated in 82% yield via a closely related procedure.

Complexes **2-IPr** and **2-SIPr** were characterized by ^{1}H, ^{13}C, and ^{19}F NMR spectroscopy. The NMR spectral data for both **2-IPr** and **2-SIPr** in THF are consistent with neutral monomeric species of general structure (NHC)Cu(CHF_2) rather than the ion pair [$(NHC)_2$Cu][Cu$(CHF_2)_2$].[12] For example, ^{13}C/^{19}F HMBC experiments show strong correlations between the metal-bound NHC carbons and the fluorine atoms of the CHF_2 ligand. Furthermore, the chemical shifts of the ^{19}F NMR resonances of **2-IPr** and **2-SIPr** do not exhibit a concentration dependence, as would be expected for a rapidly equilibrating mixture of (NHC)Cu(CHF_2) and [$(NHC)_2$Cu][Cu$(CHF_2)_2$].

X-ray crystal structures of **2-IPr** and **2-SIPr** are shown in Figure 5.1. Both solid state structures show neutral monomeric copper(I) complexes with linear geometries (C–Cu–CHF_2 angle = 175.5º and 176.6º, respectively). The Cu–CHF_2 bond distance in **2-IPr** (1.928 Å) is shorter than that of **2-SIPr** (1.970 Å).[13] However, the NHC-Cu bond lengths of **2-IPr** and **2-SIPr** are nearly identical at 1.902 and 1.895 Å, respectively. Furthermore, the steric protection to the Cu center as determined by their buried volumes is also similar (buried volume = 48.1% versus 49.4% for **2-IPr** and **2-SIPr**, respectively).[14] At the time of their discovery, these

complexes represented the first isolated examples of copper(I) complexes bearing the CHF_2 ligand.

Figure 5.1 ORTEP of **2-IPr** (left) and **2-SIPr** (right). Thermal ellipsoids drawn are drawn at 50% probability.

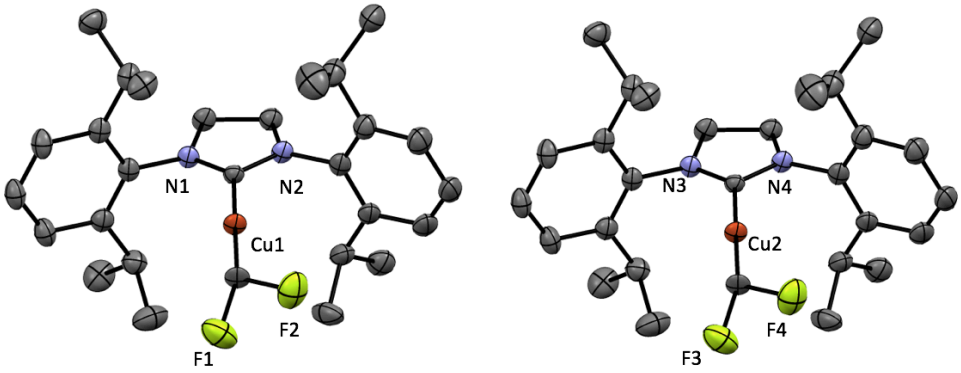

We next investigated the reactivity of **2-IPr** with a variety of electrophiles (Scheme 5.4). Acyl chlorides, aryl diazoniums salts, diaryl iodonium salts, and methyl iodide all underwent relatively clean conversion to their corresponding difluoromethylated product. Interestingly, 4-methylbenzendiaznoum tetrafluoroborate did not undergo denitrogenation under these conditions. This observation contrasts the reactivity of Cu-CF_3 derivatives, which yield benzotrifluorides upon treatment with aryl diazonium salts. Finally, methyl iodide was found to afford 1,1-difluoroethane in under 3h at room temperature but n-pentyl iodide did not react even at higher temperatures.

Scheme 5.4 The reaction of **2**-IPr with various electrophiles. Yields were determined by ^{19}F NMR spectroscopy against an internal standard.

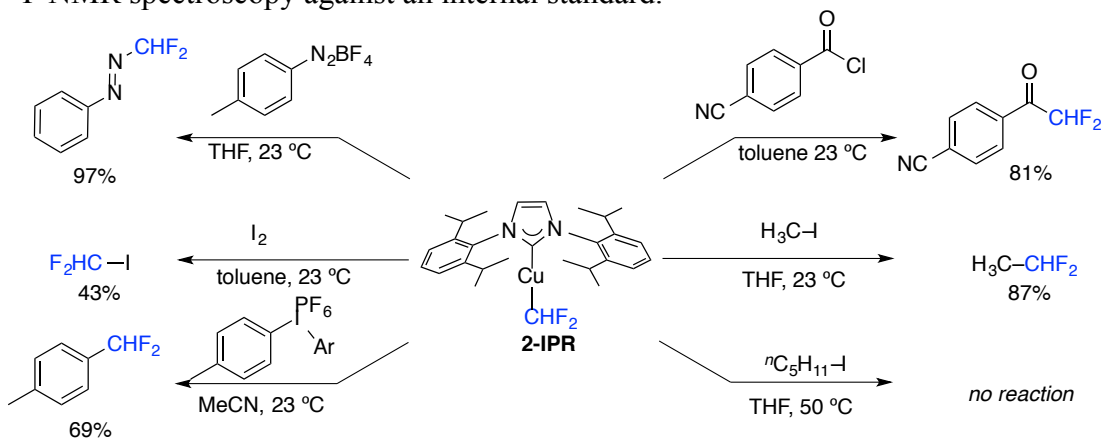

The reactions of [Cu(CHF_2)] intermediates with aryl electrophiles are proposed as a key step in Cu-catalyzed difluoromethylation reactions (Scheme 5.1, step *ii)*. As such, we next examined the reactions of **2-IPr** and **2-SIPr** with the aryl electrophile bis-(4-cyanophenyl)iodonium tetrafluoroborate[15] in greater detail. After 20 h at room temperature **2-IPr** and **2-SIPr** were fully consumed, and the formation of 4-(difluoromethyl)benzonitrile was observed in 44% and 57% yield, respectively, as determined by ^{19}F NMR spectroscopy. Benzonitrile was also detected in the crude reaction mixtures by GC/MS. Notably, competitive formation of arenes has been observed in related copper-mediated iodoarene difluoromethylation reactions.[5a]

In contrast, no reaction was observed between **2-IPr** or **2-SIPr** and 4-iodobenzonitrile at room temperature under analogous conditions. However, when these reaction mixtures were heated to 90 ºC for 20 h, 4-(difluoromethyl)benzonitrile was formed in >98% and 33% yield, respectively, as determined by ^{19}F NMR spectroscopy. Unreacted iodoarene was detected by GC/MS in the crude reaction mixture of the reaction between 2-SIPr with 4-iodobenzonitrile. Unproductive decomposition of 2-SIPr apparently competes with iodoarene difluoromethylation under these conditions. Complex **2-IPr** also reacted slowly with 4-bromobenzonitrile at 90 ºC, affording 4-(difluoromethyl)benzonitrile in 5% yield after 20 h. In contrast, **2-SIPr** afforded none of the difluoromethylated product under analogous conditions.[16] No Cu intermediates were detected by NMR spectroscopy in any of these transformations. These reactivity trends parallel the relative oxidizing strengths of the aryl electrophiles, suggesting that oxidative addition is the slow step in this sequence. Notably, Vicic demonstrated an analogous reactivity trend for related (NHC)Cu(CF_3) compounds.[8]

Table 5.1 Reactions of **2-IPr** and **2-SIPr** with aryl electrophiles[a,b]

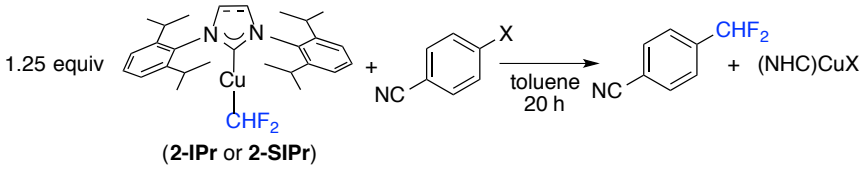

entry	[Cu]	X=	temp	yield
1	2-IPr	[I-(4-CN-C_6H_4)](BF_4)	23 ºC	44%
2	2-SIPr			57%
3	2-IPr	I	90 ºC	>98%
4	2-SIPr			33%
5	2-IPr	Br		5%
6	2-SIPr			nd[c]

[a] Reactions conducted on a 0.8 μmol scale at 0.02 M concentration; [b] Yields determined by ^{19}F NMR spectroscopy. [c] nd = not detected

We next examined the stoichiometric reactions of 2-IPr with a broader range of electronically and sterically varied aryl iodides. As shown in Table 2, electron-deficient aryl iodides generally reacted to afford high yields of the corresponding $ArCHF_2$ products (3a-e) over 20 h at 90 ºC in toluene. In contrast, electron-rich aryl iodides reacted to afford $ArCHF_2$ in lower yields, and these substrates often required more forcing reaction conditions (120 ºC). In systems where the yield of $ArCHF_2$ was moderate/low, unreacted ArI was typically observed by GC/MS at the end of the reaction, and traces of *cis*-difluoroethylene were detected by ^{19}F NMR spectroscopy. These results suggest that the decomposition of 2-IPr can be competitive with productive difluoromethylation when oxidative addition is slow. Importantly, the higher reactivity of electron deficient aryl iodides is further consistent with the electrophile trends seen in Table 1.

Table 5.2 Scope of the difluoromethylation of aryl iodides by stoichiometric **2-IPr**

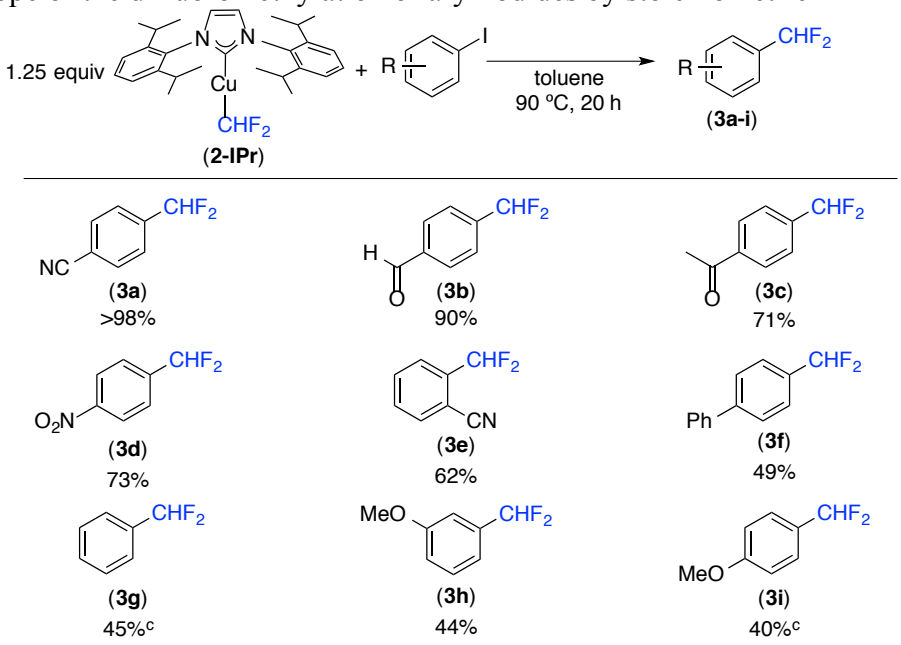

The stoichiometric reactions in Table 5.1 and 5.2 constitute the sequence of steps required for the catalytic cross-coupling of aryl iodides with $TMSCHF_2$.. As such, we next explored the use of (IPr)CuCl as a pre-catalyst for the difluoromethylation of ArI. The relatively electron-neutral substrate 4-iodobiphenyl was selected for initial optimization, with commercially available $TMSCHF_2$ as the nucleophilic source of CHF_2. Initial efforts focused on the direct merger of the transmetalation conditions developed in the synthesis of **2-IPr** with the difluoromethylation conditions in Table 5.3. However, *tert*-butoxide bases proved to be too reactive at the high temperatures required for oxidative addition, and thus yielded intractable heterogeneous mixtures upon work up. We hypothesized that fluoride salts, which are also commonly used to promote transmetalation from fluoroalkyl silicon reagents,[5a-c,6,17] might be more compatible with the reaction conditions. After surveying various fluoride salts and solvents (Table 5.3), we found that the combination of 10 mol % of (IPr)CuCl, 1 equiv of 4-iodobiphenyl, 2 equiv of $TMSCHF_2$, and 3 equiv of CsF in a 3:1 dioxane to toluene mixture at 120 ºC afforded 72% isolated yield of the difluoromethylated product **3f**.[18] Notably, this is just the second reported example of a Cu-catalyzed difluoromethylation.[4]

Table 5.3 Reaction optimization of the**2-IPr**-catalyzed aryl iodide difluoromethylation

Entry	R	Solvent	Base	Equiv. $TMSCHF_2$	mol% Cu	Yield (%)
1	CN	NMP	NaOtBu	5	15	trace
2	CN	NMP	KOtBu	5	15	<1
3	CN	NMP	KF	5	15	trace
4	CN	NMP	CsF	5	15	<1
5	CN	Tol	NaOtBu	5	15	trace
6	CN	Tol	KOtBu	5	15	trace
7	CN	Tol	KF	5	15	<1
8	CN	Tol	CsF	5	15	35
9	CN	Dioxane	NaOtBu	5	15	X
10	CN	Dioxane	KOtBu	5	15	X
11	CN	Dioxane	KF	5	15	2
12	CN	Dioxane	CsF	5	15	51
13	CN	1:1 Dioxane:Tol	CsF	5	15	62
14	CN	3:1 Dioxane:Tol	CsF	5	15	76
15	Ph	3:1 Dioxane:Tol	CsF	5	15	89
16	Ph	3:1 Dioxane:Tol	CsF	2	15	83
17	Ph	3:1 Dioxane:Tol	CsF	1	15	75
18	**Ph**	**3:1 Dioxane:Tol**	**CsF**	**2**	**10**	**80**
19	Ph	3:1 Dioxane:Tol	CsF	2	5	48

As summarized in Table 5.3, a variety of electron-rich, -neutral, and -deficient aryl iodides underwent catalytic difluoromethylation under these standard reaction conditions. The good to excellent yields obtained with electron rich aryl iodides are particularly noteworthy, as these were challenging substrates in Mikami's CuI-catalyzed difluoromethylation method.[4] We hypothesize that the IPr ligand provides sufficient stabilization of the copper center to tolerate the high temperatures required for oxidative addition with these electron rich substrates.[19] A current limitation of our method is poor tolerance of carbonyl-containing aryl iodides. Substrates bearing ketones and aldehydes afforded mixtures of products, with addition of CHF_2 into the carbonyl moiety serving as the major side reaction. However, acetal-protected

carbonyls were compatible with these conditions; for example, product **3n** was formed in 58% isolated yield.

Table 5.4. Substrate scope of IPrCuCl-catalyzed difluoromethylation. Yields determined by ^{19}F NMR spectroscopy with isolated yields in parentheses.

4

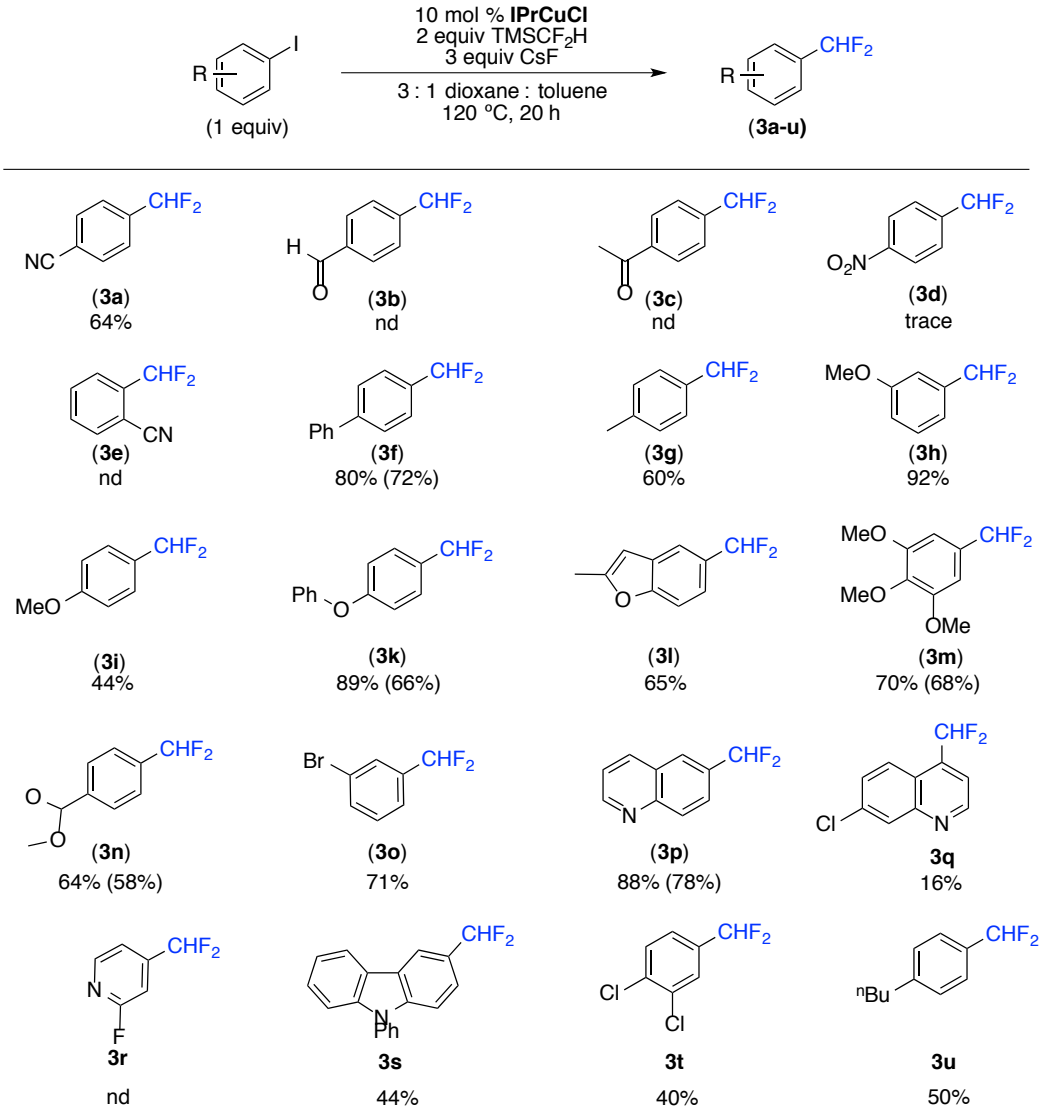

Conclusions

In summary, this chapter describes the synthesis, characterization, and reactivity of the first isolated examples of difluoromethyl copper complexes. Copper(I) compounds bearing the bulky IPr ligand were found to exhibit high stability in solution at room temperature. The bulkly ligand was not, however, found to preclude the reactions of these complexes with standard organic electrophiles. Complex 2-IPr was found to react with aryl diazoniums,

diaryliodonium salts, and acid chlorides to yield the corresponding difluoromethylated products in good yields. On account of the proposed intermediacy of $CuCHF_2$ complexes in the catalytic difluoromethylation of aryl electrophiles we investigated the scope of this aryl electrophiles in greater detail. Our studies demonstrate that (IPr)Cu(CHF_2) reacts stoichiometrically with a variety of aryl electrophiles to afford difluoromethylated arenes . Furthermore, we show that these stoichiometric studies can be translated to develop an (IPr)CuCl-catalyzed difluoromethylation of aryl iodides that utilizes a commercialy available source of CHF_2 . This catalytic method was found to difluoromethylate a wide variety of electron rich and poor arenes, though electrophilic functional groups were not well tolerated. Future studies in this area will address this limitation through investigations of alternate sources CHF_2 sources and better other ligand scaffolds that may better balance stability and reactivity.

5.3. Experimental Procedures and Characterization of Compounds

5.3.1. General Procedures and Methods

General Procedures

All manipulations were performed inside an N_2 filled glovebox unless otherwise noted. NMR spectra were obtained on a Varian VNMR 700 (699.76 MHz for ^1H; 175.95 MHz for ^{13}C), Varian VNMR 500 (500.09 MHz for ^1H; 470.56 MHz for ^{19}F; 125.75 MHz for ^{13}C), or Varian VNMR 400 (401 MHz for ^1H; 376 MHz for ^{19}F; 123 MHz for ^{13}C) spectrometer. ^1H and ^{13}C NMR chemical shifts are reported in parts per million (ppm) relative to TMS, with the residual solvent peak used as an internal reference. ^{19}F NMR chemical shifts are reported in ppm and are referenced to fluorobenzene (–113.52 ppm). Abbreviations used in the NMR data are as follows: s, singlet; d, doublet; t, triplet; q, quartet; m, multiplet; bq, broad quartet; br, broad signal; quint, quintet. Yields of reactions that generate fluorinated products were determined by ^{19}F NMR spectroscopic analysis using a relaxation delay of 25 s. Mass spectral data were obtained on a Micromass Magnetic Sector Mass Spectrometer in electrospray ionization mode. Elemental analyses were conducted by Midwest Microlabs. X-ray crystallographic data were collected on a Rigaku AFC10K Saturn 944+ CCD-based X-ray

diffractometer. Flash chromatography was performed using a Biotage Isolera One system with cartridges containing high performance silica gel.

Materials and Methods

The following compounds were prepared according to the literature procedures: IPrHCl,[20](IPr)CuCl,[21](IMes)CuCl,[2] (^{i}Pr)CuCl,[2] 2-(4-iodophenyl)-1,3-dioxolane.[22] 2-Iodobenzonitrile, 4-iodobenzonitrile, and 4-iodobiphenyl were purchased from Matrix Chemicals. Cesium fluoride was purchased from Chemetall. Spray dried potassium fluoride was provided by the Dow Chemical Company. IMesHCl, bis(4-methylphenyl)iodonium hexafluorophosphate, 4-bromobenzonitrile, and copper(I) iodide were purchased from Sigma Aldrich. Copper(I) chloride was purchased from Strem Chemicals. 3,4,5-Trimethoxyiodobenzene, 4-iodoacetophenone, 4-iodobenzaldehyde, 4-iodonitrobenzene, 3-iodobromobenzene, and 4-iodoanisole were purchased from Acros. (Difluoromethyl)trimethylsilane was purchased from Oakwood Chemicals. 6-Iodoquinoline was purchased from Ark Pharm. Dichloromethane (Fisher), pentane (Fisher), hexane (Fisher), diethyl ether (EMD), toluene (Fisher), and tetrahydrofuran (Fisher) were deaerated via a N_2 sparge and purified using an Inert Technologies alumina column solvent purification system. Anhydrous acetonitrile (Acros) was sparged and used without further purification. Anhydrous dioxane (Acros) was dried over sodium/benzophenone ketyl overnight and distilled. CD_2Cl_2, $CDCl_3$, C_6D_6, and CD_3CN were obtained from Cambridge Isotopes Laboratories and were stored over activated 4 Å molecular sieves (EMD Millipore) or basic alumina. Basic alumina (Aldrich) was dried for two days under vacuum at 210 °C. Silica gel was dried under vacuum at 130 ºC for one day. Celite was dried for 12 h under vacuum at 100 °C. Molecular sieves were dried under vacuum at 180 ºC for 3 d. CsF was crushed to a fine powder in a mortar and pestle and then dried under vacuum at 180 ºC for 6 d. Potassium fluoride was spray dried then dried further at 600 ºC overnight in an oven. Unless otherwise noted, all glassware was dried overnight in an oven at 150 °C and cooled under an inert atmosphere before use. All commercial reagents were used without further purification/drying unless explicitly stated in the experimental section.

5.3.2. Synthesis and Characterization of Complexes

Attempted Synthesis of (^{i}Pr)Cu(CHF_2):[23] A 4 mL vial was charged with (^{i}Pr)CuCl (25.3 mg, 0.10 mmol) and THF (1 mL). A separate 4 mL vial was charged with NaO^{t}Bu (19.1 mg, 0.20 mmol, 2.0 equiv) and THF (1 mL). This suspension was added to the solution of (^{i}Pr)CuCl in one portion. Upon mixing, a fine white suspension was formed. After 1 h at room temperature, $TMSCHF_2$ (26.9 mg, 0.21 mmol, 2.1 equiv) was added in one portion. The solution was then shaken for 10 s. After 1 min, the solution turned from an opaque white suspension to a deep orange solution. 4,4'-Difluorobiphenyl (19.0 mg, 0.10 mmol, 1.0 equiv) was added as a solution in 0.5 mL of THF as an internal standard. An aliquot of this solution was transferred to an NMR tube to be analyzed by ^{19}F NMR spectroscopy. Analysis of the crude reaction mixture showed the formation of difluoromethane, *cis*-difluoroethylene, and 1,1,2,2-tetrafluoroethane. After 1 h, the solvent had polymerized, and the mixture could no longer be analyzed by NMR spectroscopy.

Figure 5.2 Crude ^{19}F NMR spectrum of the attempted synthesis of **2-^{i}Pr**

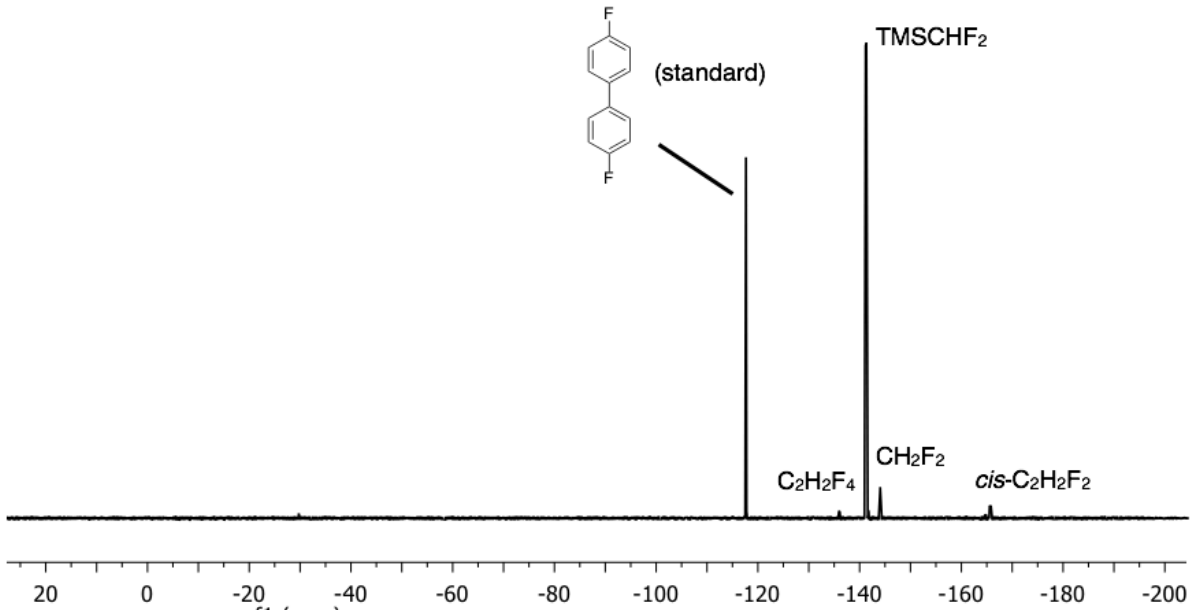

Attempted Synthesis of (IMes)Cu(CHF_2): A 4 mL vial was charged with (IMes)CuCl (41.1 mg, 0.10 mmol) and 1 mL of THF. A separate 4 mL vial was charged with NaO^{t}Bu (19.2 mg, 0.20 mmol, 2.0 equiv) and THF (1 mL). This suspension was added to the solution of (IMes)CuCl in one portion. Upon mixing, a fine white suspension was formed. After 1 h at room temperature, $TMSCHF_2$ (27.1 mg, 0.21 mmol, 2.1 equiv) was added in one portion. The solution was then shaken for 10 s. 4,4'-Difluorobiphenyl (19.0 mg, 0.10 mmol, 1.0 equiv) was added as a solution in THF (0.5 mL) as an internal standard. An aliquot of this solution was transferred to an NMR tube to be analyzed by ^{19}F NMR spectroscopy. Analysis of the crude reaction mixture showed the formation a compound consistent with **2-IMes** (–121.92 ppm, J_{CF} = 45.5 Hz) in 6% yield. Difluoromethane and *cis*-difluoroethylene were also detected by ^{19}F NMR spectroscopy. The peak tentatively assigned to **2-IMes** did not grow over the course of 2 h. After 3 h, the solvent had polymerized, and the mixture could no longer be analyzed by NMR spectroscopy.

Figure 5.3. Crude ^{19}F NMR spectrum of the attempted synthesis of **2-IMes**

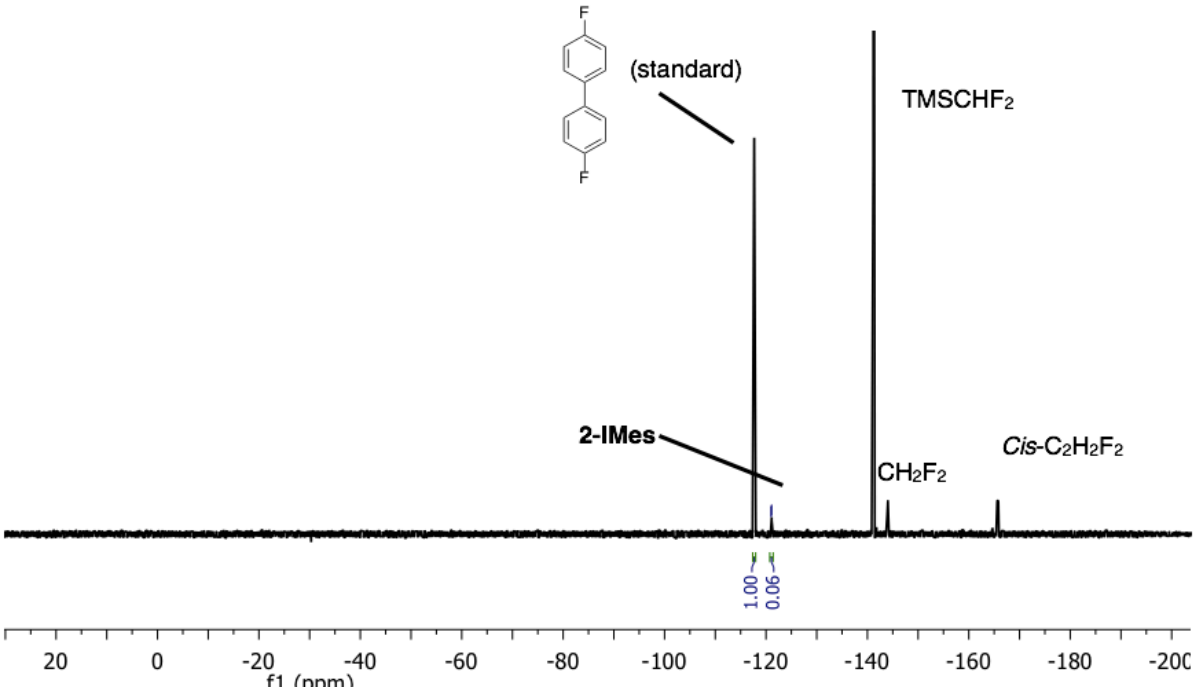

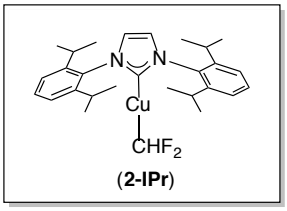

Synthesis of (IPr)Cu(CHF_2) (2-IPr): In a 20 mL vial, (IPr)CuCl (200 mg, 0.41 mmol) was dissolved in THF (5 mL). In a separate 4 mL vial, NaO^{t}Bu (78.8 mg, 0.82 mmol, 2.0 equiv) was suspended in THF (3 mL) and subsequently added to the solution of (IPr)CuCl. The mixture was shaken for 10 s and then allowed to stand for 1 h. $TMSCHF_2$ (102 mg, 0.82 mmol, 2.0

equiv) was dissolved in THF (1 mL), and then added to the solution of (IPr)CuCl and NaO^{t}Bu. The reaction mixture was allowed to stand for 1 h and was then filtered through a 2 cm thick pad of silica and concentrated. The solution was reduced to a minimum volume of THF, and a cream-colored powder was precipitated by the slow addition of pentane (10 mL) to the concentrated solution. The suspension was cooled to –35 ºC for 1 h. The powder was collected on a frit, washed with –35 ºC pentane (3 x 2 mL), and dried under vacuum to afford the product as a cream-colored powder (101 mg, 52% yield). ^{1}H NMR (700 MHz, CD_2Cl_2, 23 ºC): δ 7.55 (t, J_{HH} = 7.8 Hz, 2H), 7.36 (d, J_{HH} = 7.8 Hz, 4H), 7.16 (d, J_{HH} = 2.0 Hz, 2H), 5.84 (t, J_{HF} = 43.9 Hz, 1H), 2.59 (hept, J_{HH} = 7.0 Hz, 4H), 1.30 (d, J_{HH} = 6.9 Hz, 12H), 1.25 (d, J_{HH} = 6.9 Hz, 12H). ^{13}C NMR (176 MHz, CD_2Cl_2, 23 ºC): δ 182.78, 149.16 (t, J_{CF} = 264.6 Hz), 145.75, 134.47 130.22, 123.96, 123.08, 28.68, 24.43, 23.43. ^{19}F NMR (376 MHz, CD_2Cl_2, 23 ºC): δ –119.27 (d, J_{FH} = 42.1Hz). Elemental analysis: calculated for $C_{28}H_{37}N_2FCu$, C: 66.84, H: 7.40, N: 5.57; Found: C: 67.15, H: 7.47, N: 5.24.

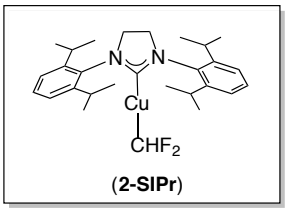

(2-SIPr)

Synthesis of (SIPr)Cu(CHF_2) (2-SIPr): In a 20 mL vial, (SIPr)CuCl (198 mg, 0.41 mmol) was dissolved in THF (4 mL). In a separate 4 mL vial, NaO^{t}Bu (78.8 mg, 0.82 mmol, 2.0 equiv) was suspended in THF (3 mL) and subsequently added to the solution of (SIPr)CuCl. The mixture was shaken for 10 s and then allowed to stand for 1 h. $TMSCHF_2$ (103 mg, 0.83 mmol, 2.0 equiv) was dissolved in THF (1 mL) and added to the solution of (IPr)CuCl and NaO^{t}Bu, and then the resulting mixture was shaken. After standing for 1 h, the reaction mixture was filtered through a 2 cm thick pad of celite. The volume of THF was reduced under vacuum, and pentane (10 mL) was added. The solution was cooled to –35 ºC for 15 h, and then the resulting precipitate was collected on a glass frit, washed with –35 ºC pentane (3 x 3 mL), and dried under vacuum to afford the product as a white solid (184 mg, 82% yield). ^{1}H NMR (700 MHz, CD_2Cl_2, 23 ºC): δ 7.45 (t, J_{HH} = 7.8 Hz, 2H), 7.30 (d, J_{HH} = 7.7 Hz, 4H), 5.74 (t, J_{HH} = 43.9 Hz, 1H), 4.00 (s, 4H), 3.10 (hept, J_{HH} = 7.1 Hz, 4H), 1.36 (dd, J = 6.9, 2.7 Hz, 24H).^{13}C NMR (176 MHz, CD_2Cl_2, 23 ºC): δ 146.84, 134.48, 129.49, 124.28, 28.82, 25.00, 23.45. Note: the **C**HF_2 and (N-**C**-N) resonances were not detected in the ^{13}C NMR spectrum at 23 ºC. However, they were detected in the ^{13}C/^{19}F HMBC : ^{19}F NMR (470 MHz, CD_2Cl_2, 23 ºC): δ –119.67 (d, J_{FH} = 44.2 Hz). Elemental analysis: calculated for $C_{28}H_{39}N_2FCu$, C: 66.57, H: 7.78, N: 5.55; Found: C: 66.32, H: 7.62, N: 5.55.

5.3.3. Reactivity Investigations

General procedure for reactions of 2-IPr and 2-SIPr with aryl electrophiles: A 4 mL vial was charged with **2-IPr** or **2-SIPr** (5.0 mg, 0.01 mmol, 1.25 equiv), the appropriate aryl electrophile (0.008 mmol), toluene (500 µL), and a magnetic stir bar. The vial was sealed with a Teflon-lined cap and removed from the glovebox. The reactions were heated to the specified temperature. After heating for 20 h, the reactions were cooled to room temperature over 30 min. The sample was then charged with fluorobenzene as an internal standard (100 µL of a 0.016 mM solution in toluene, 2.0 equiv). The solution was analyzed by ^{19}F NMR spectroscopy to determine the yield of difluoromethylated arene.

Table 5.5 Reactivity of **2-IPr and 2SIPr** with aryl electrophiles

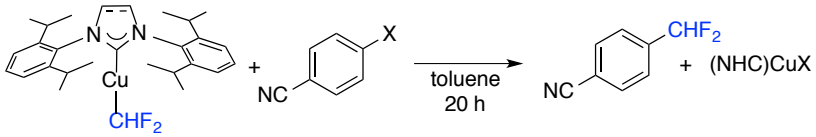

(**2-IPr** or **2-SIPr**)

entry	[Cu]	X	temperature	yield
1	2-IPr	[I(4-CN-C_6H_4)](PF_6)	23 ºC	44%
2	2-SIPr		23 ºC	57%
3	2-IPr	I	90 ºC	>98%
4	2-SIPr		90 ºC	33%
5	2-IPr	Br	90 ºC	5%
6	2-SIPr		90 ºC	nd

General procedure for the reaction of 2-IPr with aryl iodides: A 4 mL vial was charged with (IPr)Cu(CHF_2) (**2-IPr**) (5.0 mg, 0.001 mmol, 1.25 equiv) and the corresponding Ar-I (0.008 mmol, 1.0 equiv). The vial was then charged with toluene (500 µL), transferred to a screw cap NMR tube, and sealed with a Teflon-lined cap. The NMR tube was removed from the glovebox and heated at 90 °C (**3a-f**, **3h**) or 120 ºC (**3g** and **3i**) in an oil bath. After 20 h, the NMR tube was allowed to cool to room temperature, then charged with fluorobenzene (100 µL of a 0.016 mM solution in toluene) as an internal standard. The solution was analyzed by ^{19}F NMR spectroscopy to determine the yield of the difluoromethylated arene. A representative crude ^{19}F NMR spectra can be found below.

Figure 5.4. Crude ^{19}F NMR spectrum of the reaction of **2-IPr** with 4-iodobenzaldehyde to generate 4-(difluoromethyl)benzaldehyde (**3b**, δ –112.58, d, J_{FH} = 56.3 Hz). Standard = fluorobenzene (2 equiv)

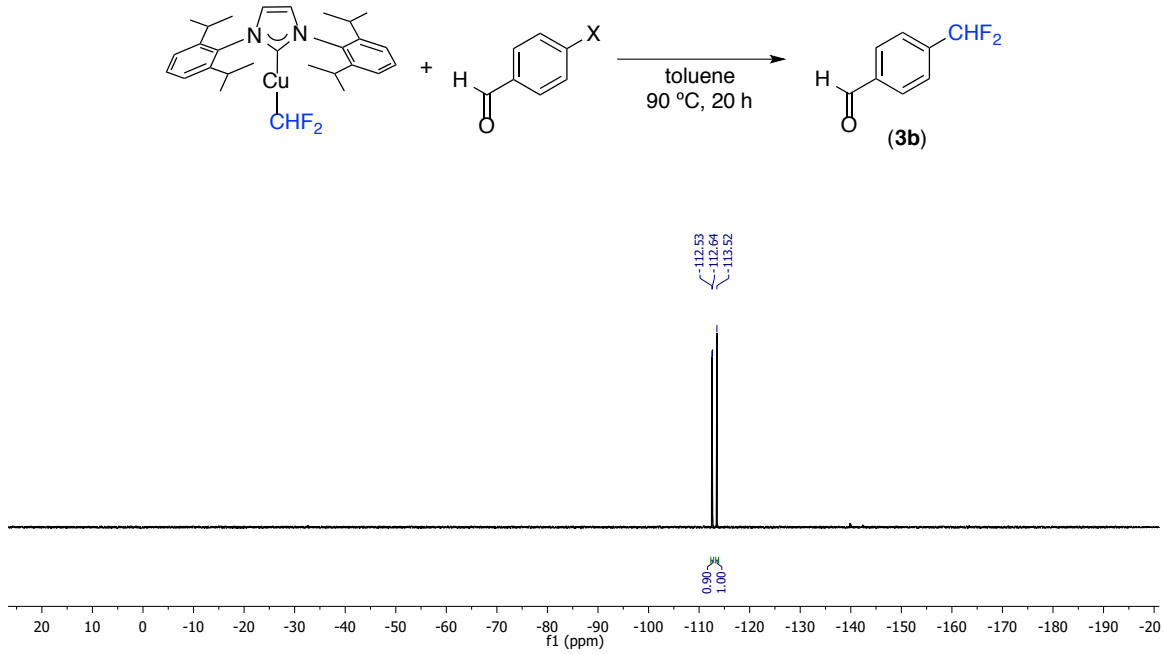

General Procedure for catalytic difluoromethylation of aryl iodides with (IPr)CuCl:

A 4 mL vial was charged with the appropriate aryl iodide (0.30 mmol, 1.0 equiv), (IPr)CuCl (15.0 mg, 0.03 mmol, 0.1 equiv), and cesium fluoride (138 mg, 0.90 mmol, 3.0 equiv). A 3 : 1 mixture of dioxane : toluene was prepared in a 20 mL vial, and 1.8 mL of this mixture was added to the reaction via syringe. $TMSCHF_2$ (77.0 mg, 0.61 mmol, 2.0 equiv) and a Teflon-coated magnetic stir bar were added to the reaction mixture. The vial was sealed with a Teflon-lined cap, wrapped with electrical tape, taken out of the glovebox, and heated at 120 °C for 20 h. The resulting mixture was allowed to cool to room temperature, and then fluorobenzene (100 µL of a 0.019 mM solution in toluene, 2.0 equiv) was added as an internal standard. An aliquot of this mixture was analyzed by ^{19}F NMR spectroscopy to determine the yield of difluoromethylated arene. Representiative NMR spectra are shown below. For isolated yields, the NMR aliquot was recombined with the bulk crude sample, and the volatiles were removed under reduced pressure. The crude residue was stirred with a 5 : 1 solution of hexanes : EtOAc (4 mL) for 1 h to dissolve the organic product. During this time, the solution was vigorously stirred and the residue was scraped from the walls of the vial with a spatula. The resulting

solution was loaded directly onto silica for purification by flash chromatography (mobile phase: hexanes/ethyl acetate with a gradient from 95 : 5 to 4 : 1).

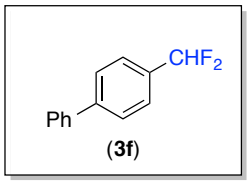

(**3f**)

Product **3f** was obtained through the general procedure as a microcrystalline white solid (45.1 mg, 72% yield). ^{1}H NMR (401 MHz, $CDCl_3$, 23 ºC): δ 7.69 (d, J_{HH} = 8.0 Hz, 2H), 7.63-7.57 (multiple peaks, 4H), 7.48 (t, J_{HH} = 7.5 Hz, 2H), 7.40 (t, J_{HH} = 7.5 Hz, 1H), 6.71 (t, J_{HF} = 57 Hz, 1H). ^{13}C NMR (176 MHz, $CDCl_3$, 23 ºC): δ 143.68, 140.16, 133.18 (t, J = 22.4 Hz), 128.90, 127.89, 127.42, 127.23, 126.01 (t, J = 6.0 Hz), 114.73 (t, J = 238.5 Hz).^{19}F NMR (376 MHz, 401 MHz, $CDCl_3$, 23 ºC): δ –110.43 (d, J_{FH} = 57.0 Hz).HRMS calcd. for $C_{13}H_{10}F_2$: 204.0751; Found: 204.0751.

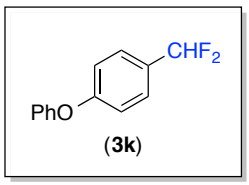

(**3k**)

Product **3k** was obtained through the general procedure as a faint yellow viscous oil (44.2 mg, 66% yield). ^{1}H NMR (700 MHz, $CDCl_3$, 23 ºC): δ 7.50-7.46 (m, 2H), 7.41-7.35 (m, 2H), 7.17 (td, J_{HH} = 7.4, 1.1 Hz, 1H), 7.08-7.02 (multiple peaks, 4H), 6.63 (t, J_{HF} = 56.6 Hz, 1H).

^{13}C NMR (176 MHz, $CDCl_3$, 23 ºC): δ 159.58, 156.16, 129.95, 128.87 (t, J = 22.7 Hz), 127.31 (t, J_{CF} = 5.9 Hz), 124.10, 119.62, 118.23, 114.59 (t, J_{CF} = 238.0 Hz). ^{19}F NMR (376 MHz, $CDCl_3$, 23 ºC): δ –109.00 (d, J_{FH} = 55.6 Hz). HRMS calcd. for $C_{13}H_{10}OF_2$: 220.0700; Found: 220.0699.

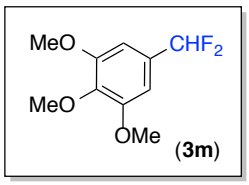

(**3m**)

Product **3m** was obtained through the general procedure as colorless crystalline solid (45.5 mg, 68% yield). ^{1}H NMR (700 MHz, $CDCl_3$, 23 ºC) δ: 6.72 (s, 2H), 6.58 (t, J_{HH} = 56.8, 1H), 3.89 (s, 6H), 3.87 (s, 3H). ^{13}C NMR (176 MHz, $CDCl_3$, 23 ºC): δ 153.51, 139.73, 129.66 (t, J = 22.6 Hz), 114.60 (t, J = 239.2 Hz), 102.54, 60.86, 56.20. ^{19}F NMR (376 MHz, $CDCl_3$, 23 ºC): δ –108.84 (d, J_{FH} = 56.4 Hz). HRMS calcd. [M^+] $C_{10}H_{12}O_3F_2$ for: 218.0755; Found: 218.0759.Product **3n** was obtained through the general procedure as a white solid (35.8 mg, 58% yield). ^{1}H NMR (500 MHz, $CDCl_3$, 23 ºC): δ 7.57 (d, J_{HH} = 8.1 Hz, 2H), 7.53 (d, J_{HH} = 8.0 Hz, 2H), 6.65 (t, J_{HF} = 56.4 Hz, 1H), 5.85 (s, 1H), 4.20-3.99 (multiple peaks, 4H). ^{13}C NMR (126 MHz, $CDCl_3$, 23 ºC): δ 140.67, 135.10, 126.77, 125.61 (t, J_{CF} = 6.0 Hz), 114.45 (J_{CF} = 239Hz), 103.02, 65.34 ^{19}F NMR (471 MHz, $CDCl_3$, 23 ºC): δ –110.94 (d, J = 56.4 Hz). HRMS calcd. for [M+H^+] $C_{10}H_9O_2F_2$: 199.0571; Found: 199.0570.

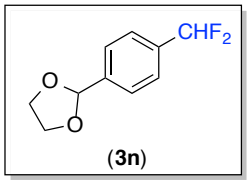

(**3n**)

Product **3n** was obtained through the general procedure as a white solid (35.8 mg, 58% yield). ^{1}H NMR (500 MHz, $CDCl_3$, 23 ºC): δ 7.57 (d, J_{HH} = 8.1 Hz, 2H), 7.53 (d, J_{HH} = 8.0 Hz, 2H), 6.65 (t, J_{HF} = 56.4 Hz, 1H), 5.85 (s, 1H), 4.20-3.99 (multiple peaks, 4H).^{13}C NMR (126 MHz, $CDCl_3$, 23 ºC): δ 140.67, 135.10, 126.77, 125.61 (t, J_{CF} = 6.0 Hz), 114.45 (J_{CF} = 239Hz), 103.02, 65.34.^{19}F NMR (471 MHz, $CDCl_3$, 23 ºC): δ –110.94 (d, J = 56.4 Hz).HRMS calcd. for [M+H$^+$] $C_{10}H_9O_2F_2$: 199.0571; Found: 199.0570.

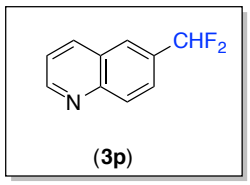

(**3p**)

Product **3p** was obtained through the general procedure as a thick yellow oil (42.9 mg, 78% yield). *Note: compound **3p** was only dried under high vacuum for 1 h, as longer periods resulted in significant loss of product. As such, minor impurities, which we attribute to solvent and semi-volatile –Si(CH$_3$)$_3$-containing compounds, were detected in the upfield region of the ^{1}H NMR.* ^{1}H NMR (700 MHz, $CDCl_3$, 23 ºC): δ 8.98 (br s, 1H), 8.23-8.15 (multiple peaks, 2H), 7.95 (s, 1H), 7.81 (d, J_{HH} = 8.2 Hz, 1H), 7.45 (dd, J_{HH} = 8.4, 3.9 Hz, 1H), 6.81 (t, J_{HF} = 56.2 Hz, 1H).^{13}C NMR (176 MHz, $CDCl_3$, 23 ºC): δ 151.79, 148.96, 136.57, 132.31 (t, J_{CF} = 22.6 Hz), 130.51, 127.53, 125.75 (t, J_{CF} = 5.6 Hz), 124.16, 121.97, 114.40 (t, J_{CF} = 239.2 Hz).^{19}F NMR (377 MHz, $CDCl_3$, 23 ºC): δ –110.92 (d, J_{FH} = 56.4 Hz). HRMS calcd. for [M+H$^+$] $C_{10}H_8NF_2$: 180.0619; Found: 180.0620.

Figure 5.5 Crude ^{19}F NMR spectrum of the (IPr)CuCl-catalyzed difluoromethylation of 4-iodobiphenyl to generate **3f** (δ –110.40, d, J_{FH} = 54.2 Hz). Standard = fluorobenzene (2 equiv)

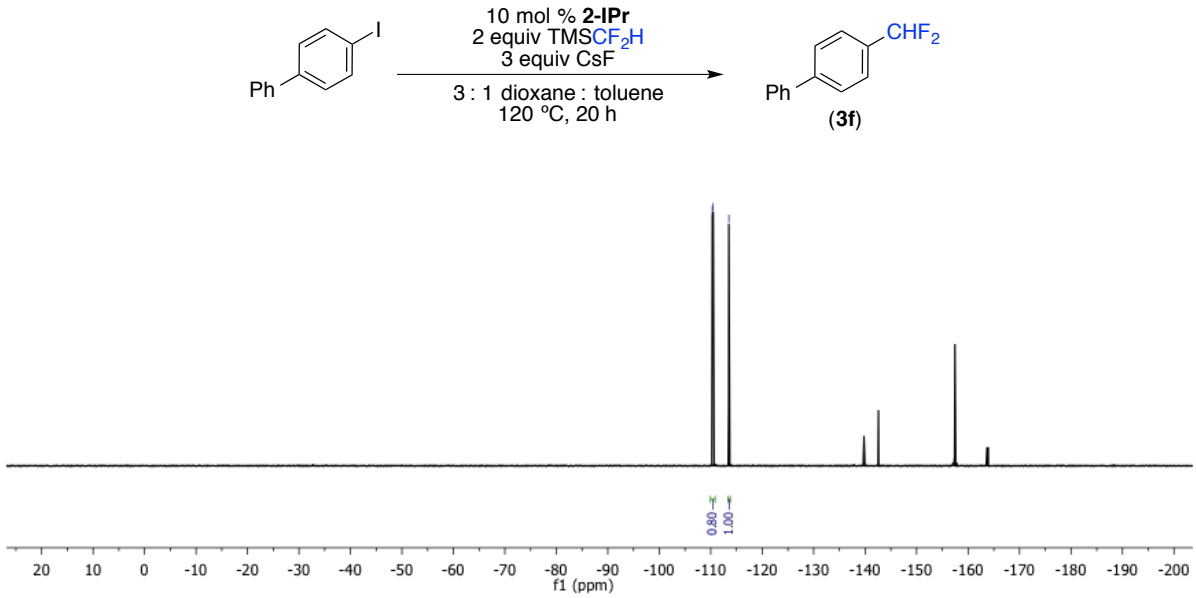

Figure 5.6. Crude ^{19}F NMR spectrum of the (IPr)CuCl-catalyzed difluoromethylation of 4-iodobenzaldehyde to generate a mixture of products consistent with addition of CHF_2 into the aldehyde. Standard = fluorobenzene (2 equiv)

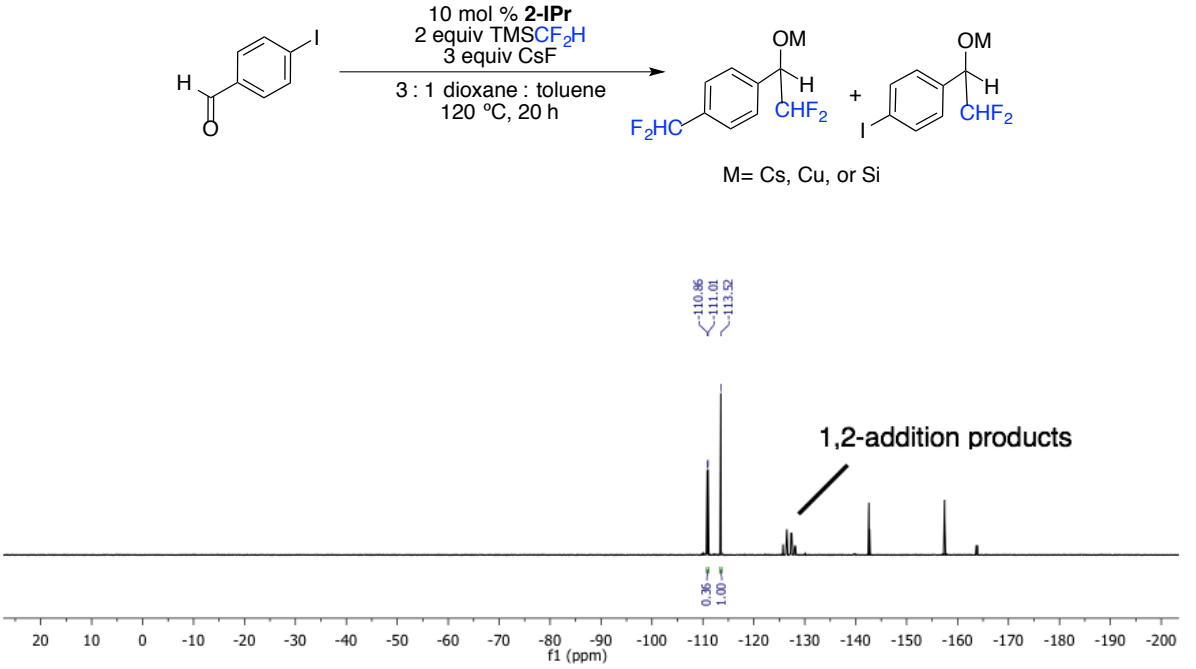

5.3.4. X-Ray Structure Determination

Structure Determination of 2-IPr

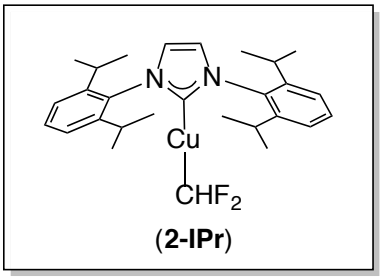

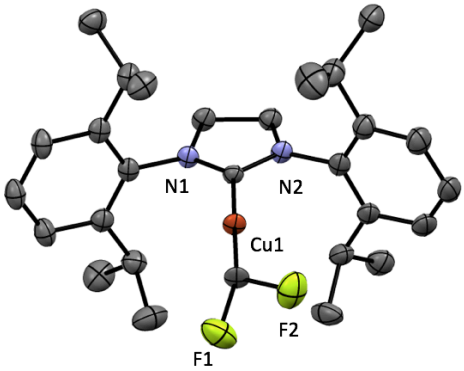

Colorless plates of **2-IPr** were grown from a toluene/pentane solution of the compound at 22 deg. C. A crystal of dimensions 0.05 x 0.03 x 0.01 mm was mounted on a Rigaku AFC10K Saturn 944+ CCD-based X-ray diffractometer equipped with a low temperature device and Micromax-007HF Cu-target micro-focus rotating anode (λ = 1.54187 A) operated at 1.2 kW power (40 kV, 30 mA). The X-ray intensities were measured at 85(1) K with the detector placed at a distance 42.00 mm from the crystal. A total of 2028 images were collected with an oscillation width of 1.0° in ω. The exposure times were 1 sec. for the low angle images, 6 sec. for high angle. Rigaku d*trek images were exported to CrysAlisPro for processing and corrected for absorption. The integration of the data yielded a total of 81781 reflections to a maximum 2θ value of 139.02° of which 9920 were independent and 8069 were greater than 2σ(I). The final cell constants (Table 1) were based on the xyz centroids 13073 reflections above 10σ(I). Analysis of the data showed negligible decay during data collection. The structure was solved and refined with the Bruker SHELXTL (version 2014/6) software package, using the space group C2/c with Z = 16 for the formula $C_{28}H_{37}N_2F_3Cu$. All non-hydrogen atoms were refined anisotropically with the hydrogen atoms placed in idealized positions. There are two crystallographically independent complexes in the asymmetric unit. For one of the complexes, the difluoromethyl ligand is disordered. Full matrix least-squares refinement based on F2 converged at R1 = 0.0497 and wR2 = 0.1144 [based on I > 2sigma(I)], R1 = 0.0640 and wR2 = 0.1222 for all data. Additional details are presented in Table 1 and are given as Supporting Information in a CIF file. Acknowledgement is made for funding from NSF grant CHE-0840456 for X-ray instrumentation.

Sheldrick, G.M. SHELXTL, v. 2014/6; Bruker Analytical X-ray, Madison, WI, 2014. CrystalClear Expert 2.0 r16, Rigaku Americas and Rigaku Corporation (2014), Rigaku Americas, 9009, TX, USA 77381-5209, Rigaku Tokyo, 196-8666, Japan. CrysAlisPro 1.171.38.41 (Rigaku Oxford Diffraction, 2015).

Table 5.6. Crystal Data and Structural Refinement for **2-IPr**

Empirical Formula	$C_{28}H_{37}F_2CuN_2$
Formula Weight	503.13
Temperature	85K
Wavelength	1.5418A
Crystal System	Monoclinic
Space Group	C2/c
Unit Cell Dimensions	a = 33.4867 A alpha = 90 deg. b =18.9543(13) A beta = 90.4160 deg c = 16.8213 A gamma = 90 deg.
Volume	10671.4 A^3
Z	16
Calculated Density	1.253mg/m^3
Absorption Coefficient	1.402 mm^{-1}
F(000)	4256
Crystal Size	0.05 x 0.03 x 0.01 mm
Theta Range for Data Collection	2.639 to 69.509 deg
Limiting Indices	$-40\leq h\leq 40$, $-22\leq k\leq 22$, $-19\leq l\leq 20$
Reflections Collected	81781
Independent Reflections	[R(int) =0.0733]
Completeness to Theta	67.684 (99.9%)
Absorption Correction	Semi-empirical from equivalents
Max and Min Transmission	1.00000. and 0.89355
Refinement Method	Full-matrix least-squares on F^2
Data / Restraints / Parameters	9920 / 0 / 620
Goodness-of-Fit on F^2	1.063
Final R Indices [$I>2\sigma(I)$]	R1 = 0.0497, wR2 = 0.1144
R indices (all data)	R1 = 0.0640, wR2 = 0.1222
Largest Difference Peak and Hole	0.580 and -0.551 $e.A^{-3}$

Structure Determination of 2-SIPr

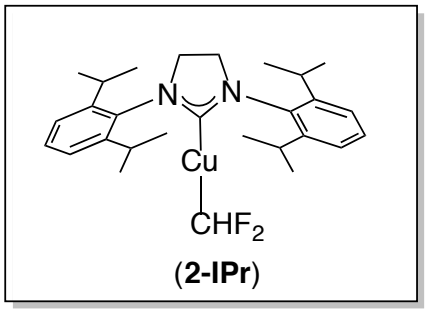

(**2-IPr**)

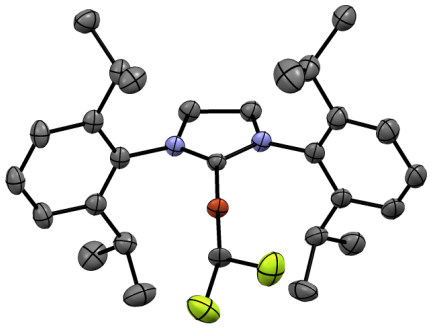

Near-colorless cubes of **2-SIPr** were grown from a tetrahydrofuran/pentane solution of the compound at 22 deg. C. A crystal of dimensions 0.15 x 0.15 x 0.15 mm was mounted on a Rigaku AFC10K Saturn 944+ CCD-based X-ray diffractometer equipped with a low temperature device and Micromax-007HF Cu-target micro-focus rotating anode (= 1.54187 A) operated at 1.2 kW power (40 kV, 30 mA). The X-ray intensities were measured at 85(1) K with the detector placed at a distance 42.00 mm from the crystal. A total of 2028 images were collected with an oscillation width of 1.0 in The exposure times were 1 sec. for the low angle images, 8 sec. for high angle. Rigaku d*trek images were exported to CrysAlisPro for processing and corrected for absorption. The integration of the data yielded a total of 126576 reflections to a maximum 2 value of 135.37 of which 16658 were independent and 13387 were greater than 2 (I). The final cell constants (Table SX) were based on the xyz centroids 30104 reflections above 10 (I). Analysis of the data showed negligible decay during data collection. The crystal was determined to be a two-component, non-merohedral twin. The two domains are related by a 89.8 degrees rotation about the reciprocal and direct (0 -1 0) axis and a refined twin volume ratio of 0.279(2). The structure was solved and refined with the Bruker SHELXTL (version 2014/6) software package, using the space group C2/c with Z = 16 for the formula $C_{28}H_{39}N_2F_2Cu$. All non-hydrogen atoms were refined anisotropically with the hydrogen atoms placed in idealized positions. The difluoromethyl ligands are rotationally disordered. Full matrix least-squares refinement based on F^2 converged at R1 = 0.1170 and wR2 = 0.3066 [based on I > 2sigma(I)], R1 = 0.1272 and wR2 = 0.3136 for all data. Additional details are presented in Table 1 and are given as Supporting Information in a CIF file. Acknowledgement is made for funding from NSF grant CHE-0840456 for X-ray instrumentation.

Table 5.7 Acquisition and Refinement parameters for **2-SIPr**

Empirical Formula	$C_{28}H_{39}F_2CuN_2$
Formula Weight	505.15
Temperature	85 K
Wavelength	1.54184 A
Crystal System	Monoclinic
Space Group	C2/c
Unit Cell Dimensions	a = 33.5944(6) A alpha = 90 deg. b =18.9208(4) A beta = 90.5685(16) deg c = 16.8763 A gamma = 90 deg.
Volume	10726. 6 A^3
Z	16
Calculated Density	1.251 mg/m^3
Absorption Coefficient	1.395 mm^{-1}
F(000)	42888
Crystal Size	0.15 x 0.15 x 0.15 mm
Theta Range for Data Collection	2.631 to 69.921 deg
Limiting Indices	$-40\leq h\leq 40$, $-22\leq k\leq 21$, $-20\leq l\leq 20$
Reflections Collected	126576
Independent Reflections	16658 [R(int) =0.1731]
Completeness to Theta	67.684 (100%)
Absorption Correction	Semi-empirical from equivalents
Max and Min Transmission	1.00000. and 0.76361
Refinement Method	Full-matrix least-squares on F^2
Data / Restraints / Parameters	16658 / 567 / 608
Goodness-of-Fit on F^2	1.415
Final R Indices [$I>2\sigma(I)$]	R1 = 0.1170, wR2 = 0.3066
R indices (all data)	R1 = 0.1272, wR2 = 0.3136
Largest Difference Peak and Hole	3.536 and 1.404 $e.A^{-3}$

5.4. References

(1) Chen, B.; Vicic, D. A. *Top. Organomet. Chem.* **2014**, *52*, 113-141.
(2) (a) Gu, Y.; Leng, X.; Shen. Q. *Nat. Commun*. **2014**, *5*, 5405. (b) Ge, S.; Chaladaj, W.; Hartwig, J. F. *J. Am. Chem. Soc.* **2014**, *136*, 4149-4152. (c) Feng, Z.; Min, Q.-Q.; Zhang, X. *Org. Lett.* **2016**, *18*, 44-47. (d) Deng, X.-Y.; Lin, J-H.; Xiao, J.-C. *Org. Lett.* **2016**, *18,* 4384-4387. (e) Aikawa, K.; Serizawa, H.; Ishii, K.; Mikami, K. *Org. Lett.* **2016**, *18*, 3690-3693.
(3) Xu, L; Vicic, D. A. *J. Am. Chem. Soc*. **2016**, *138*, 2536-2539.
(4) To our knowledge there is only one example of copper-catalyzed direct difluoromethylation of arenes. See: Serizawa, H.; Ishii, K.; Aikawa, K.; Mikami, K. *Org. Lett.* **2016**, *18,* 3686-3689.
(5) For selected examples of copper-mediated difluoromethylation of arenes see: (a) Fier, P. S.; Hartwig, J. F. *J. Am. Chem. Soc.* **2012**, *134*, 5524-5527. (b) Prakash, G. K.; Ganesh, S. K.; Jones, J.-P.; Kulkarni, A.; Masood, K.; Swabeck, J. K.; Olah, G. A. *Angew. Chem. Int. Ed.* **2012**, *51*, 12090-12094. (c) Matheis, C.; Jouvin, K.; Goossen, L. J. *Org. Lett.* **2014**, *16*, 5984-5987. (d) Jiang, X.-L.; Chen, Z.-H.; Xu, X.-H.; Qing, F.-H. *Org. Chem. Front.* **2014**, *1*, 774-776. (e) Gu, Y.; Chang, D.; X. Leng, X.; Gu, Y.; Shen. Q. *Organometallics* **2015**, *34*, 3065-3071.
(6) For examples of indirect copper-mediated and -catalyzed difluoromethylation of arenes see: (a) Fujikawa, K.; Fujioka, Y.; Kobayashi, A.; Amii, H. *Org. Lett.* **2011**, *13*, 5560-5563. (b) Belhomme, M.-C.; Poisson, T.; Pannecoucke, X. *J. Org. Chem.* **2014**, *79*, 7205-7211.
(7) (a) Hartgraves, G. A.; Burton, D. J. *J. Fluorine Chem.* **1988**, *39*, 425-430. (b) Eujen, R.; Hoge, B.; Brauer, D. J. *J. Organomet. Chem.* **1996**, *519*, 7-20. (c) Burton, D. J.; Hartgraves, G. A. *J. Fluorine Chem.* **2007**, *128*, 1198-1215.
(8) (a) Dubinina, G. G.; Furutachi, H.; Vicic, D. A. *J. Am. Chem. Soc.* **2008**, *130*, 8600-8601. (b) Dubinina, G. G.; Ogikubo, J.; Vicic, D. A. *Organometallics* **2008**, *27*, 6233-6235.
(9) Xie, W.; Chang, S. *Angew. Chem. Int. Ed.* **2016**, *55*, 1876-1880.
(10) Clavier, H.; Nolan, S. P. *Chem. Commun.* **2010**, *46*, 841-861.
(11) Notably, the saturated trifluoromethyl variant of **2-^{i}Pr** is known to be stable and isolable. See reference 8a.
(12) Related trifluoromethyl complexes were shown to exist as an equilibrium mixture of (NHC)Cu(CF_3) and [$(NHC)_2$Cu][$Cu(CF_3)_2$] in THF under analogous conditions. See ref. 8b for complete details.
(13) Interestingly, this difference is not reflected in the analogous (IPr)Ag(CHF_2) and (SIPr)Ag(CHF_2) compounds reported by Shen. These silver compounds exhibit nearly identical Ag– CHF_2 bond lengths of 2.090 and 2.092 Å, respectively. See reference 5e.
[14] Determined from the X-ray structures of **2-IPr** and **2-SIPr** using SambVca: A Web Application for the Calculation of the Buried Volume of N-Heterocyclic Carbene Ligands. See: (a) Poater, A.; Cosenza, B.; Correa, A.; Giudice, S.; Ragone, F.; Scarano, V.; Cavallo, L. *Eur. J. Inorg. Chem.* **2009**, 1759-1766. (b.) Poater, A.; Ragone, F.; Giudice, S.; Costabile, C.; Dorta, R.; Nolan, S. P.; Cavallo, L. *Organometallics* **2008,** *27*, 2679-2681.
(15) For a related reaction of a Cu–CF_3 complex with a diaryliodonium salt, see: Pandey, V. K.; Anbarasan, P. *RSC Adv.* **2016**, *6*, 18525-18529.
(16) Decomposition of **2-IPr** and **2-SIPr** appears to outcompete productive difluoromethylation at these temperatures. Analysis of the reaction mixtures by ^{19}F NMR spectroscopy showed complete consumption of **2-IPr** and **2-SIPr**, while unreacted 4-bromobenzonitrile was detected in both reactions by GCMS.

(17) (a) Cho, E.-J.; Senecal, T. D.; Kinzel, T.; Zhang, Y.; Watson, D. A.; Buchwald, S. L. *Science* **2010**, *328,* 1679-1681. (b) Maleckis, A.; Sanford, M. S. *Organometallics* **2011**, *30*, 6617-6627.

(19) Analysis of the crude reaction mixture revealed the presence of some unreacted $TMSCHF_2$ (detected by ^{19}F NMR spectroscopy). In addition, unreacted 4-iodobiphenyl was isolated from the reaction in 13% yield.

(20) The low concentration of **2-IPr** and high concentration of ArI during catalysis both likely serve to slow the competing decomposition of **2-IPr** that is observed during the stoichiometric reactions with electron rich aryl iodides.

[20] Bantreil, X.; Nolan, S. P. *Nature Protocols* **2011**, *6*, 69.

[21] Xie, W.; Chang, S. *Angew. Chem. Int. Ed.* **2016**, *55*, 1876.

[22] Ye, F.; Wang, C.; Zhang, Y.; Wang, J. *Angew. Chem. Int. Ed.* **2014**, *53*, 11625.

[23] Gu, Y.; Chang, D.; Leng, X.; Gu, Y.; Shen, Q. *Organometallics* **2015**, *34*, 3065.